



<https://theses.gla.ac.uk/>

Theses Digitisation:

<https://www.gla.ac.uk/myglasgow/research/enlighten/theses/digitisation/>

This is a digitised version of the original print thesis.

Copyright and moral rights for this work are retained by the author

A copy can be downloaded for personal non-commercial research or study,
without prior permission or charge

This work cannot be reproduced or quoted extensively from without first
obtaining permission in writing from the author

The content must not be changed in any way or sold commercially in any
format or medium without the formal permission of the author

When referring to this work, full bibliographic details including the author,
title, awarding institution and date of the thesis must be given

Enlighten: Theses

<https://theses.gla.ac.uk/>
research-enlighten@glasgow.ac.uk

**NEW METHODS IN SEISMIC REFLECTION
EXPLORATION**

SHUANG QIN M.Sc.

Department of Geology & Applied Geology
University of Glasgow

A thesis submitted for the degree of Doctor of Philosophy in the University of Glasgow.

July 1996

ProQuest Number: 10992078

All rights reserved

INFORMATION TO ALL USERS

The quality of this reproduction is dependent upon the quality of the copy submitted.

In the unlikely event that the author did not send a complete manuscript and there are missing pages, these will be noted. Also, if material had to be removed, a note will indicate the deletion.



ProQuest 10992078

Published by ProQuest LLC (2018). Copyright of the Dissertation is held by the Author.

All rights reserved.

This work is protected against unauthorized copying under Title 17, United States Code
Microform Edition © ProQuest LLC.

ProQuest LLC.
789 East Eisenhower Parkway
P.O. Box 1346
Ann Arbor, MI 48106 – 1346

Keris
10836
Copy 1



Dedicated to my parents

Summary

One of the main problems in the development of the new near-zero-offset method based on the roll-along zero-offset receiver (RAZOR) array is how to simulate this spatially extended array. In this thesis we use Sierra products (standard industry geophysical processing and geological interpretation systems) to carry out numerical experiments on synthetic RAZOR array surveys. Two array design modes are proposed for modelling these surveys. The first is the crooked line mode, which is suitable for experiments with a single RAZOR array. Its advantage is that all the data traces are sorted in the order of acquisition of the RAZOR shot gather directly, and are stored in one disk file without any extra processing. The second method is the five-line mode, which is more suitable for simulating roll-along experiments of the RAZOR array. A new Fortran-77 program RAZORSORT.F is developed for post-raytracing sorting. In addition a new quick display tool QPLOT.F has been developed, supported by the UNIRAS package.

To image the subsurface structure using the P-waves of recorded RAZOR reflection data, slant-stack processing is applied to extract the maximum reflection energy and improve the signal to noise ratio. This is called the RAZOR slant-stack in the 3-dimensional spatial domain. The aim of the slant-stack operation on the RAZOR data is to image geological structure and improve the signal/noise ratio in three dimensions, rather than to suppress multiples or achieve other purposes, for which slant-stack processing is usually performed on CDP gathers in two dimensions. Synthetic data tests are used to examine the performance of the 3-D RAZOR slant-stack. It is found that an undesired aliasing occurs in the τ - p domain during the RAZOR slant-stack processing, which leads to degradation of the images. To overcome this, two techniques, an image enhance operator (IEO) and diversity stack are proposed to suppress this aliasing noise without distorting the signal component in the stacked trace. The IEO requires careful specification of the operator parameters to avoid poor resolution of the IEO image. The RAZOR diversity slant-stack is based on the assumption that if the signal amplitude is balanced across the 12 traces in the x - t domain contributing to the RAZOR diversity slant stack, then true amplitudes are preserved. A new Fortran-77 program QDSTACK.F has been written to perform diversity slant-stack processing on the RAZOR shot gathers. Finally we examine the RAZOR point-source data from the point of view of seismic illumination, the so-called controlled directional source (CDS) method. By superposing the common-receiver traces corresponding to the continuous point source, the response of RAZOR array to a plane source is simulated. Based on the analysis of the 4-D data set from the RAZOR array rolling along a survey line, the RAZOR profile is obtained.

The new 'squeeze-filter-unsqueeze' (SFU) algorithm for removing the direct wave in uncorrelated vibroseis data is developed. It is demonstrated, using both synthetic data and field recorded data, that the filter can provide excellent correlation noise cancellation when the onset time of the direct wave sweep is known. The SFU algorithm does not require any additional conditions on field acquisition (other than that the uncorrelated data are preserved) and is suitable for all common vibroseis data acquired using linear or non-linear sweeps.

The SFU filter with the application of an optimum least-squares algorithm appears to be much more effective at cancelling noise without attenuating signal frequency components near the squeezed constant frequency than the equivalent filter using a linear recursive notch filter algorithm. When the onset time of the direct wave is only known approximately, so that the automatic picking algorithm performs poorly, the

SFU with the notch algorithm should replace SFU with the optimum least-squares algorithm. SFU filters appears to be more suitable for low-noise vibroseis data, and are more effective when the sweep tapers can be well defined. The SFU filter is still valid when the pilot sweep cannot be described as an explicit function of travel time. The SFU filter has been added to SierraSEIS Version 1.4 as a standard processor.

The new DOLS filter applies an optimum least-squares algorithm directly to remove the direct wave in the pre-correlation domain. It is a simplified version of the "squeeze-filter-unsqueeze" (SFU) algorithm, and can provide excellent correlation noise cancellation when the onset time of the uncorrelated direct wave is known. The DOLS differs from SFU filtering, in that the latter depends upon the squeezing and unsqueezing transformation pair. The DOLS filter does not require any additional constraints on field acquisition, and is suitable for all common vibroseis data acquired using linear or non-linear sweeps. The synthetic examples demonstrate that the DOLS filter requires the onset time of the uncorrelated direct wave to be known precisely, as does SFU. In cases where it is difficult to determine the onset time accurately, a correlation analysis technique should be used to minimise the resulting approximation error. Both SFU and DOLS filters can provide excellent results in cancelling the direct wave in the pre-correlation domain. The SFU filter requires more calculation time than DOLS, whereas the DOLS filter may lead to possible attenuation or distortion of the signal at and near the direct wave.

A new filter ('3CFH') is developed for enhancing P-wave reflections by using 3-component recordings. The process generates a unique 3-D velocity semblance plot for each CMP gather. By iteratively repeating the processing on each 3-component CMP shot gather, a final improved subsurface image can be extracted by using the optimum projection velocity. A new module for 3CFH filtering has been programmed and added into SierraSEIS. Another module has been added into SierraSEIS as a routine processor for gathering the 3-C CMP data into the correct format for 3CFH filtering.

Preliminary processing of the vertical component data from the crustal seismic reflection profile through the Kola superdeep well SG-3 has been carried out. It follows a conventional sequence of seismic data processing. Three new processing techniques have been developed for some preprocessing phases. Firstly, a new module carries out a timing compatibility correction for the three field recording systems which had different trigger circuits. Secondly, a new module is developed to pick up and automatically set to zero the bad traces, based on a statistical analysis of amplitudes within a certain time window of each trace, and by comparison of the traces in each shot gather. Lastly, a new notch filter is developed to cancel any stationary sinusoidal noise in the seismic data, based on a recently published digital least-squares filtering algorithm. An F-K filter has been applied to remove coherent noise such as ground roll. The notch filter suppresses a large amount of stationary sinusoidal contamination caused by the mechanical noise near the well-head. Band-pass filtering is used to attenuate very low- and high-frequency random noise. Residual statics have been applied to improve stacking quality. Post-stack deconvolution achieves compression of the wavelet to increase the temporal resolution. Coherency filtering enhances the events with lateral continuity within a specified dip range. Migration has not been applied in this preliminary processing phase. The quality of the processed Kola data is reasonably acceptable, and the stacked sections show the primary lithological layering of the Proterozoic supracrustal rocks dipping at 40-50°.

Declaration

The material presented in this thesis summarises the results of three years of research carried out in the Department of Geology & Applied Geology, University of Glasgow under the supervision of Professor D. K. Smythe. It has not previously been submitted for any degree. The study is based on my own independent research, and any published or unpublished results of other researchers used in this thesis have been given full acknowledgement in the text.

Shuang Qin

July 1996

Acknowledgements

This research was carried out at the Department of Geology & Applied Geology, University of Glasgow, under the supervision of Professor D. K. Smythe.

I would like to thank my supervisor Prof. David. K. Smythe for his initiating and supervising the work. His patient guidance, encouragement and assistance are extremely important for the research. He critically read my original manuscript and give me valuable suggestions and comments which have greatly improved the text and its general layout.

I wish to acknowledge with thanks, the benefits and assistance I have received from discussion, comments and suggestions from Dr. Doyle R. Watts, in particular when processing the Kola linear sweep data and the Ohio non-linear sweep data. I would like also to express my gratitude to Dr. J. J. Doody for his help, assistance and encouragement, in particular during the early years of the research project.

My appreciation goes to the technical staff at the Department of Geology & Applied Geology, in particular to Bob Cumberland for his efficient support in carrying out various computations and checking, and to George Gordon and Roddy Morrison for supplying materials. My thanks are also due to 'young' David Abensour for his great assistance in computer support, and the other postgraduate student colleagues of the Department of Geology & Applied Geology for their help and encouragement.

Finally it is my pleasure to express my thanks to my wife Yue-Ping Zhou for her love and continuous backing.

Contents

Summary		iii
Declaration		v
Acknowledgements		vi
Contents		vii
 Text		
1	Introduction	1
1.1	Conventional 2-D land seismic reflection acquisition	1
1.2	The conventional 2-D land 3-component reflection method	2
1.3	Use of 3-component recording in the seismic exploration industry	3
1.4	Possibilities for new acquisition geometry	4
1.5	Vibroseis <i>versus</i> impulsive sources	5
1.6	The standard industry vibroseis recording and processing method	6
1.7	The problem of sidelobes	7
1.8	Possibilities for new vibroseis data processing	9
1.9	Summary of new methods and their potential application	9
 2	 New near-zero-offset methods based on the RAZOR array	 11
2.1	Introduction	11
2.2	RAZOR array design	11
2.3	Review of the synthetic modelling of the RAZOR array using SEIS-83	15
2.4	Interaction with the Sierra seismic modelling environment	17
2.5	Geological modelling by MIMIC	17
2.6	RAZOR array design and raytracing in QUIKSHOT	18
	2.6.1 <i>Array design in the crooked line mode</i>	22
	2.6.2 <i>Array design in the five-line mode</i>	24
2.7	New Fortran-77 programs for RAZOR modelling	25

2.7.1	<i>Program RAZORSORT.F</i>	25
2.7.2	<i>Program QPLOT.F as a quick display tool</i>	26
2.8	Summary and discussion	28
3	Improving P-wave reflection images from RAZOR data	33
3.1	Introduction	33
3.2	RAZOR P-wave slant-stack processing in the τ - x domain	34
3.2.1	<i>Introduction to slant-stack technology</i>	34
3.2.2	<i>Slant-stack in RAZOR data processing</i>	36
3.2.3	<i>Synthetic examples</i>	40
3.3	Image enhancement operator for post-slant-stack processed RAZOR data	40
3.4	The diversity stack in the τ - p domain to attenuate aliasing noise	48
3.4.1	<i>Introduction to diversity stack technology</i>	48
3.4.2	<i>The diversity stack in RAZOR slant-stack processing</i>	49
3.4.3	<i>FORTRAN-77 program QDSTACK</i>	50
3.5	Plane wave decomposition for analysis of RAZOR data in three dimensions	52
3.5.1	<i>Introduction to the CDS method</i>	52
3.5.2	<i>Simulation of a planar source in the RAZOR array</i>	53
3.5.3	<i>Profiling based on the RAZOR array</i>	56
4	Filtering vibroseis data in the pre-correlation domain	64
4.1	Introduction	64
4.2	The problem of sidelobes	68
4.3	The SFU filter algorithm	69
4.3.1	<i>Squeezing a linear sweep</i>	69
4.3.2	<i>Squeezing a non-linear sweep</i>	72
4.3.3	<i>Filtering methods</i>	73
4.3.4	<i>Unsqueezing the filtered trace</i>	77
4.4	Implementation of SFU filtering	78
4.5	Synthetic examples	79
4.6	Field data example	82
4.7	Discussion	89
4.7.1	<i>Limitations of the notch and optimum least-square algorithms</i>	89
4.7.2	<i>Comparison of the notch and optimum least-squares (OLS)</i>	

	<i>algorithms in SFU</i>	90
4.7.3	<i>Filter design in SFU</i>	93
4.7	New module /QSFU in SierraSEIS 1.43	95
5	Direct optimum least-squares (DOLS) filtering of uncorrelated vibroseis data	
5.1	Introduction	95
5.2	Description of the DOLS filter algorithm	95
5.3	Implementation of DOLS filtering	101
5.4	Synthetic examples	103
5.5	Field data example	105
5.6	Discussion	108
	5.6.1 <i>Effect of onset time error on the DOLS filter</i>	108
	5.6.2 <i>Effect of operator length on DOLS filtering with incorrect onset time</i>	110
	5.6.3 <i>Comparison of the DOLS and SFU filters</i>	111
5.7	New module /QDOLS in SierraSEIS 1.4	113
6	Three-component filtering of sub-horizontal reflections	114
6.1	Introduction	114
6.2	Description of the 3CFH filter algorithm	115
	6.2.1 <i>A single flat reflector below an overlying homogeneous medium</i>	116
	6.2.2 <i>Single dipping plane reflector</i>	117
	6.2.3 <i>Horizontal isovelocity multi-layers</i>	119
6.3	3-Component data transformation and implementation of the 3CFH filter	122
6.4	Synthetic examples	124
6.5	Discussion of the projection velocity	126
6.6	New Processing modules in SierraSEIS 1.4	132
	6.6.1 <i>Module /QTCFH in SierraSEIS 1.4</i>	132
	6.6.2 <i>Module /QGATHER in SierraSEIS 1.4</i>	133

7	Processing of vertical component Kola data	134
7.1	Introduction	134
7.2	Survey geometry and acquisition parameters	134
	7.2.1 <i>Location of survey line</i>	136
	7.2.2 <i>Source type and position</i>	136
	7.2.3 <i>Receiver spread configuration</i>	138
7.3	Wave patterns	139
	7.3.1 <i>Ground roll</i>	140
	7.3.2 <i>First arrivals</i>	140
	7.3.3 <i>Shear waves</i>	143
	7.3.4 <i>P-wave reflections</i>	143
	7.3.5 <i>Noise</i>	144
7.4	New processing modules	146
	7.4.1 <i>Module /QSHIFT in SierraSEIS 1.4</i>	146
	7.4.2 <i>Module /QZERO in SierraSEIS 1.4</i>	146
	7.4.3 <i>Module /QNOTCH in SierraSEIS 1.4</i>	146
7.5	Processing parameter table	147
7.6	Preprocessing	147
	7.6.1 <i>Compatibility correction for the recording systems</i>	152
	7.6.2 <i>Data editing</i>	152
	7.6.3 <i>Geometry</i>	154
	7.6.4 <i>Application of gain</i>	154
7.7	Spectral Characteristics and filtering	156
	7.7.1 <i>Application of notch filter</i>	156
	7.7.2 <i>Application of f-k filter</i>	161
	7.7.3 <i>Application of new SFU filter</i>	161
7.8	CMP sorting	163
	7.8.1 <i>Summing shot gathers</i>	163
	7.8.2 <i>Crooked line binning</i>	163
	7.8.3 <i>Velocity analysis and NMO correction</i>	164
	7.8.4 <i>Muting</i>	164
	7.8.5 <i>Residual statics correction</i>	166
7.9	Poststack processing	166
	7.9.1 <i>Deconvolution</i>	166
	7.9.2 <i>Coherency filtering</i>	168

7.9.3	<i>Band-pass filtering</i>	168
7.10	Problems and discussion	168
7.10.1	<i>Extra moveout problem for Blue recording system</i>	168
7.10.2	<i>Separation of P- and S-waves</i>	171
7.10.3	<i>Statics estimation</i>	171
7.10.4	<i>Velocity analysis</i>	172
8	Conclusions	173
8.1	New near-zero-offset methods based on the RAZOR array	173
8.2	Removing the direct wave	175
8.3	Improving Reflection Images with 3-component filtering	177
8.4	Application of new methods to the Kola data	178
	References	182
	Appendices	
A	BIRPS S-wave experiment 1988: Field Layout of the Glasgow piggyback experiment	185
B	*Fortran-77 source code	188
C	The new processor /QDSTACK	188
D	A note on vibroseis direct wave suppression	189
E	The new processor /QSFU	191
F	The new processor /QDOLS	193
G	Note on 3-component semblance	196
H	The new processors /QTCFH and /QGATHER	198
I	The new processors /QSHIFT, /QZERO and /QNOTCH	200
J	*SierraSEIS geometry processing job file (Chapter 7).	205
K	Acronyms, abbreviations and definitions of symbols	205

*: Source files listed in the attached floppy disk.

Figures

2-1	Field areal RAZOR array pattern for seismic survey.	12
2-2	Geometry of a normal-incidence ray from a crustal reflector.	13
2-3	The geometry of a dipping reflector related to a surface line of different azimuths.	16
2-4.	The 3-D fault model calculated by MIMIC for modelling the RAZOR array.	19
2-5	The 3-D pinchout model created by MIMIC.	20
2-6	The complex 3-D model for the RAZOR array modelling.	21
2-7	The RAZOR roll-along array using the crooked line mode.	23
2-8	The roll-along RAZOR array using the five-line mode.	24
2-9	A RAZOR shot gather after sorting by program RAZORSORT.	25
2-10	Flow diagram for program QPLOT.	27
2-11	The RAZOR stacked section for a dipping reflector plotted by QPLOT.	29
2-12	The same RAZOR stacked section in variable density format.	30
2-13	Flow diagram for the numerical modelling experiments on the RAZOR array.	31
3-1	A hyperbola in a CDP gather maps onto an ellipse in a slant-stack gather.	35
3-2	RAZOR shot gather over the fault model of Figure 2-4.	38
3-3	Comparison of RAZOR slant-stack gathers with and without interpolation calculation.	39
3-4	RAZOR section over a fault model after slant-stack processing.	41
3-5	RAZOR section over a pinchout model after slant-stack processing.	42
3-6	RAZOR section over a complex model after slant-stack processing.	43
3-7	Comparison of versions before and after IEO image processing.	45
3-8	Comparison of normal and diversity RAZOR slant-stacks.	46
3-9	Flow diagram of the program QDSTACK.	51
3-10	Simulation of a dipping planar wavefront in the two-dimensional RAZOR array.	55
3-11	Relationship of the τ - p section to the constant- p section.	56
3-12	Flow diagram of seismic reflection processing for RAZOR data.	58
3-13a, b.	CDS sections with ray parameter $p=-0.0022$ and $p=-0.001467$.	60
3-13c, d.	CDS sections with ray parameter $p=-0.000733$ and $p=-0.000366$.	61
3-13e, f.	CDS sections with ray parameter $p=0.0$ and $p=+0.000733$.	62
3-13g, h.	CDS sections with ray parameter $p=+0.00146$ and $p=+0.0022$.	63
4-1	Autocorrelation of a sweep showing major lobe and side lobes.	65

4-2	Correlated synthetic data trace before and after SFU.	66
4-3	Flow chart of the squeeze-filter-unsqueeze (SFU) filter algorithm	70
4-4	Demonstration of the squeezing and unsqueezing of a sweep.	71
4-5	Flow chart of the automatic method used to determine the onset time.	78
4-6	Demonstration of squeezing and unsqueezing using interpolation.	80
4-7	Synthetic linear upsweep from 10 to 60 Hz stretched and squeezed.	81
4-8	Synthetic trace with direct wave at 0 ms and reflection at 1000 ms.	83
4-9	Synthetic trace with direct wave at 0 ms and reflection at 100 ms.	84
4-10	Correlated raw shot gather from Kola before and after SFU.	86
4-11.	Correlated raw shot gather from Ohio before and after SFU.	87
4-12.	Comparison of the Ohio stack section portion before and after SFU.	88
4-13	Comparison of two algorithms to be used in SFU.	90
4-14	Comparison of the SFU filter with two different algorithms	91
4-15	Correlograms before and after SFU filtering,	92
4-16	Linear upsweep squeezed to 60 Hz with linear tapers.	94
4-17	Effect of the unmatched tapers for the SFU filter design.	95
5-1	Flow chart showing the basic design of the DOLS filter.	98
5-2	Flow diagram of the automatic method to determine the onset time.	102
5-3	DOLS filter test using a linear sweep signal.	104
5-4	Comparison of the correlated versions in Figure 5-3.	104
5-5	DOLS filter test of the non-linear sweep signal.	106
5-6	Comparison of the correlated versions in Figure 5-5.	106
5-7	DOLS filter comparison of a Kola shot gather (linear sweep).	107
5-8	DOLS filter test of the approximation error of the onset time.	109
5-9	DOLS filter test of the operator length.	110
5-10	Comparison of SFU and DOLS filtering.	112
6-1	A single horizontal flat layer with isotropic medium and its 3CFH filter.	117
6-2	A dipping planar reflection below an overlying homogeneous medium.	118
6-3	A horizontal isovelocity multi-layer model and its 3CFH filter definition.	120
6-4	Flow chart of the 3CFH filter design and processing procedure.	123
6-5	Two-layer model with isotropic layers.	124
6-6	Roll-along array with a 24 channels system and 8 shots.	125
6-7	Conventional CDP stacked section of Z-component recordings.	127
6-8	Conventional CDP stacked section of Y-component recordings.	128
6-9	CDP stacked section after the 3CFH filter is applied with a constant velocity.	129

6-10	3-D semblance for projection velocity analysis.	132
7-1	Base map showing the location of seismic survey receiver line (triangles).	135
7-2	Base map showing the CDP coverage of the area around the SG-3 well.	137
7-3	Layout of composite CDP spread of 90 3-component stations.	139
7-4	The four types of prominent wave patterns in most Kola data.	141
7-5	Variation in the amplitude of ground roll and other waves.	142
7-6	A common source gather.	145
7-7	The geometry base map showing the location of the CDP line.	149
7-8	The base map showing the location of CMPs and the bins.	150
7-9	The elevation profile and statics profile for the CDP line in Figure 7-7.	151
7-10	The same common source gather in Figure 7-6 after compatibility correction.	153
7-11	The five shotgathers (from Z-system) from the processor /QZERO.	155
7-12	Frequency amplitude spectra.	157
7-13	Comparison of a filtered common shot.	159
7-14	Flawless analogue notch filtering on a recorded sweep from the W-system.	160
7-15	Comparisons of a filtered version.	162
7-16	Final stacked section without migration.	165
7-17	Result of poststack predictive deconvolution processing.	167
7-18	Result of poststack coherency filtering to enhance events with lateral continuity.	169
7-19	The misaligned moveout of the traces in a common source gather.	170

Tables

1-1	Summary of new methods developed in this dissertation	10
7-1	Processing Parameter List	148
7-2	Frequencies of stationary sinusoidal contamination	158

Chapter 1

Introduction

1.1 Conventional 2-D land seismic reflection acquisition

Conventional 2-D land seismic reflection acquisition is dominated by the common depth-point (CDP) recording method. It was invented by Mayne (1950) as a way of attenuating noise which could not be handled by the use of arrays. Magnetic-tape recording made CDP practical, and CDP recording began in about 1956, but it did not become extensively used until the early 1960s, when its ability to attenuate multiples and other kinds of noise led to its rapid adoption. Today its use is nearly universal.

The CDP technique is designed to cancel noise of long apparent wavelength, regardless of its origin. As with conventional cancellation, outputs of phone groups distributed over a distance comparable to a wavelength are summed. The loss of definition which averaging over such an 2-D extensive baseline would otherwise cause is averted by a special arrangement of shots and geophones that combines only those signal reflections from the same region of the subsurface. Basically, signals associated with a given reflection point but recorded at a number of different shot and geophone positions are composited after appropriate time corrections have been applied to compensate for the longer ray path as the shot-geophone distance is increased. In an actual field setup, such CDP shooting involves a greater number of shot points per unit distance along the line than conventional split-spread shooting does. For example, with 24 recording stations, threefold coverage will be obtained if the shots are separated by four geophone-group intervals, fourfold if by three intervals, and six fold if by two intervals. If the shooting is twelvefold there is a shot for every geophone group centre. To attenuate multiple reflections the spreads are much longer with CDP shooting than they were with conventional single coverage. Spreads allowing recording as much as 4 km from the shot are not uncommon in land acquisition.

The CDP coverage depends on the quality of the data and the relative amplitudes of the multiple reflections to be cancelled. In addition, CDP data are often used to compute

interval as well as average-velocity information. To attain the greatest possible precision in the resultant velocity, it may be desirable to shoot with as great a degree of multiplicity as is operationally feasible in 2-D CDP operation.

1.2 The conventional 2-D land 3-component reflection method

Until the 1970s, onshore seismic reflection acquisition methods in petroleum exploration were limited, to a great extent, to P-wave energy recorded on single-component vertical geophones. With the advent of S-wave recording in the 1970s, the use of both vertically and horizontally polarised sources and multicomponent receivers has become more common.

Two-dimensional (2-D) land 3-component seismic exploration requires acquisition equipment and data collection techniques somewhat different from those for single-component surveys. Several different valid approaches exist, and the selection of a specific approach depends on geophysical and geological objectives, environmental considerations, and cost. In a common 3-component seismic configuration, either one vertical and two horizontal geophone components are deployed as three coincident lines of single component geophones, or else one spread of 3-component geophones is laid. The approaches for determining 3-component source and receiver array lengths, group intervals, and source strengths, for example, have much in common with parameter selection for a conventional 2-D CDP survey. Source and receiver arrays are designed and implemented in a fashion similar to those used in conventional single component surveys. Likewise, data acquisition typically proceeds using standard 2-D CDP data gathering techniques that have been described in the preceding section.

Obviously, during the course of a 2-D 3-component survey, three times more seismic data are gathered than during a conventional 2-D single-component survey. The additional effort in the field and the data processing laboratory are fortunately justified, since the amount of information at hand for interpretation is significantly greater than the information content of a single component profile, and the field acquisition effort is not necessarily three times as great. Currently the significance of these 3-component data is just beginning to be fully understood. Three-component data contain information about

subsurface anisotropy, formation dips, and other properties of the rocks that affect the propagation of elastic waves that pass through them. In addition, these data can improve the signal to noise ratio and resolution of the conventional P-wave reflection images, since they contain the horizontal particle motion information of the elastic compressional wave train that is normally invisible in the conventional single (vertical) component recordings. Without question, the successful estimation of subsurface rock properties using surface seismic recording will require the acquisition, analysis and interpretation of a 3-component seismic data set. Three-component recording is necessary to record the complete wave field.

1.3 Use of 3-component recording in the seismic exploration industry

The applications of S-wave technology have led the exploration geophysicist to multicomponent recording, including use of both multicomponent sources and receivers. A great deal of interest in multicomponent studies emerged in the early to mid 1950s. Many of these studies were directed at obtaining a more complete understanding of the propagation of seismic body waves, as well as of the near-surface ground roll.

One of the primary motivations of those kind of work was to determine whether S-waves with SH polarisation could be more useful than conventional P-waves. Significant anomalies associated with under-saturation have been discovered using the ratio of the velocity of P-waves to the velocity of S-waves. This proved to be useful to the search for hydrocarbons in stratigraphic traps - oil plays which grew to prominence in the later 1960s and early 1970s. The P/S ratio was also recognised as a possible indicator of lithology and, perhaps, of porosity variation.

The second motive was that since S-wave velocities were significantly lower than P-wave velocities, while the frequencies were expected to be comparable, the wavelengths would be much smaller; hence resolution was expected to be considerably better. After years of experiment and discussion, it has been found, however, that attenuation of higher frequencies limits the useful wavelengths of S-waves to roughly the same as those of P-waves, while the frequency bandwidth is limited to almost one-half. Hence no advantage

was seen in S-wave recording over conventional P-wave recording, from the point of view of better resolution.

The third reason comes from the observation that anisotropy in S-wave velocity is an order of magnitude greater than that observed for P-wave velocities in the shallow shale section. Recently 3-component surveys have led to detection of anisotropy and its association with fracture parameters, including the presence of fracturing in the subsurface, orientation of fractures, and estimation of fracture intensity. The development of impulsive S-wave sources permits acquisition of P-wave and two polarizations of S-wave data with one pass of the sources over the line. This single-source implementation reduces some of the expense in using both P- and S-wave vibrators. The use of impulsive sources seems to be less damaging to the surface than large S-wave vibroseis units, and may thus be easier (and less costly) to permit. It also decreases the acquisition and permitting costs, along with the added benefit of fracture estimation.

In Chapter 6 a new 3-component P-wave surface-to-surface reflection filtering method 3CFH is proposed. This filter can extract the maximum P-wave energy from 3-component data recorded in a conventional CDP format. Synthetic examples demonstrate the effectiveness of the filter in boosting P-wave horizontal and dipping reflection amplitudes.

1.4 Possibilities for new acquisition geometry

The conventional multicomponent seismic survey is usually conducted by placing a number of 3-component geophones along a profile line. After a shot is fired, the whole array is successively moved or 'rolled' forward. This is the most widely used multicomponent seismic data acquisition technique. By using CDP techniques to suppress multiples and random noise, we can finally get an S-wave stacked section, as described above. However the information from the entire vector wavefield is much more than that from single vertical component recordings. Simply to copy the conventional P-wave acquisition geometry and processing procedures may lead to the loss of the additional information such as subsurface anisotropy, formation dips, and other properties of the rocks that affect the propagation of elastic waves that pass through them. Multiple source-to-geophone ray paths, as in multifold CDP recording, are usually required to extract

structural information from P-wave travel times, whereas the anisotropic information in S-waves is usually contained in the 3-D behaviour of the waveforms, which in principle can be obtained from a small number of 3-component recordings. This difference in quality and kind of information suggests that different recording configurations are desirable (Crampin and Lovell, 1991). We can divide the desired information from multicomponent seismic data into two types, wave *travel times* to image subsurface geological structure and *waveforms* to derive polarizations, S-wave splitting, and so on, caused by the anisotropy, crack or stress orientations. To extract more information about the entire vector wavefield, we introduce in Chapters 2 and 3 a new near-zero-offset acquisition array 'RAZOR' for collecting seismic data, specifically designed as an ancillary tool to onshore crustal seismic reflection surveys. As the first research phase, we initially discuss how to image subsurface structure using the P-wave travel times from the new recording configuration.

1.5 Vibroseis *versus* impulsive sources

Explosives are the most widely used impulsive energy source onshore. In operations on land, the explosive charges are placed in shot-holes drilled to depths of 10 to 100 m by a drilling rig. With an impulsive source such as an explosion, which is over in a few milliseconds, the peak energy is high enough to provide energy to record good reflections from deep interfaces. However much of the energy from impulsive sources is wasted in frequency components that are outside the band of frequencies contained in the received wavelets reflected from depth.

Vibroseis, unlike dynamite, is non-destructive, due to its limited peak force. It has been widely used in densely populated area by working along public highways. The servo-hydraulic vibrator is an electro-mechanical device which vibrates the surface at selected frequencies. The energy injected into the earth from the vibrator source consists of many cycles of quasi-sinusoidal waves that are slowly changed in frequency over a period of time called the sweep time. The vibrator source has gained much acceptance because of its unique advantages, as listed below (Pritchett 1990):

- (1) We can select the frequency band that is most favourable for a high signal to noise ratio.
- (2) We can measure the effective upper frequency limit in the field.
- (3) We can reverse the polarity of the signal injected into the earth.
- (4) We can discriminate effectively against many kinds of background noise.
- (5) Vibrators are versatile sources. With vibrators it is practical to use multiple units, to vibrate each unit at a number of surface locations, and to sum the recorded results to obtain a composited record.
- (6) Vibrators can operate on paved roads in densely populated areas.

1.6 The standard industry vibroseis recording and processing method

The conventional vibroseis technique usually uses a swept-frequency sinusoid lasting typically 14-28 s, during which the frequency changes linearly with time from a low frequency to a high frequency, or from a high frequency to a low frequency, while maintaining a constant amplitude. The sweep signal is usually simultaneously generated by several vibrator units, which are controlled by radio signals transmitted from the recording truck. The spacing of the vibrator units and their move-up between sweeps determines a source pattern which can be designed to attenuate the surface waves which originate from the vibrators. The number of elements in the source array is given by the number of vibrators used multiplied by the number of sweeps recorded at each vibrator point, and the spacing is determined by the distance between the vibrators and their move-up between each sweep. By using a repeatable source such as vibrator, we can easily employ large source arrays, which would be too costly to drill if we were using dynamite.

In the conventional processing stage for vibroseis data it is simple to sum all the individual records which are recorded at or around the same vibrator point. In addition to attenuating surface waves, this process will also increase the signal level with respect to random noise. To compress the signal to a relatively narrow wavelet or pulse, cross-correlation of geophone output with the pilot sweep signal is conducted. The process of cross-correlation involves cross-multiplying all elements of the two arrays and summing all the products to give the first sample of the output correlogram. The sweep array is then shifted down one sample and the process repeated to give the next sample, and so on.

Once they have been cross-correlated, vibroseis data can be processed in much the same manner as data recorded using impulsive sources. But some care is needed when determining the parameters used in deconvolution, since the cross-correlated vibroseis data are not minimum phase in practice, which therefore violates one of the assumptions behind deconvolution (Kirk 1981).

The recorded geophone output from any source is normally subject to phase changes caused by the recording instrument filters. With vibroseis data it is a simple matter to avoid the distortion of wavelet shape and timing caused by these phase changes, since the cross-correlation process measures the difference in phase between the data traces and the pilot sweep which is passed through the same filters as the recorded data.

For economic reasons, a great deal of vibroseis data processing is accomplished by the field recording instruments. The processes performed in this way include noise suppression or rejection techniques, summation, and cross-correlation with the pilot sweep. All of these processes can be incorporated into real time systems.

1.7 The problem of sidelobes

For each reflection coefficient in the earth response we can substitute a wavelet which is the autocorrelogram of the sweep modified in phase and amplitude by the transmission characteristics of the two-way path to the reflector. The autocorrelogram of the sweep is often referred to as the Klauder wavelet, and its characteristics are determined by the basic specifications of the sweep itself. Since an autocorrelogram is always zero phase, the wavelet is symmetrical about the central peak. A sweep with a higher mid-frequency will give a narrower Klauder wavelet and finer resolution on the seismic section. The larger the bandwidth of the sweep, the closer will the wavelet approximate to a spike. The sidelobes of the wavelet show a high-frequency ripple superimposed on a low-frequency wave.

Vibroseis data recorded at short source-receiver offsets can be swamped by direct waves from the source. After correlation, we usually think of the central peak and adjacent half-cycles as being so large in comparison to the amplitude of the later sidelobes that the sidelobes can be ignored. However the amplitude decay of the sidelobes as a function of

time for the very strong first arrivals is often much slower than the rate at which reflection amplitudes diminish in same the time period. The result is that the signal to noise ratio, where primary reflections are the signal and correlation sidelobes the noise, decreases with time, and later events are overwhelmed, leading to low seismic resolution on the vibroseis correlogram.

Sidelobes can be considered to be undesired signal-generated noise since their form is signal-dependent. Naturally, we want the sidelobes to be as small as possible so as not to obscure nearly coincident and/or weaker signals. Near to the correlation central peak, the amplitudes of first few sidelobes are large enough to interfere with the correlation peaks of desired events arriving at the same times as the unwanted sidelobes. The task of resolving the interfering events is usually carried out by spiking deconvolution, phase shifting and/or spectral whitening techniques (e.g. Yilmaz 1987), which are not the subject of this dissertation.

At late reflection arrival times, well past the arrival of the first couple of sidelobes from a strong event such as the first break, the decay envelope of the sidelobes flattens out, so that the far outlying side-lobes can still be as high in amplitude as the major lobes of desired reflection events. The result is that the signal to noise ratio, where the correlation peaks of primary reflections are the signal and correlation sidelobes are the noise, decreases with time, and later weak reflection events can be overwhelmed. The problem is one of *correlation noise*.

Correlation noise suppression has been discussed since the introduction of correlation. Klauder *et al.* (1960) described measures to reduce sidelobe levels by frequency weighting, and the sweep tapering technique has become routine for correlation noise suppression since the early 1960s. A considerable reduction of the sidelobe noise can be achieved by tapering the amplitude spectrum of the vibrator sweep, at the expense of loss of energy put into the ground (Edelmann 1966). During the 1970s, the Combisweep technique was introduced by Werner and Krey (1979), and was discussed as a correlation noise suppression technique by Edelmann and Werner (1982). This technique starts from the idea that neither a nonlinear sweep nor amplitude shaping can cope with the coupling and attenuating effects of the ground, which influence the vibroseis signal. The

Combisweep technique yields an improved recorded signal by strengthening certain spectral components which would otherwise remain below the noise level.

At around the same time as the developments described above were taking place, coding techniques to suppress correlation noise were introduced from communication theory into vibroseis exploration. One of them is the pseudo-random coding technique developed by Cunningham (1979). This encoding, however, makes great demands upon the transient response of the vibrator. Another coding technique was described by Bernhardt and Peacock (1978), designed to suppress far-correlation noise. However, near-correlation noise is only moderately reduced.

All the approaches mentioned above attack the correlation noise problem either at source (by designing better sweeps), or during *post-correlation* processing.

1.8 Possibilities for new vibroseis data processing

In Chapter 4 and 5 we propose two new filtering approaches, SFU and DOLS. They are the first attempts we are aware of to remove the direct wave sweep in the *pre-correlation* domain, resulting in the correlation noise being well suppressed, but without attenuating signals. The SFU filter described in Chapter 4 is a combination of ‘squeeze and unsqueeze’ transformation, with application of an optimum least-squares filter or linear recursive notch filter. Chapter 5 presents another new filtering approach, DOLS, based on the optimum least-square filtering algorithm. The DOLS filter also operates in the pre-correlation domain, but without any transformation calculation, so that it takes much less CPU-time than SFU filtering. These two chapters present the description of the two new filters and discussions of the algorithm performance through use of synthetic modelling data and field data examples.

1.9 Summary of new methods and their potential application

Table 1-1 summarises in chapter order the new methods discussed above. The table shows whether each method in turn is applicable to a novel or conventional source and receiver geometry, to single or 3-component receiver data, or to a particular type of source.

Table 1-1. Summary of new methods developed in this dissertation

<i>Chapter</i>	<i>New Method</i>	<i>Number of components</i>	<i>Ensemble Geometry</i>	<i>Source applicability</i>	<i>Data examples</i>
2	RAZOR geometry	1 or 3	RAZOR	Any	Synthetic
3	RAZOR imaging	1	RAZOR	Any	Synthetic
4	SFU filter	1	Single traces	Uncorrelated vibroseis	Synthetic and real
5	DOLS filter	1	Single traces	Uncorrelated vibroseis	Synthetic and real
6	3CFH filter	3	Conventional CDP	Any	Synthetic
7	Various minor new algorithms	1	Conventional CDP	Correlated vibroseis	Kola crustal CDP line

In Chapter 7 we present the results of a conventional P-wave processing sequence applied to the northernmost portion of the vertical component of the deep crustal CDP vibroseis reflection line acquired through the Kola superdeep well SG-3 in 1992 (Smythe *et al.*, 1994). The complexities of this dataset required that a number of new minor sorting and correction algorithms had be written to bring the data into a form for processing. Unfortunately this left no time for application to the data of any of the methods described in Chapters 4-6, and a final thorough test of these methods on the Kola data will have to await future work.

Chapter 2

New near-zero-offset methods based on the RAZOR array

2.1 Introduction

The conventional P-wave seismic survey is usually conducted by placing a number of vertical geophones along a profile line. After a shot is fired, the whole array is successively moved forward. This is the most widely used seismic data acquisition technique. The multi-fold CMP (common mid-point) technique is used to suppress multiples and random noise. In this chapter we will introduce a new approach to collecting seismic data, using a special areal RAZOR (Roll Along Zero Offset Receiver) array, specifically designed as an ancillary survey method for deep crustal reflection surveys.

For any new seismic approach proposed, numerical experiments are necessary and should be one of the first steps in the preliminary research phase. However we face a serious problem of how to carry out these numerical experiments in practice. As the new proposed seismic method is based on a 2-dimensional areal array the data are, in effect, 3-D. We have to find a suitable way to simulate the RAZOR array without recourse to a 3-D reflection modelling program. Ma (1990) conducted some preliminary numerical experiments of the new near-zero-offset reflection method using the SEIS-83 system. However this simulation procedure is rather time-expensive and inflexible, and it is therefore impossible for the SEIS-83 system to simulate any complex (i.e. realistic) 3-D geological model. In this chapter we propose an alternative modelling environment for the numerical experiments on the new near-zero-offset method.

2.2 RAZOR array design

The new shot-receiver array was designed by D. K. Smythe for a piggy-back experiment proposed to accompany the BIRPS WISPA line in 1988. This section is based on his note (reproduced here as Appendix A) and X. Q. Ma's Ph.D thesis dissertation (Ma, 1990). The array pattern is shown in Figure 2-1, with the shot point at the centre. Three-component

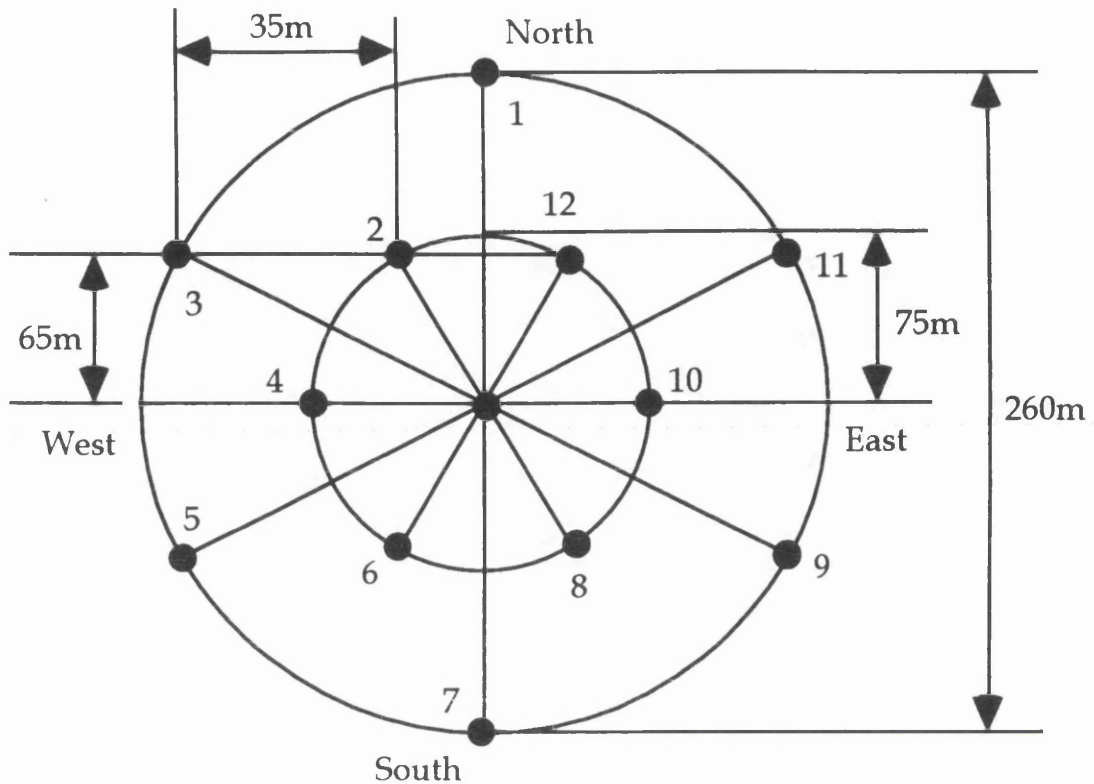


Figure 1

Fig. 2-1. Field areal RAZOR array pattern for seismic survey.

geophones lie on both concentric circles, of radii 75 and 130 m. The shot point spacing is 75 m. The determination of the array dimension is based on several factors. They are described as follows:

(1) For a maximum phase shift of half a wavelength, the radius of the array for events of interest should be of the order 200-300 m. Let us consider a normal-incidence ray leaving a reflector, which dips at an angle θ in the lower crust (Fig. 2-2). If the P-wave velocity of the crust is V , the horizontal slowness p is:

$$p = \sin \theta / V$$

The ray emerges at an angle of incidence α , corresponding to a planar wavefront dipping at the same α . We require a suitable dimension of x , the diameter of the array, over which

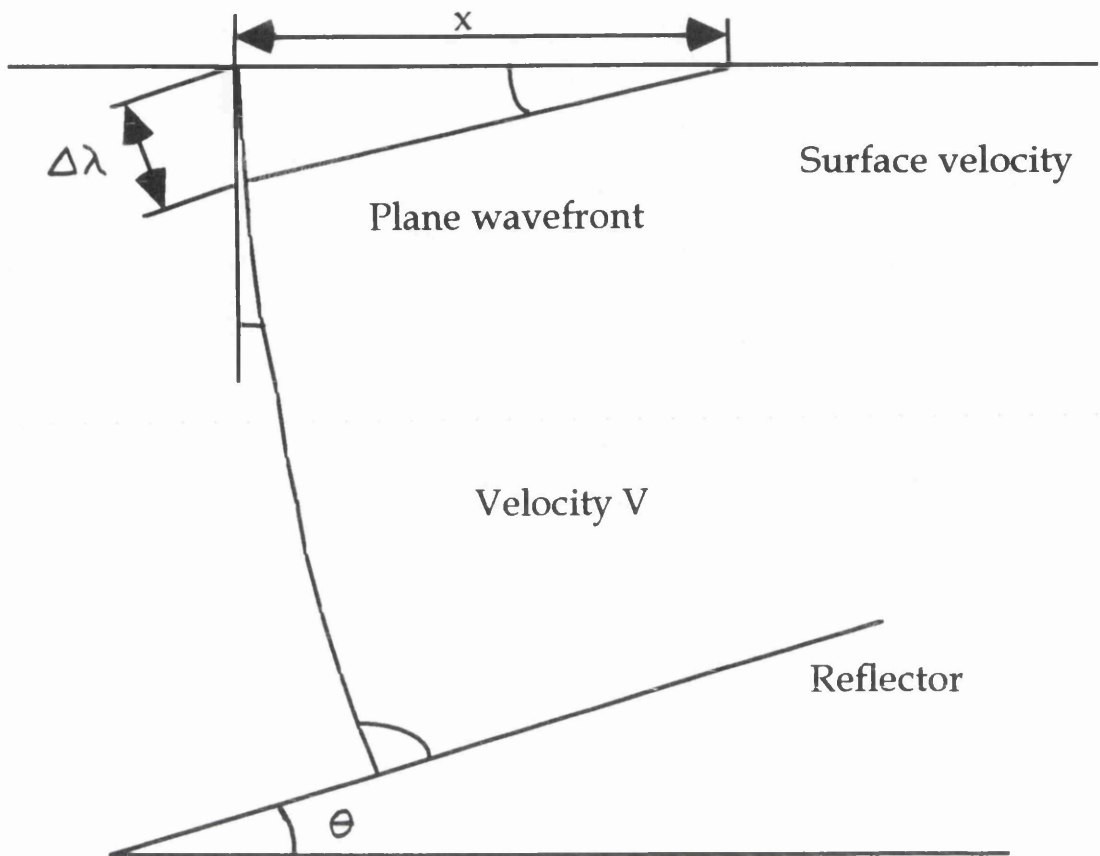


Fig. 2-2. Geometry of a normal-incidence ray from a crustal reflector dipping at q . Plane wavefront is incident across an array of receivers of horizontal dimension x .

the phase difference of a planar arrival will not differ by more than half a wavelength. The path difference across the array is:

$$\Delta\lambda = V_0\Delta t$$

where V_0 is the velocity at the surface, and Δt is the time delay. Snell's Law says that the quantity $\sin \theta / V$, which is the inverse of the horizontal phase velocity, is constant along any raypath in a horizontally stratified medium. Thus the same horizontal slowness p at depth also applies at the surface. We get:

$$p = \sin \alpha / V_0 = \Delta\lambda / (xV_0)$$

Substituting and re-arranging, we get:

$$x = \frac{V\Delta t}{\sin \theta}$$

For a half-cycle of a 25 Hz wavelet, $\Delta t = 40/2 = 20$ ms. Taking a lower crustal velocity of $V = 6.5$ km/s, and a typical dip of an event of 30° , we get:

$$x = \frac{20 \times 6.5}{\sin 30^\circ} = 260 \quad \text{m}$$

- (2) The station spacing of 75 m is big enough so that different near surface ground conditions will be sampled. Rogue stations can be identified by comparison with other stations, and rejected from the beam-steered stack.
- (3) The 75 m radius of the inner circle is large enough so that the stations will not interfere with the firing of the shots; there is no station at the shot point.
- (4) Summation of 12 stations produces a respectable signal-to-noise increase of 3.5, after polarisation filtering of each 3-component station separately. This provides near zero-offset (coincident source-receiver) 3-component 12-fold traces.
- (5) During shooting, only 6 of the 12 stations have to be shifted between each shot point, two stations (9, 11; see Figure 2-1) are used 4 times, another two stations (8,12) are used 3 times, three stations (2, 6, 10) are used twice and only 3 stations (1,4,7) are used once. thus the preparation of sites for planting the 3-component geophones is minimised.
- (6) This particular array allows slant-stack processing to be carried out along a straight line of a varied azimuth through the shot point, after the 12 stations are projected on to it. The transformed-sections can be 'turned' to maximise the amplitude of reflections from any direction, both in-line and cross-line, and supply 3-dimensional information.

- (7) Geophones with small offsets to a shot point will record good shear waves with near-vertical incidence.

2.3 Review of the synthetic modelling of the RAZOR array using SEIS-83

It is prudent to carry out 3-component modelling in 3-D for the analysis of vector waves with the RAZOR array, before going ahead with actual field tests of the new method. In this chapter only vertical component modelling is discussed, as the first phase of the numerical experiments.

Ma (1990) applied the modelling package SEIS-83 to obtain 3-D RAZOR synthetic seismograms. The SEIS-83 package was designed by Vlatislav Cerveny and Ivan Psencik of Charles University, Czechoslovakia, for the computation of rays arriving at a system of receivers distributed regularly or irregularly along the earth's surface. The generation of waves is semi-automatically determined. Optionally, amplitudes and phase shifts may be evaluated. All these quantities are stored and may be optionally plotted or used for the computation of synthetic seismograms. However the SEIS-83 package can only deal with 2-dimensional models. To obtain synthetic seismograms of the areal RAZOR array in a 3-D model, Ma (1990) had to decompose a simple 3-D model with only one dipping flat layer into six 2-D models i.e. six short profile lines. Each line has two stations on both sides of a shot point, and they are rotated relative to each other by successive intervals of 30° . Figure 2-3 (After Ma 1990) shows the simple dipping plane associated with different profile lines. In this figure, for the profile 1 lying in a north-south direction (Fig. 2-3a), the vertical distance h_z between the line and the east-dipping plane is different from its normal distance h ; Figure 2-3b is the section corresponding to line 1. In the east-west direction, the line and section are shown in Figures 2-3c and 2-3d respectively, with the true dip Ψ of the reflector. For the more general line and section shown in in Figures 2-3e and 2-3f respectively, the geometry is complicated. The dip component has to be calculated in the incident plane of seismic waves according to the vertical distance h_x of the line from a shot point at the surface to the reflector, and the normal distance h . Therefore, the synthetic data for the 3-D model is generated by running the SEIS-83 program four times based on the different input data, while keeping the source constant.

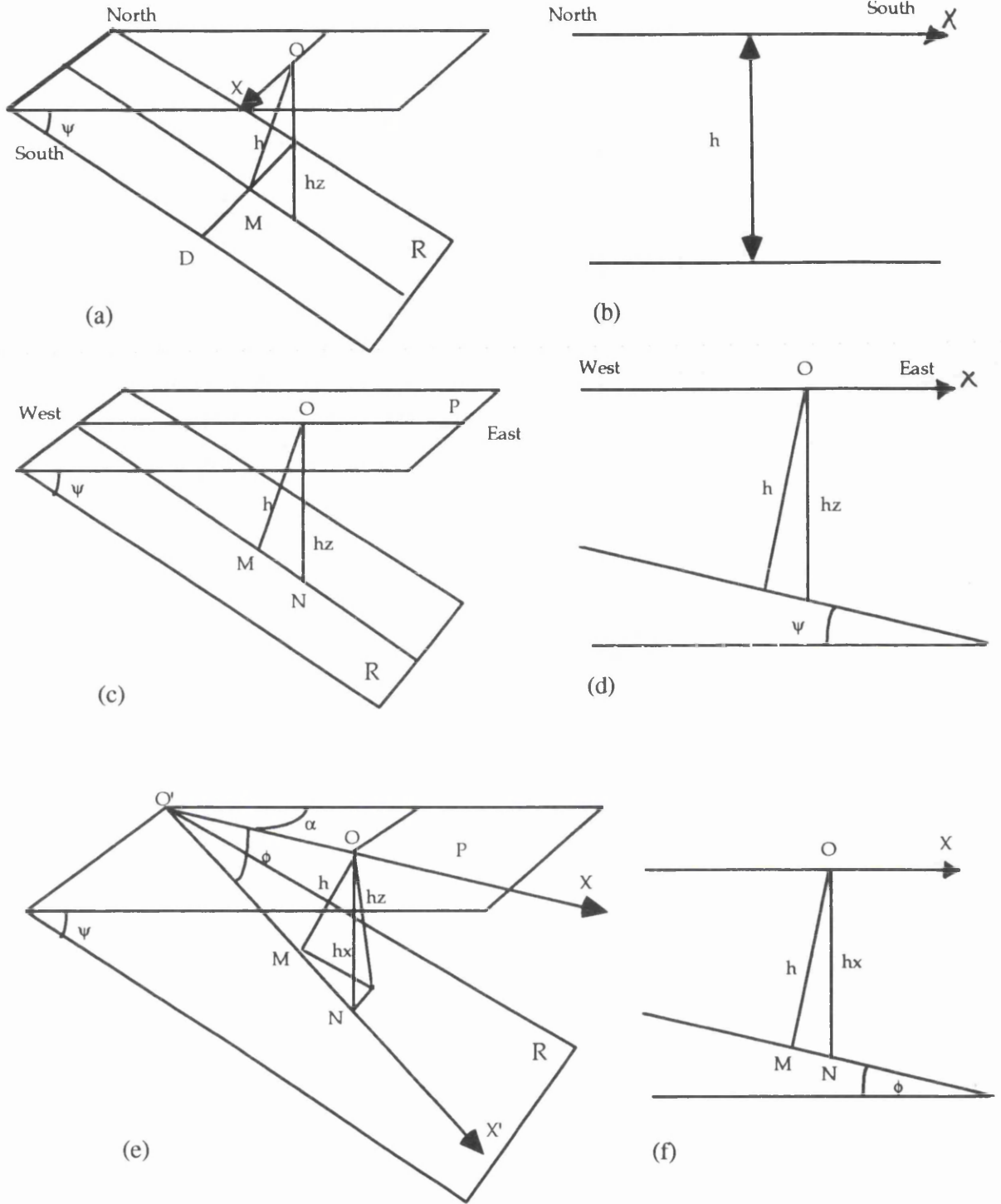


Fig. 2-3. The geometry of a dipping reflector related to a surface line of different azimuths and the equivalent 2-D models constructed from it. (a), (c) and (e) are 3-D models, (b) (d) and (f) are equivalent 2-D models constructed for input to the SEIS-83 ray tracing system (After Ma 1990).

It is obvious that we can not carry out a similar decomposition when the 3-D model becomes yet a little more complicated, for instance, if the dipping layer is not flat. It implies that the SEIS-83 package cannot accommodate the task of more realistic RAZOR array modelling. So a new simulation environment is necessary for the development of reflection methods based on the areal RAZOR array. In effect, the RAZOR array method is a 3-D acquisition method, albeit with a localised and limited array pattern.

2.4 Interaction with the Sierra seismic modelling environment

Sierra products are one of the industry-standard geophysical processing and geological interpretation systems in the oil and gas exploration field. The Sierra environment combines geophysical and geology technology with interactive window-based software engineering. It provide several benefits:

- (1) A general mapping and geological modelling capability for simulation, calculation and manipulation of geological information in three dimensions.
- (2) 2-D and 3-D raytracing modelling is included, for acquisition, planning, processing parameter estimation, depth-point smear analysis, binning analysis, simulation of observed data, and testing of interpretations.

In the numerical experiments for the new near-zero-offset reflection method, only three of the Sierra subsystems are used; MIMIC for geological model building and editing in 2-D or 3-D, QUIKSHOT for 2-D or 3-D P-wave and S-wave raytracing modelling, and SierraSEIS for batch seismic data processing.

2.5 Geological modelling by MIMIC

Sierra's MIMIC package is a tool for easy and efficient building of digital models of complex, three-dimensional geological structures. It provide some functions including simulation, calculation, storage, retrieval, manipulation, and display of geological information; the emphasis is on depth, velocity, and traveltime. In addition, MIMIC offers a generalized coordinate system and choice of spatial units. Display options include cross-sections, contour maps, isopach/isotime maps, and 3-D perspective views using elevation

lines or contour lines. Here we apply MIMIC to manipulate all the test models used later in this dissertation. The spatial units are kilometres. The procedure for MIMIC application is divided into three steps:

- Creating and editing contour maps in depth.
- Compiling these interfaces into three or two dimensional geophysical models.
- Examining and verifying maps and models using colour graphics displays.

Since the areal RAZOR array is deployed in two dimensions on earth's surface, the 3-D MIMIC geological modelling version is used in the following sections. As this is the first phase of the numerical experiments, and since one of the initial objectives of this experiment is to investigate the new methods for seismic reflection exploration, we construct all the models with a homogeneously isotropic medium, even though the variation of velocities can be defined both vertically and laterally in MIMIC. Three basic geologic models generated by MIMIC are shown in Figures 2-4, 2-5 and 2-6. As horizon depth can be shifted upon entry into the model to honour a well control point, it is easy to model the faults and pinchout geological structures shown in Figures 2-5 and 2-6, by combining two or three layers together. Construction of these 3-D geological models is one of the major steps prior to seismic raytracing modelling.

2.6 RAZOR array design and raytracing in QUIKSHOT

QUIKSHOT is part of Sierra's QUIK raytracing software, and suitable for generating common shot records from 2-D or 3-D MIMIC geological models of substantial complexity. QUIKSHOT raytracing uses asymptotic ray theory to obtain seismic amplitudes. It models offset-dependent reflection/transmission losses, geometric attenuation, and anelastic attenuation.

The first step is to design the RAZOR in the form of a survey line, because most industry-standard software, like Sierra products, is developed only for such surveys. To accommodate the RAZOR array pattern shown in Figure 2-1, with the shot point at the

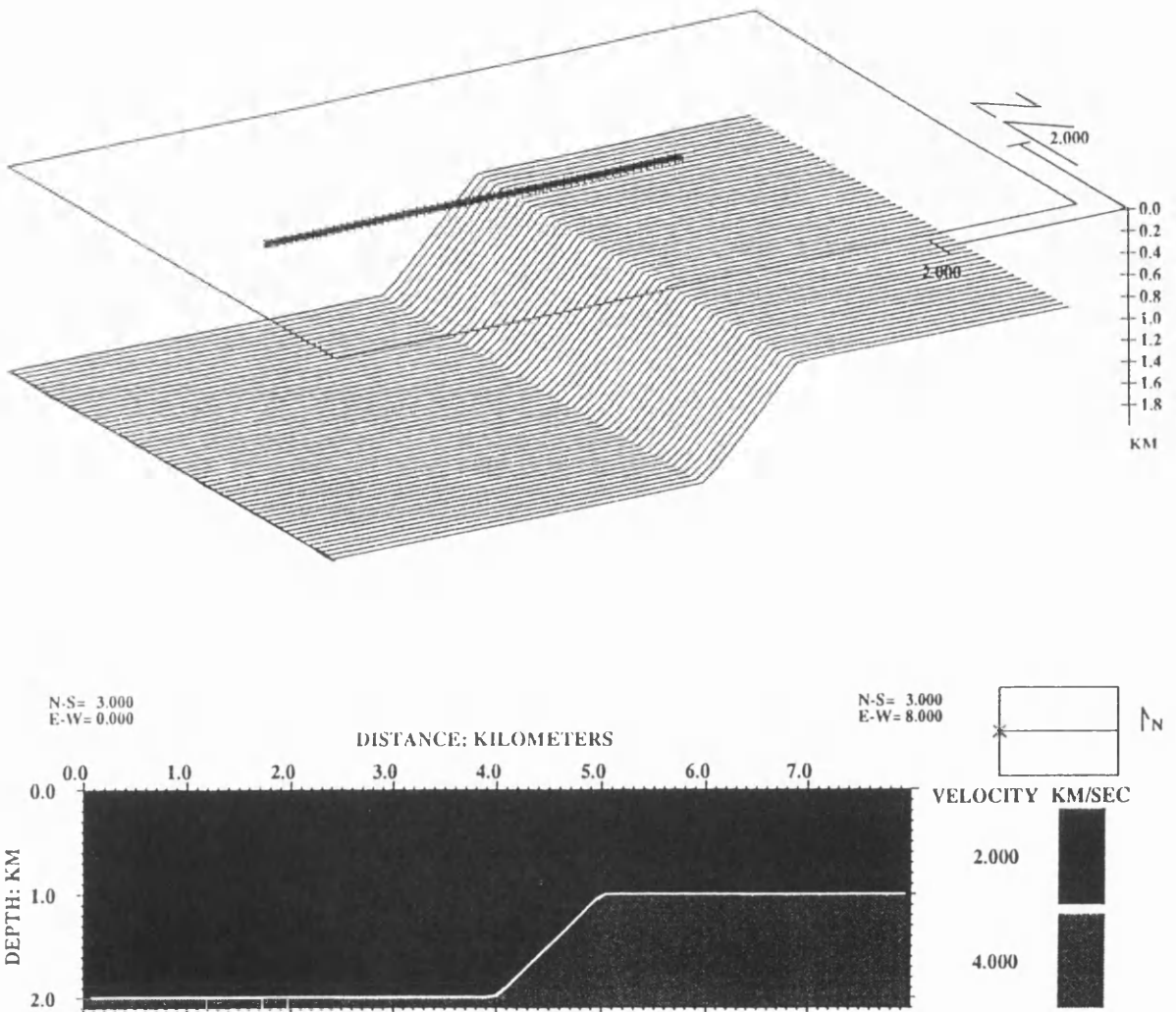


Fig. 2-4. The 3-D fault model calculated by MIMIC for modelling the RAZOR array.

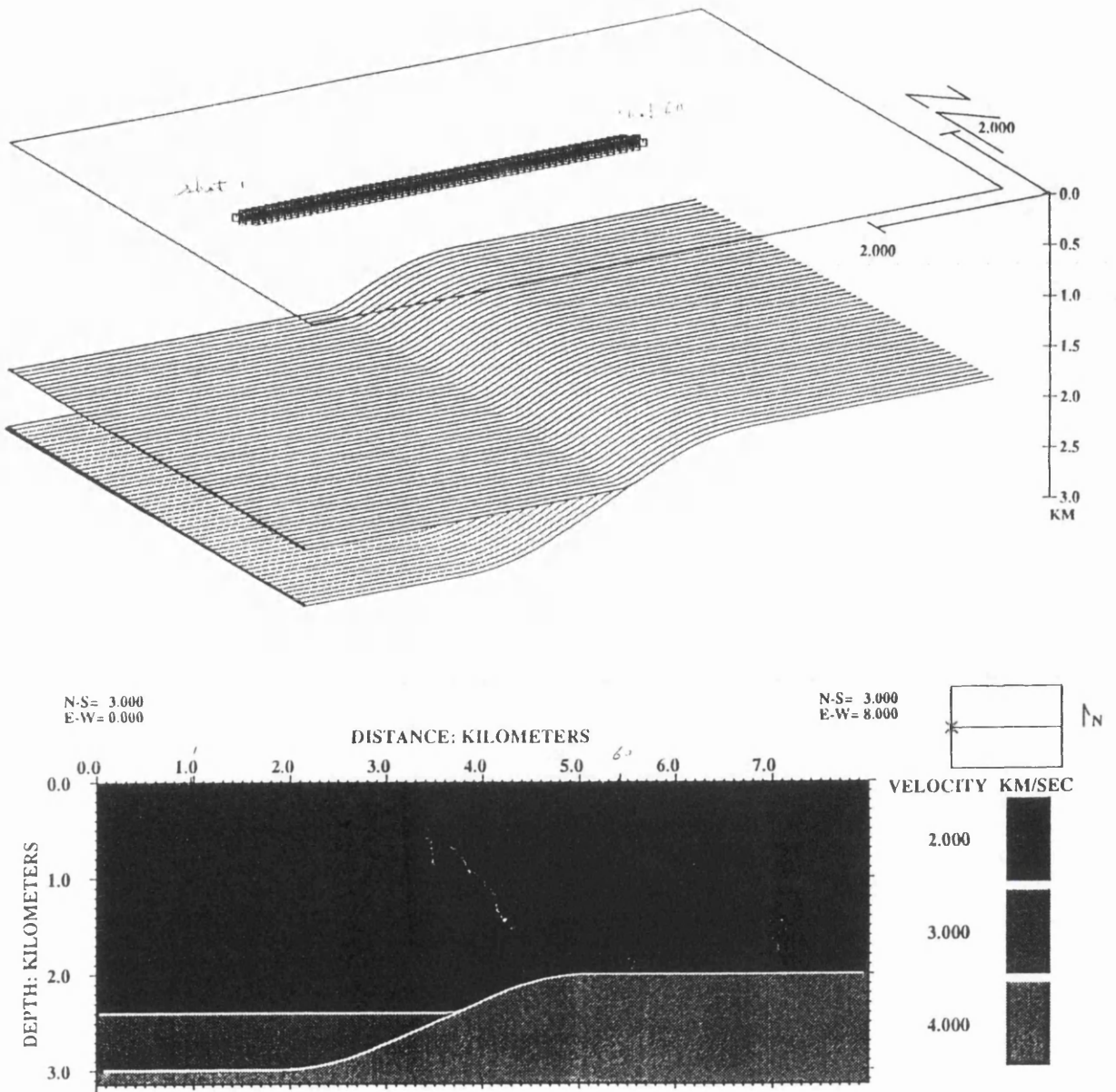


Fig. 2-5. The 3-D pinchout model created by MIMIC.

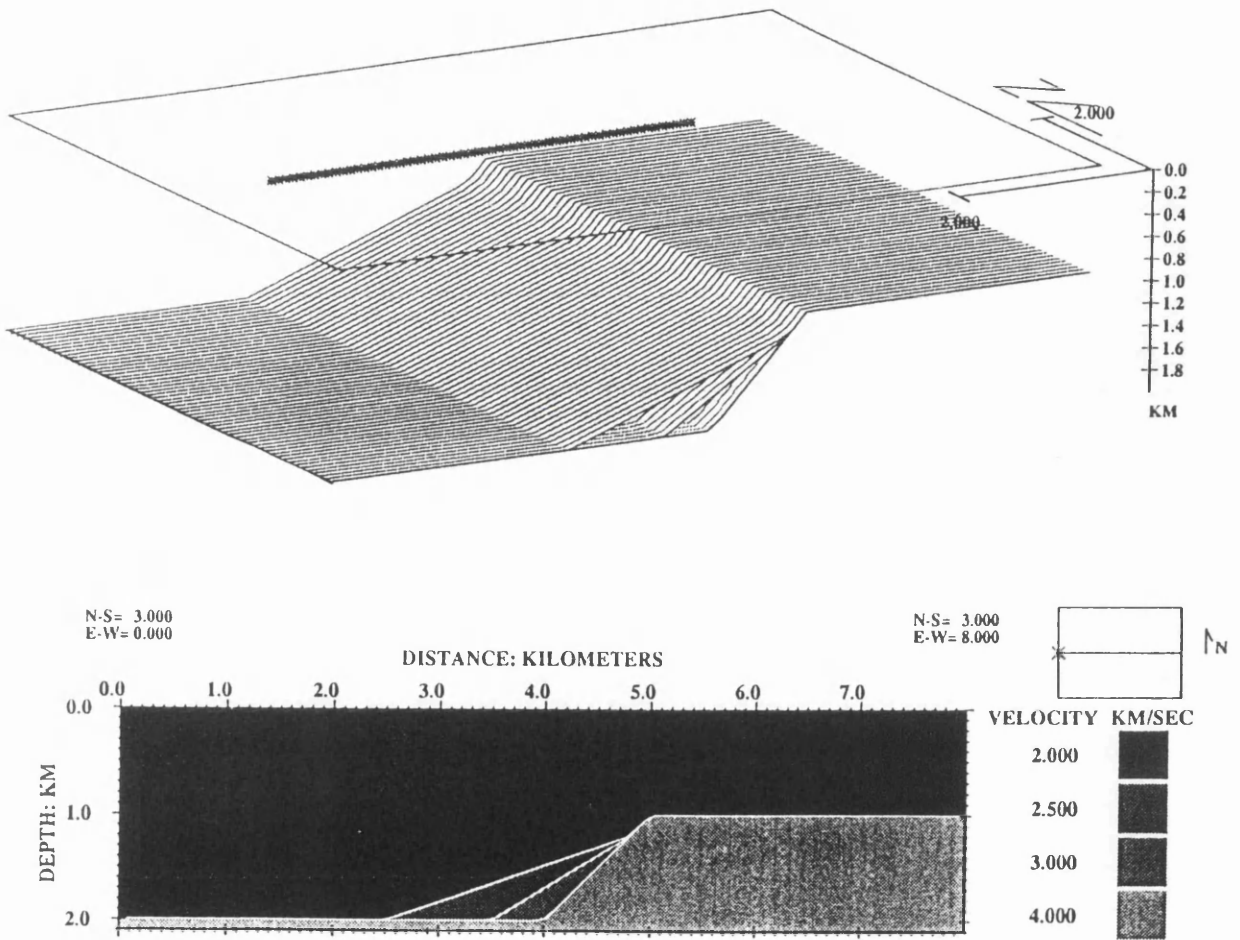


Fig. 2-6. The complex 3-D model for the RAZOR array modelling.

centre, geophones lie on either of two concentric circles of radii 75 and 130 m in the line mode only environment. We have two methods to simulate the areal array. These are described in the next two sections.

2.6.1 Array design in the crooked line mode

A crooked line geometry has been designed for single shot or roll-along modelling. Figure 2-7 shows the RAZOR array rolling along a survey line with a shot point spacing of 75 m, using the definition of the crooked line array. The input 3-D geological model can be generated by MIMIC. It implies that the raytracing of an areal RAZOR array for a complex model is possible using QUIKSHOT. Compared to RAZOR array modelling in the SEIS-83 processing system, modelling by the crooked line mode in QUIKSHOT is much easier and quicker, as it does not require any additional processing to prepare the RAZOR shot gathers.

The output of QUIKSHOT is usually a set of internal disk files, of which the file in 'AMF' format contains the calculated amplitude information, the file in 'PLT' format the raypath plot data, and the file in 'RES' format the travel time information. By using the SLIPR program, the results out from the QUIKSHOT system can be displayed on the screen as spike seismograms or wiggle traces, then transformed into Sierra HOUSE format SEG-Y data (a fixed block length version of SEG-Y), which SierraSEIS batch seismic data processing subsystem can read directly. The synthetic data from the crooked line mode array can be output and saved as one disk file in SEG-Y format for subsequent processing. The advantage of this crooked line mode design is that you need no additional processing steps to sort the RAZOR shotgathers, and all the data traces are stored in one disk file. However the RAZOR array design in this mode takes much longer than that in the second mode, the five-line mode, for a large roll-along survey project with many shots.

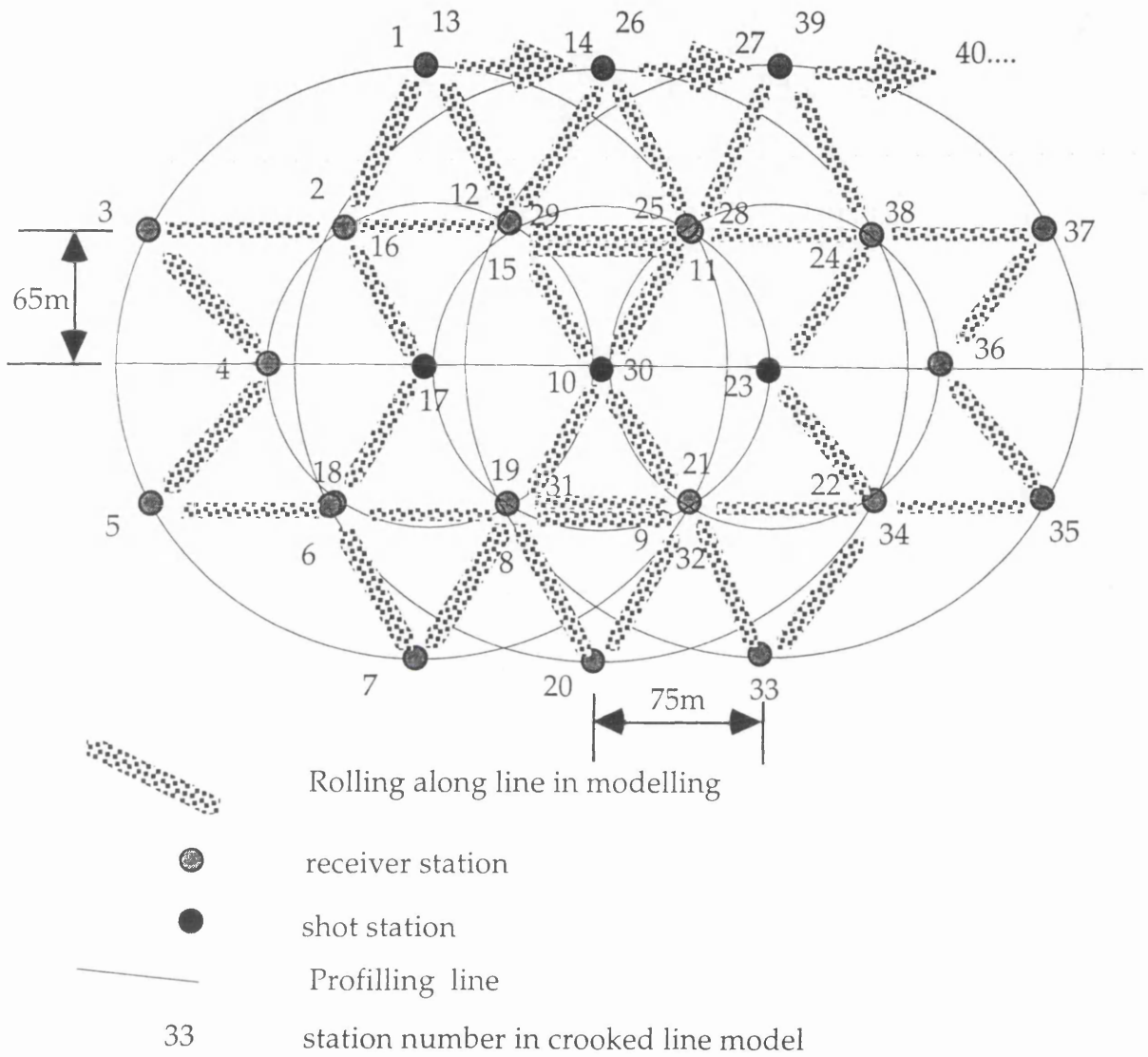


Fig. 2-7. The RAZOR roll-along array using the crooked line mode.

2.6.2 Array design in the five-line mode

For most 2-D modelling along a survey line the roll-along array is necessary to obtain a stacked section. Although the crooked line mode has the advantage of saving the RAZOR shot gather directly into a SEG-Y file without extra processing, it will take a lot of time for the roll-along RAZOR array design. To simplify the RAZOR array modelling in a roll-along survey mode, we propose an alternative, five-line mode to replace the crooked line mode described above. It consists of several processing steps, and therefore is a multi-step processing procedure. The first step is to simulate the roll-along RAZOR array with five separate straight line arrays parallel to the survey line, according to the definition of the field RAZOR array pattern in Figure 2-1. The final layout is shown in Figure 2-8, where 60 shots in total are fired along the main survey line which is at right angles to the strike of the geological structure. The second step is to save the modelling results as five separate separate SEG-Y files, which correspond to each single line array respectively. They are then transformed into ASCII files and sorted out into one shot gather file using a newly developed programme RAZORSORT.F. Compared with the crooked line mode, the five-line mode is much easier and quicker to define a roll-along RAZOR array in the QUIKSHOT subsystem, but it needs more subsequent processing after the QUIKSHOT raytracing.

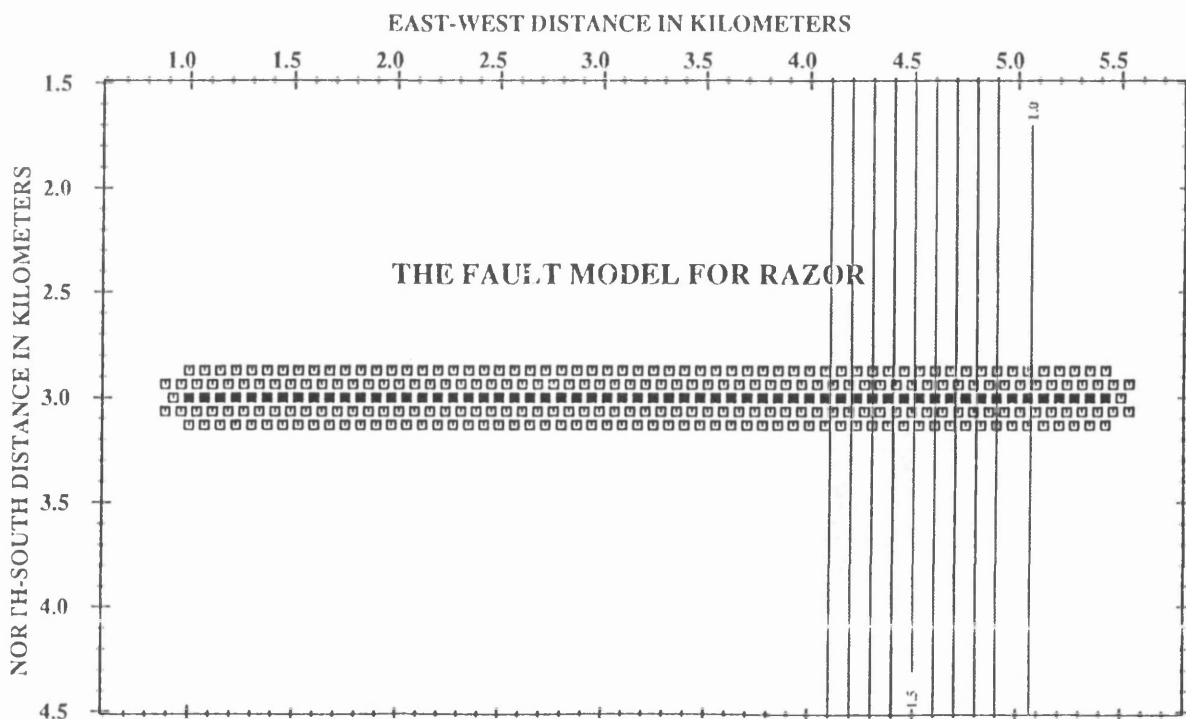


Fig. 2-8. The roll-along RAZOR array using the five-line mode.

2.7 New Fortran-77 programs for RAZOR modelling

Two application programs have been developed in association with the later RAZOR processing steps. These are described below.

2.7.1 Program RAZORSORT.F

In order to apply subsequent processing to the data collected from QUIKSHOT by the five-line mode array, a Fortran-77 program RAZORSORT.F is developed for sorting the RAZOR shot gather. This is an independent module without any direct interface to the Sierra products. It can read the five ASCII data files directly as input, and outputs a shot gather data file in 'QR' format, which is designed to save disk space and allow easy editing in the ASCII domain. All of the subsequent processing programs require this kind of shot gather data file as the input. The trace number is in the same order as defined in Figure 2-1, from trace 1 to trace 12 for each shot. The latest version of RAZORSORT.F handles data with a fixed number of samples per trace of 1000, however, it is easy to modify the definition of the trace sample number in the program if required. No parameters are needed to run the program under the UNIX operating system. Figure 2-9 presents a shot gather from this new program RAZORSORT as an example.

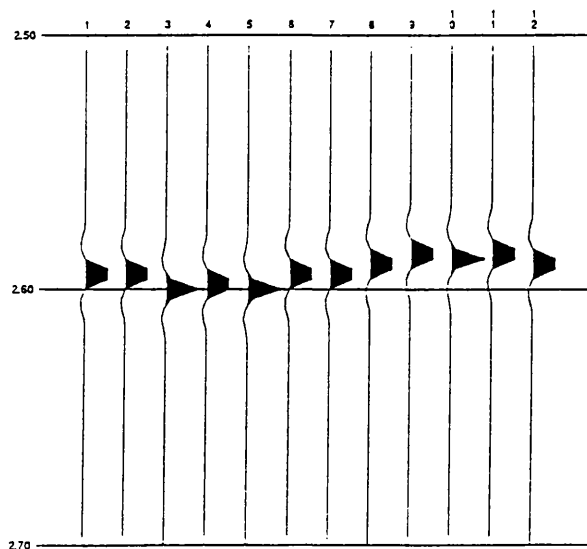


Fig. 2-9. A RAZOR shot gather after sorting by program RAZORSORT.

2.7.2 Program QPLOT.F as a quick display tool

To obtain more useful illustration of the RAZOR array shot gather with only 12 traces, or else display a stacked section, we have developed new display software within the UNIRAS environment. The new display application QPLOT (see also Appendix B) was written to perform multi-purpose plotting quickly on screen, or make hard copy in PostScript format. It uses the popular UNIRAS package as a support system environment.

UNIRAS is a graphics package which is composed of two basic parts, the first being the interactive programs. These provide facilities to draw charts and maps of all kinds. UNIGRAPH is for drawing charts and graphs, while UNIMAP is for contour maps and surface views etc. UNEDIT is for editing of picture. The second main section of UNIRAS is the subroutine libraries which can be called from a user's own program in the normal manner. SEISPAK and GEOPAK are the subroutine libraries for colour display of seismic or geoscience data in 2-D or 3-D, if a colour terminal or colour print device is available.

The newly developed QPLOT makes best use of the available UNIRAS package, including the sublibraries of UNIMAP, UNIGRAPH, SEISPAK, and GEOPAK. As shown in Figure 2-10, the program firstly reads the ASCII data trace by trace into an array X1(I,J) after a data file name and display parameters are specified in the dialog box main- and sub-menus. The user can define almost all the display limits or patterns related to the UNIRAS subroutine library without having to learn any of the details of the packages. When the program is run under UNIX, interactive menus will appear on screen as follows:

```

Main Menu
-----
1: Scaling parameter T= ***
2: Interval of samples= *** ; Colm= ***
3: The time window from : ** to **
4: The colour table from : *** to ***
5: The sheredom= ***
6: Go to sub-menu
-----
% Enter your option to change these parameters (1,2,3,...)

```

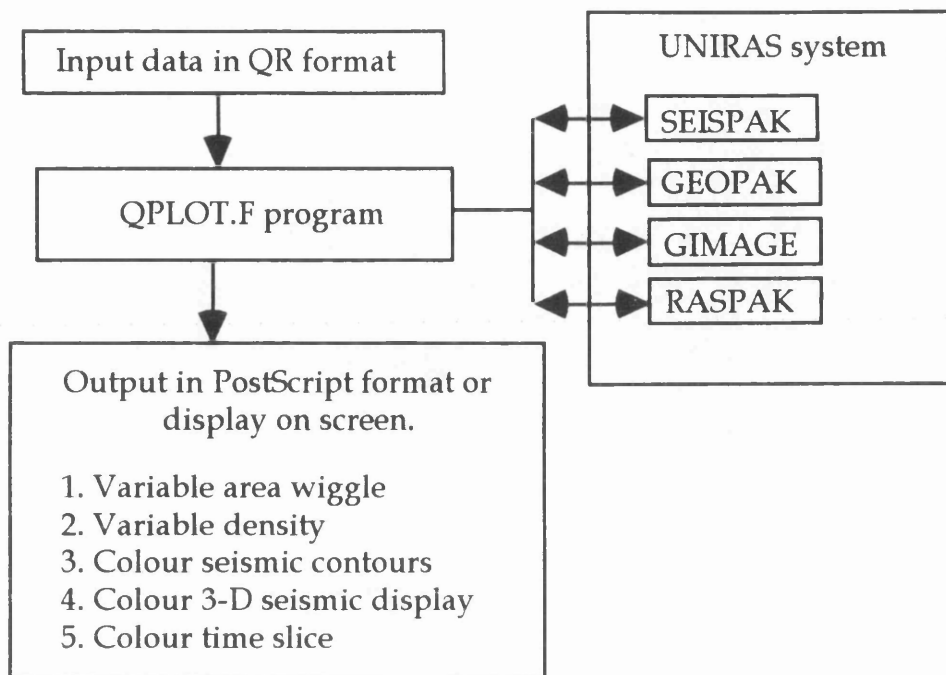


Fig. 2-10. Flow diagram for program QPLOT.

and:

Sub-Menu for Traces

-
- 1: Wiggle variable area plotting
 - 2: Coloured seismic contour plotting
 - 3: Coloured seismic grid plotting
 - 4: Wiggle trace line overlaid on contour plotting
 - 5: Wiggle trace line overlaid on grid plotting
-

% Enter your option please (1 or 2,3,...)

```
Sub-menu for Output
-----
0: Quit
1: To hardcopy by Versatec plotter
2: To re-display with new parameters
3: To input another file
-----
% Enter your option please (0 or 1, 2, 3)
```

The original SEG-Y files output from the QUIKSHOT or SierraSEIS subsystems were reformatted using the MASEGY program (Ma 1990) into ASCII coded decimal data in the 'QR' format. The program QPLOT then enables the user to examine the test results quickly, without the additional complications of batch seismic processing.

Examples of stacked section displays produced by QPLOT are shown in Figure 2-11 (wiggle and variable area mode) and Figure 2-12 (variable density mode).

2.8 Summary and discussion

We have introduced a new approach to collecting seismic data, using a special areal RAZOR (Roll Along Zero Offset Receiver) array, specifically designed as an ancillary survey method for deep crustal reflection surveys. As the new proposed seismic method is based on a 2-dimensional areal array the data are, in effect, 3-D. We have had to find a suitable way to simulate the RAZOR array without recourse to a 3-D reflection modelling program. Ma's (1990) preliminary numerical experiments using the SEIS-83 system proved to be rather time-expensive and inflexible, and thus unable to simulate any complex (i.e. realistic) 3-D geological model. Therefore an alternative modelling environment for the numerical experiments has been developed.

The flow diagram of the modelling is shown in Figure 2-13. In this chapter we propose two array design modes for modelling a RAZOR array survey line. The first is the *crooked line* mode, which is best suited for modelling of a single RAZOR array. Its advantage is that all of the data traces are sorted in the same order as the RAZOR shot gather directly. However the RAZOR array design in the crooked line mode usually takes a lot of effort if a large (multi-shot) roll-along survey project is to be modelled or processed.

Filename =f-roll60-70%-d

Shots= 60 :Noise=70 :a=27 :Date= 10/2/1992

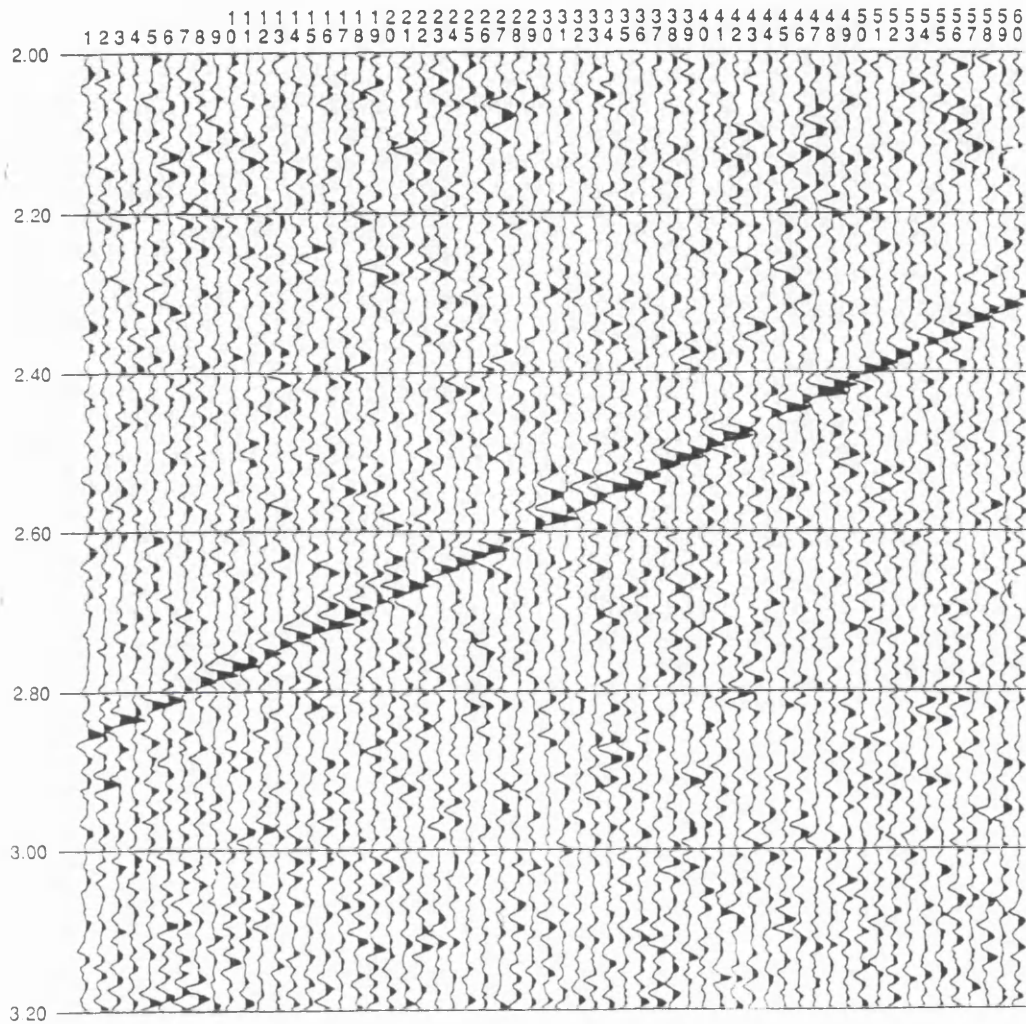


Fig. 2-11. The RAZOR stacked section for a dipping reflector plotted by program QPLOT in the variable area and wiggle mode.

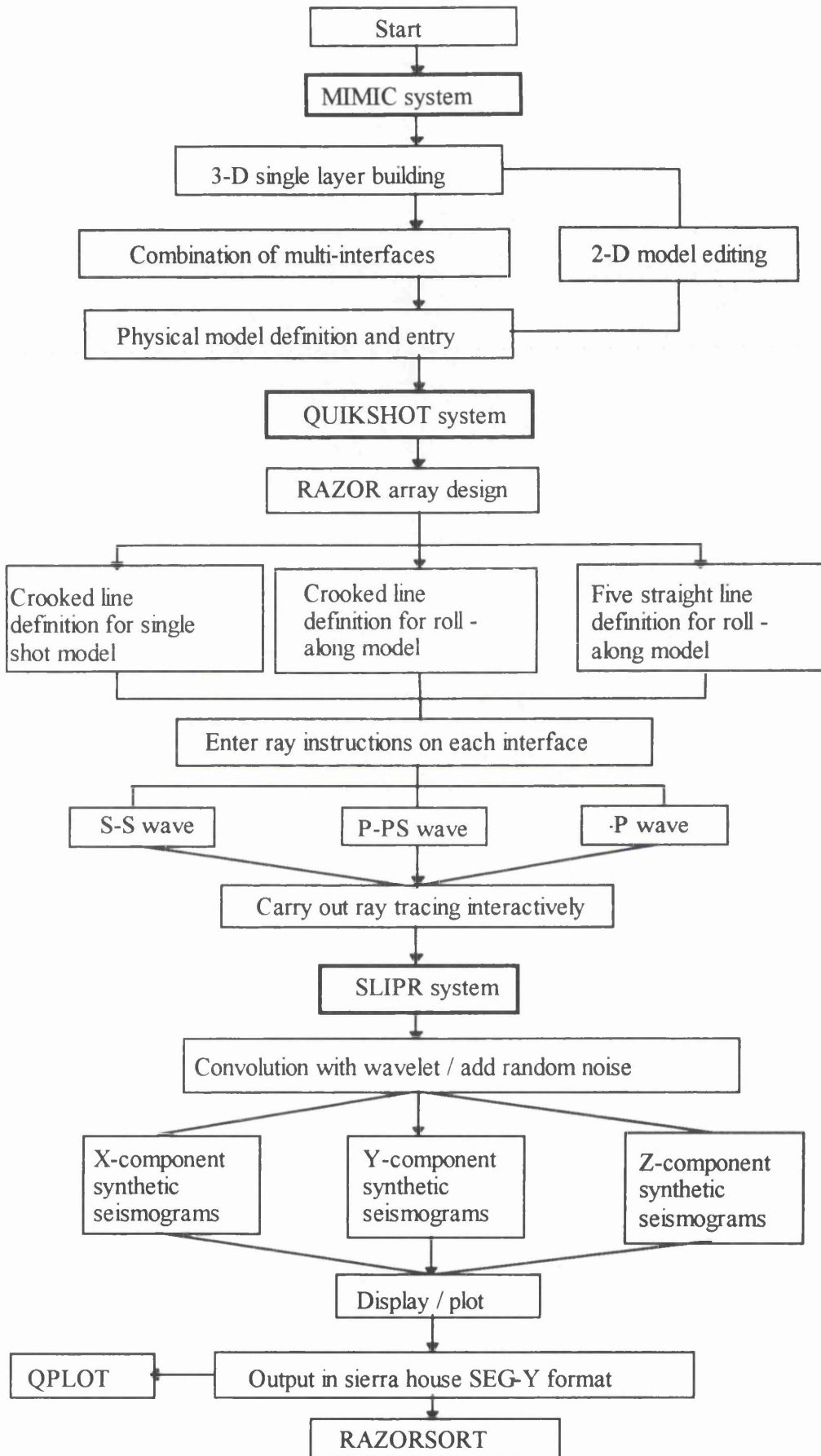


Fig. 2-13. Flow diagram for the numerical modelling experiments on the RAZOR array.

The second is the *five-line* mode, which is more suitable for roll-along RAZOR array modelling. The new Fortran-77 programme RAZORSORT.F is developed for the post-raytracing sorting required in this instance. The five-line mode is used to define the standard roll-along RAZOR array to obtain the RAZOR stacked section described in the Chapter 3. The new Fortran-77 display tool QPLOT.F makes illustrations of both the RAZOR array 12-trace shot gather and the subsequent stacked sections. It is a multi-purpose tool to plot quickly on screen or make hard copy in PostScript format. QPLOT is supported by the UNIRAS package.

In this chapter only vertical component modelling tools have been developed, as the first phase of numerical experiments on the 12-channel RAZOR array. However, the array is intended to use 3-component receivers. Chapter 3 describes the imaging methods developed for the vertical component of the RAZOR array, whereas Chapter 6 describes a new 3-component filter as applicable at present only to conventional linear (CDP) 3-component arrays. The combination of full 3-component processing and filtering into the RAZOR array method is a future task.

Figure 2-13 demonstrates that the current stage of model development for the RAZOR array is inherently complex, using several different proprietary software packages. However, this should not detract from the fact that the acquisition of the real data, as opposed to synthetic data, is relatively straightforward.

Chapter 3

Improving P-wave reflection images from RAZOR data

3.1 Introduction

This chapter discusses ways to image subsurface structure using the P-waves from recorded RAZOR data. With these new processing and analysis techniques, we can easily stack the near-zero-offset RAZOR shot gather data volume without the need for velocity analysis.

Conventional P-wave reflection processing usually results in a CDP stacked section. It assumes that the Earth consists of a series of plane horizontal isovelocity layers and that the travel times are a function of offset. After estimating the stacking velocity, we carry out normal moveout (NMO) to correct the time difference between a given offset and zero offset in a CDP gather, subsequently summing all the traces to obtain the final stacked section. The most prominent factor influencing the CDP stack is defining the NMO correction velocity. When the assumption is violated, e.g. the layers are dipping steeply and/or their boundaries are arbitrary shapes, the traveltimes equation is complex, and NMO correction velocity may be a poor estimate.

Since in the RAZOR array the offsets between the shot and receivers are small relative to the depth of the subsurface target, the three-dimensional reflection wavefronts can be approximated by planes, rather than by spherical surfaces. It implies that the traveltimes as a function of offset can be simply expressed as a linear function, and the traditional hyperbolic NMO correction is unnecessary. So we can process and image subsurface structure from the RAZOR data without stacking velocity analysis. In this chapter we will first present the application of slant-stack technology to RAZOR P-wave reflection data processing. However, serious aliasing noise occurs in the τ - p domain with 3-D slant-stack processing. Two techniques, *image enhancement* and *diversity stack* are proposed here to suppress this kind of noise in pre-stack RAZOR shot gathers without distortion of the signal content of the stacked trace. Finally we will examine the RAZOR point-source data

from the point of view of seismic illumination by using the *controlled directional source* method (CDS).

3.2 RAZOR P-wave slant-stack processing in the τ - x domain

The imaging principle by the RAZOR P-wave reflection data is based on the picking of the P-wave reflection information, which consist of certain seismic parameters. One of those is the travel time t from the source in the centre of RAZOR array to the 12 receivers located on two concentric circles. The second is the ray parameter p defined as the variation of travel time corresponding to the dip of reflections. The third one is the parameter which indicates the azimuthal orientation of reflections. As the offsets between the source in the centre of RAZOR array and the receivers are small relative to the depth of the subsurface survey target, the wavefront can be approximated by a flat plane. So it is possible to use 3-D linear slant-stacking over a planar wavefront to extract the maximum P-wave reflection energy from a subsurface interface.

3.2.1 Introduction to slant-stack technology

The applications of conventional slant stacking to reflection data were first demonstrated by Schultz (1976) and Schultz *et al.* (1978). Slant stacking, a term introduced by Claerbout, usually refers to a shift-and-add process. The continuous version, in which the sum is replaced by an infinite integral, can be distinguished by use of the term Radon transform. A related procedure is commonly known as plane-wave decomposition or τ - p processing. The procedure refers to the problem of synthesising a spherical wavefront from plane waves, and similar problems. A τ - p transform can be expressed as a weighted sum of slant stacks. An underlying assumption of slant stacking is that of a horizontally layered earth. Conventional processing primarily is done in midpoint-offset coordinates. Slant-stacking replaces the offset axis with the ray parameter p axis. A family of traces with a range of p values is called a slant-stack gather.

To construct a slant-stack in a common-midpoint-gather, a linear moveout correction (LMO) is applied to the data through a coordinate transformation (Claerbout 1978):

$$\tau = t - px \quad (3-1)$$

where p is the slowness or ray parameter, x is the offset, t is the two-way traveltime, and τ is the linearly moved out time. After LMO, an event with slope p on input is flat. Next, the data are summed over the offset axis to obtain:

$$S(p, \tau) = \sum_x P(x, \tau + px) \quad (3-2)$$

Here, $P(x, t)$ are the observed seismic data, and $S(p, \tau)$ represents a plane wave with ray parameter $p = \sin \theta / V$. By repeating the LMO for various values of p and performing the sum according to equation 3-2, the complete slant-stack gather, which consists of all the dip components in the original offset data, is constructed. A schematic description of the slant stacking described by equations 3-1 and 3-2 is shown in Figure 3-1.

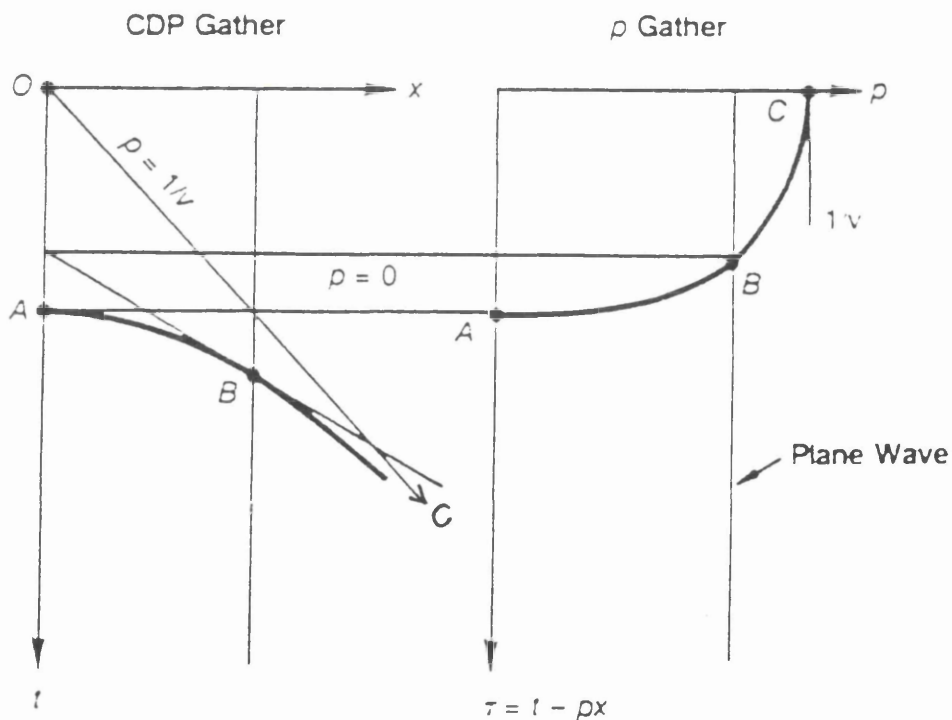


Fig. 3-1. A hyperbola in a CDP gather maps onto an ellipse in a slant-stack gather.

In the conventional processing domain the slant stacking is usually applied to suppress multiples based on different characteristics of multiples in two dimensions. Its other application includes of dip filtering, refraction inversion, and trace interpolation, for which the forward and inverse transforms are important. The physical meaning of slant-stack is not the primary concern, but rather the ability to transform the data, modify the transformed data, and apply the inverse transform (Yilmaz 1987). In addition, based on downward continuation of a slant stack gather, a technique has been developed to estimate interval velocity (Schultz 1982).

3.2.2 *Slant-stack in RAZOR data processing*

The dimension of the RAZOR array is defined such that the phase difference of a planar arrival will not differ by more than half a wavelength. For a horizontal reflector from a deep target area, say 3 km, the seismic wavefront of the reflection event will behave as an approximate plane wave across the areal array. Based on the assumption that the dimension of the RAZOR array is much smaller than the depth of the survey target area, the variation of the reflection wavelet arrival times in the t - x section is predominantly due to the dip of the reflectors or subsurface structure rather than the different offsets between the source and receivers on the earth surface (Appendix A).

As the wavefront of P-wave reflection from RAZOR data can be approximated by a plane, it is possible to apply slant-stack processing to extract the maximum reflection energy and to improve the signal to noise ratio. A RAZOR shot gather with 12 traces is decomposed into a set of new data traces, each of which contains information about a different dip component of the data. Comparing with slant-stacking of a CDP gather in conventional seismic data processing, P-wave slant-stacking in RAZOR data processing is carried out in the shot gather over a 3-dimensional flat plane by summing all 12 traces.

The equation used to define the slant stack in a RAZOR shot gather can be written

$$h(p, \tau, \alpha) = \sum_{i=1}^{12} g(x_i, \tau + px_i, \alpha) \quad (3-3)$$

where p is the ray parameter, τ is the linearly moved out time, and α is the azimuth of linear move out, also called the projection azimuth. x_i are the projected offsets between the i receivers and source at a certain projection azimuth α . g represents the observed seismic traces from the 12 receivers located on two concentric circles $i = 1, 2, \dots, 12$. With the variation of the projection azimuth α , a 3-D τ - p domain can be constructed by repeating the LMO for various values of p . For a given projection azimuth α_0 , equation 3-3 becomes:

$$h(p, \tau, \alpha_0) = \sum_{i=1}^{12} g(x_i, \tau + px_i, \alpha_0) \quad (3-4)$$

and can be rewritten as:

$$h_{\alpha_0}(p, \tau) = \sum_{i=1}^{12} g_{\alpha_0}(x_i, \tau + px_i) \quad (3-5)$$

where g_{α_0} represents the projected version of the RAZOR shot gather on the cross section at the azimuth α_0 . Comparing equation 3-5 with the equation 3-2, we find that it performs a conventional slant-stack operation, the same as in equation 3-2, and that equation 3-2 is a simplified version of equation 3-3. Similarly, an event with slope p on an input 3-D RAZOR gather becomes flat after LMO correction. The data are then summed over the offset axis to extract the maximum reflection energy as $h_{\alpha_0}(p, \tau)$. In other words, the value of $h_{\alpha_0}(p, \tau)$ at the point (p, τ) in the τ - p domain is obtained by adding the data $g_{\alpha_0}(x, t)$ along a flat plane $t = \tau + px$ and $y = \tau$ where p is the slope of this plane and τ is the intercept time when $x = 0$. Figure 3-2 shows one of the typical RAZOR shot gathers over a fault model (see Figure 2-4). The upper flat event corresponds to the flat interface on the downthrown side of the fault, and lower sinuous event is from the dipping interface representing the fault plane. Note that the 'normal' 2-D display of the RAZOR shot gather (e.g. Fig. 3-2) is not a projection, but comprises merely the 12 traces numbered in an anticlockwise fashion (Fig. 2-1) and displayed in ascending order 1-12 from left to right.

(VERTICAL COMPONENT) :Shots No. =23
 Noise = 0 % :Date = 23/2/1992 :The name of model = faul2km

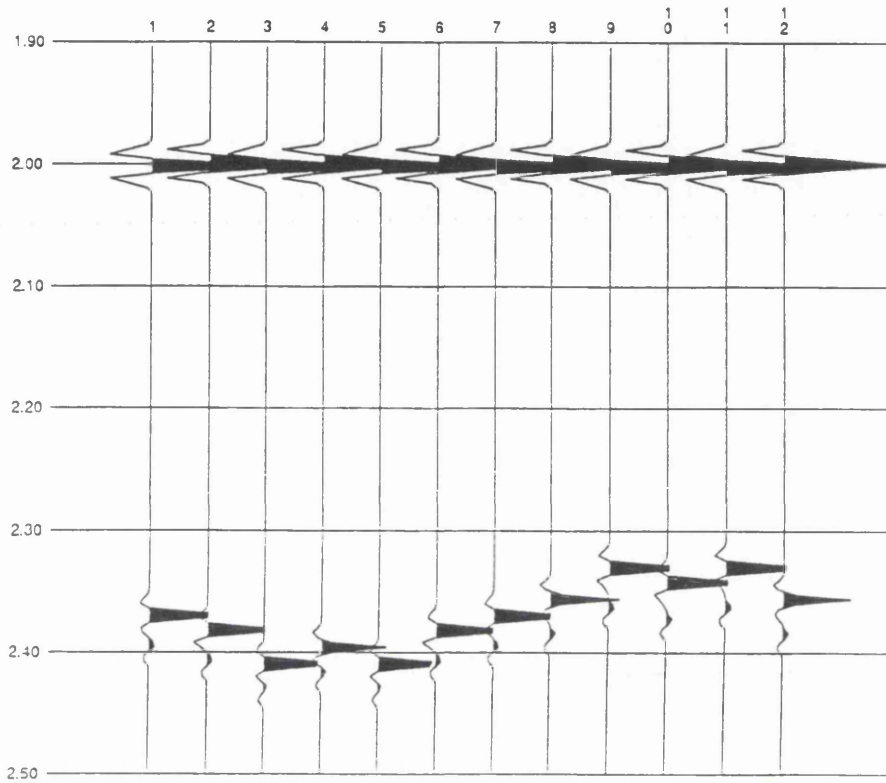


Fig. 3-2. RAZOR shot gather over the fault model of Figure 2-4. The corresponding slant-stack is shown in Figure 3-4 below; this gather is at station 23. Vertical scale - seconds of two-way time.

During the slant-stack operation the stacking plane intersects the data traces at a time t that may occur between sample points, so the value of $g_{a_0}(x, t)$ should be calculated by interpolation. Figure 3-3 shows the comparison of the RAZOR slant-stack gathers with and without the interpolation calculation. In summary, the slant-stack processing in one RAZOR shot gather can be divided into a series of conventional slant-stack operations.

Note that there is a significant distinction between the conventional slant-stack operation and the slant-stack processing in RAZOR shot gathers. The slant-stack operation in the RAZOR array aims to image geological structure in three dimensions and improve the signal/noise ratio, rather than to suppress multiples or pursue other purposes, for which slant-stack processing is usually performed on conventional CDP gathers in two

dimensions. The analysis of the slant-stack result, $h(p, \tau, \alpha)$ in the 3-D domain at each RAZOR shot gather may offer more information, such as a detailed subsurface image and the orientation of dipping interfaces. We will discuss the further application of the $h(p, \tau, \alpha)$ result in a later section of this chapter.

3.2.3 Synthetic examples

Figures 3-4 through 3-6 test our confidence in the usefulness of the RAZOR slant-stack processing to image the subsurface structure. The method yields satisfactory results, which look similar to what would be expected from a conventional CDP stacked section.

As we stated in Chapter 2, the geological models are initially built assuming a homogeneously isotropic medium by the Sierra MIMIC software subsystem. The three basic geological models in Figures 2-4, 2-5 and 2-6 above correspond to the test results shown in Figures 3-4, 3-5 and 3-6, respectively. The synthetic RAZOR roll-along recordings are simulated by the QUIKSHOT raytracing subsystem, which is suitable for generating common shot records from 2-D or 3-D MIMIC geological models of substantial complexity. The RAZOR roll-along array is modelled here by the five-line mode (Fig. 2-8). The data from the QUIKSHOT and SLIPR subsystems are converted into the ASCII domain in 'QR' format (see section 2.6.2 above), and the processing program based on equation 3-5 is applied to reconstruct the subsurface image. Here the projection azimuth α_0 is specified as 90° , so that the projection line of each RAZOR shot gather along the survey line is always perpendicular to the strike of the geological structure. After analysis in the τ - p domain for each RAZOR shot gather, the 12-fold stacked sections are presented in Figure 3-4, 3-5 and 3-6.

3.3 Image enhancement operator for post-slant-stack processed RAZOR data

The RAZOR array is designed to be an ancillary, 'piggy-back' method to take advantage of the shots from a primary CDP profile. It is intended as a cost-effective and feasible way to obtain valuable additional information on 3-D structure, for example to help in identifying out-of plane reflectors in the primary profile. However, it is worthwhile

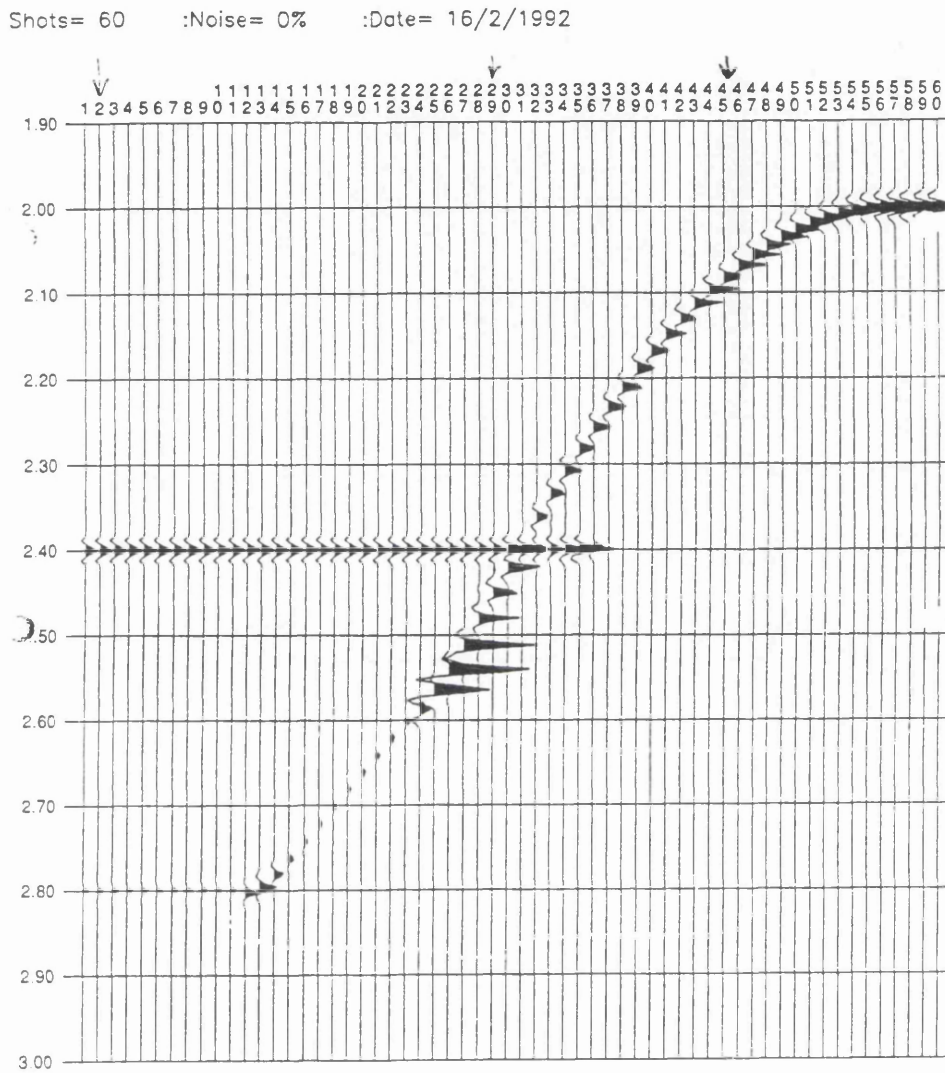


Fig. 3-5. RAZOR section over a pinchout model after slant-stack processing of 60 shot gathers. Horizontal axis - channels 1-60; vertical axis - two-way time in seconds.

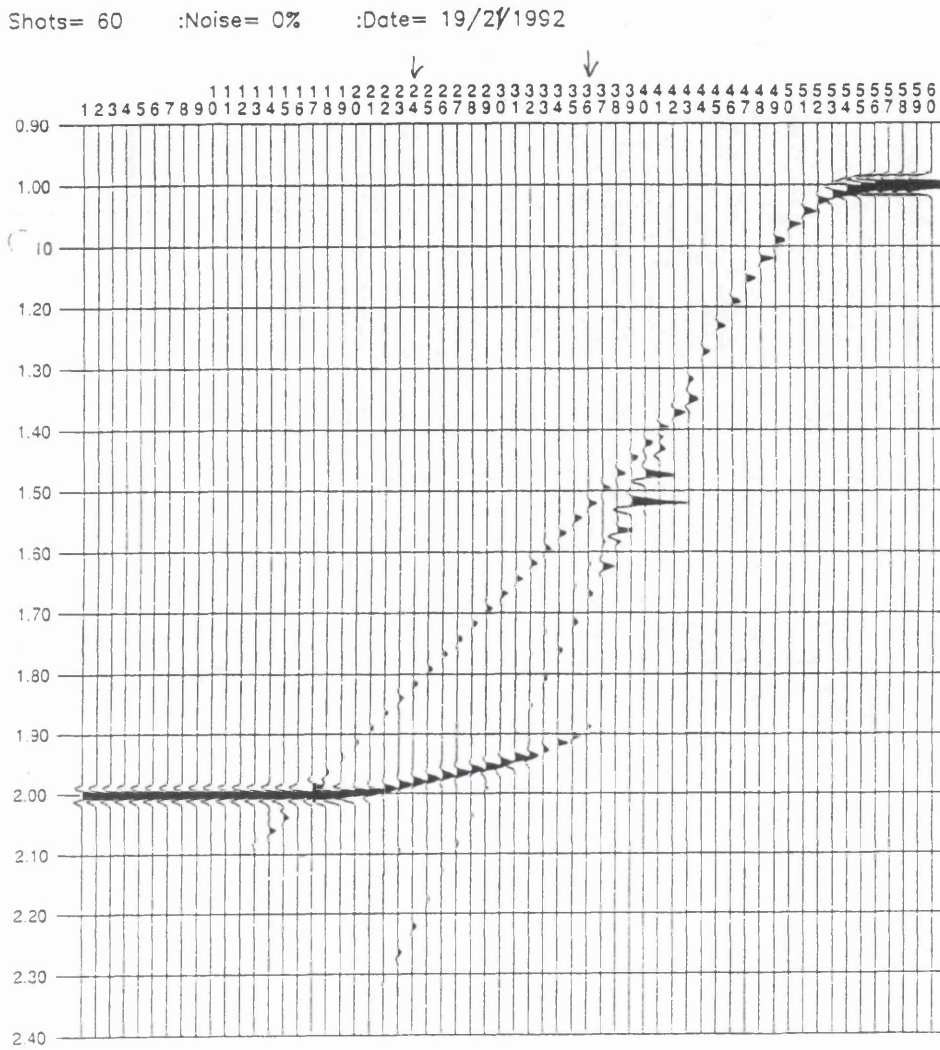


Fig. 3-6. RAZOR section over a complex model after slant-stack processing of 60 shot gathers. Horizontal axis - channels 1-60; vertical axis - two-way time in seconds.

investigating whether the stacked RAZOR image can be improved.

Stacking of the RAZOR shot gather data is effectively a filtering operation designed to select plane waves arriving at the surface with given ray parameters and along a certain azimuth α_0 . However an undesired aliasing effect occurs in the τ - p domain, when signals propagating in directions significantly different from the primary reflection signal are not sufficiently attenuated, as shown in Figures 3-3, 3-7a and 3-8a. Aliasing noise always degrades the post-slant-stack processed (SSP) RAZOR data quality, and is a serious problem for the analysis in the τ - p or t - p domains. In this and next sections, two new methods are proposed and examined to suppress the aliasing noise, without attenuating the desired signals. The first is an image enhancement operator (IEO).

The new image processing operator IEO developed here is classified as an image enhancement technique. It utilises the characteristics of aliasing noise, i.e. the constant cross-shaped pattern for any interfaces in the converted τ - p domain, to design the filter parameters. It ignores the physical causes of the seismic reflection events in the τ - p domain during its operation, treating any 2-D RAZOR slant-stack gather like a common digital image. By using the image enhancing principle, the IEO operator is defined as equation 3-6 below to superimpose all signals over laid on the cross pattern of the aliasing noise, which always corresponds to a reflection event in the form of the plane wavefront. The reflection events in a RAZOR slant-stack gather could be caused by dipping or horizontal subsurface interfaces .

Generally, the image enhancement approaches are divided into two broad categories; (1) frequency domain, and (2) spatial domain. The new operator is performed in the spatial domain, so that we can directly design the IEO based on the measurement and manipulation of pixels in the RAZOR τ - p image. For the spatial dimension of the RAZOR array, the IEO can be defined as:

$$f(p, \tau) = T[h_{\alpha_0}(p, \tau)]$$

where:

$h_{\alpha_0}(p, \tau)$ = the input image from the slant-stack processing with azimuth α_0 for one RAZOR shot gather,

$f_{\alpha_0}(p, \tau)$ = the processed version of $h_{\alpha_0}(p, \tau)$, and

T = the IEO defined as:

$$T[h_{\alpha_0}(p_0, \tau_0)] = A \exp \left\{ B \sum_{i=1}^5 \int_{-\infty}^{+\infty} h_{\alpha_0} \left[\frac{(p-p_0)}{K_i} + \tau_0, p \right] dp \right\} \quad (3-6)$$

A and B in equation 3-6 are the parameters dealing with the resolution and travel time or depth of reflections. K_i is the slope of the i th linear noise aliasing event, and since there are 5 linear alias patterns used in this IEO operation, $i = 1, 2, \dots, 5$. After $h_{\alpha_0}(p, \tau)$ is sampled with the period dp equal to unity from $p = -0.03$ to $p = +0.03$ s m^{-1} ($j = 1, 2, 3, \dots, 60$) by summing over the parameter p axis, the $T[h_{\alpha_0}(p, \tau)]$ is evaluated numerically as shown in the following equation:

$$T[h_{\alpha_0}(p_0, \tau_0)] = A \exp \left\{ B \sum_{i=1}^5 \sum_{j=1}^{60} h_{\alpha_0} \left[\frac{(p_j - p_0)}{K_i} + \tau_0, p_j \right] \right\} \quad (3-7)$$

so that the image at point (p_0, τ_0) from IEO processing can be described as

$$f_{\alpha_0}(p_0, \tau_0) = A \exp \left\{ B \sum_{i=1}^5 \sum_{j=1}^{60} h_{\alpha_0} \left[\frac{(p_j - p_0)}{K_i} + \tau_0, p_j \right] \right\} \quad (3-8)$$

The comparison of the versions before and after the IEO image processing is illustrated in Figure 3-7.

From Figure 3-7 it is obvious that the aliasing noise in the processed version on the right is completely attenuated. We can easily identify the reflection event at about $j = 30$, $\tau = 1.95$ s, which corresponds to the plane wave reflected from a horizontal interface with

a two-way travel time $t = 1.95$ s. At the same time, we find that the parameters A and B play important roles in the IEO processing. Improper specification of those parameters can lead to degradation of the resolution of the IEO image. For this reason an alternative treatment is proposed in following section.

3.4 The diversity stack in the τ - p domain to attenuate aliasing noise

The technique of diversity τ - p transformation is proposed as an alternative to suppress the aliasing noise caused by signals propagating in the different directions. The method utilises diversity scaling of the traces prior to slant stacking. A direct τ - p representation of data can be determined which minimises the response of linear events, so that aliasing effects in the RAZOR τ - p domain are much reduced.

3.4.1. Introduction to diversity stack technology

The problem of weighting seismic traces prior to summation has been an interesting area. Embre (1968) described a trace weighting scheme called ‘diversity stack’, which could be applied to any summation of seismic data to achieve the effect of improving the signal to noise ratio. His ‘diversity stack’ concept led the way for later work in other areas. Potts and Wason (1986) showed that power diversity stack weighting of the traces to be stacked leads to a stacked trace which has a S/N ratio closer to that of the optimum stack, and much better than a straight stack of the traces. Even in the presence of noise, the power diversity stack can be an amplitude preserving process. The diversity stack was proposed by Lynn *et al.* (1987) as a method of improving the CDP stack when large levels of noise are present in the pre-stack data. The diversity stack has recently been introduced into the τ - p domain, called the diversity slant stack (Monk 1991). In this section, the technique of diversity stack is extended to the slant-stack processing of the pre-stack RAZOR shot gathers, to suppress the aliasing noise without distortion of the signal content of the stacked trace.

3.4.2 The diversity stack in RAZOR slant-stack processing

In the normal RAZOR slant-stack processing described in section 3.2, the data which are not aligned along the particular dip being stacked will still contribute to the output slant stacked τ - p trace, and this leads to the common ‘butterfly’ impulse response in τ - p which is generated from a single flat event in the 3-D RAZOR t - x - α domain.

For a given projection azimuth α_0 there exists a certain x - t domain g_{α_0} which represents the projected version of the RAZOR shot gather on the cross-section at the azimuth of α_0 . The normal RAZOR slant-stack in this x - t domain g_{α_0} can then be replaced by the RAZOR power diversity slant-stack $h^1_{\alpha_0}(p, \tau)$ as expressed below:

$$h^1_{\alpha_0}(p, \tau) = \left[\sum_{i=1}^{12} \frac{g_{\alpha_0}(x_i, \tau + px_i)}{\bar{g}_{\alpha_0}^2(x_i, \tau + px_i)} \right] / \left[\sum_{i=1}^{12} \frac{1}{\bar{g}_{\alpha_0}^2(x_i, \tau + px_i)} \right] \quad (3-9)$$

where:

- g_{α_0} = projected version of the RAZOR shot gather at the azimuth α_0
- \bar{g}_{α_0} = the time averaged version of g_{α_0} , or dispersion aperture
- τ = time at zero offset.
- p = the ray parameter, or slope of dipping stack plane.
- x_i = projected offset of i th receiver station in a RAZOR gather.
- i = station number of a RAZOR array, or trace number of a RAZOR gather.

In the performance of this RAZOR power diversity slant-stack, a set of scalars is determined as the square of the inverse of the trace amplitudes, i.e. the division term in equation 3-9. In practice, a small amount of noise should be added to ensure computational integrity for those samples which are zero. So the practical formulation of the RAZOR power diversity slant-stack, e.g. equation 3-9, would be:

$$h_{\alpha_0}^1(p, \tau) = \left[\sum_{i=1}^{12} \frac{g_{\alpha_0}(x_i, \tau + px_i)}{\bar{g}_{\alpha_0}^2(x_i, \tau + px_i)} + n \right] / \left[\sum_{i=1}^{12} \frac{1}{\bar{g}_{\alpha_0}^2(x_i, \tau + px_i)} + n \right] \quad (3-10)$$

where n is additive noise.

The RAZOR diversity slant-stack minimises artifacts normally generated in the normal RAZOR slant-stack processing, and protects against contribution from aliased energy. As long as it is valid to assume that the signal amplitude was balanced across the 12 traces in the x - t domain contributing to the RAZOR diversity slant stack, then true amplitudes are preserved.

To demonstrate the performance of the diversity slant-stack in the RAZOR data processing, comparison of the $h_{\alpha_0}^1(p, \tau)$ with $h_{\alpha_0}(p, \tau)$ is presented in Figure 3-8, according to equations 3-5 and 3-10. A RAZOR shot gather is projected onto the cross-section as g_{α_0} at the azimuth of $\alpha_0 = 90^\circ$, which is perpendicular to the strike of a geological structure with one horizontal and one dipping interface. Figure 3-8a shows the result from the normal RAZOR slant-stack technique. This process appears to result in coherent linear aliasing noise artefacts in the τ - p domain which are so strong that the two reflection events at trace numbers 20 and 31 cannot be identified at all. However the result from the RAZOR diversity slant-stack is a great improvement, as shown in Figure 3-8b. The aliasing noise is considerably attenuated, without the attenuation of those two events which correspond to the horizontal and dipping interfaces respectively.

3.4.3 FORTRAN-77 program QDSTACK

A new Fortran-77 program called QDSTACK is independent module written by the author to perform diversity slant-stack processing in the RAZOR shot gathers based on equation 3-10. The main program reads the input file, which must comprise the RAZOR shot gathers in 'QR' format, into an array. Then it will ask the user to define the dispersion aperture, or the local time average of trace power, which is related to the resolution of the processed version. The additive noise n in the equation 3-10 is usually specified as 0.1% of the average input signals. The programme will first calculate scalar traces, scale the data trace g_{α_0} , then carry out the usual slant-stack for the scaled data trace g_{α_0} . The flow

diagram of the program QDSTACK is shown in Figure 3-9. Details of how to run the program are given in Appendix C.

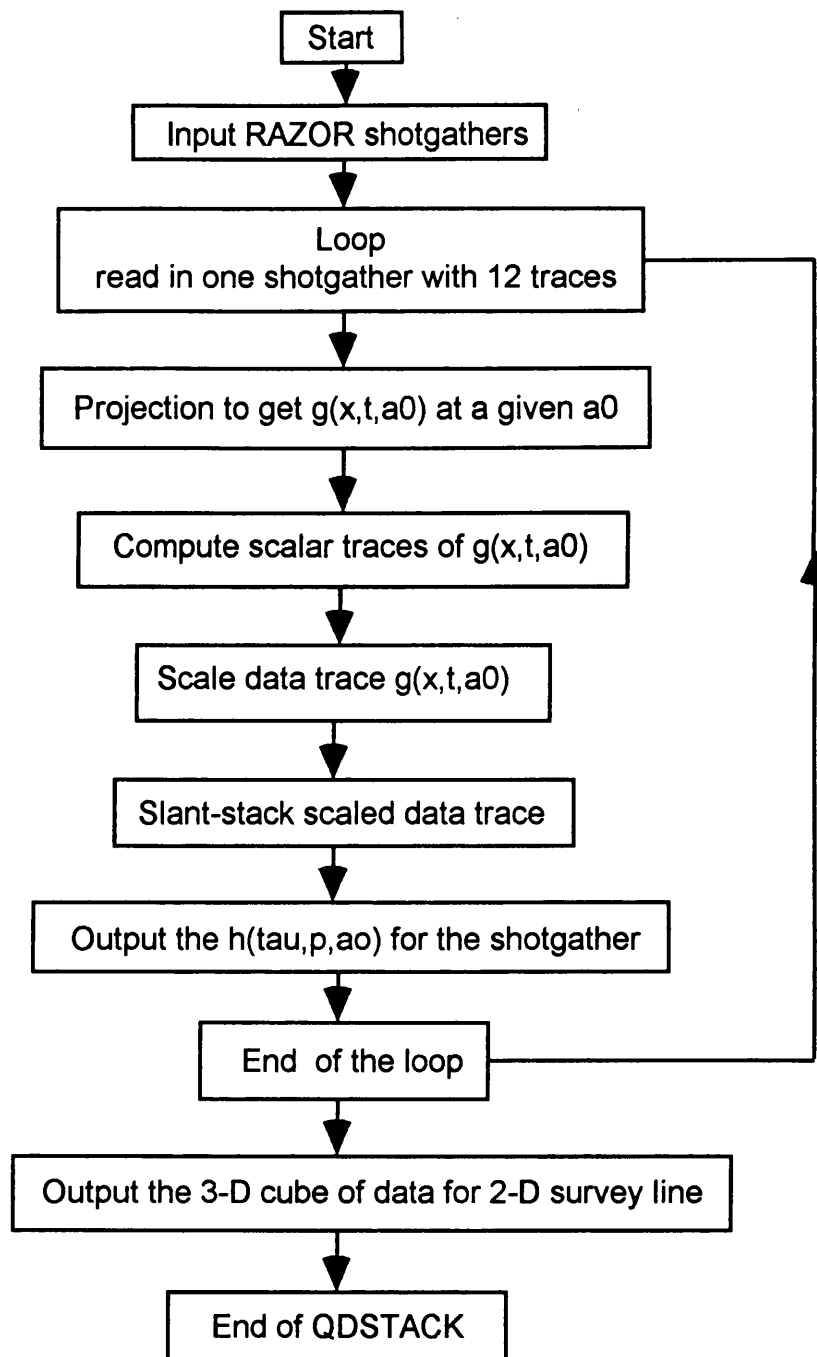


Fig. 3-9. Flow diagram of the program QDSTACK.

3.5 Plane wave decomposition for analysis of RAZOR data in three dimensions

In this section, we will examine the RAZOR point-source data from the point of view of seismic illumination, or so called controlled directional source (CDS) method.

3.5.1 Introduction to the CDS method

While common point-source processing based on common midpoint (CMP) stacking techniques progresses in its own direction, an alternative method of processing and producing seismic images, the 'controlled direction source' (CDS) method was proposed based on a line source to generate a linear wavefront (Taner *et al.* 1988).

Reflection seismic processing can be classified into three main streams, which correspond to three kinds of source used in the seismic survey. They are:

- (1) Processing based on a point source,
- (2) Processing based on a line source, and
- (3) Processing based on a planar source.

Point-sources are omni-directional, so that the subsurface is illuminated by a spherically spreading source wavefront. Due to their omni-directionality, point sources have poor penetration characteristics across high velocity contrast interfaces. The higher velocity contrast results in a smaller critical angle and thus a smaller portion of the spherical front penetrates to the next medium as a pressure wavefront. In contrast, a planar source is generated at a constant incidence angle, so that the subsurface is illuminated by a directional planar source wavefront. The reflection from a planar interface appears as a flat planar event in a two-dimensional array, or as linear event in a one-dimensional array at a certain azimuth. Because of its higher level of directionality, due to the constant incidence angle, planar sources have better penetration characteristics across high velocity contrast interfaces.

Experimental procedures using line sources were introduced to combat the problems associated with point sources, primarily horizontally travelling waves and ground roll, in

the 1950s and early 1960s (Mitchell 1951; Pierau and Muller 1960; Pierau and Rosenbach 1960; Bortfeld *et al.* 1960). While the results were superior to those of point sources, line sources did not become generally accepted because of the introduction and popularity of the CDP method. After Claerbout (1971), Taner (1976, 1978), and Garotta (1980) showed that long line source arrays can be simulated by combining conventionally generated point-source records, the controlled direction source (CDS) method based on line sources received some attention again.

In this section we propose the controlled directional source (CDS) method based on planar sources simulated by the two-dimensional RAZOR array, and demonstrate its application to RAZOR data analysis. CDP-stack-like sections can then be generated.

3.5.2 Simulation of a planar source in the RAZOR array

Planar source recording is much too expensive to be practical, as each source direction must be shot in the field. However, planar sources can be simulated by the proper combination of point source recordings from the two-dimensional RAZOR array, which makes its use economically feasible. The simulation is based on two basic principles.

The Dutch physicist, Huygens, developed the well-known Huygen's principle of wave propagation. The principle is *wave superposition*. It states that any wave shape can be simulated by proper superposition of many secondary point sources. In other words, a planar source can be simulated by firing many smaller closely spaced point-source simultaneously or sequentially. In this way, it is possible to simulate wave propagation in any desired direction, simply by controlling the sequence of firing. The second important physical rule is the principle of *reciprocity*, which states that if we exchange the source and receiver positions, we would record the same seismic trace at the source position as was previously recorded at the receiver position.

A RAZOR shot gather represents a single source at the centre of two concentric circles where 12 geophones record the seismic wave field. Based on the reciprocity law, each seismic trace can be treated as if it were recorded at the shot location in the centre while the source is located at the receiver positions on the two circles. In the reciprocal mode

these 12 traces represent the common-receiver traces. Therefore, in order to simulate a planar source array as large as a whole RAZOR array, we invoke the superposition rule and sum the 12 traces horizontally, thereby obtaining a single trace, which represents the simultaneous firing of all 12 'shots' located at the receiver locations. It means that the simulated planar wavefront propagates vertically downward. To generate a slant planar wavefront, the 12 'shots' must be fired sequentially, spaced apart in time by a firing interval T_i , which can be computed from the geometrical relationships in the RAZOR array:

$$T_i = \frac{x_i \sin \theta \cos \beta}{v_o} \quad (i = 1, 2, 3 \dots 11) \quad (3-11)$$

where x_i is the projected source interval along the dipping wavefront direction at the i th source station. As there are only 12 'shot' positions, the number of total source intervals x_i is 11, e.g. i ranging from 1 to 11. v_o is the medium velocity near the surface. θ is the desired source wavefront direction, and β is the azimuth of wavefront inclination as shown in Figure 3-10. The RAZOR roll-along survey line is defined as the X axis, and the Y axis is parallel to the zero azimuth of the RAZOR array. O represents the original field shot point in the RAZOR array.

For a given projection azimuth β , and as the quantity $\sin \theta / v_o$ is a constant along a raypath in a layered medium by the Snell's law, we can define:

$$\frac{\sin \theta \cos \beta}{v_o} = p$$

where the p is the ray parameter. Equation 3-11 is then rewritten as:

$$T_i = px_i \quad (3-12)$$

The angle of propagation of the planar wavefront is controlled by adjusting the p value. Setting $p = 0$ corresponds to a plane wave from the RAZOR array travelling vertically. Note that the physical meaning of the calculation by equation 3-12 is in effect the normal

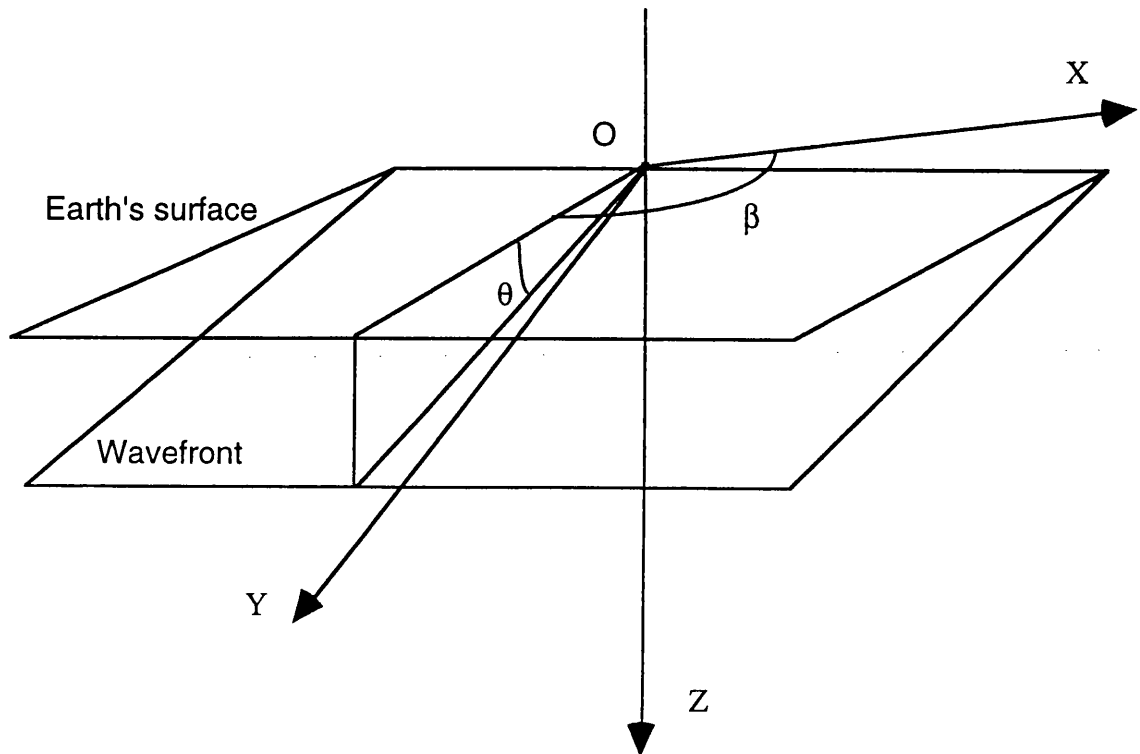


Fig. 3-10. Simulation of a dipping planar wavefront in the two-dimensional RAZOR array.

RAZOR slant-stack process. Except for some small computational differences, the section in the t - p domain calculated by equation 3-12 is identical to the normal RAZOR slant-stack in the τ - p domain for the same input RAZOR shot gather.

According to some authors (e.g. *Taner et al.* 1988), the point sources should be spaced less than $1/4$ of the shortest wavelength apart in order to generate a plane wave or controlled wavefront properly. For the geometrical definition of the RAZOR array, the simulated planar wave obeying this criterion would be suitable for 20 Hz reflections at the station spacing of 75 m used here (Fig. 2-1), if the velocity is 5000 m/s.

3.5.3 Profiling based on the RAZOR array

By superposing the common-receiver traces corresponding to the continuous point source, the response of the RAZOR array to a planar source is simulated. This process is essentially as same as that in the RAZOR slant-stack, but is in three dimension rather than in two dimensions.

Since the RAZOR slant-stack is performed on 12 split-spread data traces g_{α_0} projected from one RAZOR shot gather, there will be one transformed 3-D data cube for each shot gather, with a family of projection azimuth α_0 . The parameters τ , p and α represent its three axes. When the RAZOR array rolls along a survey line as shown in Figure 2-7 and 2-8, we can obtain a four-dimensional data set with an additional geometric axis along the survey line. The RAZOR profiling is based on the analysis of this 4-D data set. For a given projection azimuth α_0 which is applied to all shot gathers, the 4-D data set becomes a 3-D cube along the survey line as demonstrated schematically in Figure 3-11, where the coordinates represent the inclination of the source wavefront (p), the intercept time (τ), the RAZOR array reference direction (x) and the RAZOR shot station are located along the line (y).

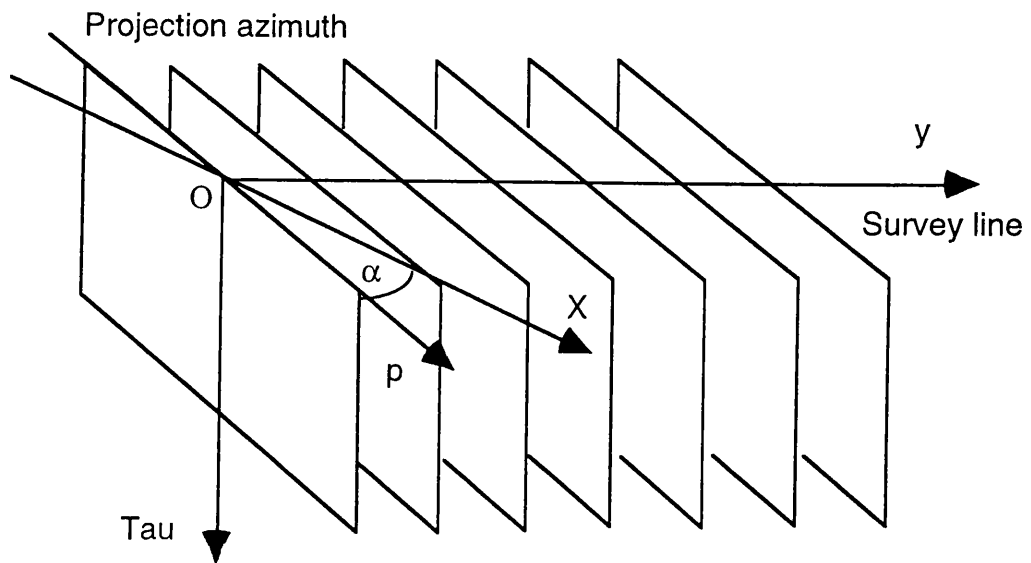


Fig. 3-11. Relationship of the τ - p section to the constant- p section.

If the data cube is cut parallel to the x - τ plane, the traces will have the same p value, and this constant p plane is the seismic section, called a CDS section, which contains the simulated response to a planar-source with a controlled source direction at azimuth α_0 and with inclination:

$$\theta = \sin^{-1} \left(\frac{v_0 p}{\cos \alpha_0} \right)$$

where v_0 is the medium velocity. The analysis of the RAZOR data in the τ - p and y - τ domains is based on the point of view of seismic illumination. Therefore a horizontal reflection appears horizontal in these sections without any normal or linear moveout, so that the processing and interpretation of the RAZOR CDS section are facilitated. Note that all of the CDS sections from the RAZOR data were generated without consideration of a velocity function, which is usually needed for building the subsurface image in routine CDP methods.

The aliasing noise in the τ - p image usually becomes stronger with increase of receiver spacing. As the station spacing is 75 m in the RAZOR array, this type of coherent aliasing noise could become a serious problem if the normal RAZOR slant-stacking method is applied to the three-dimensional shot gathers. Hence, in practice, the trace spacing of RAZOR shot gathers should be reduced by interpolation in order to overcome the aliasing problem. An alternative treatment is the application of the diversity stack technique, which has been described above.

3.5.4 Synthetic data example of plane wave decomposition

The synthetic RAZOR shot gather data are generated for a pinchout model by using Sierra's MIMIC, QUIKSHOT, SierraSEIS and the new Fortran-77 program RAZORSORT as described in Chapter 2. The modelling flow diagram is presented in Figure 3-12. The model is in a isovelocity medium with $v_1 = 2500$ m/s., $v_2 = 2700$ m/s, and $v_3 = 3000$ m/s. The RAZOR array rolls along a survey line which is perpendicular to the strike of the geological structure, i.e. the projection azimuth is defined as $\alpha = 90^\circ$. A total

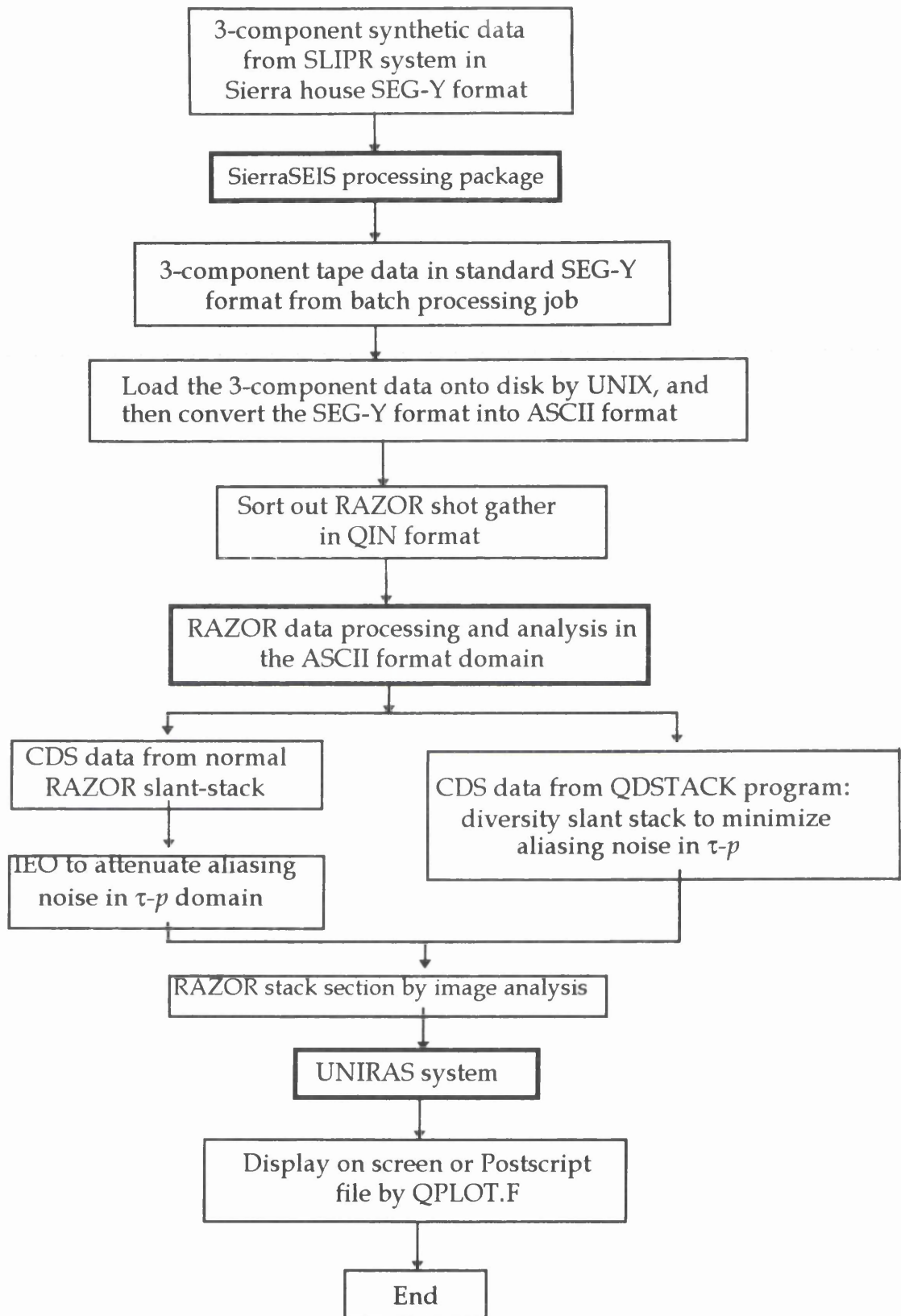


Fig. 3-12. Flow diagram of seismic reflection processing for RAZOR data.

of 60 shot stations is laid out from west to east with a constant interval of 75 m. We just apply the normal RAZOR slant-stack to the processing of each shot gather to obtain their corresponding τ - p images. After these τ - p images are placed according to their centre shot station coordinates as indicated in Figure 3-11, a 3-D data cube with axes, y - p - τ is obtained. By cutting the data cube along the survey line with same p value, we obtain the constant p planes shown schematically in the eight Figures 3-13a through 3-13h.

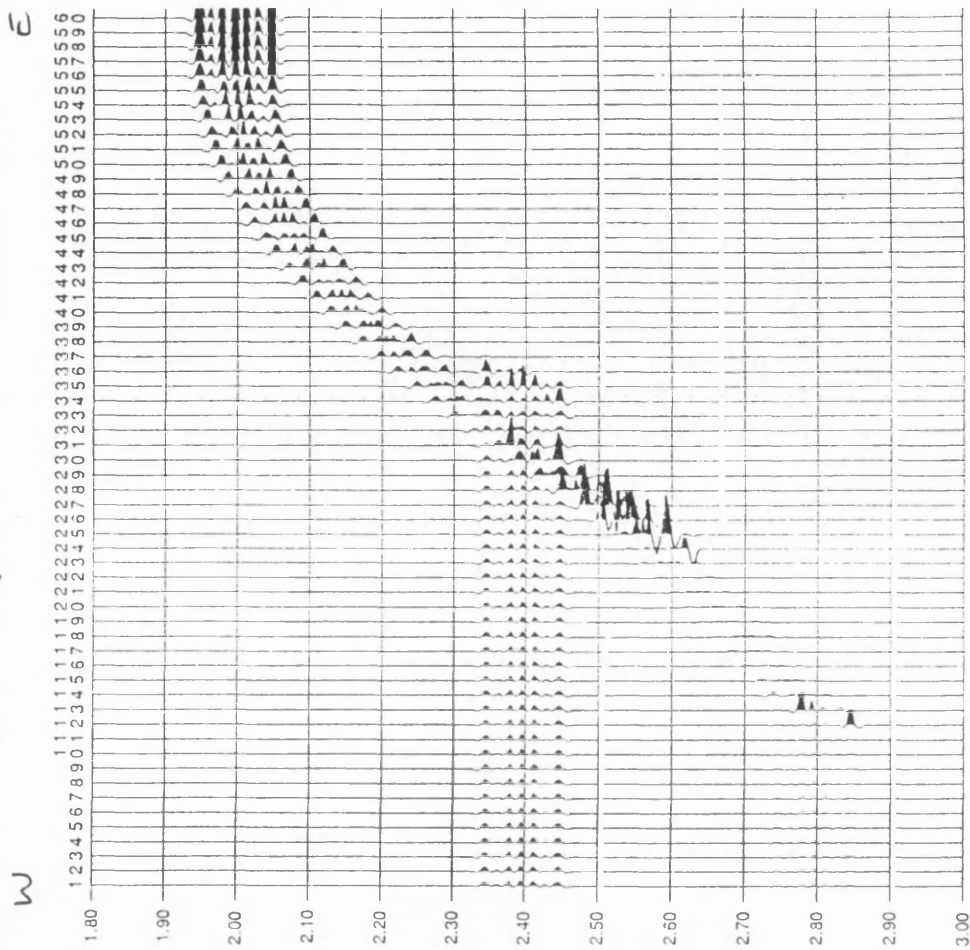
Sequentially through Figure 3-13a-h, the source plane wave illuminates a constant subsurface structure (the pinchout model of Figure 2-5) with the source inclination varying from west to east, i.e. from $p = -0.0022$ (Fig. 3-13a) to $p = +0.0022$ (Fig. 3-13f). When $p = -0.0022$ (Fig. 3-13a), the inclination of the source wavefront dips too steeply west to get much reflection energy from the fault plane, which is dipping in the same direction, as seen in the traces 14 to 45. The repeated events are scattered aliasing noise caused by the usual RAZOR slant-stack. As the dip of the source plane wave is reduced, the maximum reflection energy from the fault plane is extracted when the source plane wavefront is parallel to the dipping fault plane (e.g. Fig. 3-13d). When the source plane wave is injected vertically ($p = 0.0$; Fig. 3-13e), the reflections from the three horizontal interfaces reach their maximum amplitudes, while the amplitudes of the events from the fault decrease. When the ray parameter p becomes positive the source plane wave is dipping eastward. As there are no interfaces dipping in this direction, only scattered aliasing noise is visible, as shown in the end-member example of Figure 3-13h. In a similar way, the analysis of another 3-D data set y - p - τ can be conducted when a new projection azimuth is given.

Here we used the usual RAZOR slant-stack without IEO filtering to obtain the 3-dimensional data cube, so that the CDS sections of Figure 3-13 are heavily contaminated by aliasing noise. In practice, the IEO filter should be applied to remove this kind of noise in the τ - p domain. Alternatively the RAZOR diversity slant-stack can replace the normal RAZOR slant-stack and IEO filtering in most cases. We recommend the use of the RAZOR diversity slant-stack in the RAZOR data processing, although it costs more in computational time. In conclusion, each RAZOR CDS section represents the reflections generated by an invariant subsurface illuminated by a planar source wave with a particular inclination and azimuth.

SUBTITLE : pp10

(VERTICAL COMPONENT) :T = 0.0020000

Noise = % :Date = Fri Aug 14 15:29:44 1992 :SAMPMM = 0.600



SUBTITLE : ~~sd~~pp1

(VERTICAL COMPONENT) :T = 0.0020000

Noise = % :Date = Thu Aug 13 17:27:54 1992 :SAMPMM = 0.600

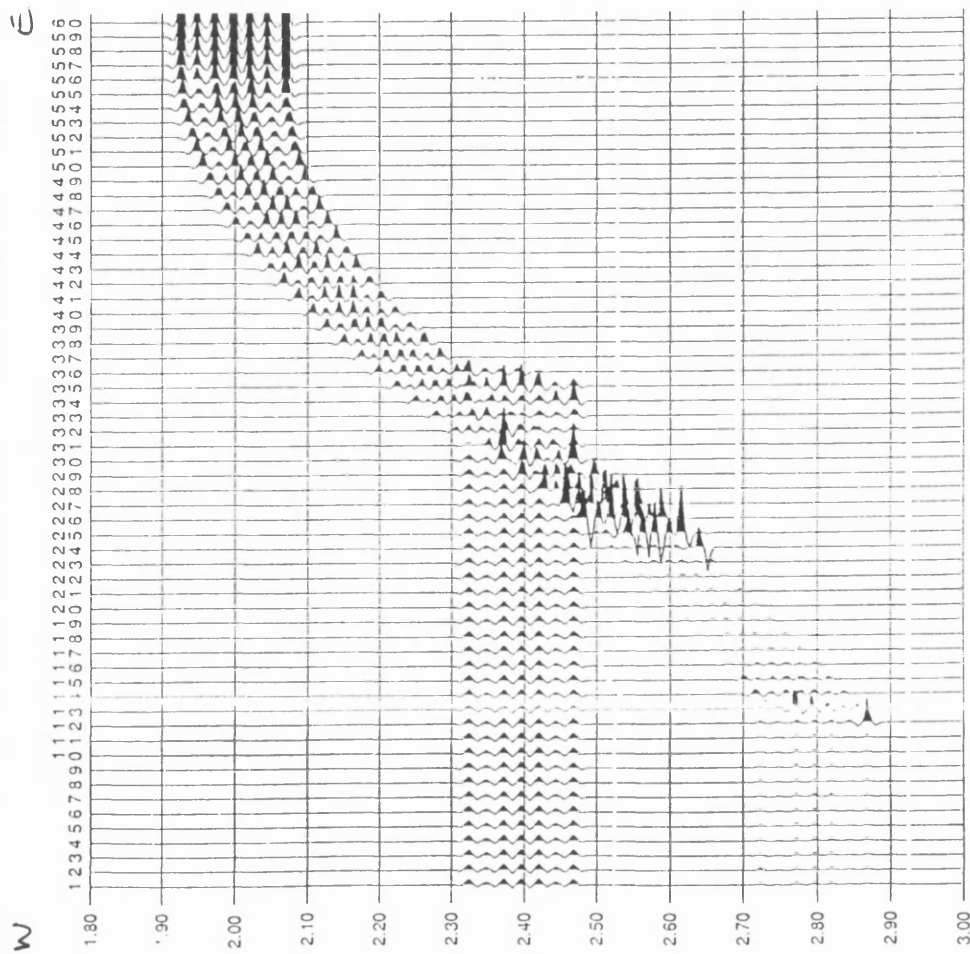
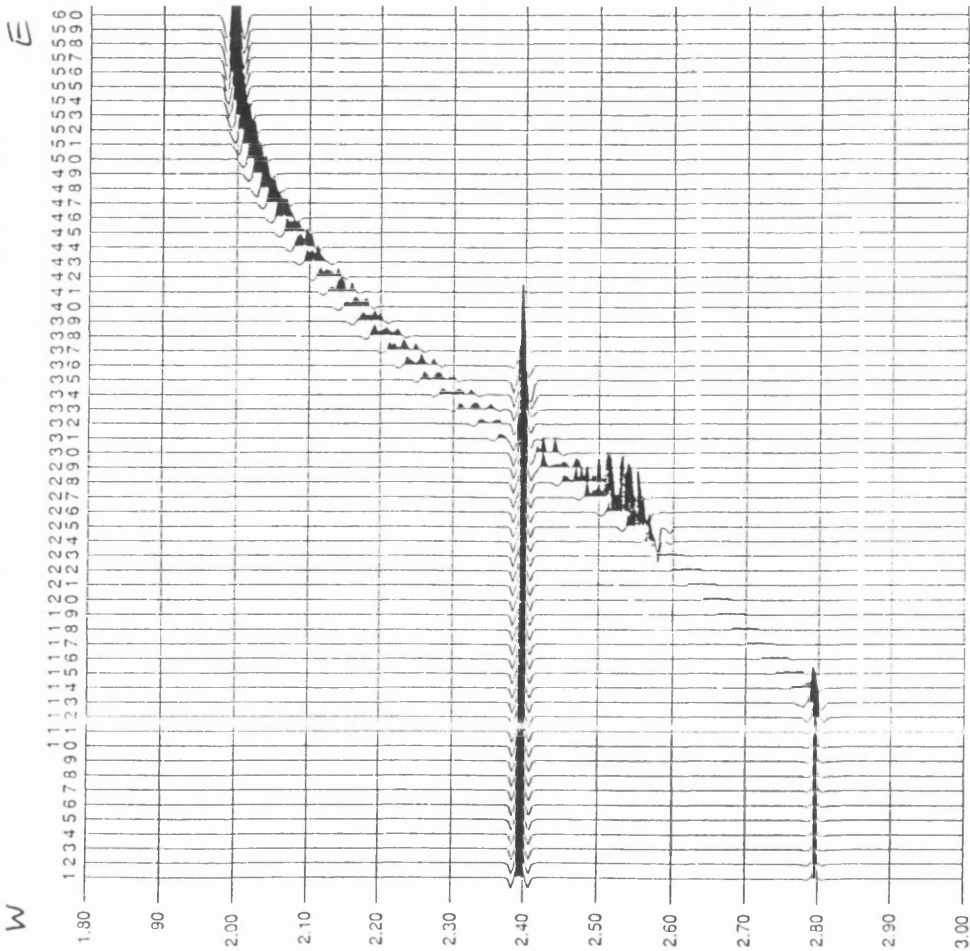


Fig. 3-13a, b. CDS sections with projection azimuth $\alpha=90^\circ$ and ray parameter $p=-0.0022$ (a), and $p=-0.001467$ (b). Horizontal axis - channels 1-60; vertical axis - two-way time in seconds.

SUBTITLE : pp3C

(VERTICAL COMPONENT) :T = 0.0020000

Noise = % :Date = Fri Aug 14 15:37:49 1992 :SAMPMM = 0.600



SUBTITLE : pp4O

(VERTICAL COMPONENT) :T = 0.0020000

Noise = % :Date = Fri Aug 14 15:40:20 1992 :SAMPMM = 0.600

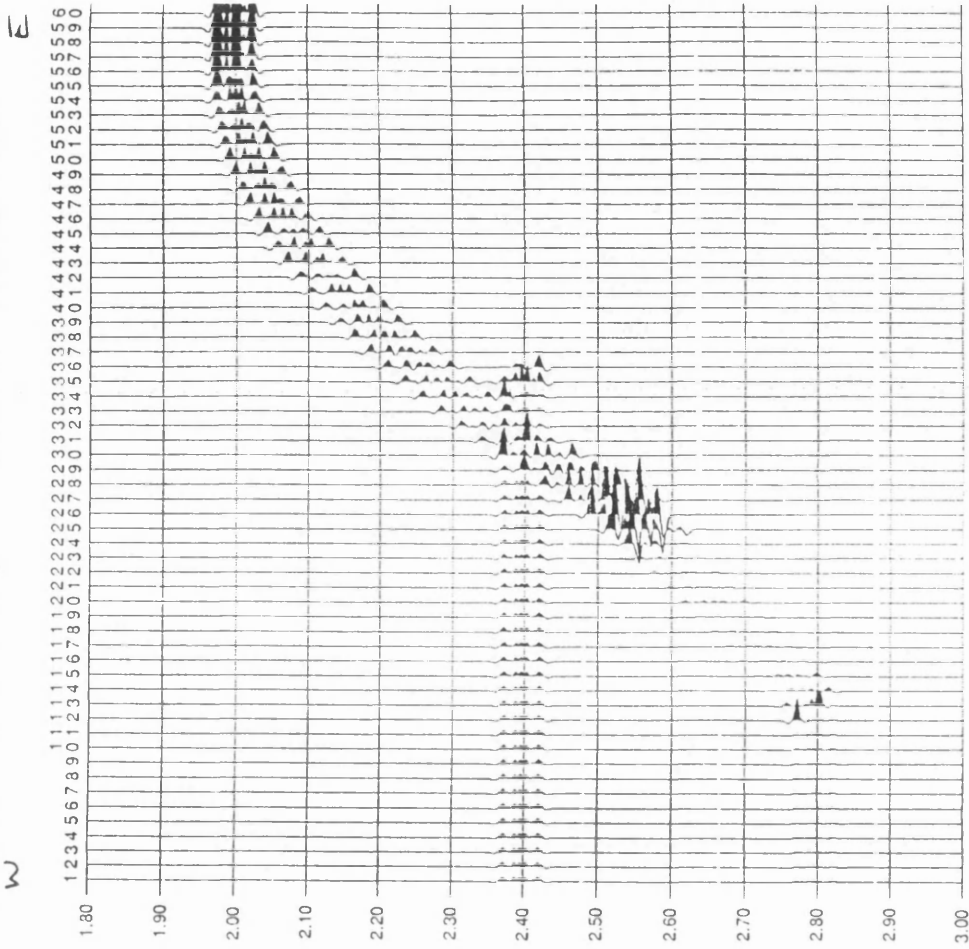
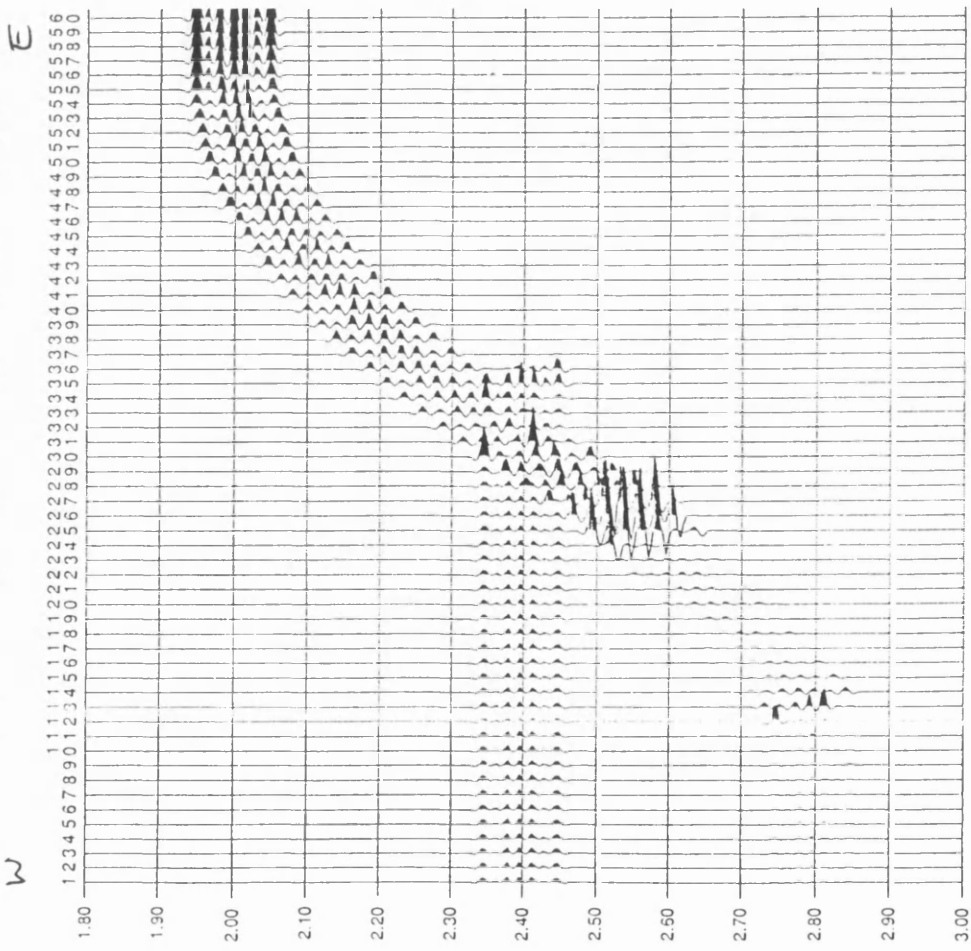


Fig. 3-13e, f. CDS sections with projection azimuth $\alpha=90^\circ$ and ray parameter $p=0.0$ (e), and $p=+0.000733$ (f). Horizontal axis - channels 1-60; vertical axis - two-way time in seconds.

SUBTITLE : pp50

(VERTICAL COMPONENT) :T = 0.00200000

Noise = % :Date = Fri Aug 14 15:41:42 1992 :SAMPMM = 0.600



SUBTITLE : pp60

(VERTICAL COMPONENT) :T = 0.00200000

Noise = % :Date = Fri Aug 14 15:44:04 1992 :SAMPMM = 0.600

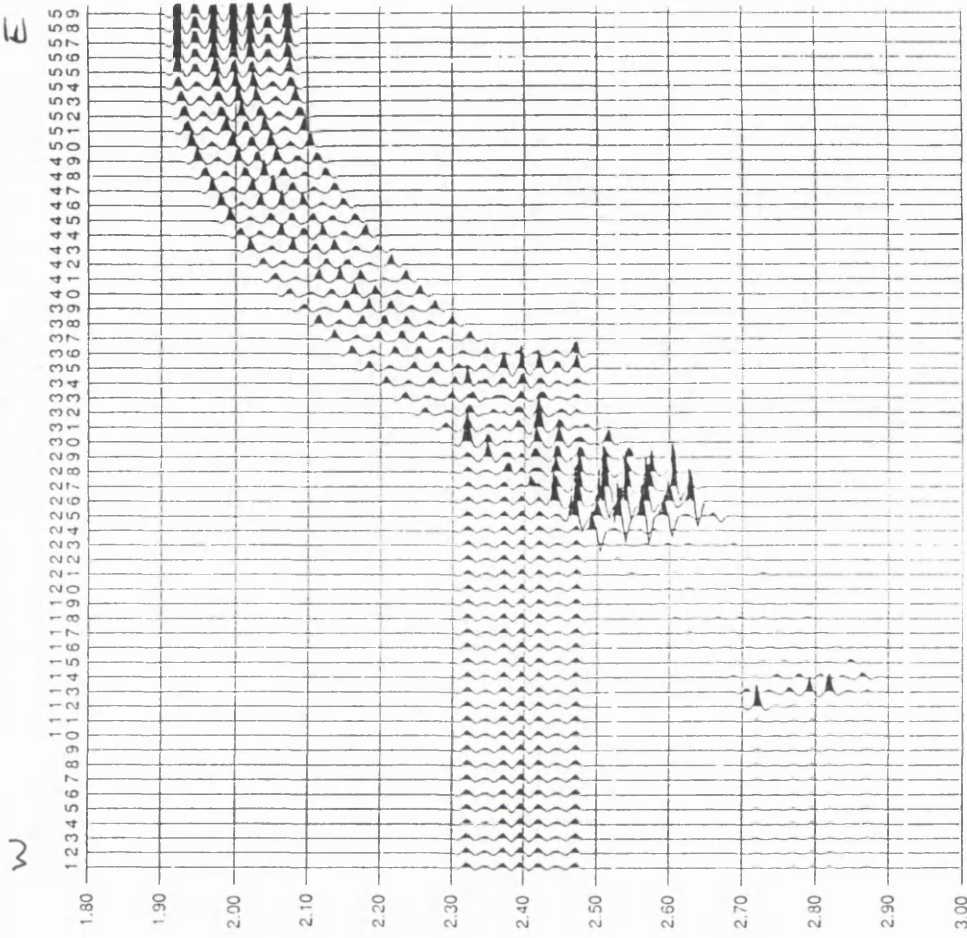


Fig. 3-13g. h. CDS sections with projection azimuth $\alpha = 90^\circ$ and ray parameter $p = +0.00146$ (g), and $p = +0.0022$ (h). Horizontal axis - channels 1-60; vertical axis - two-way time in seconds.

Chapter 4

Filtering vibroseis data in the pre-correlation domain

4.1 Introduction

Vibroseis reflection data recorded at short source-receiver offsets can be swamped by direct waves from the source. After correlation, we usually think of the central peak and adjacent half-cycles as being so large in comparison to the amplitude of the later sidelobes that the sidelobes can be ignored. Sidelobes can be considered to be undesired signal-generated noise since their form is signal-dependent. Naturally, we want the sidelobes to be as small as possible so as not to obscure nearly coincident and/or weaker signals. The first sidelobe of a conventional linear sweep can be as high as 22% of the peak and second sidelobe as high as 13% of the peak (Fig. 4-1). These will interfere with the correlation peaks of desired events arriving at the same times as the unwanted sidelobes. The task of resolving the interfering events is usually carried out by spiking deconvolution, phase shifting and/or spectral whitening techniques (e.g. Yilmaz 1987), which are not the subject of this dissertation.

However, at time ranges outside the first couple of sidelobes shown in Figure 4-1 the decay envelope of the sidelobes flattens out, so that the far outlying side-lobes from first arrivals, for example, can still be as high in amplitude as the major lobes of desired reflection events. The result is that the signal to noise ratio, where the correlation peaks of primary reflections are the signal and correlation sidelobes are the noise, decreases with time, and later events can be overwhelmed. The problem is one of correlation noise. The synthetic example in Figure 4-2a shows that sidelobes from a large event such as the first break can dominate much later, low amplitude signals. The sweep is a 10-60 Hz linear sweep with 0.5 s linear tapers. The amplitude of the first signal at 100 ms (the first break) is 4000 times larger than that of the second signal (reflection) arriving 2200 ms later. An exponential gain has been applied to the correlated trace to make the two signals visible; this gain makes the first break look asymmetrical. The reflection signal correlation peak is

2.7 times bigger than the sidelobe contamination in its vicinity. We define this ratio as the signal-to-noise (S/N) ratio.

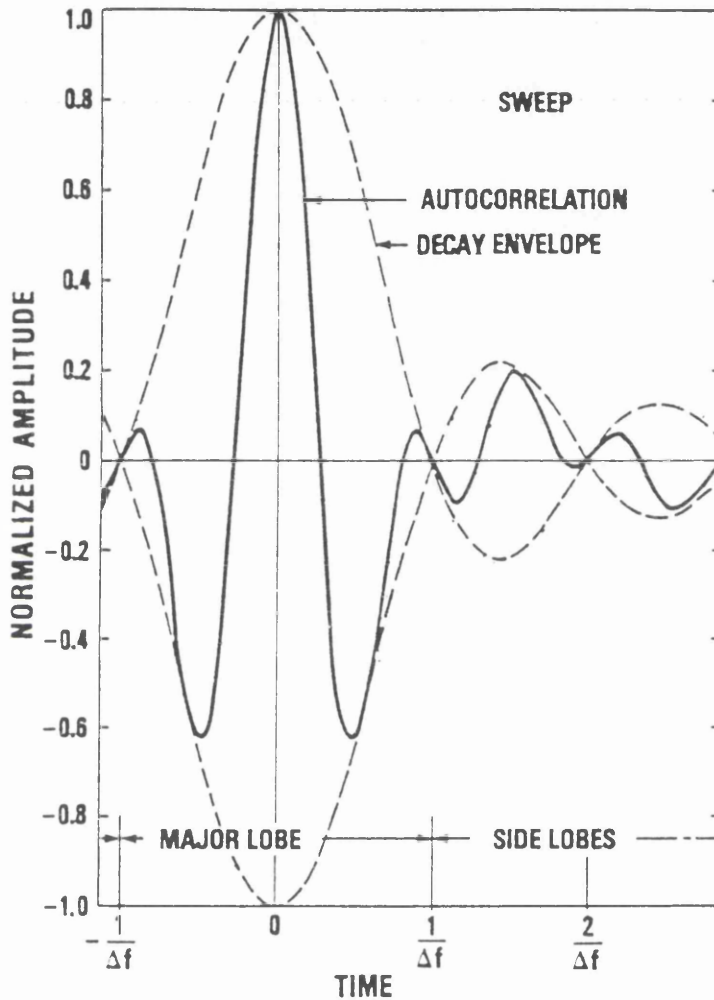


Fig. 4-1. Autocorrelation of a sweep (after Cunningham 1979), showing the definition of major lobe and side lobes.

Correlation noise suppression has been discussed since the introduction of correlation. Klauder *et al.* (1960) described measures to reduce sidelobe levels by frequency weighting, and the sweep tapering technique has become routine for correlation noise

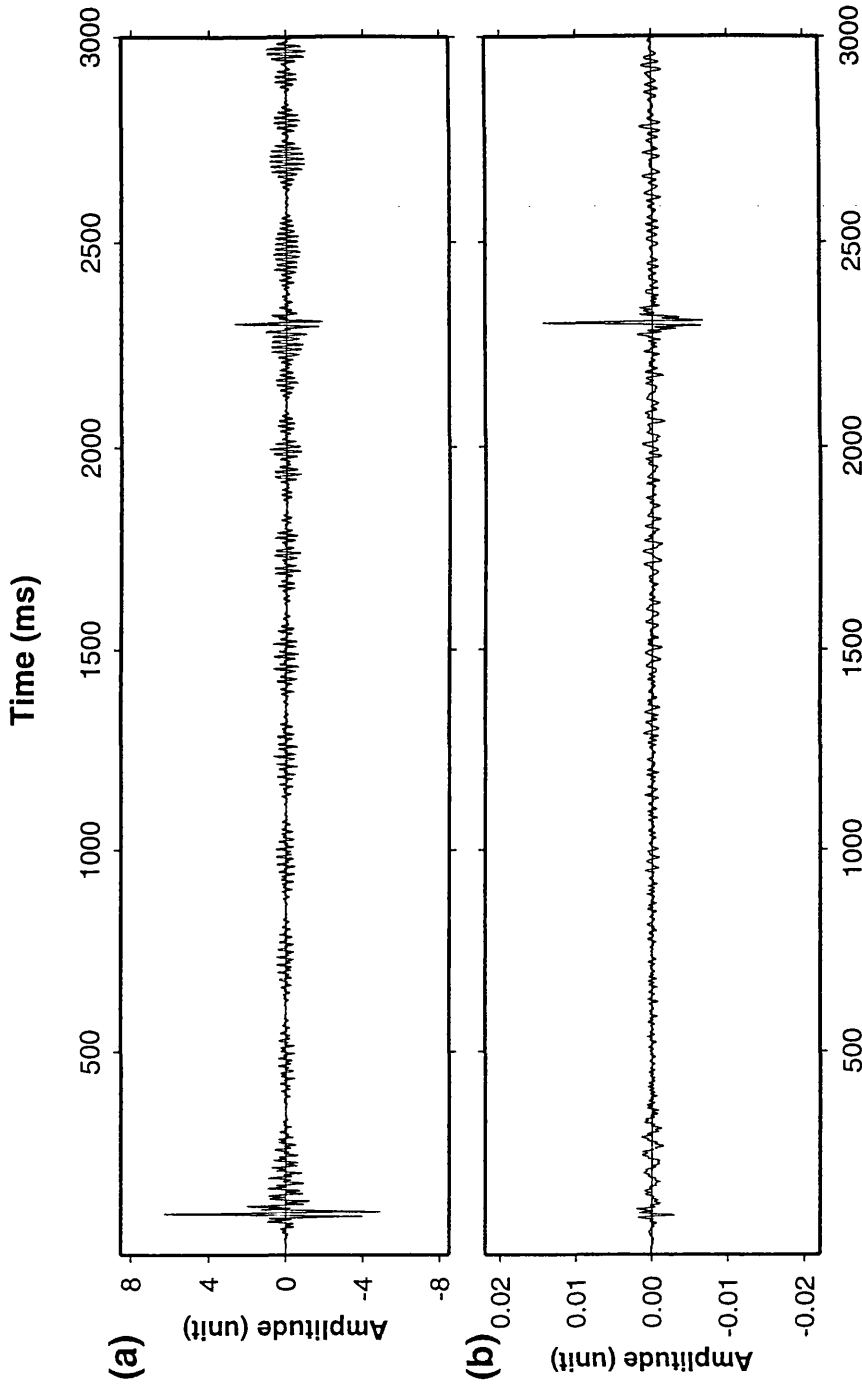


Fig. 4-2. Correlated synthetic data trace from 10-60 Hz linear sweep with 500 ms linear tapers. Direct wave is at 100 ms and reflection at 2300 ms, with 1/4000 of the amplitude of the direct wave:(a) Before SFU; spherical divergence gain applied; (b) After removal of the direct wave by SFU, constant gain applied.

suppression since the early 1960s. A considerable reduction of the sidelobe noise can be achieved by tapering the amplitude spectrum of the vibrator sweep, at the expense of loss of energy put into the ground (Edelmann 1966). During the 1970s, the Combisweep technique was introduced by Werner and Krey (1979), and was discussed as a correlation noise suppression technique by Edelmann and Werner (1982). This technique starts from the idea that neither a nonlinear sweep nor amplitude shaping can cope with the coupling and attenuating effects of the ground, which influence the vibroseis signal. The Combisweep technique yields an improved recorded signal by strengthening certain spectral components which otherwise would remain below the noise level.

At around the same time coding techniques to suppress correlation noise were introduced from communication theory into vibroseis exploration. One of them is the pseudo-random coding technique developed by Cunningham (1979). This encoding, however, makes great demands upon the transient response of the vibrator. Another coding technique was described by Bernhardt and Peacock (1978), designed to suppress far-correlation noise. However, near-correlation noise is only moderately reduced.

All the approaches mentioned above attack the correlation noise problem either at source (by designing better sweeps), or during post-correlation processing. Our approach (based on a note by D.K. Smythe in 1992; Appendix D) is to remove the events causing the problem before correlation. These events will usually be large-amplitude events such as first breaks, ground roll and air blast. The synthetic example shown in Figure 4-2a has had the first break removed before correlation (Fig. 4-2b). This output trace is displayed at a constant gain. The amplitude of the desired reflection at 2300 ms has been increased by about 18,000 relative to the first break at 100 ms, and there is a 3.2 increase in S/N ratio in the vicinity of the reflection event. The first break was removed with our 'Squeeze-Filter-Unsqueeze' algorithm (SFU for short), which is a combination of squeeze and unsqueeze transformations, together with application of either an optimum least-squares (OLS) filter or a linear recursive notch filter prior to the inverse transform. We squeeze the uncorrelated trace in a non-linear way so that the unwanted signal is transformed into a constant quasi-sinusoidal wave of known phase and duration. We then filter this signal out, without removing any other signal components. Lastly, we unsqueeze

the trace. SFU is a single trace process applied to uncorrelated data. The following sections present the description of the new filter, its implementation, and a discussion of the algorithm performance examined through use of both synthetic modelling data and field data examples.

4.2 The problem of sidelobes

To demonstrate an example of the correlation sidelobe problem we examine the conventional linear swept-frequency sine wave from start frequency f_1 to end frequency f_2 over the duration T . Its autocorrelation function $\Phi(\tau)$ can be well approximated for seismic applications (Cunningham 1979) by

$$\Phi(\tau) = \frac{A^2}{2} \frac{T \sin \pi \Delta f \tau}{\pi \Delta f \tau} \cos 2\pi \left(f_0 + \frac{\Delta f \tau}{2T} \right) \tau$$

$$\text{for } 0 \leq |\tau| \leq T, \quad (4-1)$$

where τ = processed record time

A = signal amplitude

$\Delta f = f_2 - f_1$: bandwidth, and

$$f_0 = \frac{(f_2 + f_1)}{2} : \text{centre frequency}$$

The autocorrelation is plotted as the solid curve in Figure 4-1, representing the product of a constant, a $(\sin x)/x$ decay envelope, (where $x = \pi \Delta f \tau$; the dashed curve), and a cosine term. The decay envelope has zero amplitude values at integer multiples of $\frac{1}{\Delta f}$, the reciprocal of the sweep bandwidth, and oscillates within the decay envelope at a rate governed by the arguments of the cosine term. The portion of the autocorrelation between $-\frac{1}{\Delta f}$ and $\frac{1}{\Delta f}$ is defined as the major lobe and that portion outside these points as the

sidelobes. The sidelobes are undesired signal-generated noise since their form is signal-dependent, and, as we see from the synthetic example in Figure 4-2a, they resemble coherent noise which can dominate later arriving signals. Naturally, we want the sidelobes to be as small as possible so as not to obscure nearby and/or weaker signals.

The principle of SFU filtering is based on the fact that the sidelobes caused by strong direct waves may be the dominant coherent noise problem. If the direct wave can be cancelled in the pre-correlation domain, this source of correlation noise can be removed without attenuating the signal, so that the signal to noise ratio will be improved as shown in Figure 4-2b.

4.3 The SFU filter algorithm

Figure 4-3 shows the flow chart of the SFU algorithm. The squeezing and unsqueezing transformations are the fundamental components of SFU. Figure 4-4 illustrates their operation on a synthetic linear sweep. Firstly, a forward transformation linearly squeezes the portion of the trace from the beginning of the undesired signal (e.g. the direct wave) to the end of it (Fig. 4-4a), to turn the direct wave into a constant frequency signal (Fig. 4-4b). A suitable filter can then remove it. The resulting output of such a filter is not shown; instead we show that the inverse transformation (unsqueezing) successfully restores the original trace (Fig. 4-4c). Since vibroseis data are recorded with sources using both linear and non-linear sweeps, different approaches to the squeezing and unsqueezing transformations have been developed separately for each, and are discussed below.

4.3.1 Squeezing a linear sweep

Generally the vibroseis direct wave can be considered as a copy of the source sweep, which in this case takes the form of a sinusoidal linear up-sweep ranging from start frequency f_1 to end frequency f_2 , with a duration T , at a constant amplitude A , where:

$$s(t) = A \sin 2\pi(f_1 + Kt)t \quad (4-2)$$

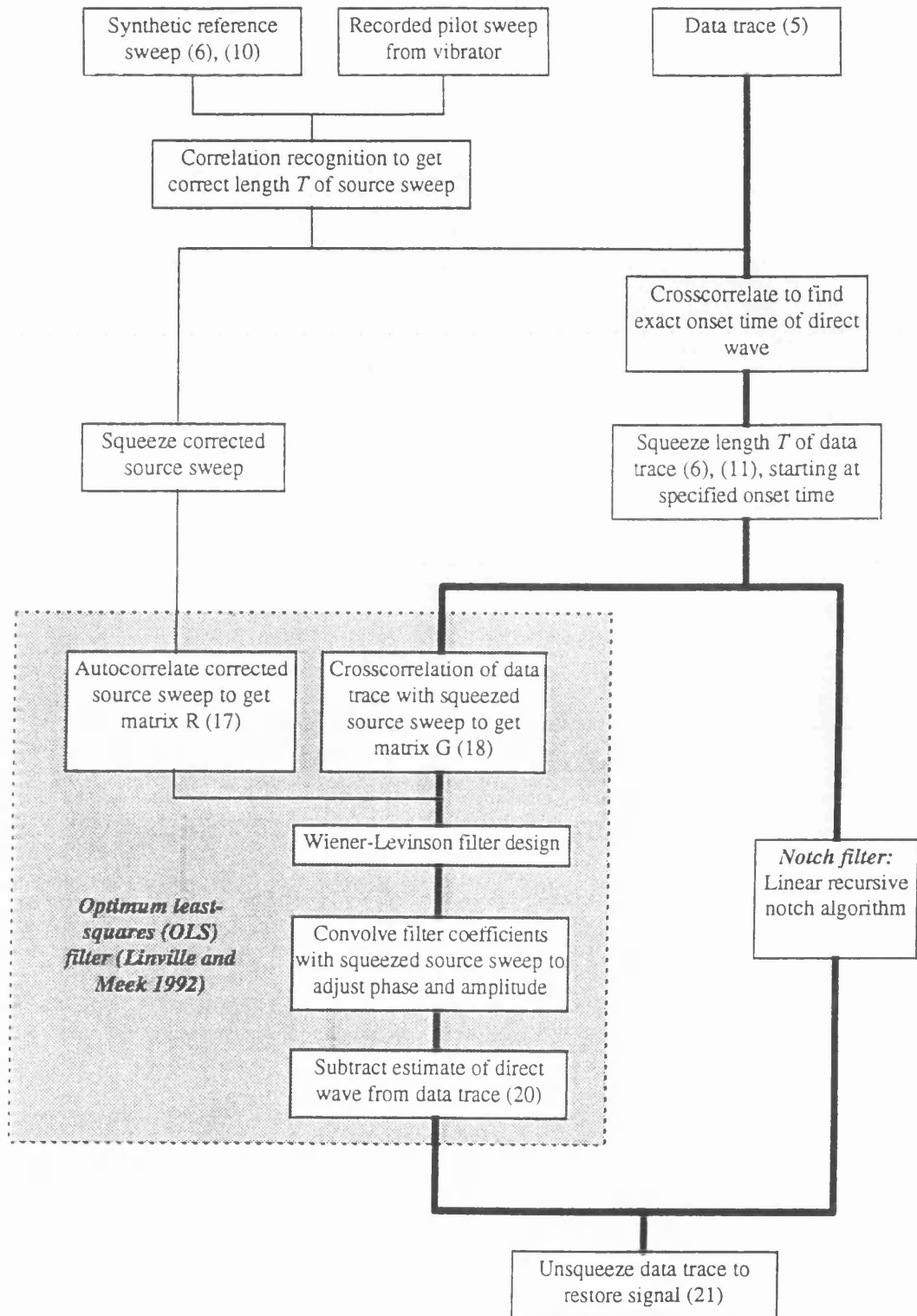


Fig. 4-3. Flow chart of the squeeze-filter-unsqueeze (SFU) filter algorithm. Equations in the text are referred to by the numbers within brackets. Heavy linking lines show trace data flow paths; light lines show reference sweep flow paths. Shaded area shows algorithm of Linville and Meek (1992).

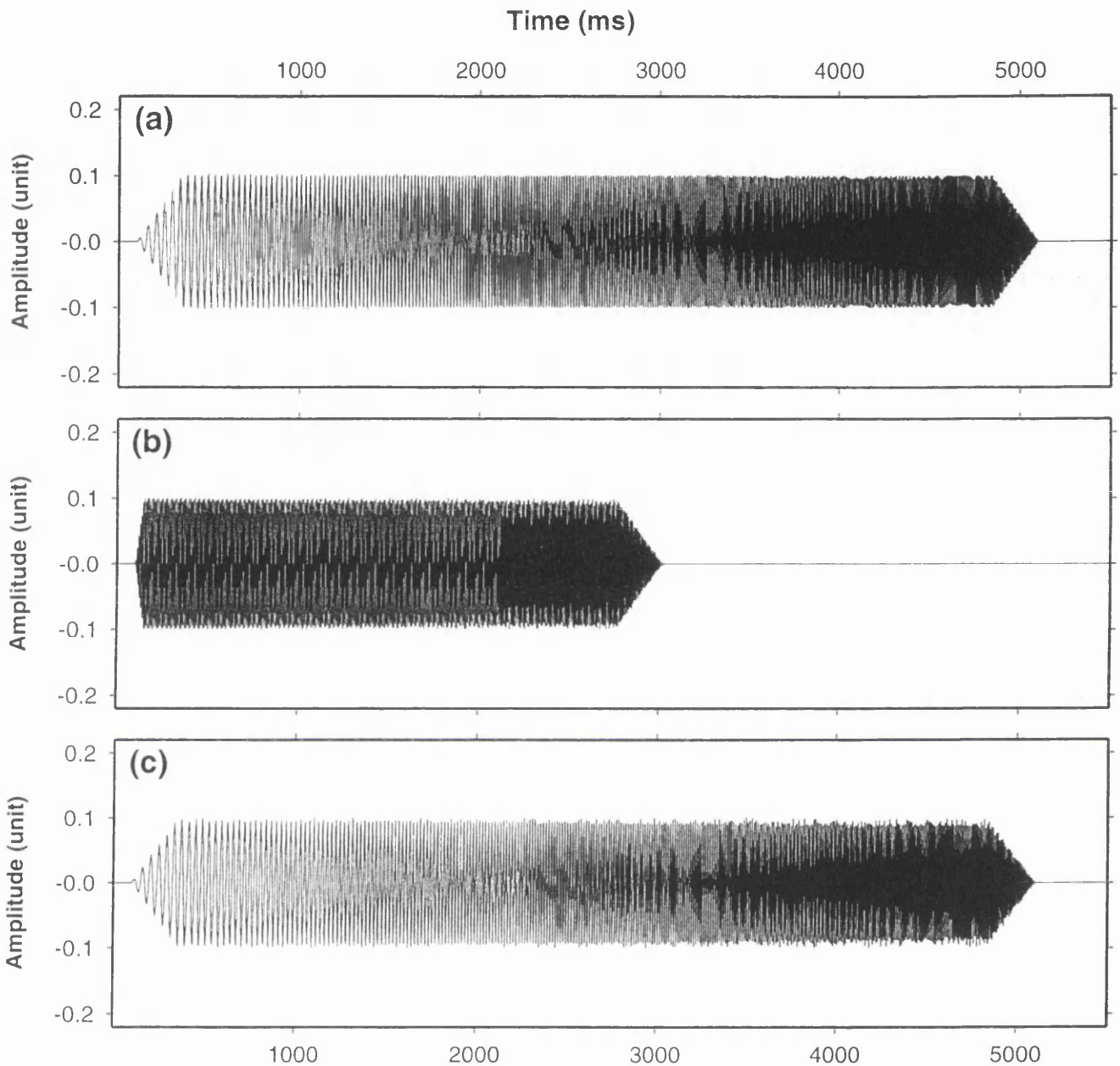


Fig. 4-4. Demonstration of the squeezing and unsqueezing of a sweep: (a) a linear sweep from 10 Hz to 60 Hz over 5 s; (b) squeezed to a constant 60 Hz, and (c) the unsqueezed (recovered) sweep from (b). Slight deformation of the waveform in the unsqueezed version (c) is caused by the operation of squeezing and unsqueezing transformations with linear interpolation.

$$K = \frac{f_2 - f_1}{2T} \quad (4-3)$$

Substituting equation 4-3 into 4-2, we get:

$$s(t) = A \sin \frac{\pi}{T} [2Tf_1 t + (f_2 - f_1)t^2]$$

We assume that the data trace $x(t)$ comprises the vibroseis direct wave $s(t)$ and signal $y(t)$, e.g. the reflections:

$$x(t) = s(t) + y(t) \quad (4-5)$$

The data trace after the squeezing transform should be:

$$\begin{aligned} x^1(t_1) &= S\{s(t) + y(t)\} = s^1(t_1) + y^1(t_1) \\ &= A \sin 2\pi f_0 t_1 + y^1(t_1) \end{aligned} \quad (4-6)$$

where S denotes the squeezing transform, $s^1(t_1)$ is the squeezed direct wave sweep with constant frequency f_0 , $y^1(t_1)$ is the squeezed version of $y(t)$, and

$$t_1 = \frac{[2Tf_1 + (f_2 - f_1)t]}{2Tf_0} \quad (4-7)$$

4.3.2 Squeezing a non-linear sweep

The vibroseis source sweep (and therefore the direct wave) may alternatively be defined as a sinusoidal non-linear upsweep ranging from start frequency f_1 to end frequency f_2 , with a duration T , at a constant amplitude A , where, for example:

$$s(t) = A \sin 2\pi(f_1 + K\sqrt{t})t \quad (4-8)$$

$$K = \frac{2(f_2 - f_1)}{3\sqrt{T}} \quad (4-9)$$

Substituting equation 4-9 into 4-8, we get

$$s(t) = A \sin \frac{2\pi}{T} [Tf_1 t + 2(f_2 - f_1)\sqrt{Tt^3}] \quad (4-10)$$

Similarly we obtain the data trace after the squeezing transform;

$$\begin{aligned} x^1(t_1) &= S\{s(t) + y(t)\} = s^1(t_1) + y^1(t_1) \\ &= A \sin 2\pi f_0 t_1 + y^1(t_1) \end{aligned} \quad (11)$$

where S denotes the squeezing transform, $s^1(t_1)$ is the squeezed direct wave sweep with constant frequency f_0 , $y^1(t_1)$ the squeezed version of $y(t)$, and

$$t_1 = \frac{[Tf_1 + 2(f_2 - f_1)\sqrt{Tt}]t}{Tf_0} \quad (4-12)$$

4.3.3 Filtering methods

In the following discussion, the squeezing transform is carried out by setting $f_0 = f_2$. In other words the uncorrelated direct wave signal is squeezed, to turn it into a constant sinusoidal signal with a frequency equal to the upper limit of the vibroseis source sweep; however, this particular choice of frequency is not an essential feature of the transformation.

In order to remove the squeezed constant frequency sweep $s^1(t_1)$, either a notch filter or an optimum least-squares (OLS) filter can be applied. In the application of a *notch filter*, a linear recursive notch algorithm is used to remove the narrow frequency band around the squeezed fiducial frequency $f = f_2$. The output trace sequence y_n^1 of the notch filter for an input trace sequence x_n^1 (Press 1989) is:

$$y_n^1 = \sum_{k=0}^M c_k x_{n-k} + \sum_{j=1}^N b_j y_{n-j} \quad (4-13)$$

In equation 4-13, the $M+1=3$ filter coefficients c_k and the $N=2$ coefficients b_k are used here in the form below, and are obtained from the response function:

$$c_0 = \frac{1 + f_2^2}{(1 + \theta f_2)^2 + f_2^2}$$

$$c_1 = -2 \frac{1 - f_2^2}{(1 + \theta f_2)^2 + f_2^2}$$

$$c_2 = \frac{1 + f_2^2}{(1 + \theta f_2)^2 + f_2^2}$$

$$b_1 = 2 \frac{1 - \theta f_2^2 - f_2^2}{(1 + \theta f_2)^2 + f_2^2}$$

$$b_2 = \frac{(1 - \theta f_2)^2 + f_2^2}{(1 + \theta f_2)^2 + f_2^2}$$

where the parameter θ is the desired width of the notch.

In the application of an OLS filter (Ensing 1983; Linville and Meek 1992) to remove the squeezed constant frequency signal from equations 4-6 and 4-11, the squeezed data trace

is assumed to comprise the useful signals caused by reflectivity and the squeezed vibroseis direct wave signal s_t^1 , which is defined as a sinusoidal noise at the frequency f_2 with a constant amplitude A and tapers on both ends.

The aim of the OLS filter is to find the optimum Wiener-Levinson filter coefficients, which are then used to adjust the amplitude and phase of a squeezed reference sweep to match those of squeezed direct wave sweep s_t^1 . When the onset time of the first arrival is accurately known, the squeezed synthetic reference sweep is defined as

$$h_t = \sin 2\pi \cdot f_2 t$$

where f_2 is the terminal frequency of vibroseis direct wave sweep. To match the amplitude of squeezed direct wave signal s_t^1 in the data trace x_t^1 , h_t must be adjusted by convolution with a filter v_t :

$$h_t^1 = v_t * h_t \quad (4-14)$$

Usually the direct wave amplitude in the data trace is larger than any other signal, and the least-squares error L between the direct wave and reference sweep is defined as (Wiener 1949; Yilmaz 1987):

$$L = \sum_t (s_t^1 - h_t^1)^2 \quad (4-15)$$

Substituting equation 4-14 into equation 4-15:

$$L = \sum_t \left(s_t^1 - \sum_t v_t h_{t-t} \right)^2$$

We wish to compute the filter coefficients (v_0, v_1, v_2, \dots) so that the error L is a minimum. Taking the partial derivatives of L with respect to the filter coefficients v_j and setting them equal to zero, we get:

$$\frac{\partial L}{\partial v_j} = -2 \sum_t s_t^1 h_{t-i} + 2 \sum_t \left(\sum_t v_t h_{t-t} \right) h_{t-j} = 0$$

or

$$\sum_t v_t \sum_t h_{t-t} h_{t-j} = \sum_t s_t^1 h_{t-j} \quad j = 0, 1, 2, \dots, (n-1). \quad (4-16)$$

By using

$$\sum_t h_{t-\tau} h_{t-j} = r_{j-\tau} = R \quad (4-17)$$

and

$$\sum_t s_t^1 h_{t-j} = g_j = G \quad (4-18)$$

equation 4-15 becomes

$$\begin{bmatrix} r_0 & r_1 & r_2 & \dots & r_{n-1} \\ r_1 & r_2 & r_3 & \dots & r_{n-2} \\ \cdot & \cdot & \cdot & \dots & \cdot \\ r_{n-1} & r_{n-2} & r_{n-3} & \dots & r_0 \end{bmatrix} \begin{bmatrix} v_0 \\ v_1 \\ \cdot \\ v_{n-1} \end{bmatrix} = \begin{bmatrix} g_0 \\ g_1 \\ \cdot \\ g_{n-1} \end{bmatrix} \quad (4-19)$$

This Toeplitz matrix can be solved rapidly using Levinson's recursion algorithm.

The data trace after the suppression of the direct wave is obtained by subtracting the corrected, squeezed and filtered synthetic sweep:

$$y_t^1 = s_t^1 - v_t * h_t \quad (4-20)$$

Due to the cyclic nature of the squeezed sweeps on both the recorded reference and on the data trace, a short filter length generally satisfies the requirement of the processing.

4.3.4 Unsqueezeing the filtered trace

After the direct wave has been removed, the inverse transformation is applied to unsqueeze linearly the squeezed portion $y^1(t)$ of the recorded data trace. This restores the signal deformed by the squeeze transformation. According to equations 4-5 and 4-6, the recovered data trace $y(t)$ becomes:

$$y(t) = S^{-1}\{y^1(t)\} = y^1(t_1) \quad (4-21)$$

where S^{-1} denotes the unsqueezeing transformation. For a linear sweep:

$$t_1 = \frac{\sqrt{T^2 f_1^2 + (f_2 - f_1)f_2 t} - T f_1}{f_2 - f_1}$$

and for a non-linear sweep, t_1 can be obtained by the corresponding squeeze transformation, since t_1 cannot be represented as an explicit function of t .

Figure 4-4 demonstrates the operation of the squeezing and unsqueezeing transformations without the intervening filter operation, to show that there is no distortion for a synthetic linear upsweep when the onset time of the sweep is known. When the pilot sweep cannot be described analytically, or it is otherwise impossible for it to be described as a function of time, we can still carry out the squeezing and unsqueezeing transformations directly by searching and picking the zero nodes on the recorded pilot sweep trace, without having to derive a transformation algorithm. This method can also be applied to vibroseis data recorded with a sweep describable analytically.

4.4 Implementation of SFU filtering

Because the squeezing and unsqueezing transformations of SFU must be performed from the start of the uncorrelated first break, the exact onset time of this unwanted signal must be determined. Due to static delays, the onset time of the direct wave usually varies from trace to trace in a somewhat irregular way - it cannot be specified simply as a function of headwave velocity and offset. To circumvent this problem, an automatic method based on crosscorrelation analysis has been developed to find the actual start time. The method is summarised in the flow chart of Figure 4-5. A synthetic sweep defines the start and end time of the recorded pilot sweep from the vibrator to correct the sweep length T . We then correlate the corrected reference source sweep with each data trace individually to determine the onset time of the direct wave for that data trace.

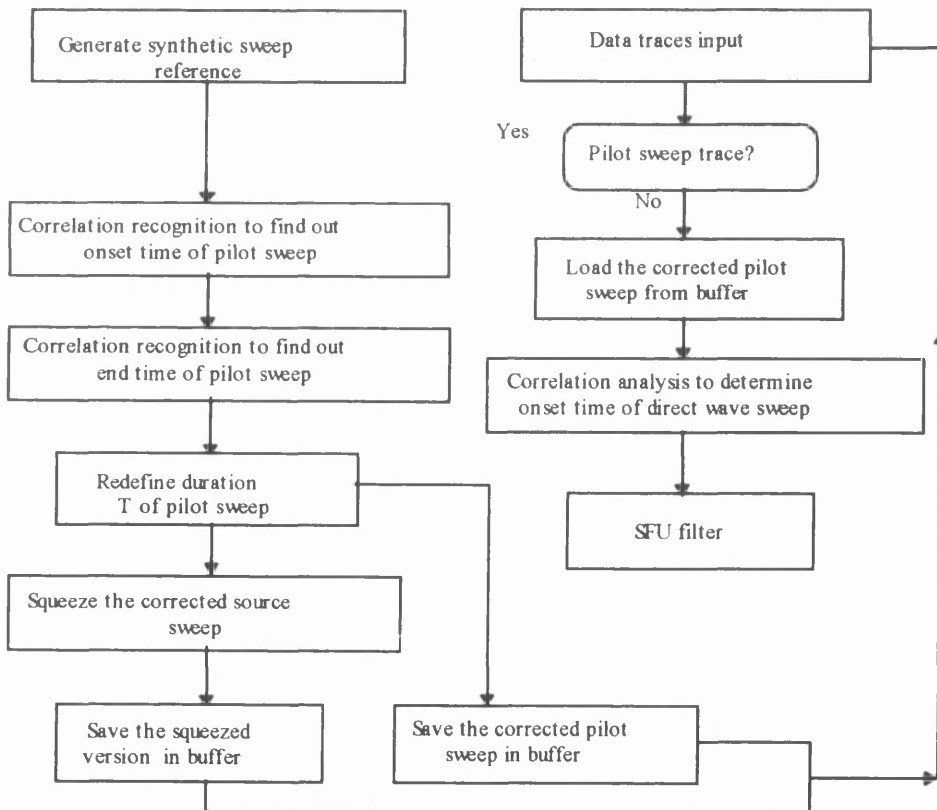


Fig. 4-5. Flow chart of the automatic method used to determine the onset time of the direct wave sweep in the SFU filter.

Deformation of the waveform has been caused to a certain extent by the simple linear interpolation used in the squeezing procedure, as shown in Figure 4-4. To minimise the distortion of the waveform, a 4-point cubic spline interpolation must be applied in association with the squeezing and unsqueezing transformations. The interpolation process is divided into two stages:

- (1) Fit an interpolation function to the data at the 4 sampling points provided.
- (2) Evaluate that interpolating function at the new target sampling time t . By comparing the unsqueezed version using linear interpolation (Figure 4-4c), with the 4-point cubic spline interpolation (Figure 4-6c), it can be seen that the latter method avoids the distortion inherent in the linear interpolation method.

In a similar way, the squeezing and unsqueezing transformation can be operated in reverse order to obtain a transformed sinusoidal sweep at any desired stationary frequency point, as shown in Figure 4-7. It is helpful to consider or analyse the pre-squeezed frequency bandwidth in order to apply various filters in the frequency domain. When using SFU with the notch algorithm, we should more carefully determine the frequency at which to remove the direct wave in the pre-correlation domain, as there always exists a narrow frequency band around the squeezed fiducial frequency point. This means that not only the direct wave will be removed, but also the other nearby signals would be attenuated during the processing.

4.5 Synthetic examples

In this section, two examples are presented to illustrate and evaluate SFU. The synthetic upsweep representing the direct wave ranges from 10 to 60 Hz, 5 s duration, with amplitude of 0.1 (arbitrary units) and with 0.5 s linear tapers on both ends (Figs. 4-8a, 4-9a). All records are displayed with the same gain for comparison. Six seconds of data were generated at a sample interval of 2 ms.

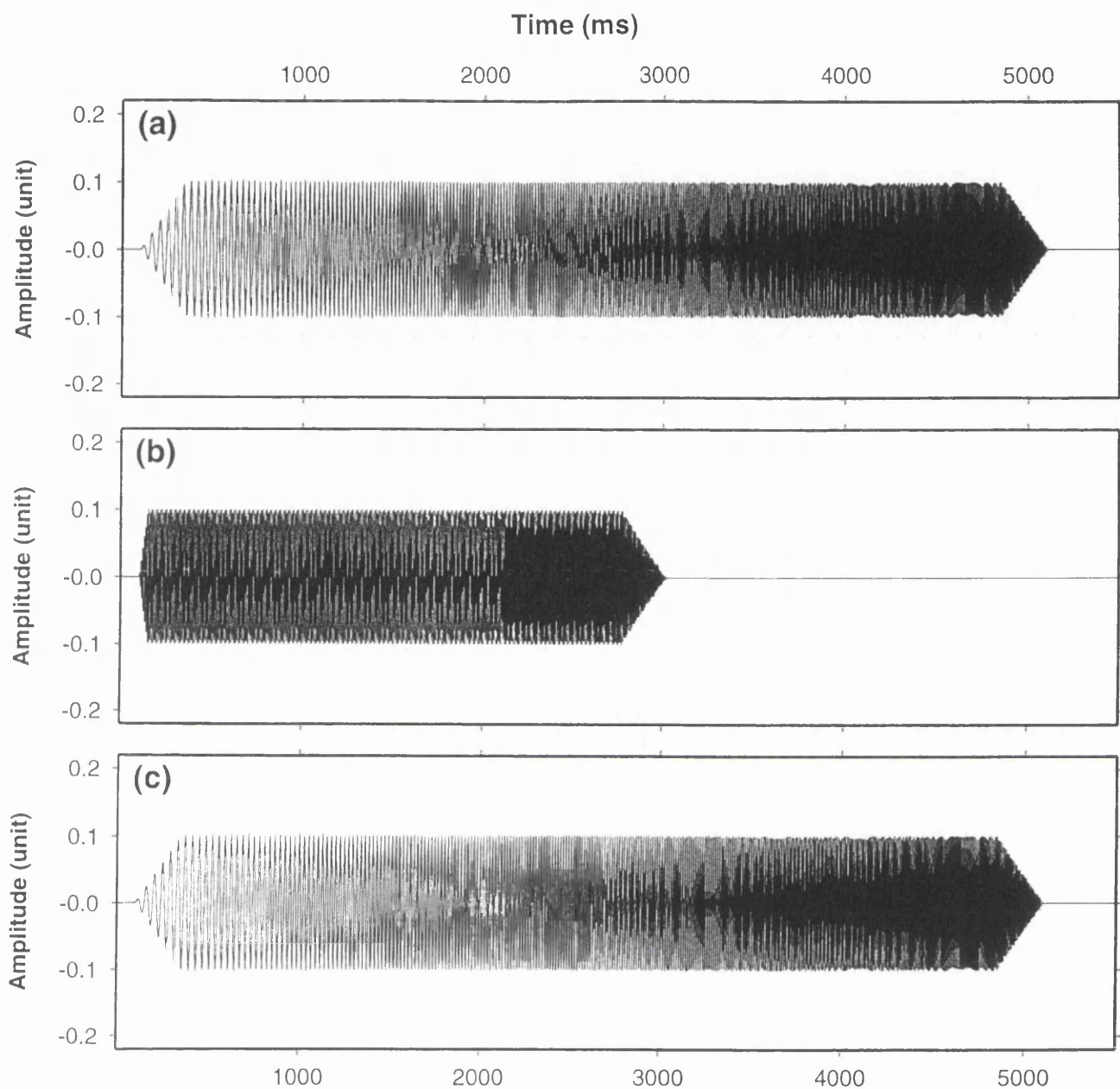


Fig. 4-6. Demonstration of squeezing and unsqueezing transformations using 4-point cubic spline interpolation resulting in no distortion. (a) is the same synthetic linear upswEEP as in Figure 4-4a, from 10 to 60 Hz over 10 s, (b) is the squeezed version, and (c) is the unsqueezed version.

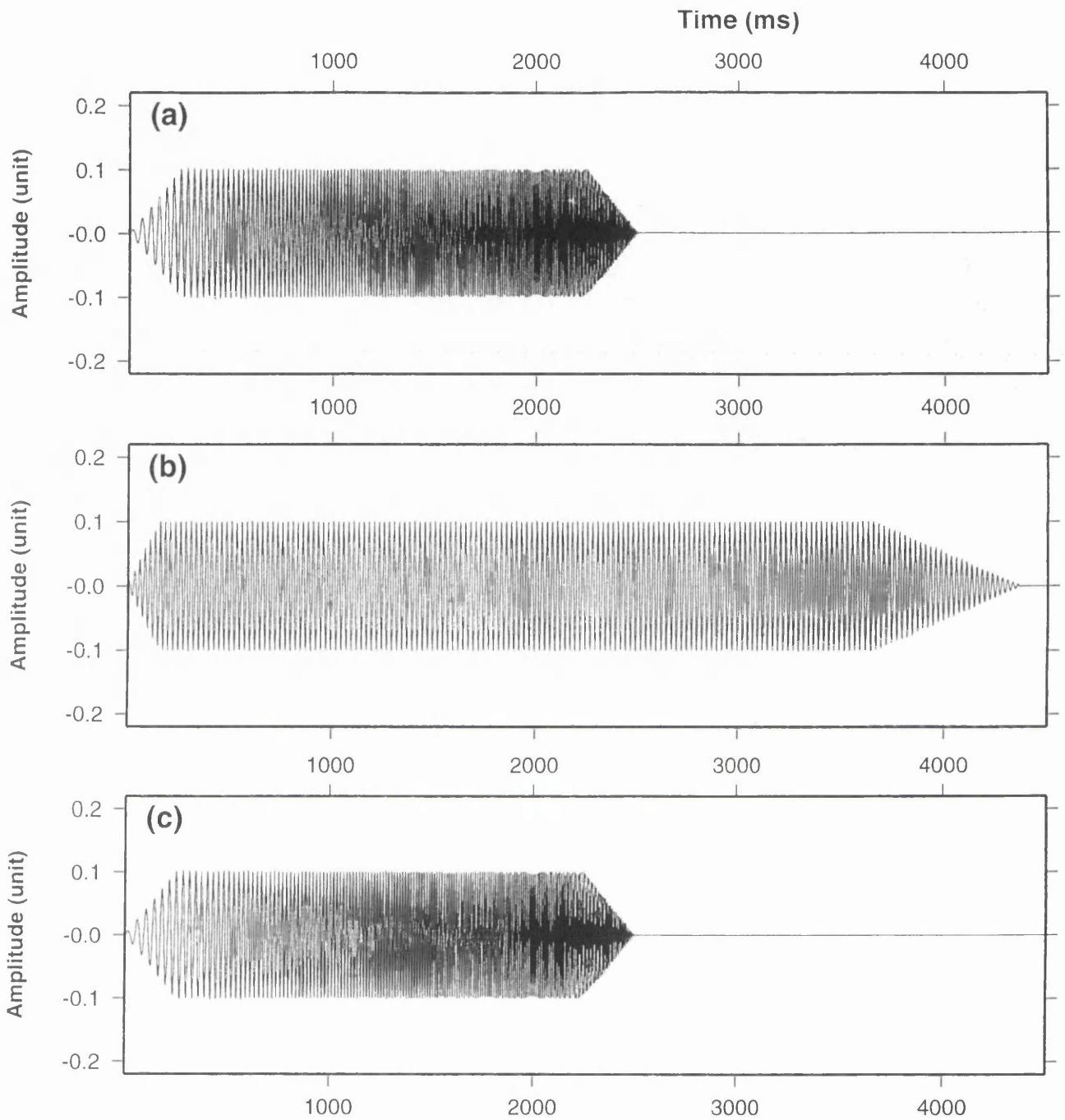


Fig 4-7. A synthetic linear up-sweep (a) from 10 to 60 Hz over 2.5 s is stretched (unsqueezed) into a 30 Hz stationary frequency signal (b), then squeezed back into version (c), which is the same as the original one (a).

In the first example, an uncorrelated reflection event is generated using the same up-sweep as the direct wave, with the same amplitude of 0.1, but delayed by 1 s, as shown in Figure 4-8b. The synthetic seismogram is the superimposition of the direct wave and this reflection signal (Fig. 4-8c). We then apply SFU to this synthetic trace in two different ways, producing the filtered records shown in Figures 4-8d and 4-8e. Figure 4-8d is the output of SFU with the application of an optimum least-squares (OLS) filter, and Figure 4-8e is the output of the SFU with the application of a linear recursive notch filter. The correlated versions both before and after the application of SFU are shown in Figure 4-8f and 4-8g respectively. SFU has effectively removed the uncorrelated direct wave from the synthetic trace. However, this example is a somewhat limited test, in that the two events (Figs. 4-8a and b) are well separated in time and of equal amplitude.

We show next a more stringent test in which the two signals are very close together, and in which the desired signal is also much smaller than the undesired signal. Figure 4-9 shows the same uncorrelated direct wave (Fig 4-9a), but with a ten times smaller amplitude for the reflection (Fig. 4-9b) than that in Figure 4-8b. The reflection event is only 100 ms behind the undesired direct wave. These two events are summed to give the synthetic trace (Fig. 4-9c). Application of SFU successfully removes the uncorrelated direct wave, whichever of the two methods of applying it is used. Figure 4-9d shows the output of SFU with the OLS filter, and Figure 4-9e shows the output of SFU using the notch filter. The significant improvement in signal to noise ratio is illustrated by the comparison of the correlated versions before and after the removal of the direct wave (Figure 4-9f and g respectively). The strong direct wave has been removed in the pre-correlation domain without attenuating the nearby signal. The example in Figure 4-2 also shows that the weaker signals obscured by far-correlation noise can be much improved after filtering in the pre-correlation domain.

4.6 Field data example

This section shows two field examples, with a linear and a non-linear sweep respectively. The first example shows SFU with the stationary sinusoidal noise cancelling algorithm applied to a shot gather recorded with a linear sweep source, acquired in a crustal seismic

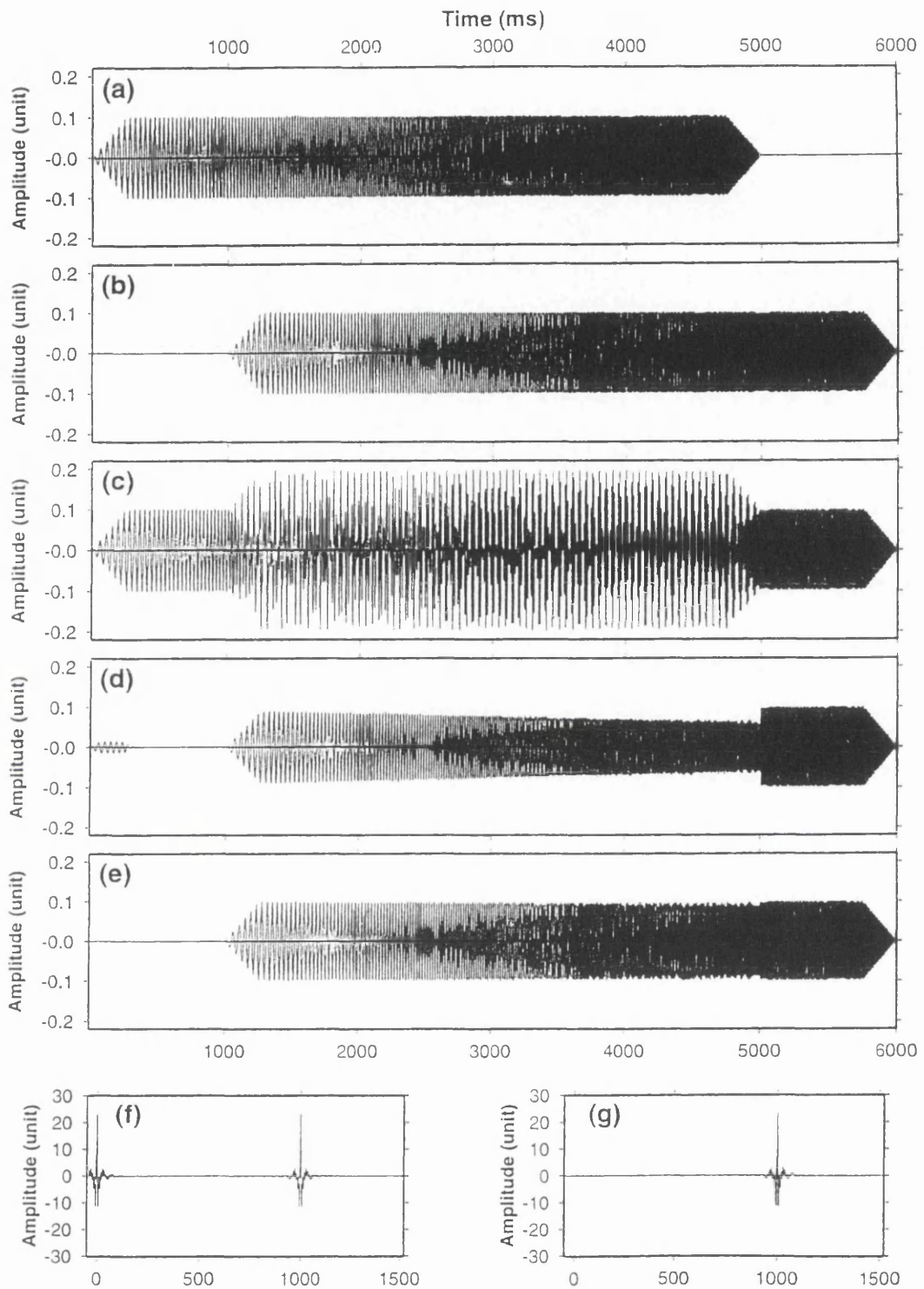


Fig. 4-8. Synthetic trace made up of (a) direct arrival at time 0 ms, amplitude 0.1 unit, and (b) reflection arriving at 1000 ms, amplitude 0.1, giving (c) recorded trace. The direct wave is removed by application of either (d) an optimum least-square filtering algorithm, or (e) a linear recursive notch algorithm. The correlated trace is shown (f) before application of SFU, and (g) after application of SFU.

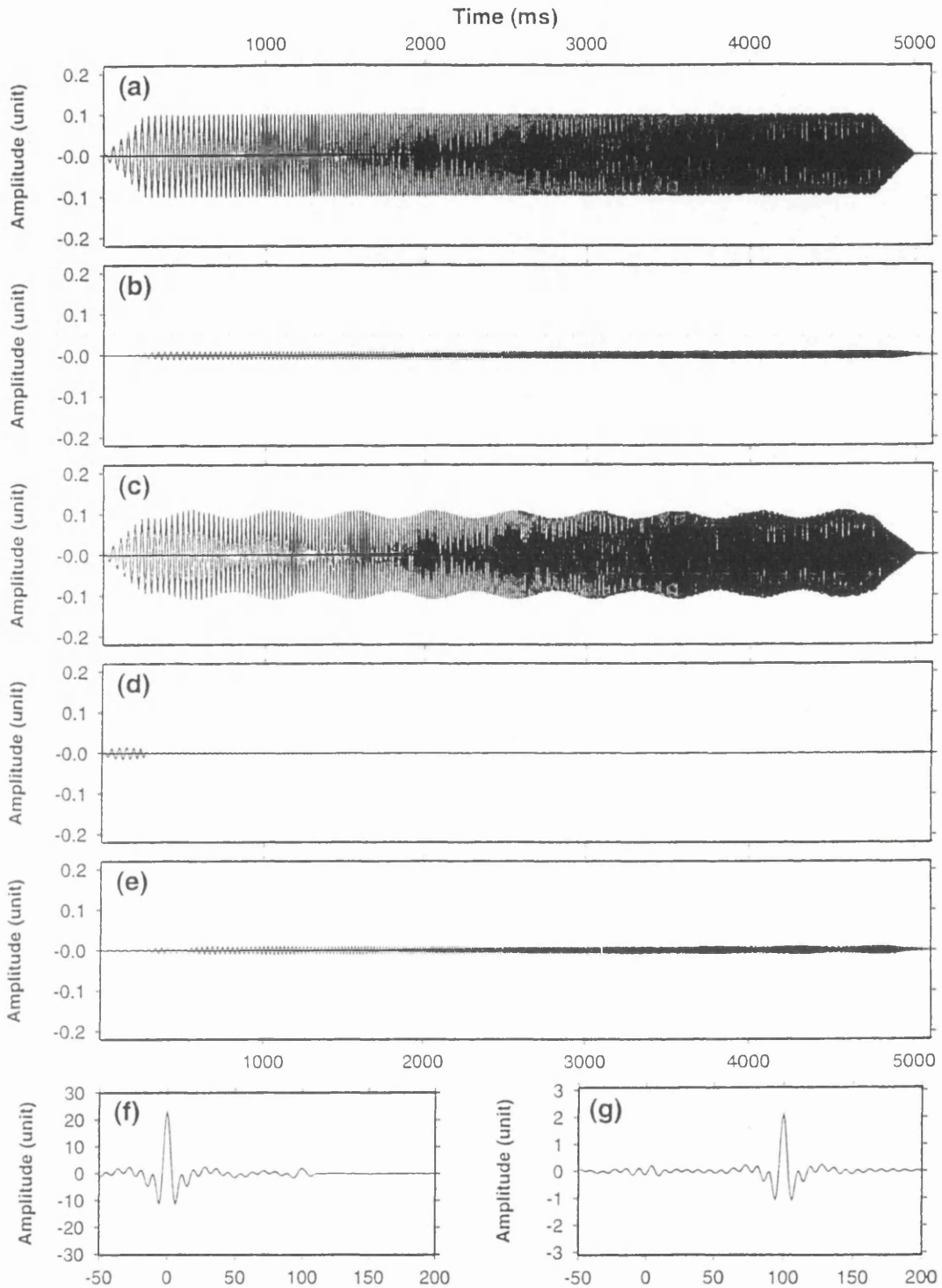


Fig. 4-9. Synthetic trace made up of (a) direct arrival at time 0 ms, amplitude 0.1 unit, and (b) reflection arriving at 100 ms, amplitude 0.01, giving (c) recorded trace. The direct wave is removed by application of either (d) an optimum least-square filtering algorithm, or (e) a linear recursive notch algorithm. The correlated trace is shown (f) before application of SFU, and (g) after application of SFU.

reflection profile in the Kola Peninsula, Russia in 1992 (Smythe *et al.* 1994). The reflection data shown here are the 90 vertical component channels; the 180 other channels per shot, not shown here, recorded the two horizontal components. The source is a 20 s upsweep ranging from 10 Hz to 60 Hz, with 0.5s linear tapers on each end. Both gathers are displayed with the same AGC window of 1 s for comparison purposes.

The unfiltered correlated shot gather is shown in Figure 4-10a. The 90 trace record is highly contaminated by mechanical sources near the Kola superdeep well, particularly on the channels to the right of the gather. The direct wave arrives between 0.3 and 0.9 s. The filtered output is shown in Figure 4-10b. Correlation analysis was used to pick automatically the onset time of the uncorrelated direct wave. SFU has done a good job of cancelling the first arrivals in the pre-correlation domain, so that the amplitude of any correlation noise will be reduced to less than the amplitude of the genuine correlation signals from weak reflections. As mentioned above, the direct wave is removed without attenuating signal near the first arrivals. If, after the application of the filter, some trace of the first arrivals remains, it usually indicates that the onset time of sweep is not precisely determined enough for SFU to work properly.

The second example is a split-spread shot gather using a non-linear sweep source, with frequency ranging from 20 Hz to 120 Hz over 7 s, acquired over the Serpent Mound structure in Ohio, USA. The direct wave is much stronger than that in the first example. Figure 4-11a is the correlated shot gather without application of SFU. Figure 4-11b show the correlated outputs of SFU for the same shot gather as in Figure 4-11a. The filtered version has a much better signal to noise ratio, particularly in the shallow part of the section. This improvement is due to the fact that SFU suppresses the direct wave without having any adverse effect on the signal.

Figure 4-12 illustrates a comparison of the filtered CDP stack version with the unfiltered version. To emphasis the relative amplitude the plot are made only with variable area trace plotting. Comparing the result obtained after applying the SFU filter in Figure 4-12b with that by applying only the orthodox CDP processing routines, one can see some improvement in the processed version. There is an improvement in the major horizontal

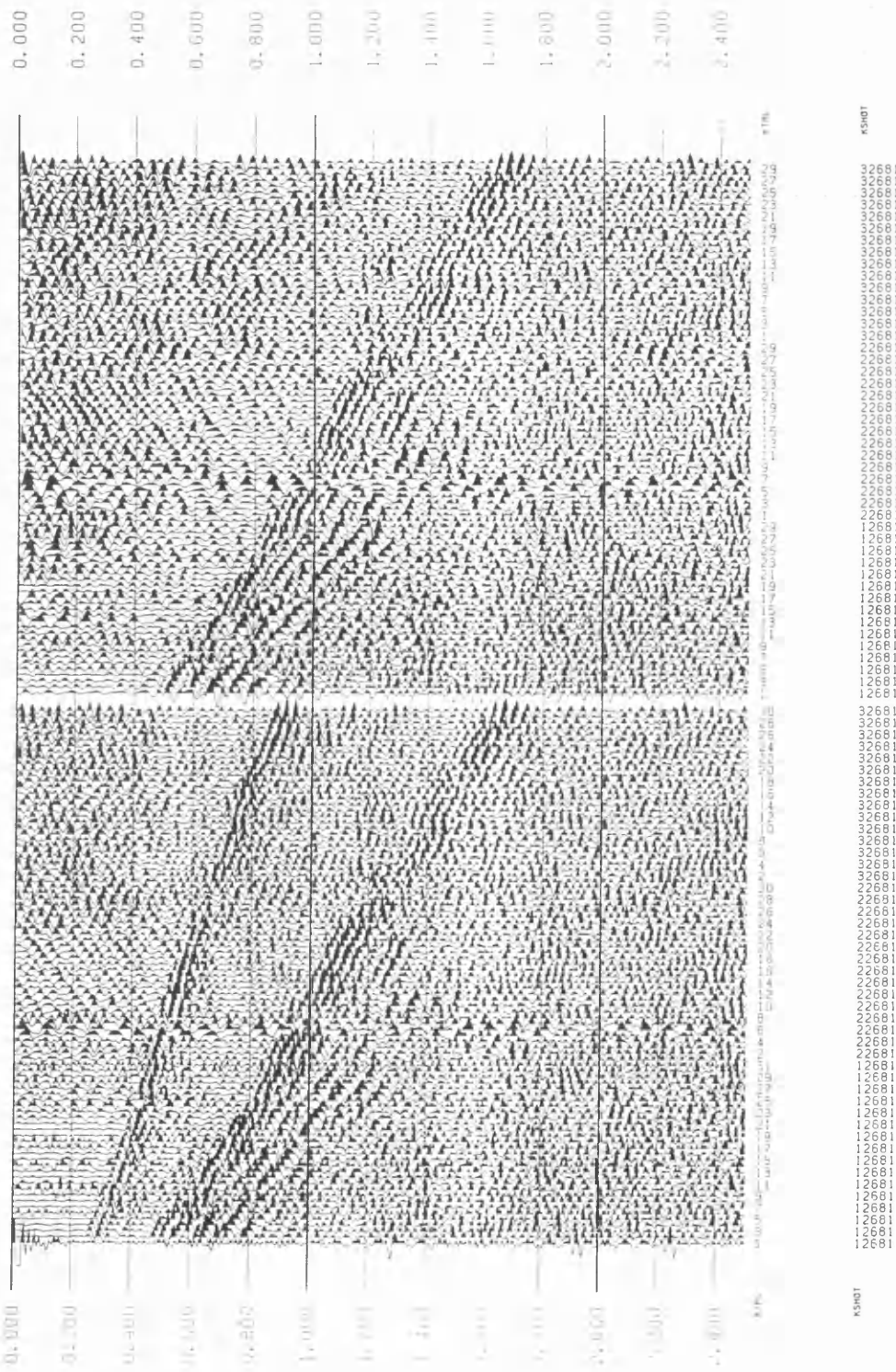


Fig. 4-10. Correlated raw shot gather from Kola; linear sweep, 10-60 Hz over 20 s. Left: before SFU and right: after SFU to remove first arrival. Same exponential gain applied to both panels. Trace interval 50 m. Vertical scale in seconds.

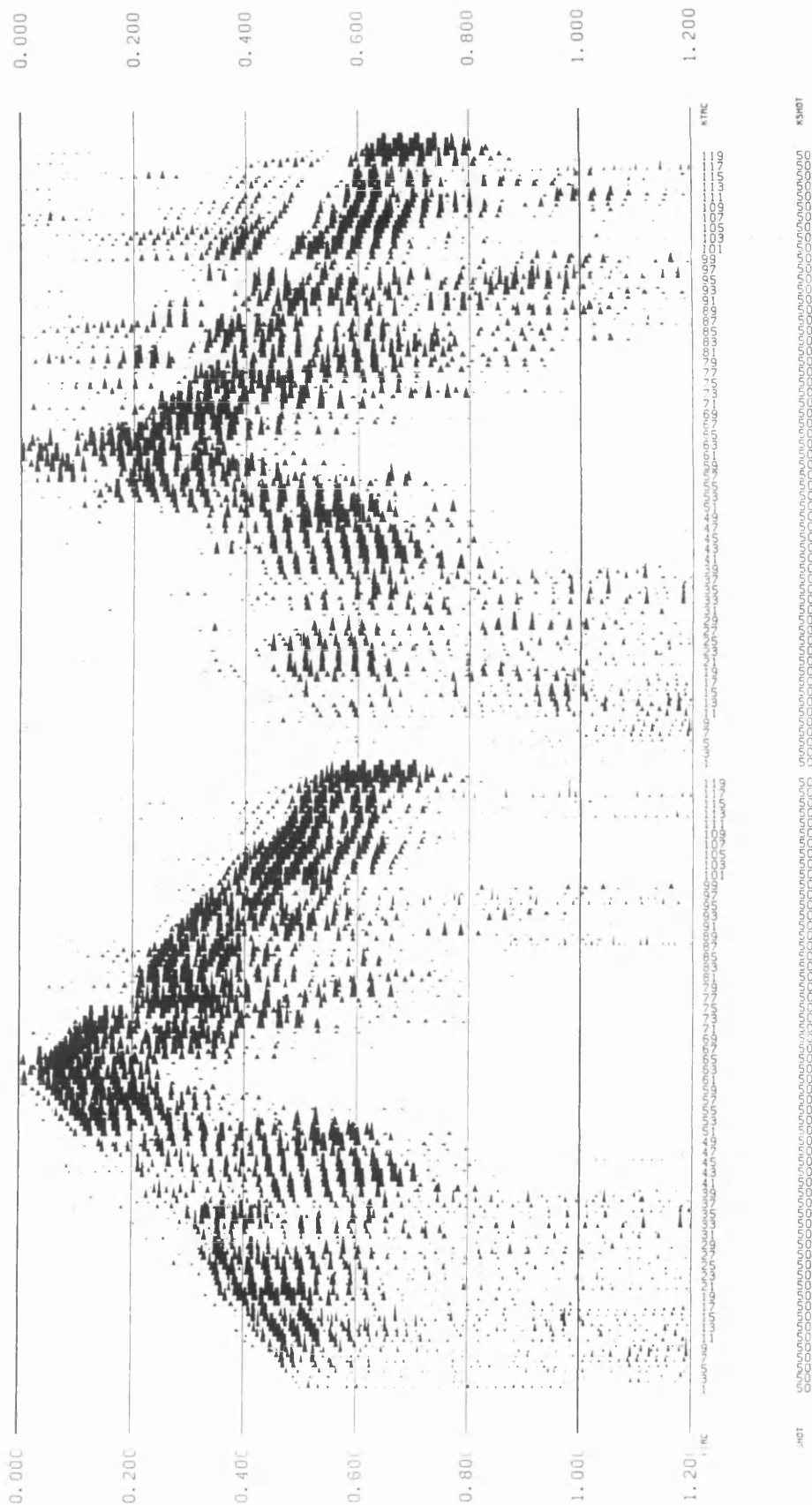


Fig. 4-11. Correlated raw shot gather from Ohio: non-linear sweep, 20-120 Hz over 7 s. Left: before SFU and right: after SFU to remove first arrival. Same exponential gain applied to both panels. Trace interval 33 m. Vertical scale in seconds.

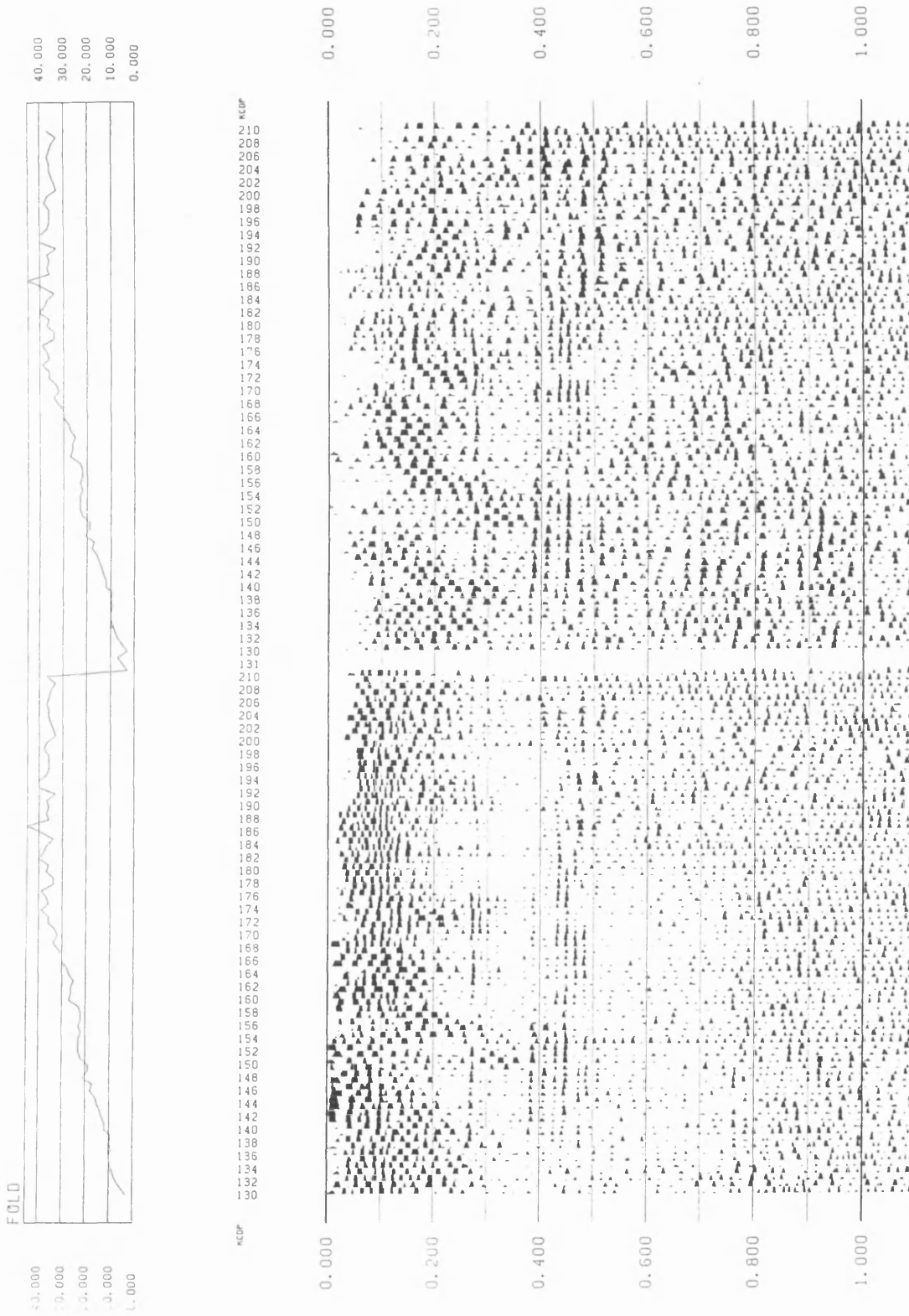


Fig. 4-12. Comparison of the Ohio stack section portion, (a) before SFU filtering, and (b) after SFU filtering, both with an AGC of 500 ms. Trace interval 33 m. Vertical scale in seconds.

reflection between 400 ms and 500 ms, and dipping reflection events can be seen in the shallow section above 200 ms, between CDPs 150 and 186, after the strong direct wave is attenuated. In the deeper area of between the 500 ms to 1000 ms. the relative amplitude of the signal is improved, so that the events near 900 ms between CDPs 140 and 154 can be extracted.

4.7 Discussion

This section is a discussion of the problems and difficulties in the SFU filter design associated with the notch filter and with the optimum least-squares (OLS) algorithm.

4.7.1 Limitations of the notch and optimum least-squares algorithms

The notch algorithm is one of the most frequently used routines in seismic data processing worldwide. It is easy to use and can effectively attenuate any undesired stationary sinusoidal frequency component from data. Unfortunately this algorithm also attenuates all signals at the notch frequency, as well as at frequencies around the notch point. Figure 4-13a show a 40 Hz sinusoidal signal mixed with a linear sweep from 10 Hz to 60 Hz. Figure 4-13b shows the resultant rather distorted sweep after a 40 Hz notch filter has been used. The notch algorithm removes any signal at and near the frequency notch point, regardless of the overall signal characteristics.

The least-squares filtering algorithm is optimally designed to provide the least amount of prediction error, and can provide much better attenuation of an undesired stationary sinusoidal signal, without notching the desired signal as well around the notch point. Figure 4-13c shows that the original sweep is restored with very little distortion after applying the least-squares filtering algorithm. However, it requires more computer time than simple notch filtering, usually taking five to seven times longer. Another limitation is that the frequency of the undesired stationary sinusoidal signal must be known exactly.

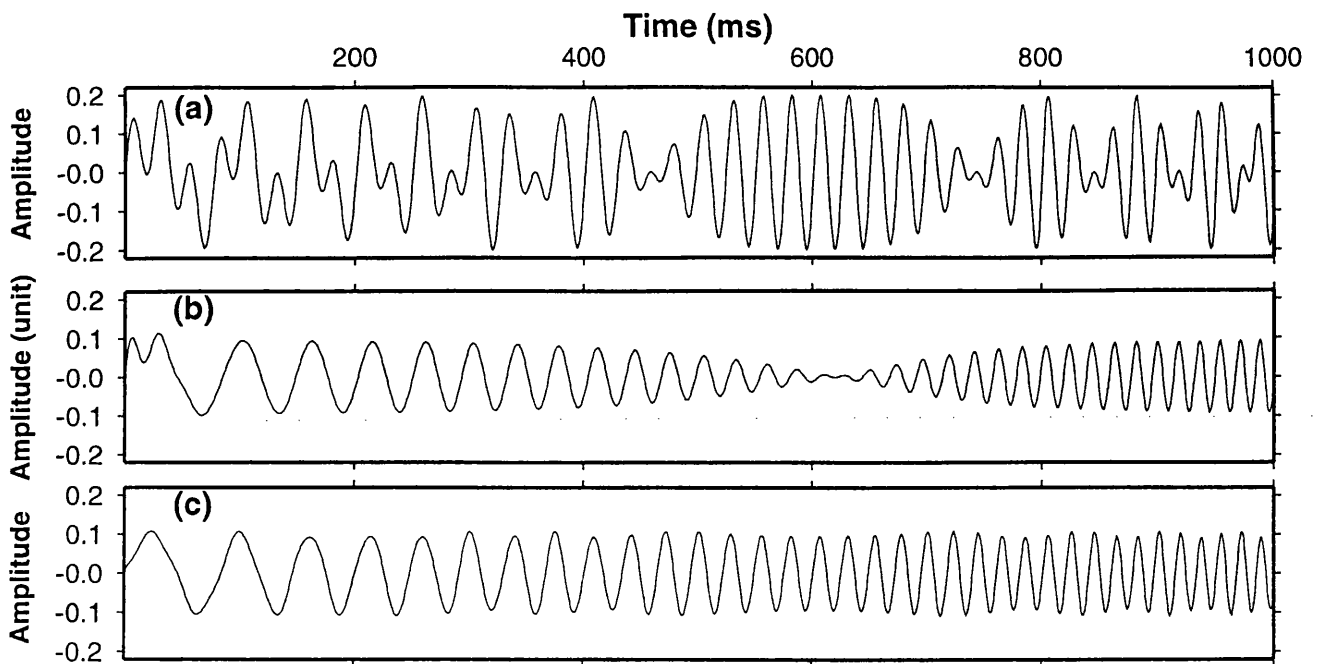


Fig. 4-13. Comparison of two algorithms to be used in SFU: (a) the upsweep contaminated by 40 Hz noise before SFU filtering; (b) after SFU filtering with the linear recursive notch algorithm; (c) after SFU filtering with the optimum least-squares algorithm.

4.7.2 Comparison of the notch and optimum least-squares (OLS) algorithms in SFU.

So far we have learned that both the notch and optimum least-square algorithms have some disadvantages and limitations respectively. What will happen when they are applied in SFU filtering and how we should make the correct choice between both? To discuss these problems, Figure 4-14 presents the correlated versions corresponding to the numerical example in Figures 4-8d and e. The unfiltered version is shown in Figure 4-14a with the direct wave at zero time and a reflection at 1000 ms. In this example, the reflection event is far away from the direct wave and the amplitude of the event is strong enough to be easily identified. Comparing the filtered versions in Figures 4-14b and c, there is no significant difference between them, except for the smaller amplitudes in the version filtered with the notch algorithm, and the fact that the SFU version (Fig. 14-4b) is slightly asymmetric. Despite the fact that the amplitude of the non-correlated reflection is

distorted near the merge point after SFU filtering with the notch algorithm as shown in Figure 4-8d, both algorithms seem to work well for data with strong reflections.

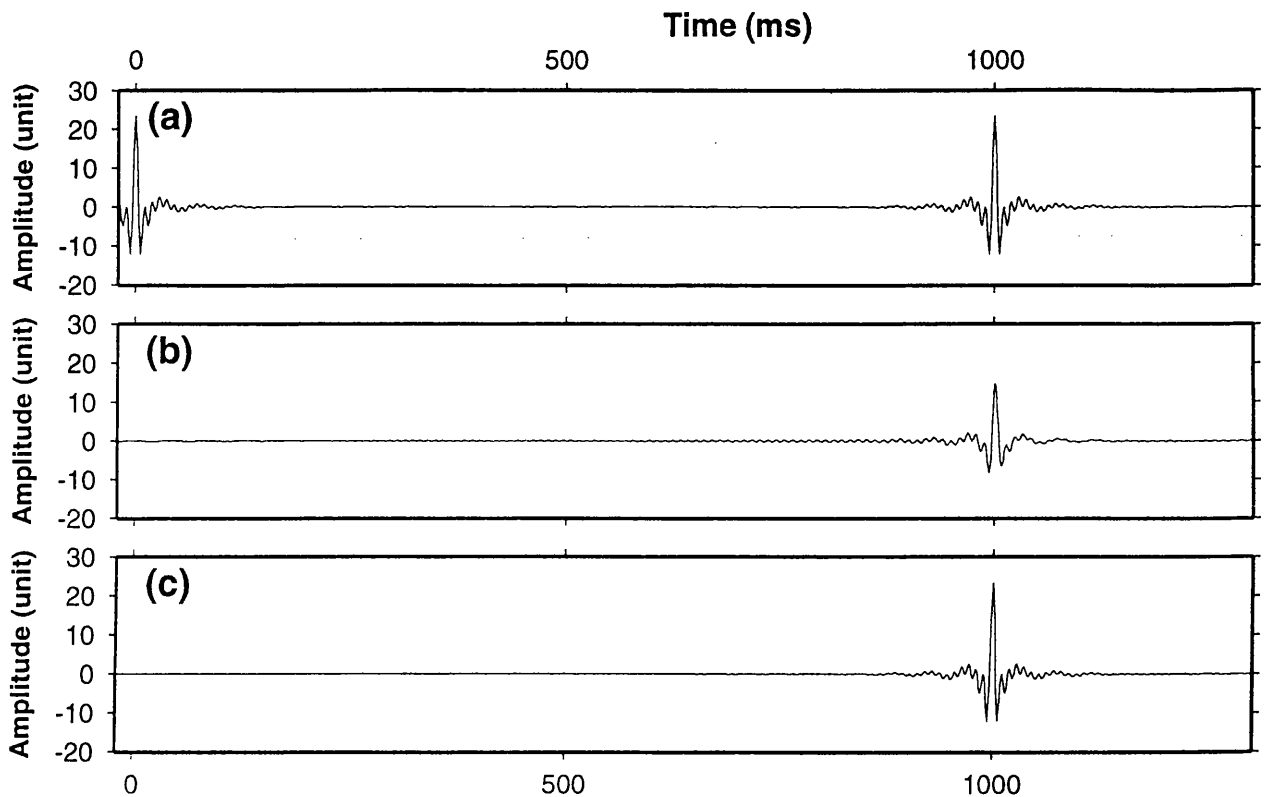


Fig. 4-14. Comparison of the SFU filter with two different algorithms: (a) the correlogram without SFU; (b) after SFU filtering with linear recursive notch algorithm; (c) after SFU filtering with the optimum least-square (OLS) algorithm.

For the case where the amplitude of the desired reflection is much smaller than that of direct wave and also close to the direct wave, as in the example shown in Figure 4-9 above, comparison of the correlated versions is presented in Figure 4-15. Note that the reflection event at 100 ms is almost overwhelmed by the correlation sidelobes of the strong direct wave, leading to low seismic resolution on the vibroseis correlogram. Although the SFU filtered versions, whether filtered with the notch or OLS algorithms, both achieve considerable improvement in the signal to noise ratio for the primary reflection, this does not mean that the improvements are of the same quality. Figure 4-15b show a slight delay of the reflection event, which is now also mixed phase, associated with the harmonic from the start time. The absolute amplitude of the reflection after SFU with

the notch algorithm is much smaller than that using the OLS algorithm, because of the attenuation of the signals near the notch frequency point. Refer also to the respective uncorrelated versions in Figures 4-9d and e.

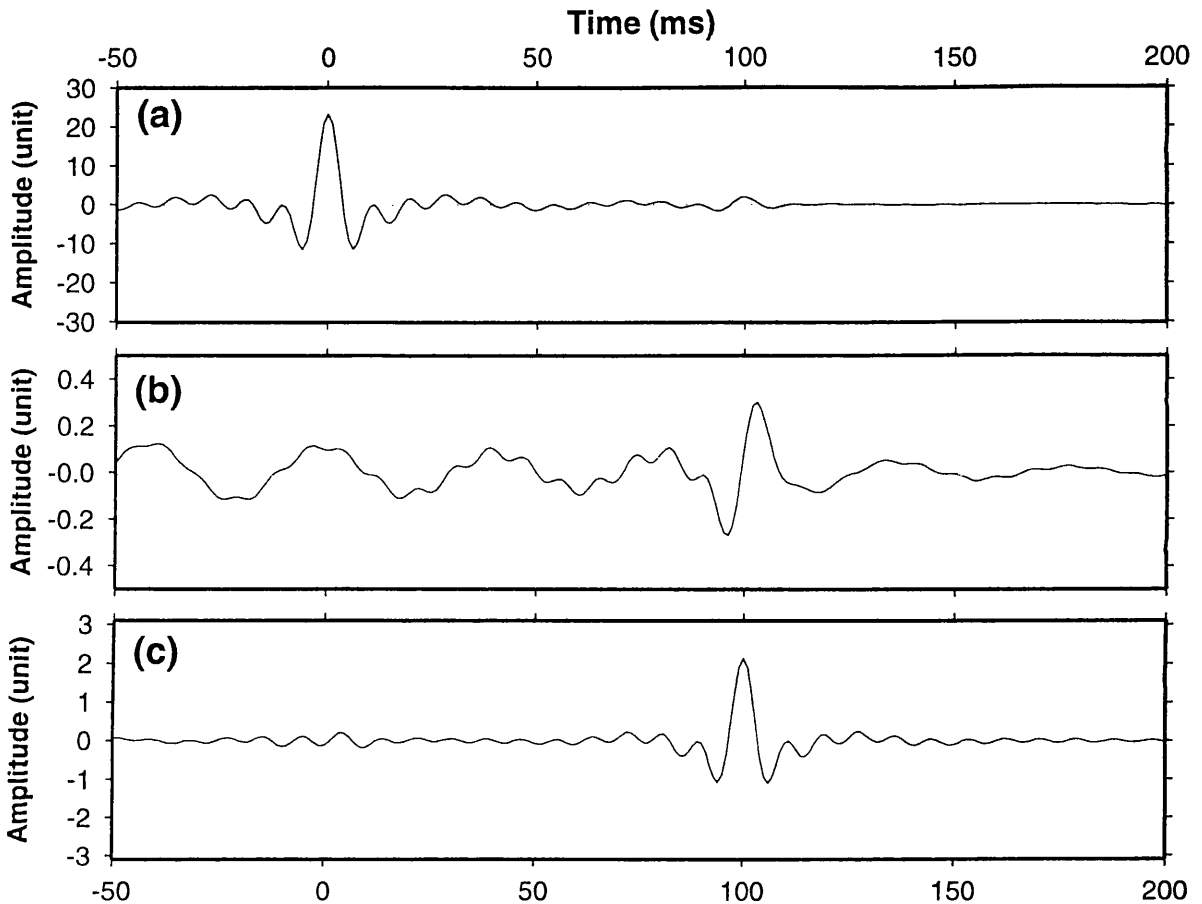


Fig. 4-15. (a) Correlogram before SFU filtering; (b) after SFU filtering with linear recursive notch algorithm; (c) after SFU filtering with the optimum least-squares (OLS) algorithm.

Based on this numerical experiment and analysis, the SFU filter with the OLS algorithm is strongly recommended if the squeezing and unsqueezing transformations are to operate properly. This necessitates that the onset time of the direct wave sweep is known. Otherwise the frequency will shift away from the desired frequency point in the squeezed version, violating the assumption for the OLS algorithm that the frequency of the undesired stationary sinusoidal signal must be known exactly. In practice, we are unlikely

to ensure that the onset time of direct wave sweep can be determined without any error in the pre-correlation domain.

In conclusion, as these assessments are dictated by the signal to noise ratio, the choice of which algorithm should be used in SFU is dependent upon the balance of the benefits desired:

- (1) SFU with the notch algorithm is more tolerant of the slight frequency shift caused by estimating the onset time of direct wave sweep with error, whereas
- (2) SFU with the OLS algorithm can extract the weak signals with less distortion. The OLS algorithm is discussed further in Chapter 5.

4.7.3 Filter design in SFU

With regard to the real data by conventional vibroseis techniques, one of the practical difficulties we encounter is the taper problem at each end of direct wave sweep when computing the filter coefficients in the OLS algorithm. Since a reduction of the sidelobe noise can be achieved in the field by tapering the amplitude of the vibrator pilot sweep, the sweep tapering technique has become routine since the early 1960s.

If the tapers of the source sweep are precisely known, SFU with the OLS filter causes less distortion of the uncorrelated reflection than with the notch filter. But when the tapers of the reference sweep do not accurately match those of the direct wave, for whatever reason, we find that harmonic noise results. To illustrate this problem, a synthetic linear upsweep of 10 Hz to 60 Hz over 3000 ms with linear tapers of 500 ms on both ends is generated as a synthetic direct wave, which is subsequently squeezed into an undesired 60 Hz stationary sinusoidal signal by the squeeze (Figure 4-16a). Note that the tapers on both ends still remain linear, but the one at the low frequency end is shorter after squeezing than the other taper at the high end. If a reference sweep with no tapers (Fig. 4-16b) is used to design the OLS filter, a harmonic will be introduced into filtered version, as shown in Figure 4-16d. The unmatched tapers in the filter design lead to the heavy distortion of

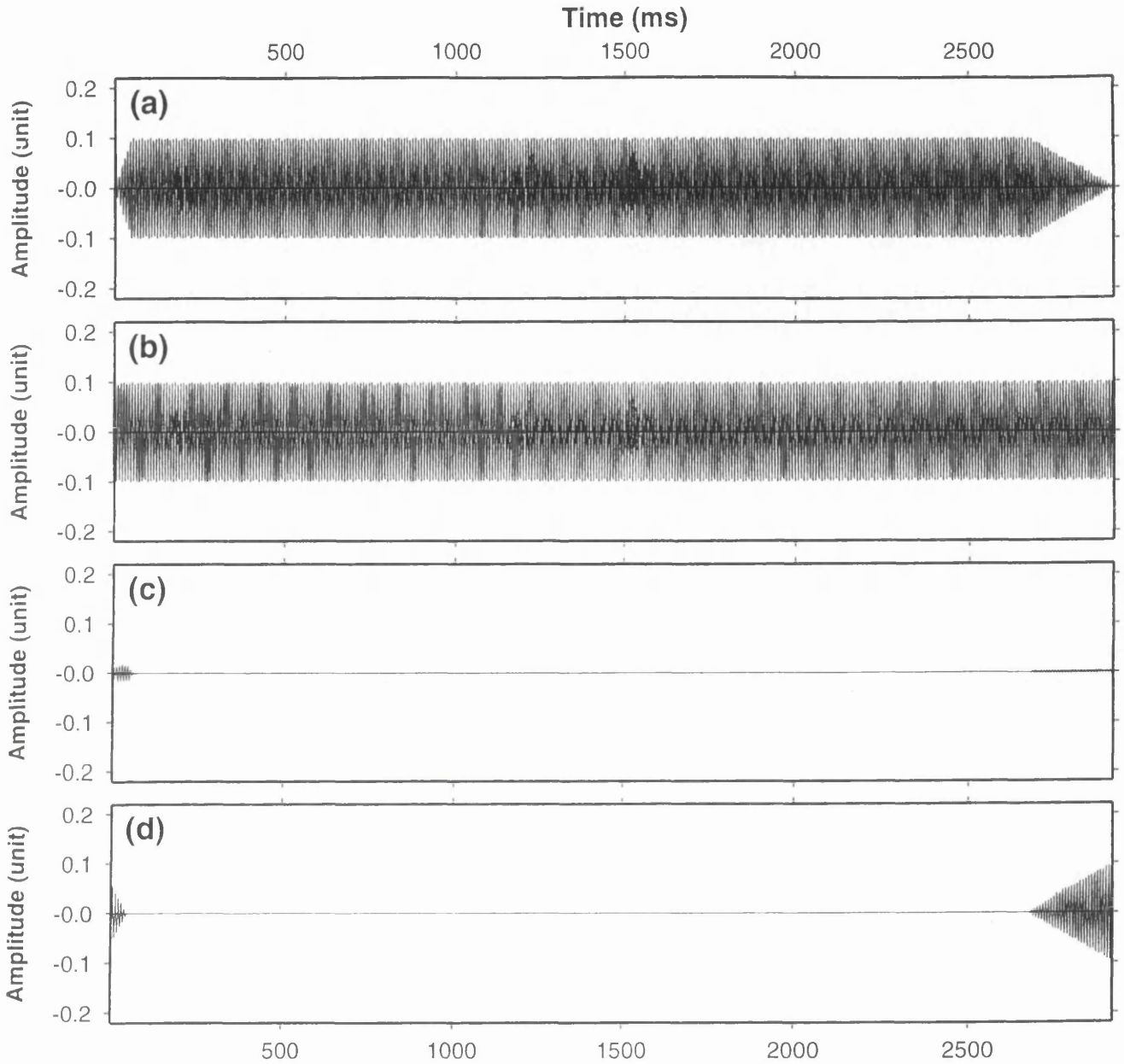


Fig. 4-16. (a) Linear up-sweep (10-60 Hz over 2500 ms) squeezed to 60 Hz with linear tapers at each end. (b) 60 Hz stationary sinusoidal reference sweep without any tapering, used in filter design to remove signal (a). (c) Resulting output from the notch algorithm method, and (d) from the optimum least-squares filtering algorithm method.

the reflection sweep in the filtered version, as shown in Figure 4-16d, because the OLS algorithm operates as a linear adjuster for the amplitude and phase of the reference sweep in the filter design. This type of harmonic caused by unmatched tapers will degrade the performance of SFU so that a known pilot sweep is required if we wish to use the OLS filter. In cases where the pilot sweep specification is incomplete or not available (due, for example, to missing observer's logs), a linear taper should be assumed. This will minimise the harmonic distortion. However, the result obtained from the notch filter (Fig. 4-16c) shows that only slight harmonic distortion occurs at each end, implying that SFU with the notch filter is insensitive to unmatched tapers in the filter design. In conclusion, we must use a known pilot sweep as the reference sweep in SFU with the OLS algorithm, whereas we do not need to worry about taper matching if we use a simple notch filter.

If the harmonic distortion is serious, we have to use SFU with the notch filter. In practice, we should use the OLS algorithm in SFU only when both the sweep tapers *and* the onset time of the direct wave (or other undesired signal) are known exactly.

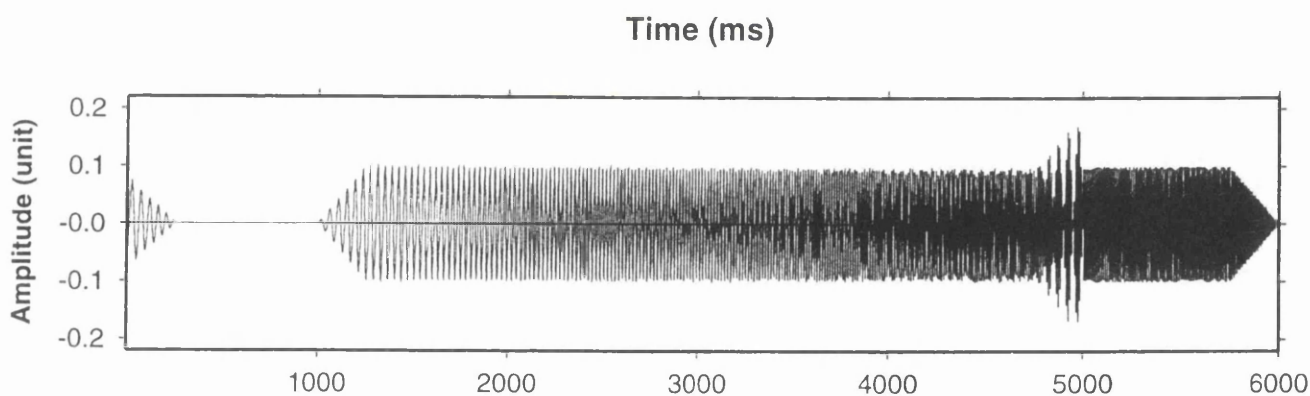


Fig. 4-17. Effect of the unmatched tapers for the SFU filter design with optimum least-square algorithm in the synthetic example of Fig. 4-8.

4.8 New module /QSFU in SierraSEIS 1.43

The SFU filter has been added into the SierraSEIS package as a routine processor named /QSFU, and has been used in processing real data from Kola deep seismic reflection and

Ohio seismic reflection projects. The only disadvantage of /QSFU is that it is expensive in CPU-time.

The correlation analysis scanning plays a very important role in the determination of precise onset time of direct wave. We must define as carefully as possible the scanning time window, which contains the first break information. Usually it is helpful that correlated shot gathers are plotted to check out window specification prior to the application of SFU. Notes on usage and the source code listing are described in Appendices E and B respectively.

Chapter 5

Direct optimum least-squares (DOLS) filtering of uncorrelated vibroseis data

5.1 Introduction

The correlation sidelobes caused by a strong direct wave are one of the major problem in vibroseis data processing, leading to low seismic resolution on the vibroseis correlogram. The SFU filter, proposed and discussed in Chapter 4, suppresses this sort of coherent noise with its squeezing and unsqueezing transformation pair. It does a very good job both on synthetic data and on real field data. However, the squeezing and unsqueezing transformations take a lot of CPU time. To overcome this disadvantage, this chapter discusses another new filtering approach, 'DOLS', to remove the direct wave in the pre-correlation domain, which is Direct[*ly based on the*] Optimum Least-Squares filtering algorithm - hence 'DOLS'. The DOLS filter operates in the pre-correlation domain without any transforming calculation, so that it takes much less CPU time than SFU filtering. In this chapter we will present the description of the new filter, its implementation, and a discussion of the algorithm performance, through use of synthetic modelling data and field data examples. The comparison of DOLS and SFU filter methods, and the effect of error in determining onset times, in particular, will be illustrated.

The principle of the DOLS filtering developed here is based on the assumption that the sidelobes caused by a strong direct wave are the dominant coherent noise problem. If the direct wave can be cancelled in the pre-correlation domain, the sidelobe noise can be removed, so that the signal to noise ratio will be thereby improved

5.2 Description of the DOLS filter algorithm

There are no squeezing and unsqueezing transformations in the DOLS filter, in contrast to the SFU filter, in which they are fundamental. The direct wave is removed in the pre-correlation domain by a digital optimum least-squares filtering algorithm without any

transforming calculation. Figure 5-1 shows a flow chart of the DOLS filter. Since it uses the original pilot sweep as a reference trace to design the Wiener filter directly, we do not have to consider whether the vibroseis data were recorded with a linear sweep or a non-linear sweep. Remember that these had to be treated in different ways in the SFU algorithm.

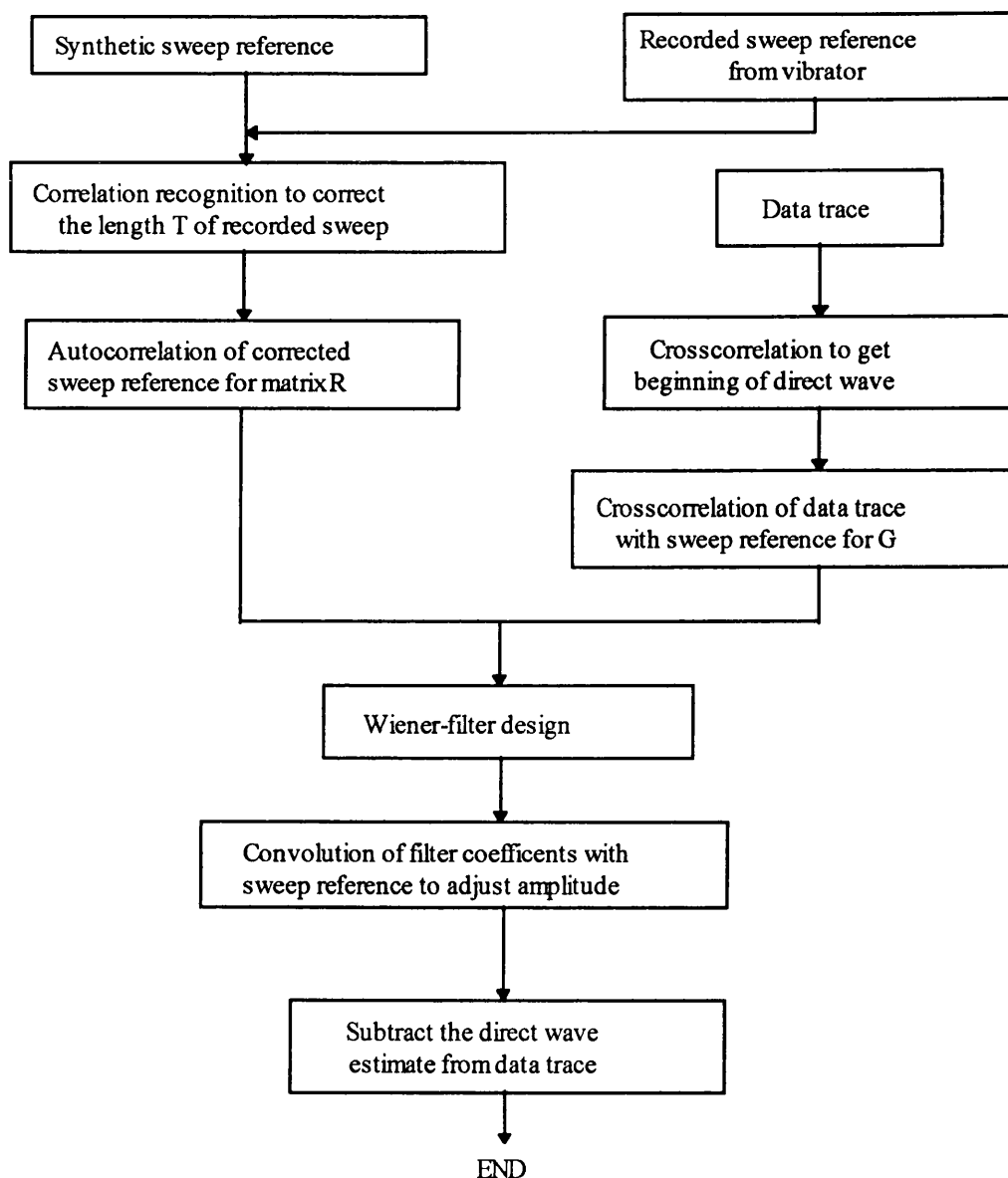


Fig. 5-1. Flow chart showing the basic design of the DOLS filter.

The design of the DOLS filter is based on two assumptions. The first is that the overall characteristics of direct wave, i.e. the sweep duration and taper length, remain consistent with the pilot sweep, and only the amplitude and phase vary depending upon source-receiver offset and direct wave propagation velocity. The second is that the amplitude of the direct wave in the recorded data trace is much larger than that of any other signal.

To remove the direct wave sweep in the pre-correlation domain, a data trace x_t is assumed to comprise a signal y_t associated with reflectivity, and vibroseis direct wave sweep s_t , which can be defined as a function in any form.

$$x_t = s_t + y_t \quad (5-1)$$

The basic design of the DOLS filter is to find the optimum Wiener filter coefficients, which are used to adjust the amplitude and phase of a pilot sweep reference to match those of direct wave s_t . When the onset time of the first arrival is well determined, the pilot sweep reference h_t is defined (Ensing 1983; Linville and Meek 1992) as:

$$h_t = \zeta(t)$$

where $\zeta(t)$ is the implicit presentation of any vibroseis direct wave, either as a linear or non-linear sweep.

To match the amplitude of the direct wave sweep s_t in data trace x_t , h_t must be adjusted by carrying out a convolution with a filter v_t :

$$h_t^1 = v_t * h_t \quad (5-2)$$

As assumed above, the direct wave amplitude in the data trace is much larger than any other signal, so that the least-squares error L (Wiener 1949; Yilmaz 1987) between the direct wave and pilot sweep reference is defined as:

$$L = \sum_t (s_t - h_t^1)^2 \tag{5-3}$$

Substituting equation 5-2 into equation 5-3:

$$L = \sum_t \left(s_t - \sum_{\tau} v_{\tau} h_{\tau-t} \right)^2$$

The goal is to compute the filter coefficients (v_0, v_1, v_2, \dots) so that the error L is a minimum. Then taking the partial derivative of L with respect to the filter coefficient v_j and setting them equal to zero, we get:

$$\frac{\partial L}{\partial v_j} = -2 \sum_t s_t h_{t-j} + 2 \sum_t \left(\sum_{\tau} v_{\tau} h_{\tau-t} \right) h_{\tau-j} = 0$$

or

$$\sum_{\tau} v_{\tau} \sum_t h_{t-\tau} h_{t-j} = \sum_t s_t h_{t-j} \quad j = 0, 1, 2, \dots, (n-1). \tag{5-4}$$

By using

$$\sum_t h_{t-\tau} h_{t-j} = r_{j-\tau}$$

and

$$\sum_t s_t h_{t-j} = g_j$$

equation 5-4 becomes

$$\begin{bmatrix} r_0 & r_1 & r_2 & \dots & r_{n-1} \\ r_1 & r_2 & r_3 & \dots & r_{n-2} \\ \vdots & \vdots & \vdots & \dots & \vdots \\ r_{n-1} & r_{n-2} & r_{n-3} & \dots & r_0 \end{bmatrix} \begin{bmatrix} v_0 \\ v_1 \\ \vdots \\ v_{n-1} \end{bmatrix} = \begin{bmatrix} g_0 \\ g_1 \\ \vdots \\ g_{n-1} \end{bmatrix} \tag{5-5}$$

This Toeplitz matrix can be solved rapidly using Levinson's recursion algorithm, just as we did in the SFU filter.

Then the data trace after the suppression of vibroseis direct wave can be obtained directly as:

$$y_t = s_t - v_t * h_t$$

Based on both the assumptions, a short filter length is, in general, enough to meet the requirement of the processing. If the first assumption is violated, some harmonics and distortion will result, due to the non-constant cyclic nature of the sweep signal. A detailed discussion of this is given below.

As the algorithm does not require the pilot sweep to be described analytically, or as a function of time explicitly, the DOLS filter can be applied to any conventional uncorrelated vibroseis data with a recorded pilot sweep trace.

5.3 Implementation of DOLS filtering

As we do not need the squeezing and unsqueezing transformations to suppress the unwanted wave, the implementation of the DOLS filter is much easier than SFU, which can give rise to two kinds of error. One is associated with approximating the onset time of the unwanted signal during the squeezing and unsqueezing transformations. The other is the error associated with the application of the stationary sinusoidal interference cancelling method or notch filters. For the DOLS filtering approach, there only is the error associated with the application of the optimum least-square filtering algorithm, called here the *approximation error* of the onset time. That means that we can eliminate the potential error from the squeezing and unsqueezing transformations, though we still need a knowledge of the exact onset time of the direct wave in the pre-correlation domain.

As we considered in the implementation of the SFU algorithm, the exact onset time of the direct wave will vary from trace to trace in a somewhat irregular way due to static delays.

To circumvent this problem, the same automatic method, based on crosscorrelation analysis, is used here to search for the start time. In the same way, a synthetic sweep is used to find the end of the reference pilot sweep. We then correlate the reference pilot sweep with each data trace to determine the onset time of the direct wave for that data trace. A flow diagram of the method is shown in Figure 5-2.

Since there is no re-sampling, as required in the squeezing and unsqueezing transformations, it is possible to avoid losing any desired frequency components, which is usually caused to a certain extent by the various interpolation methods.

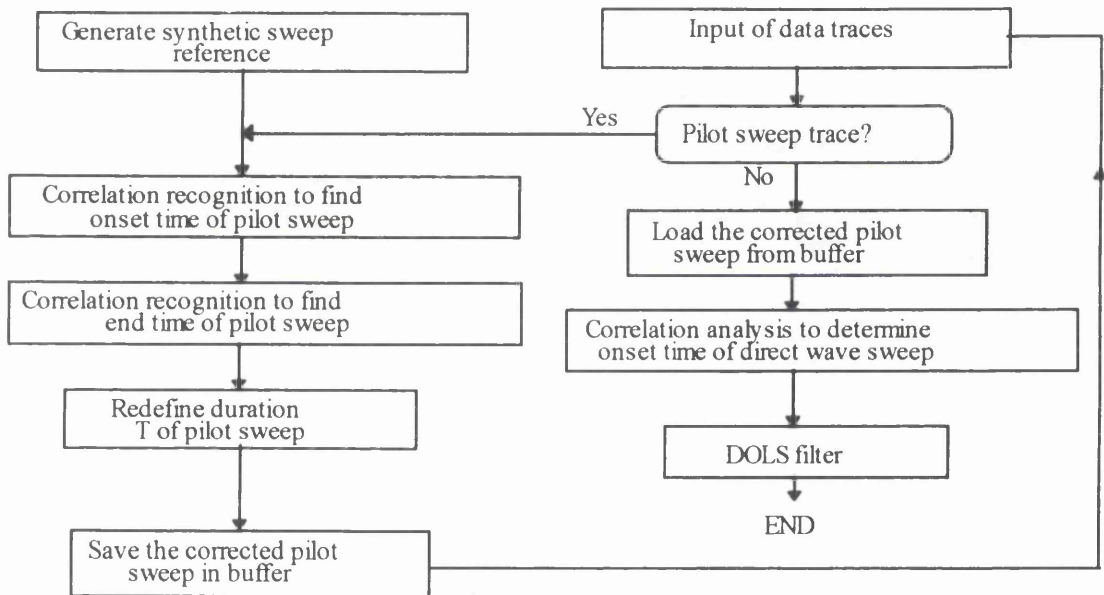


Fig. 5-2. Flow diagram of the automatic method to determine the onset time of the direct wave sweep in the DOLS filter.

5.4 Synthetic examples

Two synthetic examples - one linear and one non-linear - are presented to evaluate the effectiveness of the DOLS filter. In the first example, the synthetic linear upsweep representing the direct wave ranges from 10 to 60 Hz, 2 s duration, with an amplitude of 0.1 unit, and with 0.5 s linear tapers on each end. An uncorrelated reflection event is assumed to have the same upsweep as the direct wave, but with an amplitude of 0.01 unit, i.e. one-tenth of the direct wave amplitude and arriving 100 ms later. The synthetic seismogram is the superimposition of the direct wave and the signal, recorded at a sample interval of 4 ms, as shown in Figure 5-3a. We then apply the DOLS filter to this synthetic trace, producing the filtered record shown in Figures 5-3b. Figure 5-4 is the comparison of the correlated version before and after DOLS filtering. The DOLS filter does a very good job of removing the direct wave in the pre-correlation domain. All records are displayed with the same gain for comparison.

The second example is shown in Figure 5-5. A synthetic non-linear sinusoidal upsweep ranging from beginning frequency f_1 to terminal frequency f_2 over an interval T , with a constant amplitude A , is defined as:

$$s(t) = A \sin 2\pi(f_1 + K\sqrt{t})t \quad (5-6)$$

where

$$K = \frac{2(f_2 - f_1)}{3\sqrt{T}}$$

Accordingly the direct wave is represented by a signature record ranging from 10 to 60 Hz, 2.5 s duration, with amplitude of 0.1 unit and with 0.5 s linear tapers on both ends as shown in Figure 5-5a. An uncorrelated reflection event is assumed to have the same non-linear upsweep as the direct wave, but with an amplitude of 0.01 unit (i.e. one-tenth of the direct wave amplitude), and delayed by 100 ms, as shown in Figure 5-5b. The synthetic seismogram is the superimposition of the direct wave and the signal, as shown in Figure 5-

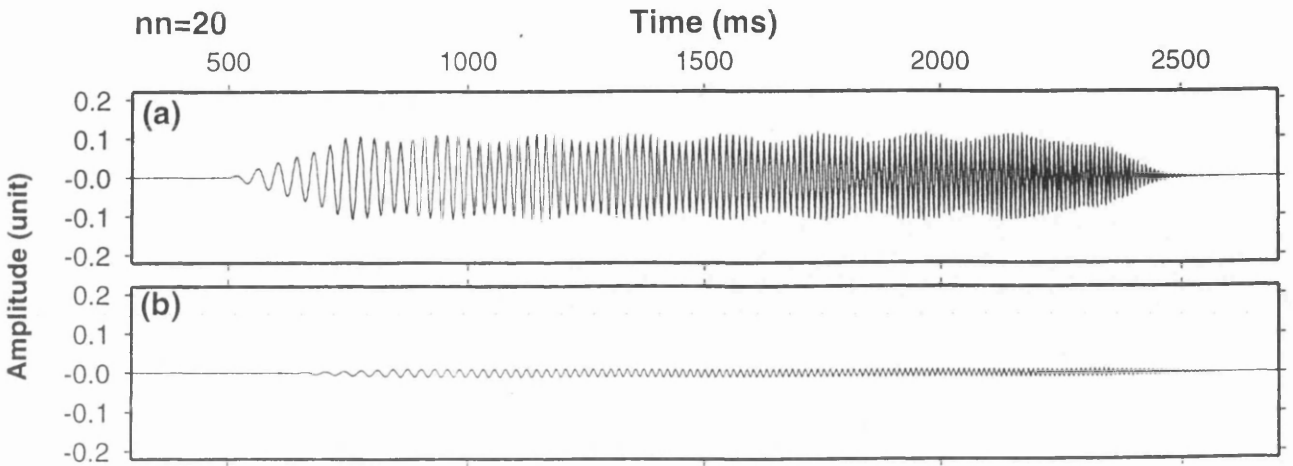


Fig. 5-3. Test using a linear sweep signal: (a) the synthetic input trace made up of a direct wave starting at 500 ms and a reflection at 600 ms, but with one tenth of the direct wave amplitude; (b) the DOLS-filtered version, with only the reflection sweep remaining.

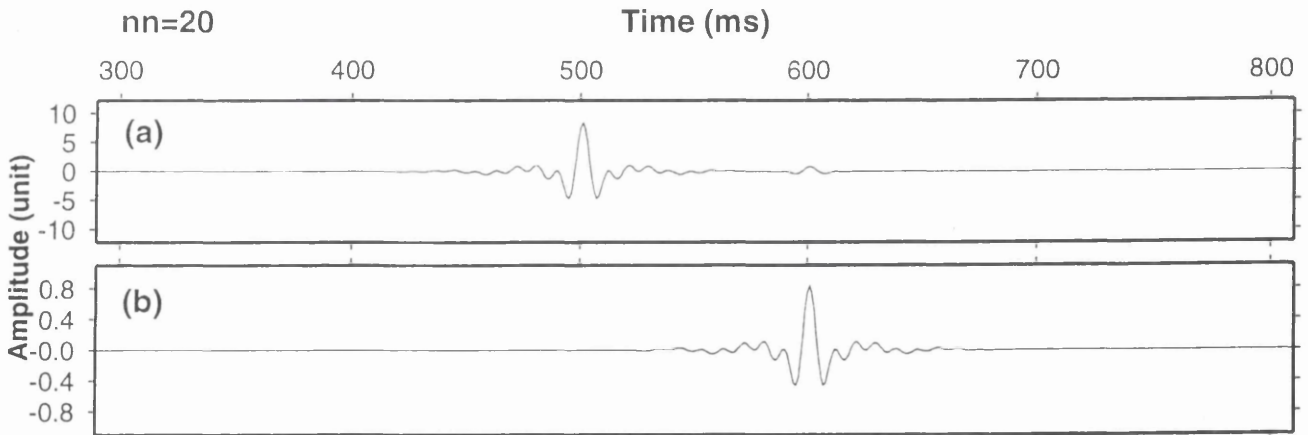


Fig. 5-4. Comparison of the correlated versions in Figure 5-3: (a) the synthetic input trace with the direct wave at 500 ms and a reflection at 600 ms; (b) the DOLS-filtered version, with only the reflection event remaining. The same gain is applied to both data traces.

5c. We then apply the DOLS filter to this synthetic trace, producing the filtered record shown in Figure 5-5d. Figures 5-6a and b show a comparison of the correlated versions of Figure 5-5c and 5-5d respectively, before and after DOLS filtering. Notice that the direct wave is successfully removed and the weaker signals obscured by correlation noise can be improved after filtering in the pre-correlation domain. Also we find that the correlogram differs from that of the linear sweep shown in Figure 5-4. All records are displayed with the same gain for comparison.

5.5 Field data example

The Kola field data used in the section is as the same shot gather as that used in the section 3.6 for SFU testing. The source is a 20 s linear upswEEP ranging from 10 Hz to 60 Hz, with 0.5s linear taper on both ends. The gathers are displayed with the same AGC window of 1 s for comparison.

The unfiltered correlated shot gather is presented in Figure 5-7a. The direct wave arrives between 0.3 and 0.9 s. The filtered version is shown in Figure 5-7b. The correlation analysis was used to pick automatically the onset time of the direct wave in the pre-correlation domain. The DOLS filter has done a good job of cancelling the first arrivals in pre-correlation domain so that the amplitude of the correlation noise is removed, leading to possible improvement in genuine correlation signals from weak reflections. Comparing with the results from the SFU filter in Chapter 4, Figure 4-10, we find with the DOLS filter that the signals near the first arrivals are also attenuated to some extent while the direct wave is removed. This could indicate that the onset time of the direct wave is not determined as precisely as the DOLS algorithm requires. This means that the DOLS filter may be more sensitive to the approximation error of the onset time of direct wave in the pre-correlation domain than is the case with the SFU filter. The adverse effects of various errors of the DOLS filter will be discussed in the following sections.

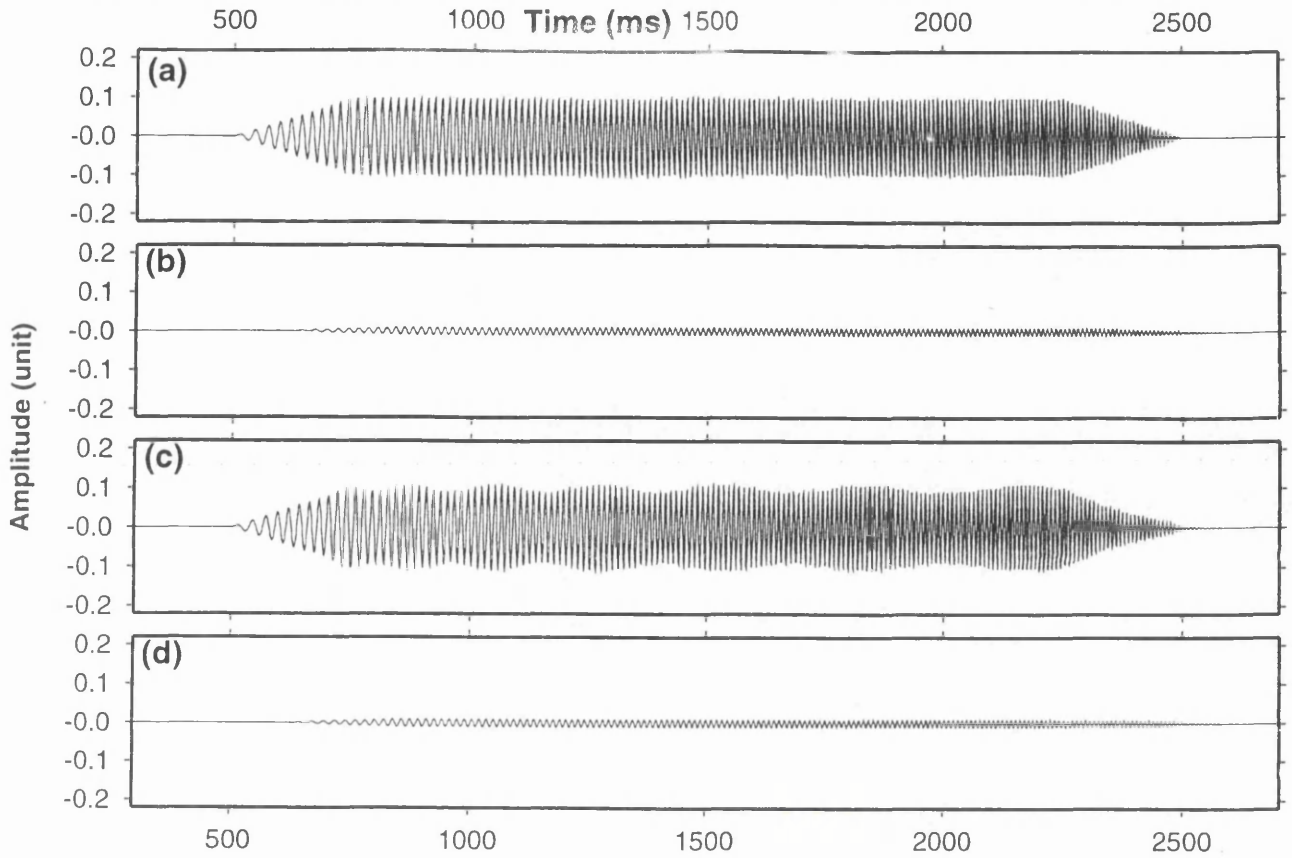


Fig. 5-5. The test of the non-linear sweep signal: (a) the synthetic direct wave sweep with the onset time at 500 ms, (b) a reflection sweep at 600 ms, but with only one tenth of the direct wave amplitude, (c) the final version of superimposed direct wave and reflection event as input data trace, (d) the DOLS-filtered version with only the reflection sweep remaining.

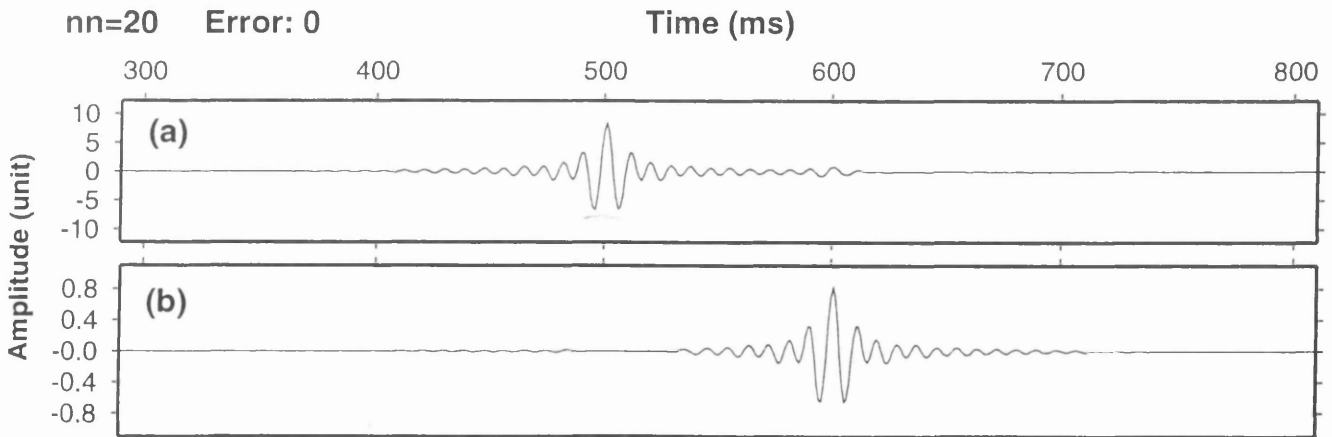


Fig. 5-6. Comparison of the correlated versions in Figure 5-5: (a) the synthetic input trace with the direct wave at 500 ms and a reflection at 600 ms; (b) the DOLS-filtered version with only the reflection event remaining. The same gain is applied to both data traces.

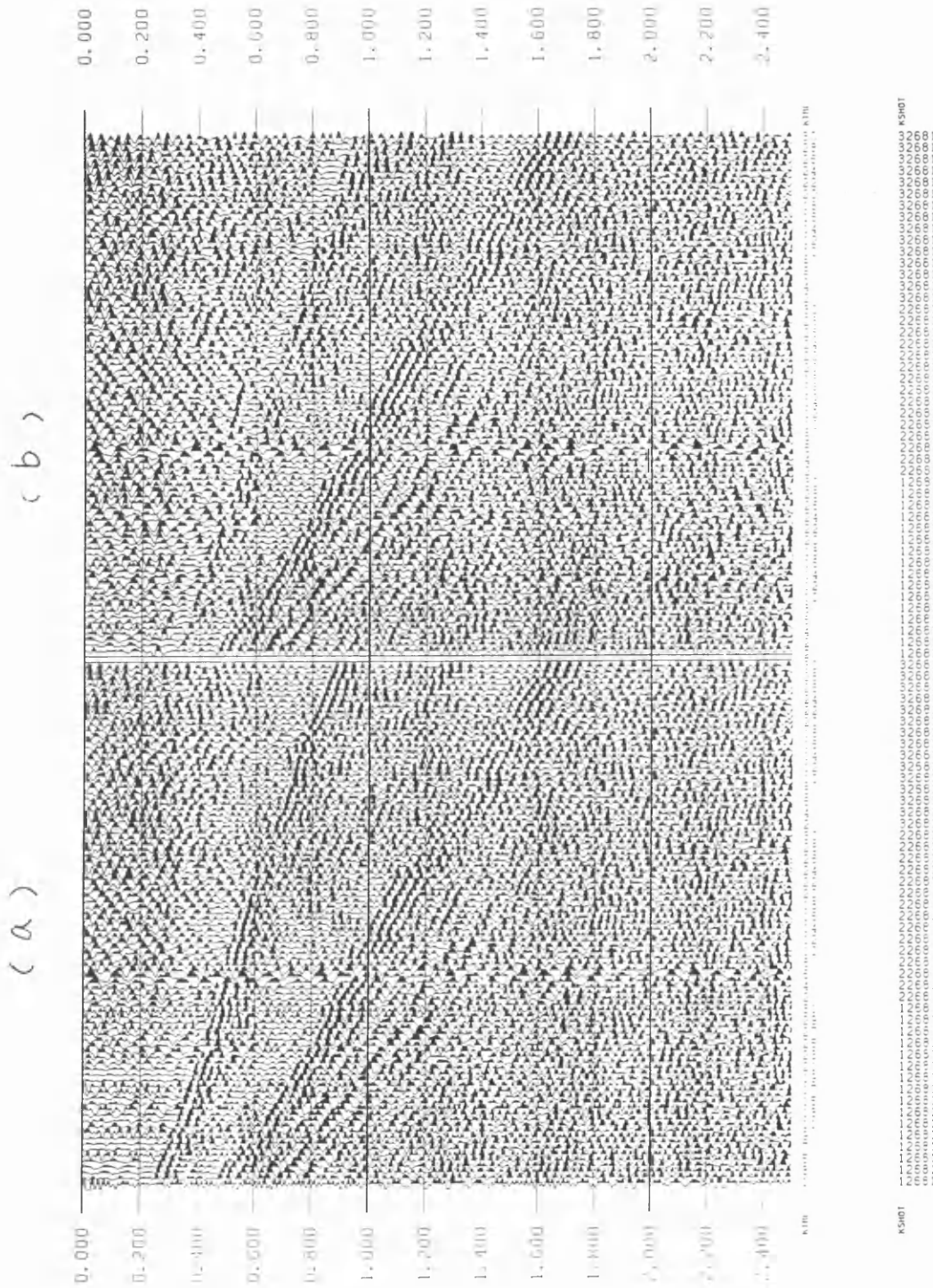


Fig. 5-7. Comparison of a Kola shot gather (linear sweep): (a) before DOLS filtering, and (b) after DOLS filtering. Vertical scale is in seconds.

5.6 Discussion

Although the DOLS filter can provide a much quicker suppression of the direct wave than SFU, it leads to more signal attenuation due to the sensitivity of DOLS filter to the onset time error. To further understand the problem the effect of the error on the performance of DOLS and the filter design will now be discussed, based on a numerical examination.

5.6.1 *Effect of onset time error on the DOLS filter*

As mentioned above, there is only one kind of error related to approximating the onset time of the direct wave. It is impossible to get rid of this error in practice, although we can define an error-free experiment in synthetic data. Given the direct wave sweep $x(t)$, we want to remove it by the DOLS filter with reference sweep $x(t+e)$, where e is the approximation error of the onset time, and t the correct onset time of sweep. The effect of the approximation error of the onset time on the performance of DOLS filtering is examined in Figure 5-8. Consider a synthetic trace with the direct wave at 500 ms and a later arriving reflection event at 1000 ms. We keep the DOLS operator length constant ($nm = 20$) and vary the approximation error of the onset time of the direct wave in the pre-correlation domain. The correlograms of the output from the DOLS filter are depicted in Figure 5-8, where nm refers to the operator length in milliseconds of the DOLS filter, and *Error* is the approximation error of the onset time of the direct wave in the pre-correlation domain. The approximation error varies from $e = +10$ ms to $e = -10$ ms, as indicated in the figure. An almost perfect performance of the DOLS filter is achieved when the approximation error e of the onset time is zero. The positive error yields the double spikes at about 500 ms with a constant gap. The amplitude of these noise spikes decreases regularly as the error becomes smaller. When the error is as large as $e = +10$ ms, the DOLS filter does almost nothing to remove the direct wave at 500 ms, and the high-frequency tails of the spike at 1000 ms become worse, which is associated with the reflection event.

However, note that the negative error does not lead to any noise spikes around 500 ms, even when $e = -10$ ms. The negative approximation error means that the estimated onset time is ahead of the correct onset time, or the truncated point is shifted forward to earlier

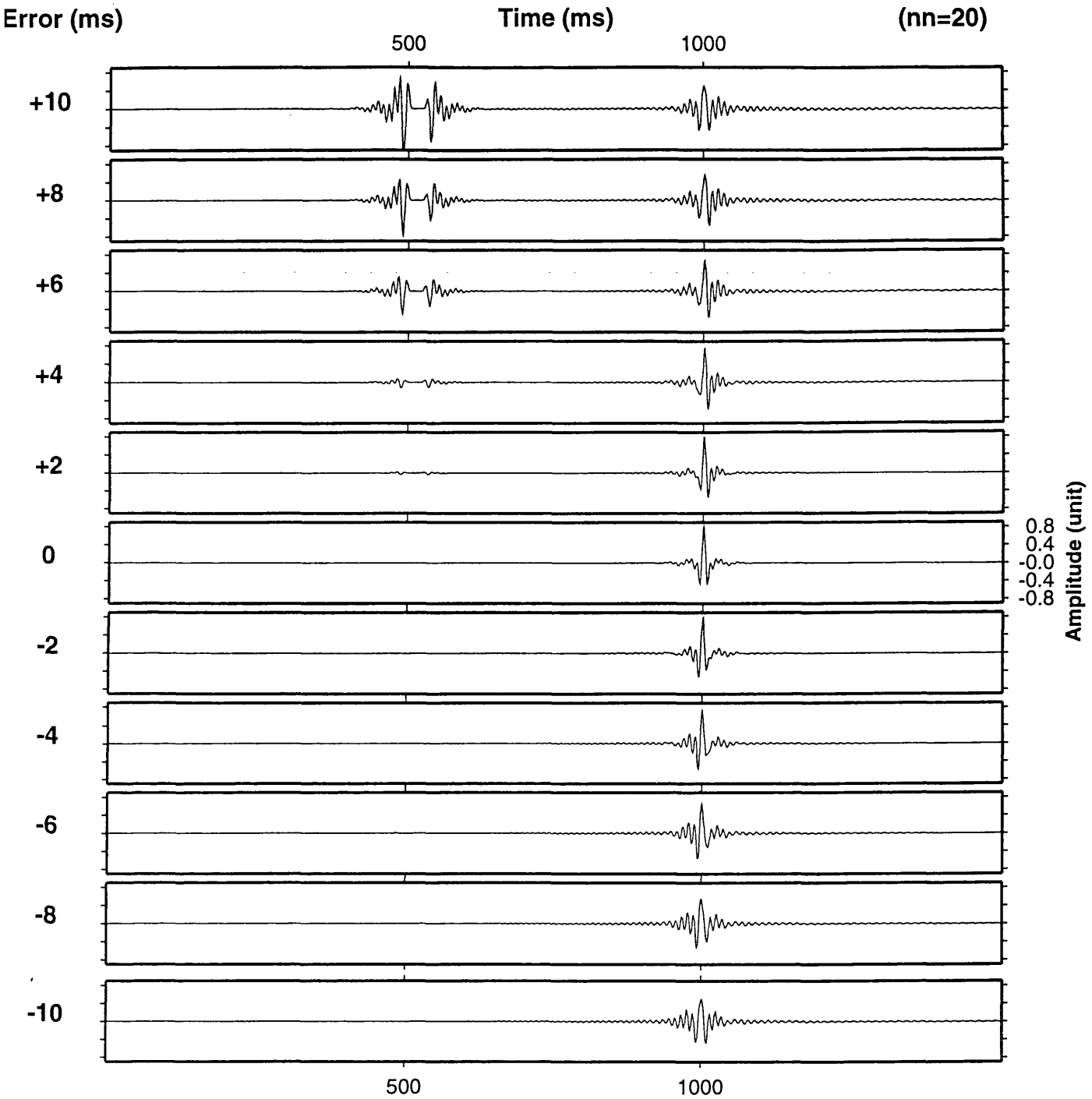


Fig. 5-8. Test of the approximation error of the onset time on the performance of DOLS filtering, where nn = operator length and Error = approximation error of the onset time. A positive error means the approximated onset time is delayed behind the correct onset time, and negative means that it is ahead of the correct onset time.

time. It implies that DOLS filter needs the information of the onset time to be included in the filter coefficient design. This assumption is satisfied only for those negative approximation errors e of the onset time. In conclusion, we prefer the approximation error of the onset time to be negative rather than positive in the application of DOLS filtering. So the auto-search procedure for the onset time in DOLS could be designed based on the point with a time shift function to make the approximation error as positive as possible. This can be specified manually.

5.6.2 Effect of operator length on DOLS filtering with incorrect onset time

Consider the same synthetic data trace as above. The direct wave arrives at 500 ms and reflection energy is later, arriving at 1000 ms. Here, the approximation error of the onset time for direct wave is kept constant ($Error = +6$), while the operator length of the DOLS filter is varied from 30 lags to 60 lags as indicated in Figure 5-9. One lag of the

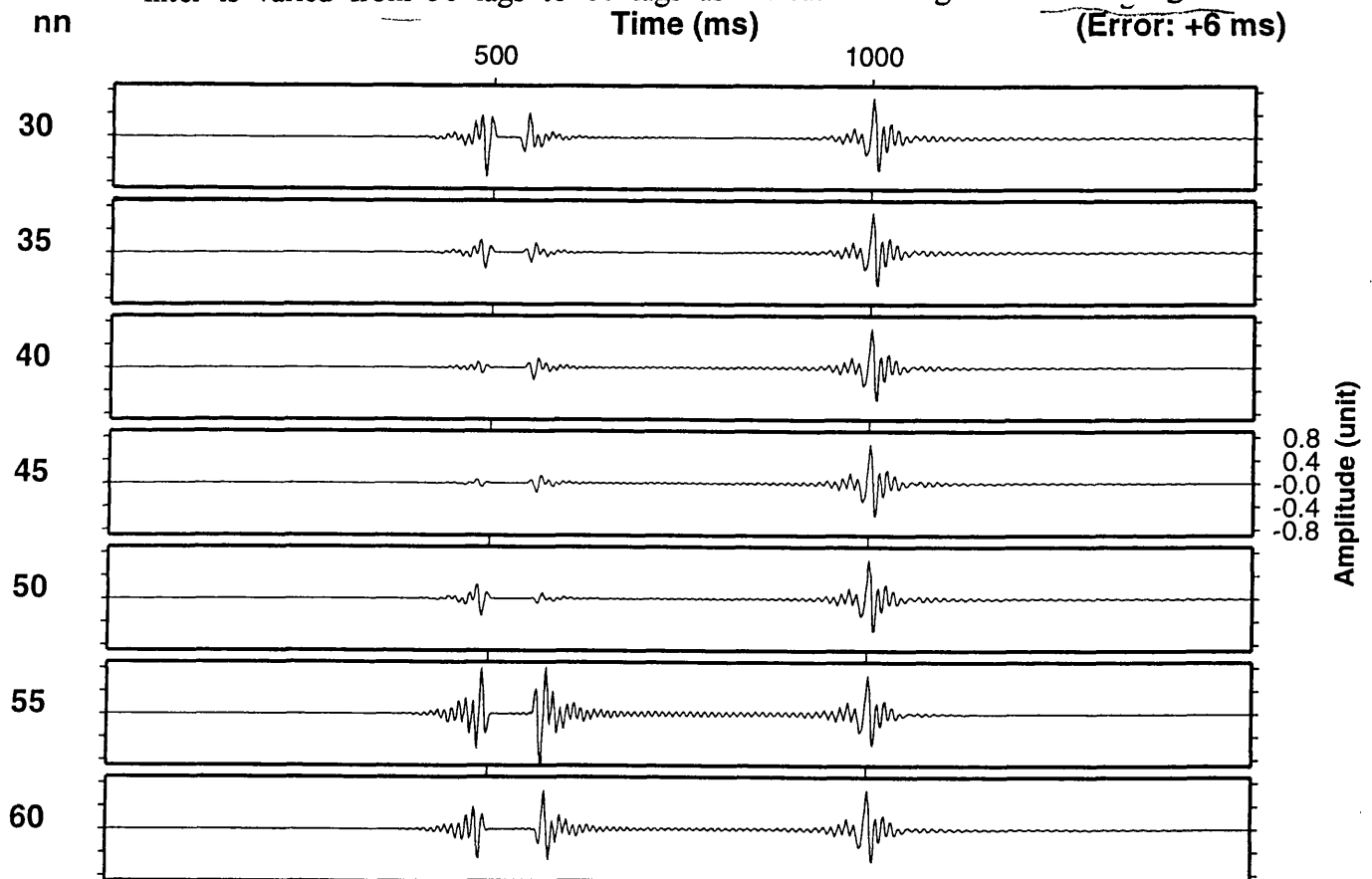


Fig. 5-9. Test of the operator length where $nn = operator\ length$ and $Error = the\ approximation\ error\ of\ the\ onset\ time,$ for direct wave at 500 ms.

operator length is equal to the sample interval. The 45-lag-long operator of DOLS almost perfectly removes the direct wave in the pre-correlation domain. Shorter operators result in poorer performance. However, increasing the operator length does not indefinitely improve the results; on the contrary, more and more strong spurious noise spikes are introduced. We can not give an adequate explanation as to why only an operator of a specific length does the best job of suppressing the direct wave energy, but it is probable that the optimum operator length of the DOLS filter is dependent upon the specification of the injected source sweep, e.g. the duration of sweep, the start and end frequency, the taper, etc. At the same time, we find that the correlated reflection spike become a non-zero phase wavelet, and is independent of the variation of operator length. Comparing these results (Figure 5-9) with those in Figure 5-8 for the events at 1000 ms, it is possible to conclude that this kind of phase change is due to the approximation error of the onset time for direct wave.

What kind of operator length should be used for DOLS filtering? To select an operator length, ideally we could carry out the test with varied operator length for the pilot sweep trace as we did in Figure 5-9, then find out which operator length gives the best result. In practice, the operator length usually ranges from 20 to 50 samples, which depends upon the specification or characteristics of the injected sweep. In the Kola data example above, a 20-lag operator length is used in the DOLS filter.

5.6.3 Comparison of the DOLS and SFU filters

The SFU filter is a combination of squeezing and unsqueezing transformations with a least-squares filtering algorithm, but the DOLS filter is the application of a least-squares filtering algorithm directly to cancel the non-stationary sinusoidal signal, without any transformations. Although both filters use the same least-squares filtering algorithm, the filter designs differ. For SFU the least-squares filtering algorithm is optimally designed to provide the least amount of prediction error between the squeezed reference sweep and squeezed direct wave in the pre-correlation domain, while for DOLS the filter is optimally designed to provide the least amount of prediction error between the original unmodified reference sweep and unsqueezed direct wave. As the SFU filter requires the squeezing and

unsqueezing transformation pair, before and after the least-squares filtering respectively, it usually takes more CPU time than DOLS.

A comparison of SFU and DOLS is conducted on an input synthetic trace, whose correlated version is shown in Figure 5-10a. The synthetic trace consists of two linear sweeps from 10 to 60 Hz with a duration of 8 s and with 0.5 s linear tapers at both ends, representing the direct wave and reflection event respectively. The onset time of the first sweep (direct wave) is at time zero with the amplitude of 0.1 units. The second (reflection) is delayed by 100 ms with the amplitude of only 0.01 units. The filtered versions from SFU and DOLS are correlated with the pilot sweep, then presented in Figure 5-10b and 5-10c respectively.

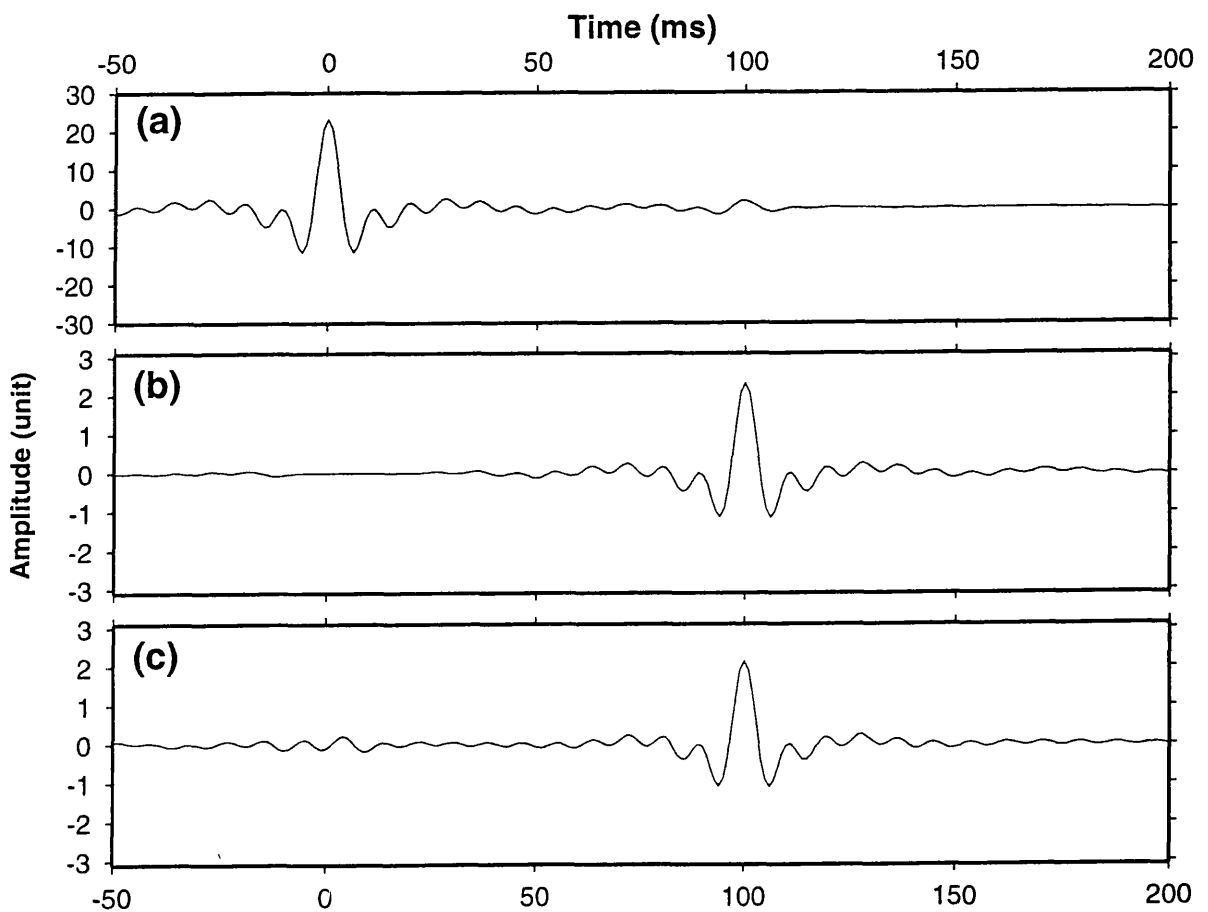


Fig. 5-10. Comparison of SFU and DOLS filtering: (a) the correlated version of the input synthetic trace with the direct wave at 0 ms and reflection at 100 ms; (b) the DOLS-filtered version, and (c) the SFU-filtered version.

Both the SFU and DOLS filters can provide excellent attenuation for removing the direct wave in the pre-correlation domain, as shown the correlated versions in Figure 5-10. Comparing Figure 5-10b and 5-10c, we see that the DOLS filter does a better job in cancelling the direct wave energy at zero time than SFU. However, by comparing the field examples in Figures 4-10 and 5-7, it seems that the DOLS filter leads to some attenuation or distortion of the signal around the times of the direct wave, which has been effectively removed in Figure 4-10, but not well removed in Figure 5-7.

In conclusion, both SFU and DOLS filters can provide excellent results in cancelling direct wave in the pre-correlation domain, based on the experiments with synthetic data. The SFU filter takes more calculation time than the DOLS filter, whereas the DOLS filter can lead to attenuation or distortion of the signal at and near the time of the direct wave. This disadvantage of DOLS may be related to the approximation error of the onset time for the direct wave.

5.7 New module /QDOLS in SierraSEIS 1.4

The DOLS filter has been added into SierraSEIS package as a routine processor, named /QDOLS. It has been used in processing data from the Kola deep seismic reflection profiling project. The advantage of /QDOLS is the smaller CPU time required, as compared with /QSFU. The disadvantage of /QDOLS is that the operator length could be more sensitive to the characteristics and definition of the injected sweep than /QSFU.

Correlation analysis scanning is still applied, to detect the precise onset time of the direct wave. We should define the scanning time window, which must contain the first break information, as carefully as possible. Usually it is helpful that the normal correlated shot gathers are plotted to check out the window specification prior to the application of SFU. The notes on usage are described in Appendix F, and the Fortran source code is given in Appendix B.

Chapter 6

Three-component filtering of sub-horizontal reflections

6.1 Introduction

A 40 km long crustal seismic reflection profile through the Kola superdeep well SG-3 has been shot with 3-component recording (Smythe *et. al.* 1994). There is exciting evidence of both present and past fluid flow at great depth from physical property and logging data. However, until this experiment was done, the well lacked the deep crustal seismic section required for the correlation. So one important element of the processing that we would like to do is to highlight any possible sub-horizontal reflections indicating fluids at depths of 6-9 km. These are expected to cross-cut the lithological layering, which dips at about 50°.

Until the 1970s, applications of seismology in petroleum exploration were limited, to a great extent, to P-wave energy recorded on single-component vertical geophones. With the advent of S-wave recording in the 1970s, the use of multicomponent receivers has become somewhat more common. Appropriate technology for practical 3-component recording (i.e. enough recording channels) has only become readily available over the last ten or fifteen years. Three-component reflection surveys are usually related to application requiring shear-waves. For example, the use of both seismic P- and S-wave information allows a crude separation of the effects of elastic constants, and the dimensionless ratio between P- and S-wave velocity (V_P/V_S) is applied as diagnostic of both gas saturation and gross lithology. But so far only a small number of 3-component shear-wave surface reflection surveys have been reported, and it has been concluded that this kind of shear-wave reflection information is useful only in particular circumstances, because the near-surface structure will perturb the S-wave polarisations from the deeper zones of interest. However, we wish to consider the potential application of the 3-component surface seismic reflection method to improve P-wave reflection processing, such as to extract additional signals or to enhance the overall interpretation system.

Both conventional reflection and refraction exploration seismology have been concerned predominately with P-wave energy. The use of explosive sources and the servo-hydraulic vibrator have been part of the reason for this emphasis, along with the simplicity of single vertical component seismometer recorded data. Furthermore, at the frequencies of interest, instruments sensitive to vertical motion have proven more robust in field applications than those for recording horizontal ground motion. As a final note, the requirement of determining transit times of seismic energy is indeed best served by the early arriving P-waves. In this chapter a new 3-component P-wave surface-to-surface reflection filtering method 3CFH is proposed on the basis of an idea by D. K. Smythe (Appendix G). The 3CFH filter is able to extract the maximum P-wave energy from 3-component data on the assumption that the earth is made up of horizontal isotropic layers of constant velocity, and that the velocities of the multi-layered model do not vary too much. We will demonstrate the effectiveness of the 3CFH filter in boosting P-wave horizontal and dipping reflections using a synthetic example.

6.2 Description of the 3CFH filter algorithm

For an isotropic medium, the particle motion associated with conventional P-wave propagation is defined entirely by the ray geometry. The P-wave source is a vertical impulse on the earth's surface. This impulse leads to a P-wave that is reflected from depth and recorded at some position along a line of detectors. By Snell's law, the reflected rays lie in a plane which contains the source, the receiver, and the reflection point.

To enhance the horizontal reflection events, the new 3CFH filter algorithm is developed for use in 3-component recording. The P-wave energy travels downwards as a wave from a source, strike the interfaces and is partially reflected back to the surface. The wave received at one station at time t can be expressed by a spatial vector, which has not only quantity but direction. The 3CFH filter algorithm is developed based on three assumptions:

- (1) The earth is made up of horizontal isotropic layers of constant velocity,
- (2) P-wave energy predominates in the 3-component data compared with other modes, and

(3) the velocities of the multi-layered model do not vary much.

6.2.1 A single flat reflector below an overlying homogeneous medium

For a flat reflector, the plane defined by the source, receiver, and reflection point is vertical, and is sometimes referred to as the ‘sagittal’ or ‘arrowhead’ plane. For P-wave propagation in such a flat earth, particle motion is in the direction of the ray, and lies entirely in the vertical plane defined by the source and receiver.

Figure 6-1 illustrates the 3CFH filter design for a single horizontal reflection. At a given midpoint location M, the traveltime along the raypath to receiver position G is $t(x)$ in a homogeneous, isotropic medium with velocity v . Using the reflection principle (Snell's Law):

$$\left(\frac{tv}{2}\right)^2 = \left(\frac{x}{2}\right)^2 + d^2$$

the angle θ between vertical component and raypath of a plane wave can be represented at the receiver point G as:

$$\tan \theta = \left(\frac{x}{2d}\right) = \frac{1}{\sqrt{\left(\frac{tv}{x}\right)^2 - 1}}$$

$$\theta = \arctan \left[\frac{1}{\sqrt{\left(\frac{tv}{x}\right)^2 - 1}} \right]$$

where the x and t of any raypath associated with the input traces are known in a CMP gather. When a estimated projection velocity is given, the 3CFH filter will project all of these 3-component measurements along the travel-path direction, to obtain the maximum of P-wave energy reflected from the horizontal flat interface as:

$$U(t,x) = Z(t,x)\cos\theta - H(t,x)\sin\theta \quad (6-1)$$

where $Z(t,x)$ is the vertical component of the measurements, $H(t,x)$ the horizontal component in the 'sagittal' or 'arrowhead' plane, and the filtered output $U(t,x)$ is a new scalar measurement of the 3-component recordings along the direction of DG in Figure 6-1.

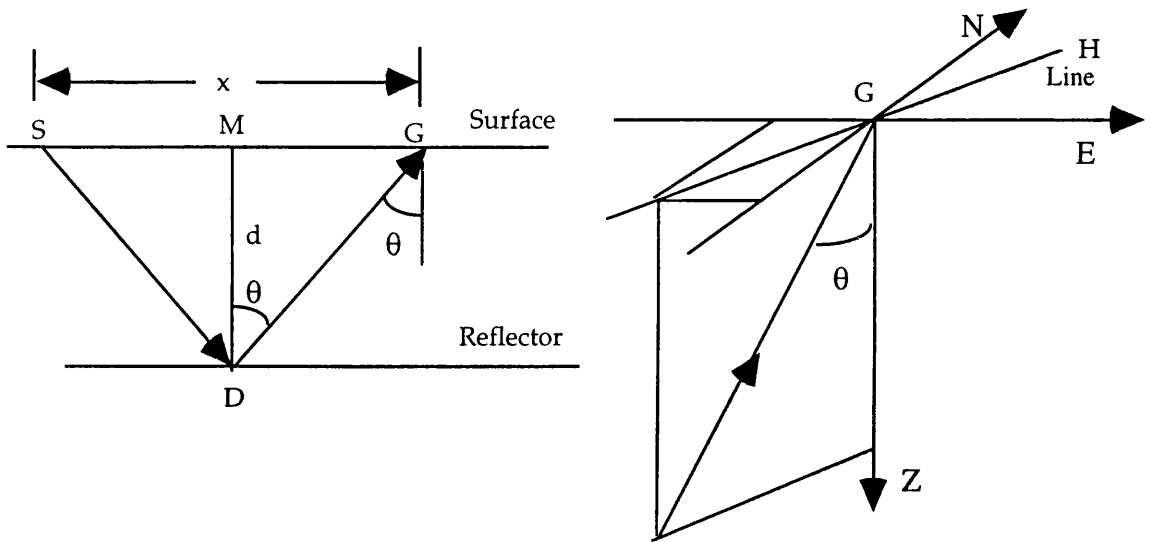


Fig. 6-1. A single horizontal flat layer with isotropic medium and its 3CFH filter definition.

6.2.2 Single dipping plane reflector

For a horizontal flat reflector below an overlying homogeneous medium, the 3CFH filter can extract the maximum of P-wave energy when the assumed projection velocity V' is equal to the velocity of the medium above the interface. But for a dipping reflector, only partition of P-wave energy can be detected if the same principle is applied.

From Figure 6-2 we can see:

$$\angle GPD = \angle GG' D$$

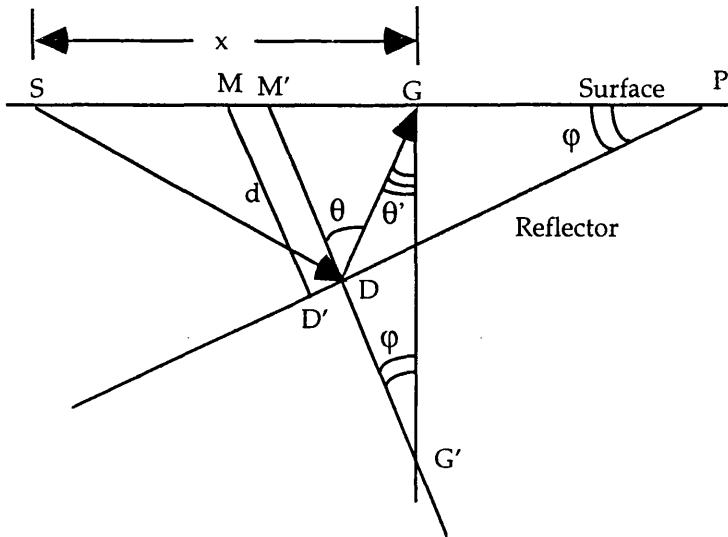


Fig. 6-2. A dipping planar reflection below an overlying homogeneous medium, with P-wave reflection raypath from S to G via D.

and

$$\angle M' DG = \angle GG' D + \angle G' GD$$

For a dipping interface

$$\angle GG' D = \phi > 0$$

then

$$\angle M' DG \geq \angle G' GD$$

That is:

$$\theta \geq \theta'$$

So:

$$U(t, x) \leq U'(t, x)$$

where:

$$\begin{aligned} U(t, x) &= Z(t, x) \cos \theta - H(t, x) \sin \theta \\ U'(t, x) &= Z(t, x) \cos \theta' - H(t, x) \sin \theta' \end{aligned}$$

then the projection of 3-component vector on to raypath DG from a dipping reflector is always smaller than that from a horizontal reflector at the same travel time. This is the reason why the 3CFH filter $U(t, x)$ is able to suppress dipping reflections while extracting the horizontal events. This unique feature of the 3CFH filter can be applied to the Kola data to enhance the possible sub-horizontal reflections at depths of 6-9 km, which cross-cut the lithological layering dipping at about 50°.

6.2.3 Horizontal isovelocity multi-layers

When a subsurface medium composed of a few horizontal isovelocity layers as shown in Figure 6-3. the 3CFH filter definition may become more complicated, but is still tractable, using the third assumption above that the velocity of the multi-layered model does not vary much. Each layer has a certain thickness that can be defined in terms of two-way zero-offset travel time. The layers have interval velocities ($V_1, V_2, V_3, \dots, V_N$) in Figure 6-3a, where N is the number of layers, and v_{rms} is the RMS velocity from the surface to the n th reflector. Then the filter $U(t, x)$ is defined as:

$$U(t, x) = Z(t, x) \cos \theta - H(t, x) \sin \theta \quad (6-2)$$

where

$$\theta = \arctan \left[\frac{1}{\sqrt{\left(\frac{tv_{rms}}{x}\right)^2 - 1}} \right]$$

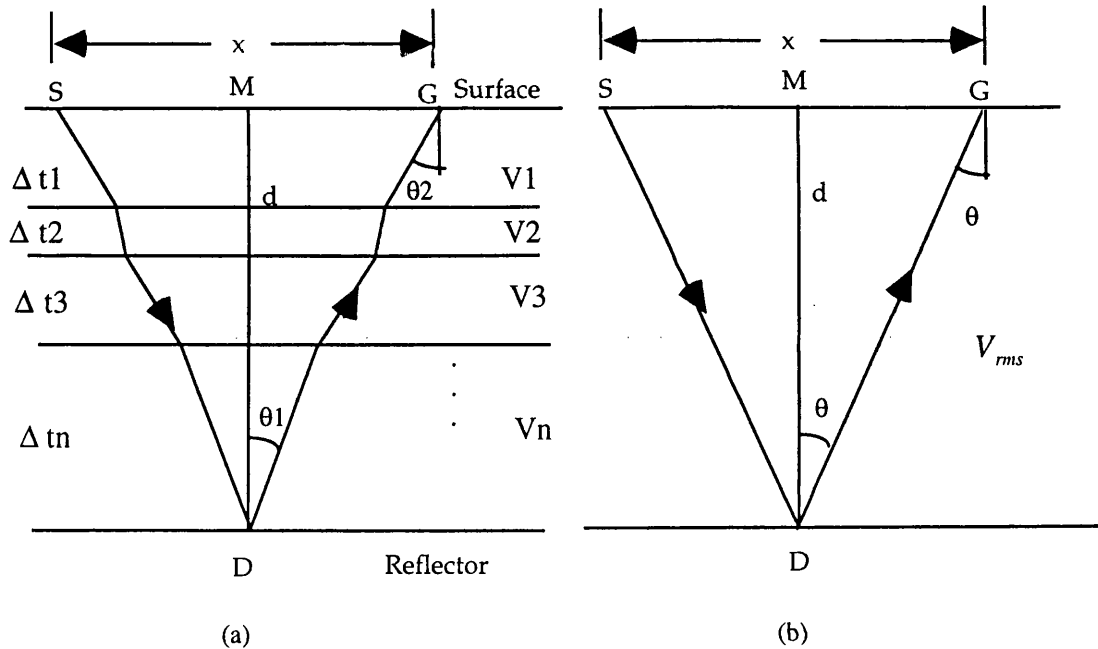


Fig. 6-3. A horizontal isovelocity multi-layer model and its 3CFH filter definition after the simplification under assumption 3.

It is obvious that the $U(t,x)$ for a single flat layer (6-1) is just a simplified case of equation (6-2).

Consider the real raypath from source S to depth point D back to receiver G, associated with offset x at midpoint location M. Taner and Koehler (1969) derived the travel time equation for this path as:

$$t^2(x) = c_0 + c_1 x^2 + c_2 x^4 + c_3 x^6 + \dots \quad (6-3)$$

Where $c_0 = t(0)$, $c_1 = 1/V_{rms}^2$, and $c_2 \dots$, are complicated functions that depend on layer thickness and interval velocities. By making the small-spread approximation, the series in equation 6-3 can be truncated to the travelttime equation for an equivalent single layer (Figure 6-3b) as follows:

$$t^2(x) = t(0) + \frac{x^2}{V_{rms}^2}$$

It is proved that the traveltimes are slightly different for both the computations with a given interval velocity model and with an RMS velocity V_{rms} . In the case of a horizontally layered model and small spread length, which satisfies the first assumption, that the earth is made up of horizontal isotropic layers of constant velocity:

$$V_{nmo} = V_{rms} = V_{st}$$

where V_{st} is the stacking velocity and V_{nmo} is NMO velocity defined (Hubral and Krey 1980) as:

$$V_{NMO}^2 = \frac{l}{t(0) \cos^2 \beta_0} \sum_{i=1}^N V_i^2 \Delta t_i(0) \prod_{k=1}^{i-1} \left(\frac{\cos^2 \alpha_k}{\cos^2 \beta_k} \right)$$

(V_i is the interval velocity shown in Figure 6-3)

So we can present:

$$\theta \cong \theta_1 \cong \theta_2$$

Accordingly we can use stacking velocity V_{st} or rms velocity V_{rms} instead of interval velocities ($V_1, V_2, V_3, \dots, V_N$) to calculate θ in the 3CFH filter for a horizontally layered model with small array spread length.

6.3 3-Component data transformation and implementation of the 3CFH filter

A field coordinate system $O_1(N, E, V)$ is often used to record data, where N stands for North, E for East, and V stands for vertical. The first step of the 3CFH processing is to transform the recorded field data to the coordinate system required, $O_2(X, Y, Z)$, where X stands for the radial, Y for the transverse, and Z for the vertical component, respectively. If the origins of the two system are at the same point with a coincident vertical axis, the vertical component V is as same as the Z component, and the X, Y components can be represented as:

$$\begin{aligned} X &= N \cos \beta + E \sin \beta \\ Y &= -N \sin \beta + E \cos \beta \end{aligned}$$

where β is defined as the angle of rotation from the N axis clockwise to the X axis. Since the calculation of $U(t, x)$ is defined as:

$$U(t, x) = Z(t, x) \cos \theta - H(t, x) \sin \theta$$

and $H(t, x)$ is the projected horizontal component of the vector along the profiling section, only converted Y for transverse component and Z for vertical component are needed for the 3CFH filter, if we define the Y as the profiling direction.

In order to calculate $U(t, x)$ in equation 6-2, the second step is to obtain the P-wave velocity for the projection calculation. In this chapter we propose a new technique to estimate this projection velocity. It starts with the conventional velocity analysis for the Z component to get an initial velocity model. Once the initial stacking velocity V_{st} is available, the projections of the vector associated with the reflected P-wave energy can be calculated along the wave raypath direction, and the potential maximum of the P-wave energy from horizontal and near horizontal interfaces can be extracted in the new composed 3-C measurements $U(t, x)$. By giving a range of the stacking velocity V_{st} around the initial velocities, a 3-D velocity semblance can be generated.

The subsequent 3-D velocity analysis for $U(t,x)$ is different from the conventional velocity analysis for Z component in the second step. The new stacking velocity V'_{st} will put more weight on horizontal reflections. The interactive picking of the 3-D velocity spectrum would play an important role in the estimation of the projection velocity. The related techniques and software need further development in the future.

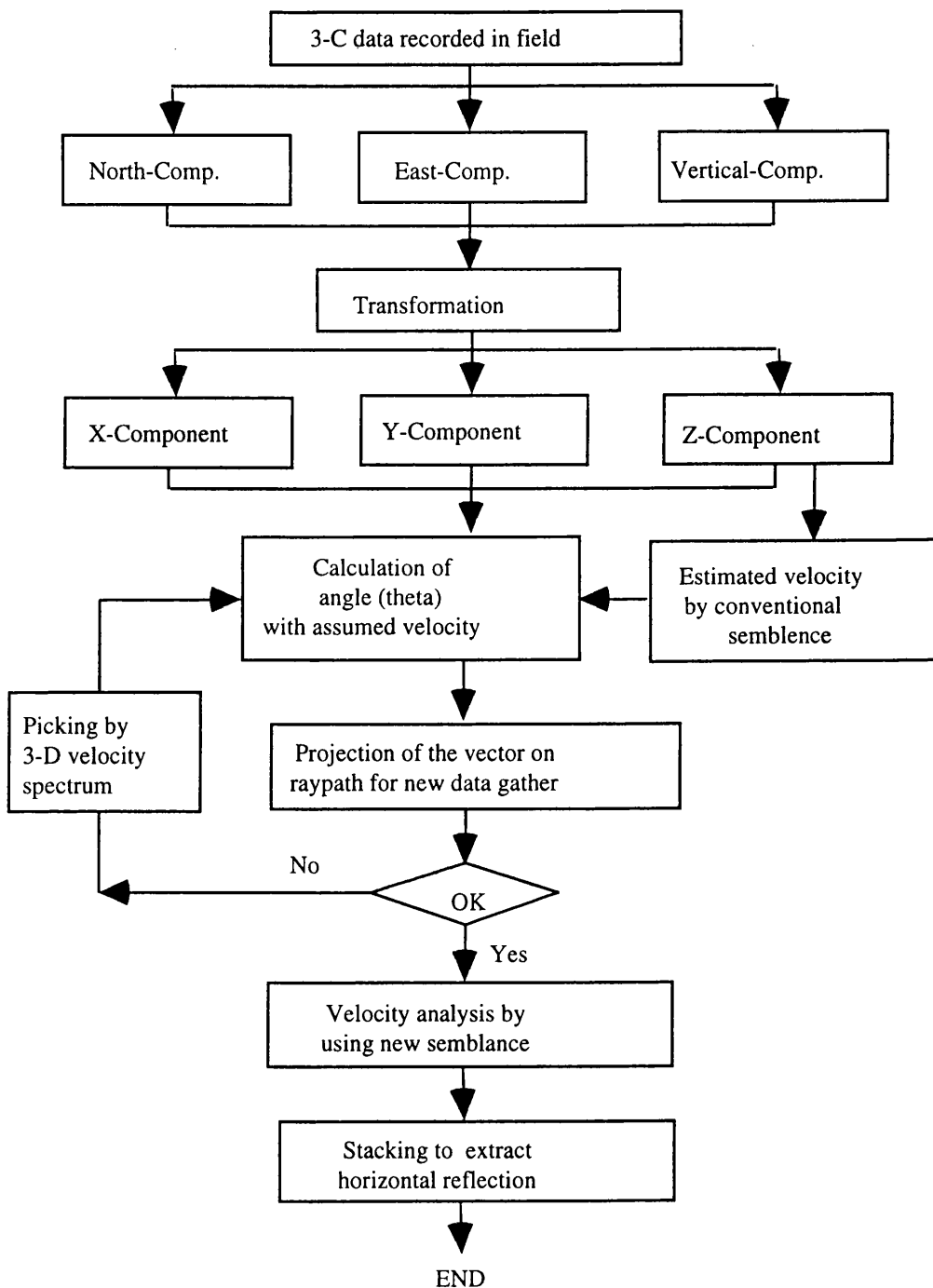


Fig. 6-4. Flow chart of the 3CFH filter design and processing procedure.

6.4 Synthetic examples

One synthetic example is presented in this section to illustrate an important application of 3-component seismic data in P-wave reflection processing, and to evaluate the effectiveness of the new 3CFH filter in extracting the P-wave reflection energy.

Modelling is conducted using Sierra products. Firstly, a two-layer model is interactively built by the MIMIC package with an isotropic medium and P-wave velocities are specified from 3000 m/s to 4000 m/s as shown in Figure 6-5. A 24 channel array is adopted here as shown in Figure 6-6 (following Al-Sadi 1980). The station spacing is 25 m, and there are 8 shots at a spacing of 50 m. The QUIKSHOT package is used to carry out offset raytracing for simulation of the field shot records, based on the above model and using a roll-along array. The SLIPR time domain program then transforms these travel times and amplitude data from QUIKSHOT into 3-component synthetic field data, and saves them as SEG-Y format files. Finally the SierraSEIS batch seismic data processing system is used to complete the subsequent processing with two new modules to obtain a comparison of the stacked sections. Since SierraSEIS is unable to handle 3-component data sorting, a new SierraSEIS gathering processor 'QGATHER' has been developed for Version 1.4.

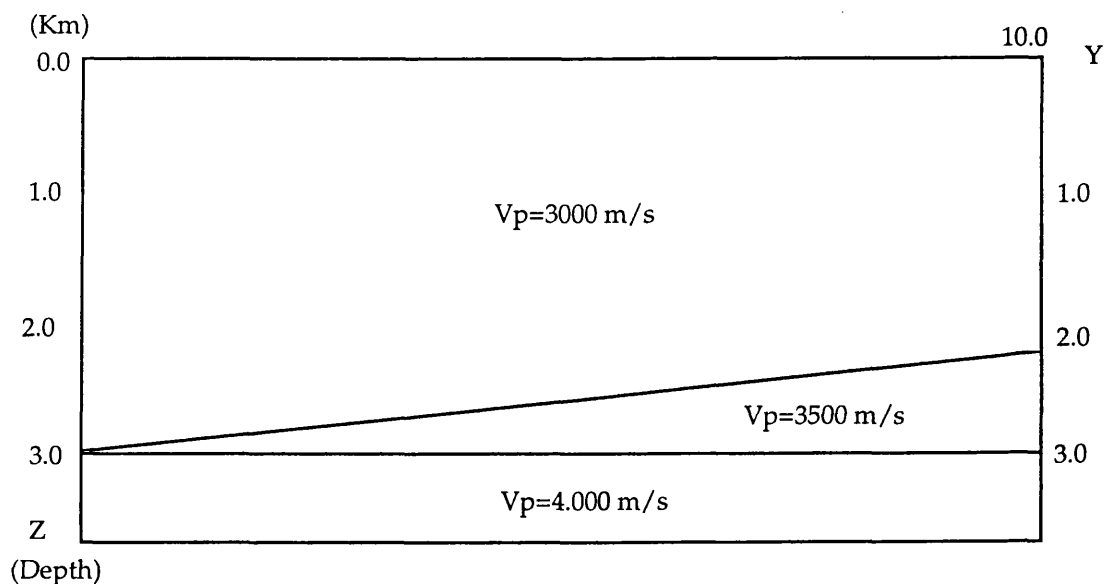
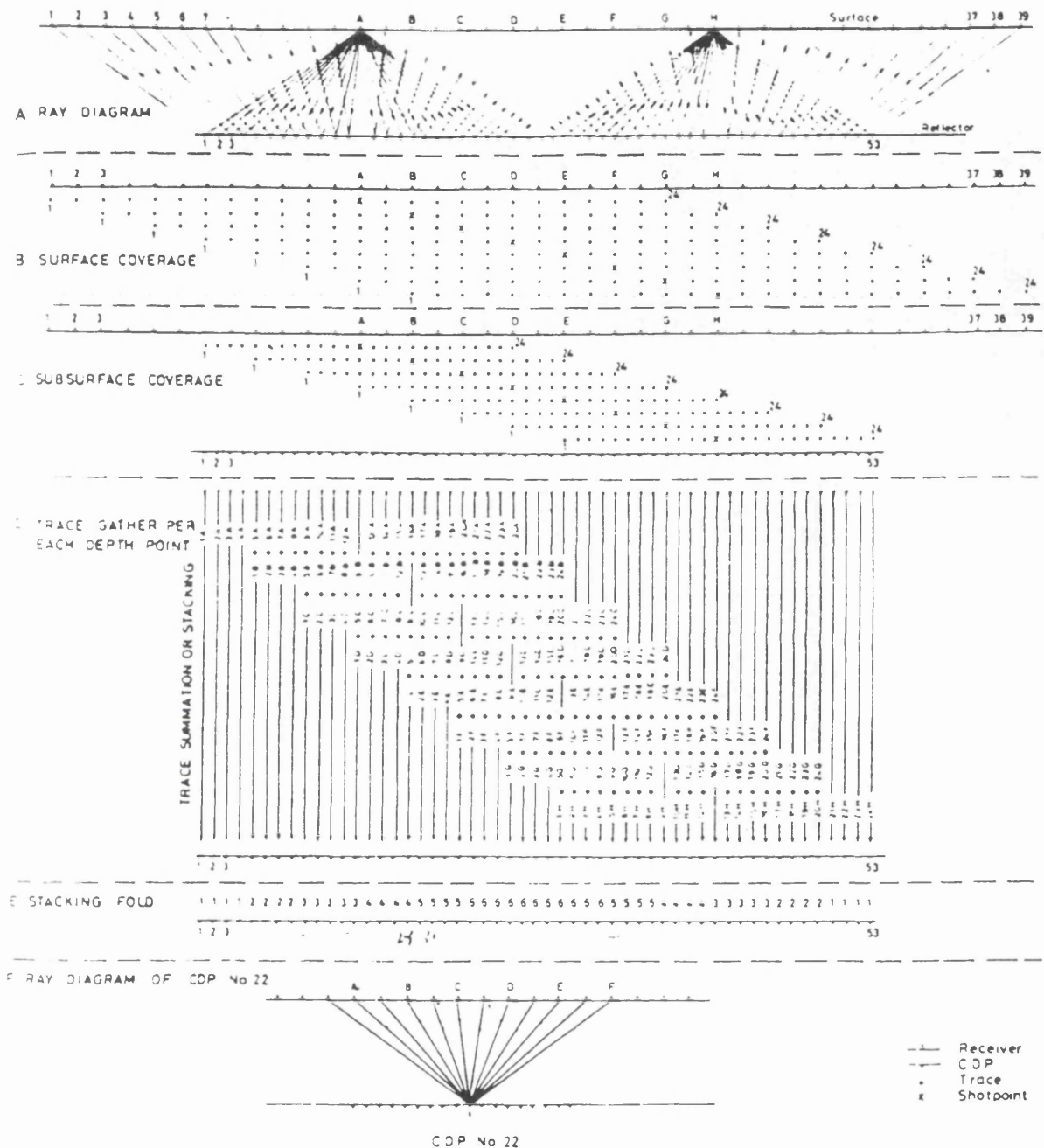


Fig. 6-5. Two-layer model with isotropic layers.



Configuration of a 24-trace, centre-shooting spread of a constant offset and constant move-up rate. In this example the shooting system is so designed as to ensure continuous 6-fold coverage. (A) Raypath diagram drawn only for the first and last shotpoints. (B) Actual surface locations of the shotpoints and their respective traces. (C) Locations of each reflection point which belongs to each shotpoint. (D) The trace-gather of each common depth point. The arrows indicate the traces which are summed up to produce the stacked trace for each CDP. (E) The coverage-fold map. (F) Raypath diagram of reflections belonging to depth point No. 22 which is taken at random.

Fig. 6-6. Roll-along array with a 24 channels system and 8 shots. The station spacing is 25 m and the shot spacing 50 m (Reproduced from Al-Sadi 1980).

Figure 6-7 shows the conventional stacked section of the Z-component and Figure 6-8 the stacked section of the Y-component from SierraSEIS. The ratio of the signal to background (random) noise is 100%. The rotated component geometry is as follows:

- X: transverse component (not needed in processing);
- Y: in-line component, parallel to the recording direction;
- Z: remains as the recorded vertical component.

The X-component data can be disregarded here. In the Z-component stack (Fig. 6-7) both primary reflections are just visible, but they are buried in strong ambient noise. In the Y-component stack (Figure 6-8), the reflection from the dipping interface is much stronger than the horizontal one, which has become almost invisible under the noise. The 3CFH filter is applied with a constant assumed velocity 4 km/s to extract the P-wave reflection by using Z and Y component data to obtain the new stacked section. This is shown in Figure 6-9. Obviously the filtered version in Figure 6-9 has a much higher signal to noise ratio than either the Y-component stacked section or the Z-component one, and the reflections are boosted successfully. However we have to admit that the 3CFH filter has boosted both the dipping and horizontal reflectors. This could be due to the relatively short offsets used, relative to for the buried depth of these interfaces. Note that both the left and right margins of all these stacked sections look more noisy because of the lower CDP fold of coverage there. In this synthetic example only constant assumed velocities are used in the 3CFH filtering as there no routines within the Sierra products for handling 3-D velocity analysis interactively. We expect that the performance of the 3CFH filter would be much improved if a 3-D velocity spectrum analysis tool were available and used for picking the projection velocity in this case. The detailed discussion about the projection velocity is presented in the following section.

6.5 Discussion of the projection velocity

We have demonstrated the effectiveness of the 3CFH filter to enhance P-wave horizontal reflections. However the image of the dipping reflections in those numerical examples above is improved as well since the dip angle j is so small that the dipping interface responds like an approximated flat plane to the downgoing wave. The angle between the

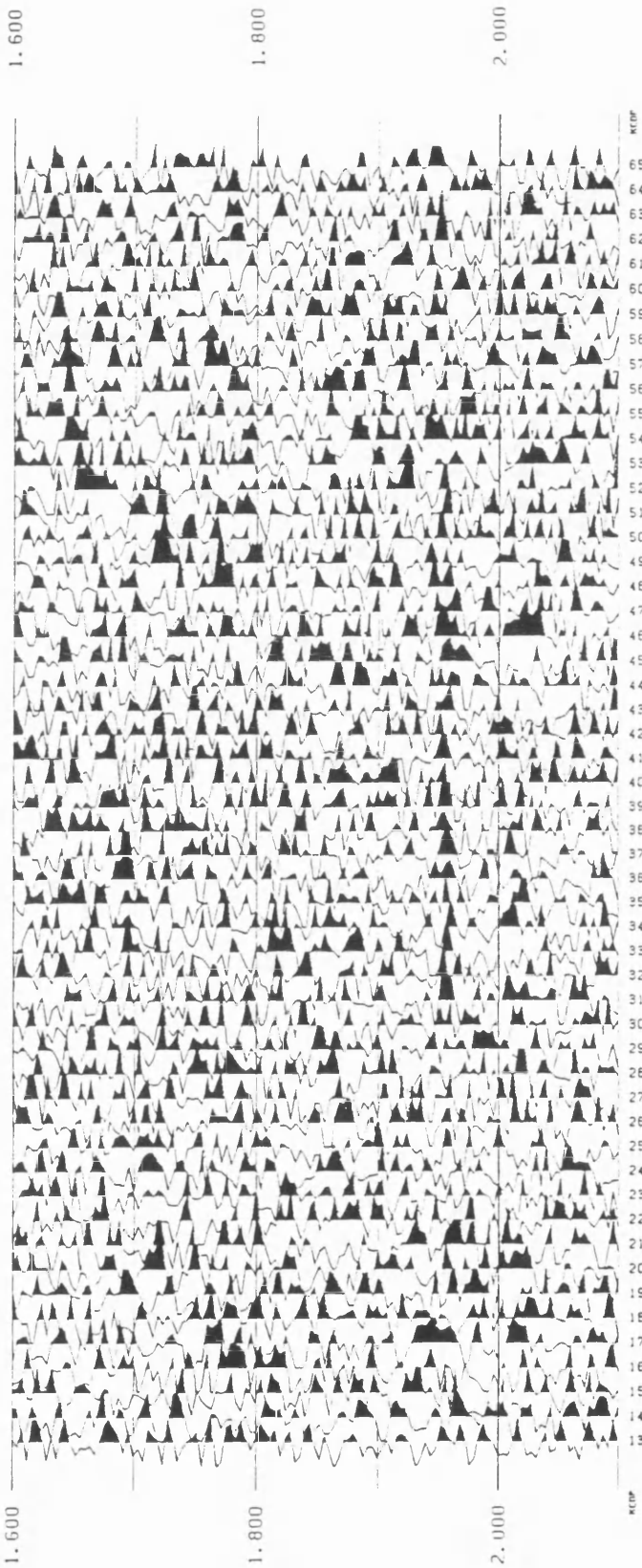


Fig. 6-7. Conventional CDP stacked section of Z-component recordings.
CDP interval 12.5 m; vertical scale in seconds of two-way time.

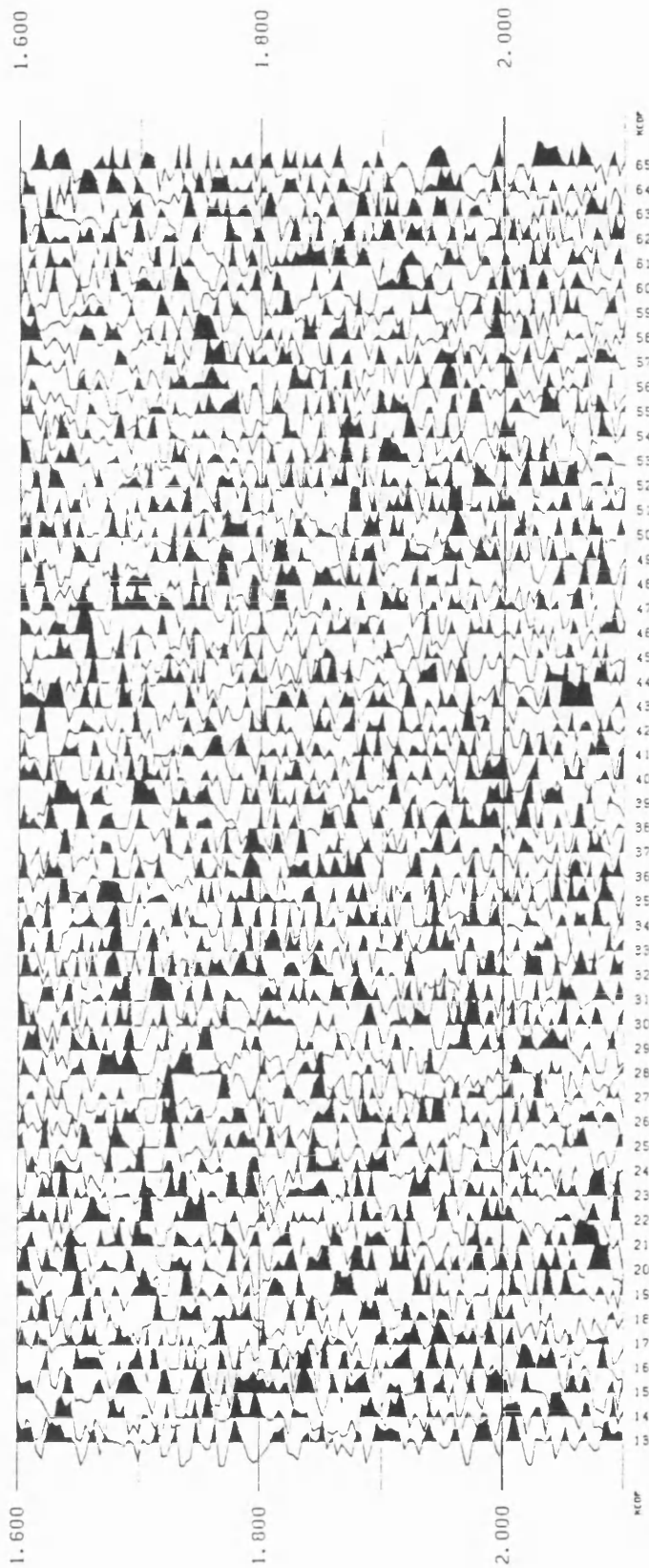


Fig. 6-8. Conventional CDP stacked section of Y-component recordings.
CDP interval 12.5 m; vertical scale in seconds of two-way time.

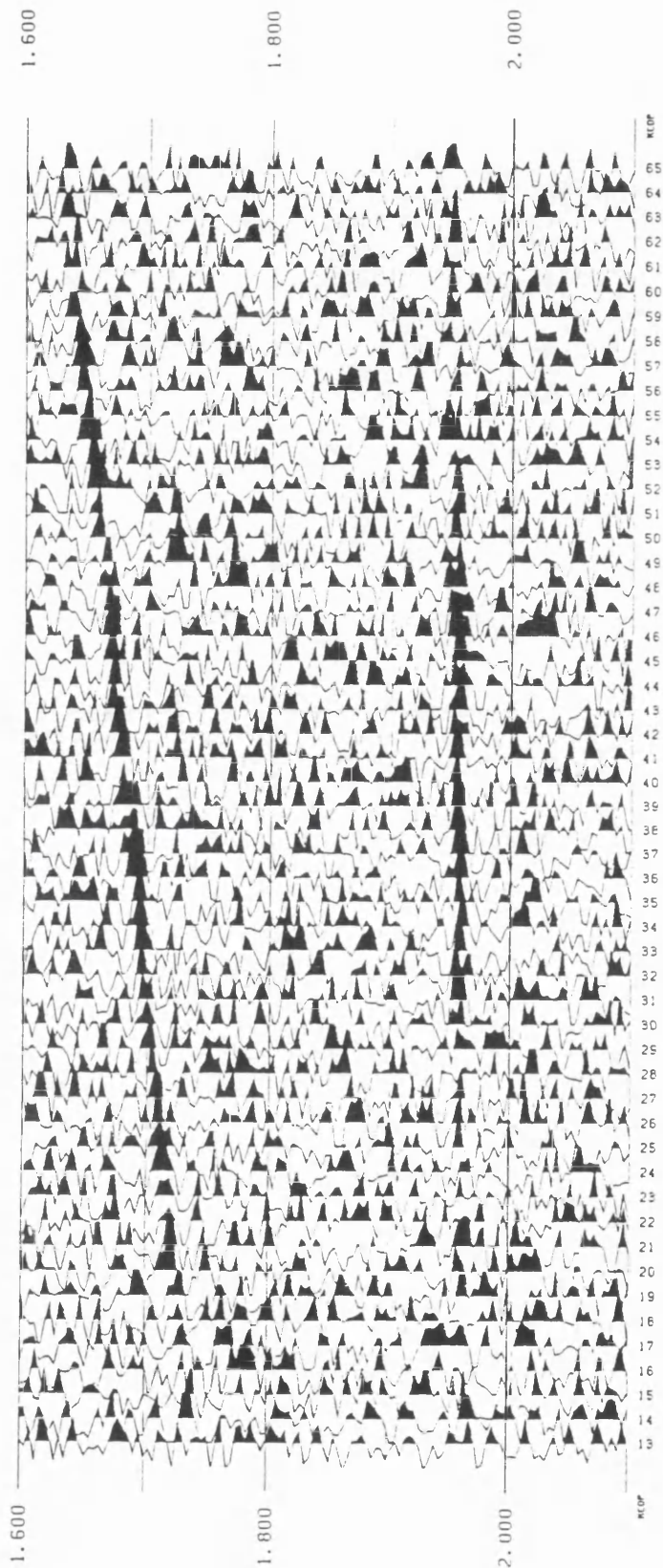


Fig. 6-9. CDP stacked section after the 3CFH filter is applied with a constant assumed velocity of 4 km/s. CDP interval 12.5 m; vertical scale in seconds of two-way time.

raypath and the Z axis plays a important role in the projection calculation in the 3CFH filter design, and is dependent upon the projection velocity obtained by the assumed velocity analysis.

The data acquired with large offsets is especially suited for the 3CFH filter to enhance P-wave horizontal reflections because the filtering would discriminate much more against P-wave energy from dipping interfaces. However a large offset usually violates the assumption that $V_{nmo} = V_{rms} = V_{st}$, only with the case of a horizontally layered model and small spread length. Thus the projection velocity (which is in fact rather insensitive to projection angle) is estimated with much more error. For a small-offset relative to the depth of the interfaces, the angle θ between the vertical component and the raypath of a plane wave becomes small, so that the horizontal component $H(t,x)$ of the P-wave also becomes small and the vertical component $Z(t,x)$ will dominate in the composition of the 3-C measurement $U(t,x)$. The projection velocity is estimated with less error than that for large offsets.

We define the 3CFH filter above by making the small-spread approximation for the horizontal isovelocity multi-layered model. However the assumption of the small spread approximation will degrade the effectiveness of the filtering in enhancing the horizontal reflections, as discussed above. If the velocity is not estimated correctly, it will result in the filter being applied over an incorrect projection angle θ in Figure 6-3, where:

$$\theta \neq \theta_1 \neq \theta_2$$

We could improve the performance of the 3CFH filter by replacing the semblance velocity estimation for single Z-component data with other data, such as velocities from well logs, or else we could redefine the filter as:

$$U(t, x) = Z(t, x)\cos \theta - H(t, x)\sin \theta$$

where

$$\theta = \arctan \left[\frac{2}{\sqrt{\left(\frac{tV_{A_n}}{x}\right)^2 - 1}} \right]$$

and N is the number of layers, V_{A_n} is the average velocity down to n th reflector, which is defined as:

$$\bar{V}_n = \frac{\sum_{i=1}^n V_i t_i}{\sum_{i=1}^n t_i} = \frac{\sum_{i=1}^n V_i (t_{o,i} - t_{o,i-1})}{t_{o,n}}$$

but

$$V_{A_n}^2 = \frac{t_{o,n} V_{rms,n}^2 - t_{o,n-1} V_{rms,n-1}^2}{t_{o,n} - t_{o,n-1}}$$

so

$$\begin{aligned} \bar{V}_n &= \sum_{i=1}^n \sqrt{\frac{t_{o,i} V_{rms,i}^2 - t_{o,i-1} V_{rms,i-1}^2}{t_{o,i} - t_{o,i-1}}} \cdot \frac{(t_{o,i} - t_{o,i-1})}{t_{o,n}} \\ &= \sum_{i=1}^n \frac{\sqrt{(t_{o,i} V_{rms,i}^2 - t_{o,i-1} V_{rms,i-1}^2)(t_{o,i} - t_{o,i-1})}}{t_{o,n}} \end{aligned}$$

where $t_{o,i}$ is the traveltime from surface to the i th reflector; $V_{rms,i}$ is the RMS velocity from surface to the i th reflector.

If neither of the velocity estimators are reliable on the data, a range of constant velocity values can be applied, similarly to that in the conventional velocity spectrum (Taner and Koehler 1969). Then we may focus attention on the interesting horizontal reflections, or else pick velocities in the form of a 3-D gated row plot or a contour plot, as shown schematically in Figure 6-10.

These proposed 3-D velocity analysis methods need new interactive velocity picking tools to be developed. So far the scheme outlined above has not been tried; its usefulness and its practicality still are uncertain, but it should be examined further.

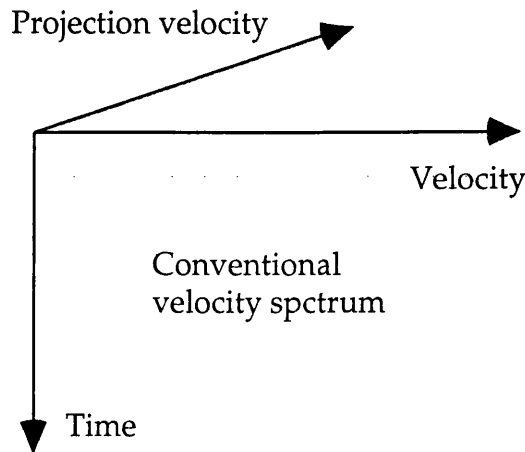


Fig. 6-10. 3-D semblance for projection velocity analysis.

6.6 New Processing modules in SierraSEIS 1.4

To carry out experiments on the new 3-component P-wave processing approach, a module /QTCFH has been programmed and added into SierraSEIS Version 1.4. As almost all industry-standard processing systems, including SierraSEIS, are specially designed for vertical component recording, they cannot sort out the 3-component CMP gathers in the order $X_1, Y_1, Z_1, X_2, Y_2, Z_2, \dots, X_i, Y_i, Z_i$, where i is in the term for their offset. To accommodate the application of the processor /QTCFH another new module /QGATHER has been developed as well, for the synthetic data experiment in this chapter. The detailed notes of usage for the two new processors are described in Appendix H, and their Fortran source codes are given in Appendix B.

6.6.1 Module /QTCFH in SierraSEIS 1.4

The 3CFH filter has been added into SierraSEIS package as a routine processor, named /QTCFH. It is used in processing 3-component data to obtain the enhanced P-wave

reflections, based on the three assumptions. /QTCFH must be applied to the 3-component CMP gather data stream prior to NMO correction and stacking. The 3-component trace stream should be in the order of $X_1, Y_1, Z_1, X_2, Y_2, Z_2, \dots, X_i, Y_i, Z_i, \dots$. The /QTCFH processor can extract the offset and velocity information attached to each trace attribute to calculate the angle between the raypath and vertical axis. However, you can also alternatively manipulate those input information by specifying the parameters in the batch job file.

6.6.2 Module /QGATHER in SierraSEIS 1.4

Industry-standard processing systems such as SierraSEIS are specially designed for vertical component recording, and they do not have routine processors for sorting out the 3-component CMP gathers in the order $X_1, Y_1, Z_1, X_2, Y_2, Z_2, \dots, X_i, Y_i, Z_i, \dots$. This kind of data sorting operation usually uses a large amount of temporary disk buffers to store multi-trace data, and needs the manipulation of multi-address points, so its programming becomes quite complicated. Since SierraSEIS is a trace sequential processing system with input of trace by trace controlled by 5 major parameters for each trace, it is extremely difficult to develop a new 'gathering' module with full features similar to the original one. To accommodate the application of the processor /QTCFH for the synthetic data experiment, a new module /QGATHER, with a limited trace sorting and handling capability, has had to be developed first.

Chapter 7

Processing of vertical component Kola data

7.1 Introduction

The Kola SG-3 superdeep well in the Kola Peninsula, Murmansk Region, Russia, has been cored with more than 80% recovery. Investigation has yielded exciting evidence of current and past fluid flow, as well as physical property and logging data. However, until now it has lacked the deep crustal common-depth-point (CDP) seismic section required for borehole correlation efforts. To remedy this gap in our knowledge, a major multinational experiment, incorporating truck-mounted vibrators was performed during the winter of 1992 (Smythe *et al.* 1994).

The principal aim of the seismic profiling project was to determine the reflection characteristics of the upper crystalline crust, and obtain a whole crustal image, where the primary lithological layering of the Proterozoic supracrustal rocks dips at 40-50°. A secondary priority was to acquire high resolution 3-component surface seismic data for the experiments on newly developed 3-component reflection processing methods.

In this chapter, we present a description of the conventional P-wave processing sequence for the vertical component of the Kola data acquired along the northern portion of the main survey line through the well (Fig. 7-1; Line 1), together with the preliminary processing results.

7.2 Survey geometry and acquisition parameters

This section summarises the fieldwork described by Smythe *et al.* (1994) in which the present author was not involved.

The 38-km long crustal seismic reflection profile was recorded first from south to north along the main survey Line 1, which passes through the well in a direction at right angles

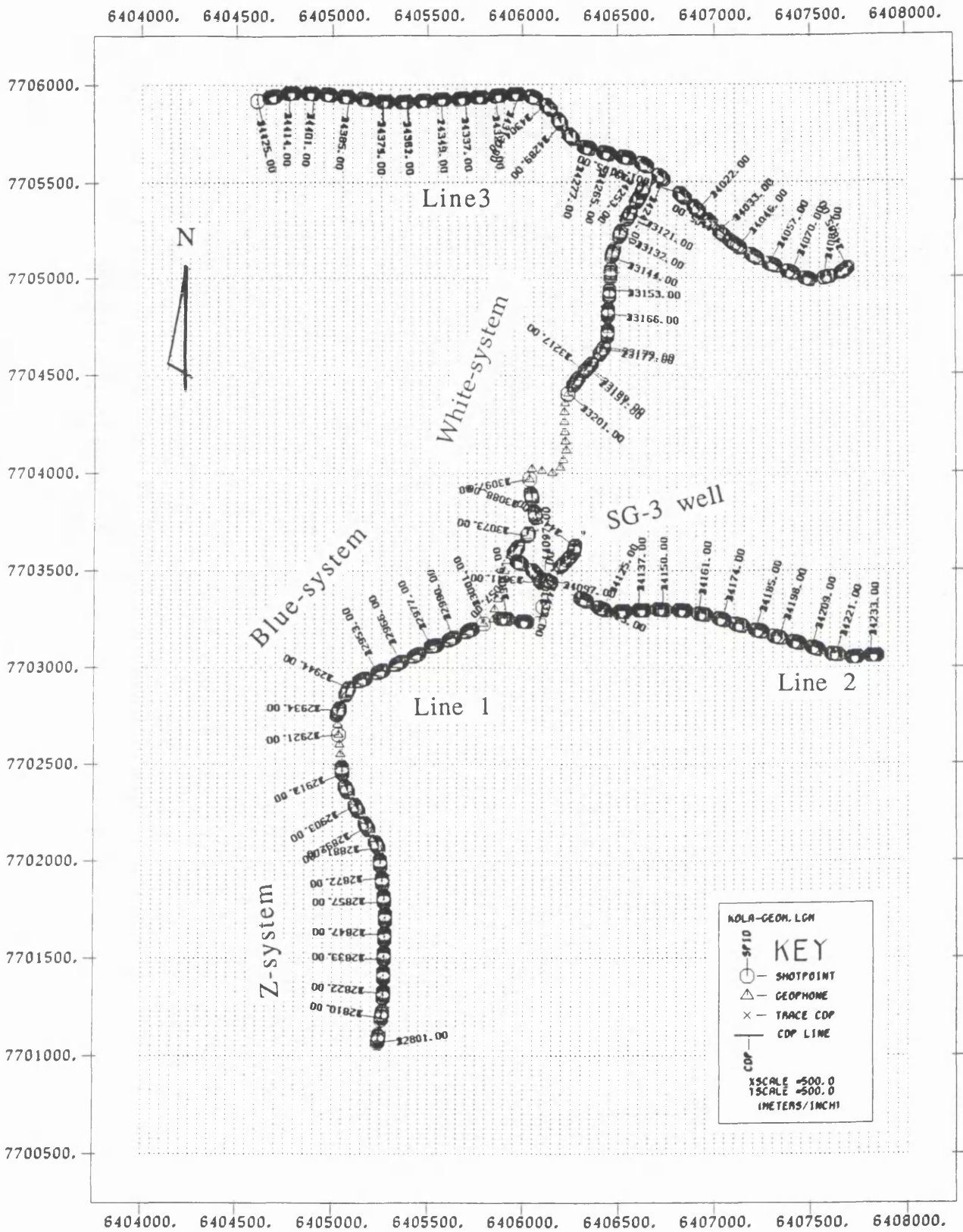


Fig. 7-1. Base map showing the location of seismic survey receiver line (triangles) and the three shot lines (circles) at the northern end of the profile.

to the regional strike. At the north end of the main survey line, there are other two east-west cross-lines which were shot into the fixed N-S receiver array to generate a unique 3-dimensional 3-component coverage of a CDP area around the SG-3 well, as shown in Figure 7-2. However, due to data handling problems within SierraSEIS it has not been possible to include the data from these two lines (Fig. 1; Line 2 and Line 3) in the dataset discussed in this dissertation

7.2.1 Location of survey line

At the north end of the survey, about 6 km of surface reflection data were collected along main survey line in a NNE-SSW crooked line through the SG-3 well, as shown in Figure 7-1. This main line was shot from south to north. Away from the well the lateral deviation of shots or receivers from a mean straight line was less 300 m. Two east-west shot lines were extended to carry out a three-dimensional survey around the well. This three-dimensional, 3-component coverage of a CDP area covers about 6 km² around the SG-3 well, with offsets from 50 m to 5 km.

The data were recorded in 3-component mode - ground motion in X, Y, and Z directions - to give the full wavefield, permitting separation of P-and S-waves. The surface seismic survey was recorded in both 3-component and 3-dimensional formats by using three 90-channel digital recording systems, named the Z, Blue and White systems, with real-time 50 Hz notch filtering applied in the field. The acquisition parameters were chosen on the basis of field tests and, of necessity, represent a compromise between those that were considered ideal and those that the available equipment and budget allowed.

7.2.2 Source type and position

The area near SG-3 well site had previously been the target of VSP surveys. It is covered by Proterozoic volcanics and Archaean gneisses with steeply dipping discordant interfaces and numerous tectonic faults. The seismogeological environment is very complex. So a repetitive source such as vibroseis is used to produce high-frequency energy with a consistent spectrum to suppress large-amplitude ground roll, and improve signal-to-noise

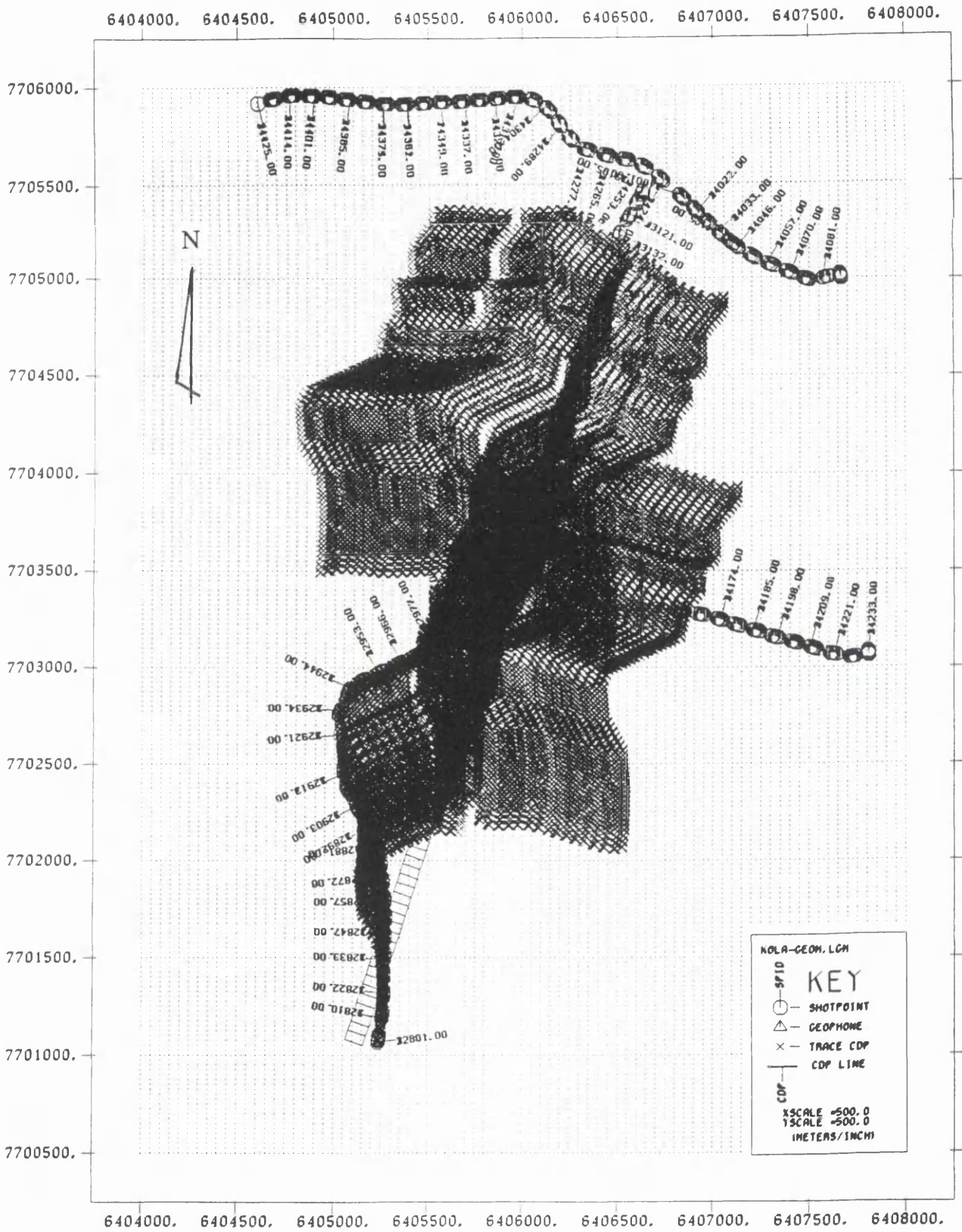


Fig. 7-2. Base map showing the CDP coverage of the area around the SG-3 well.

ratio and trace rejection. Although truck-mounted vibrators are hardly ideal for the terrain, they are powerful. This vibrator source is also equipped with control electronics compatible with the recording equipment being used to collect data.

The decision to use 4 vibrators in a nose-to-tail configuration, to make a linear array, was made in an attempt to inject as much energy as possible to obtain the reflections from the middle crust. Due to mechanical breakdowns, the normal source turned out to be three out of the four vibrators. In practice, the source array usually consisted of 2-3 nose-to-tail vibrators moved up between each of eight sweeps to give an array length of approximately 35 m. This was sufficient to maintain adequate resolution. The source array moved along three different lines. Line 1 (the main line) lies on the main survey station line as marked in Figure 7-1. Line 2 (the East Road line) is oriented from east to west to join the main survey line near the SG-3 well. Line 3 (the Nikel Road line) is oriented in similar direction to Line2, but at the northern end of the survey area (Fig. 7-1).

The production mode sweep was linear, from 10 Hz to 60 Hz with a duration of 20 s and 0.5 s linear tapers on both ends. The long duration of sweep ensured that sufficient energy was injected into the deep crust. Record length was 40 s at a 4 ms sample interval.

7.2.3 Receiver spread configuration

For the CDP data discussed herein, three 90-channel digital recording systems were deployed in a stationary position along the main line from south to north in the order of Z, Blue, and White systems, while the source array moved along the three different lines. Each 90-channel system has its own spread in a 3 x 30 channel mode at a 50 m channel spacing, giving a composite spread 4.5 km long. One recording cabin (Fig. 7-3; G = Glasgow) with two systems (Blue and White) sat between two spreads, and the other, recording with the Z-system (Fig. 7-3; W = Wyoming), triggered source-firing and the recording cycle of all three instruments as shown in Figure 7-3. Thus it is equivalent of a 3 x 90 channel system for recording 3-component data, i.e. vertical, north and east directions at 90 receiver stations simultaneously. To facilitate the recovery of static corrections, no near-source gap was used while the source array was on the main line. This spread results in a wide-angle 3-dimensional cover of the CMP positions as shown in

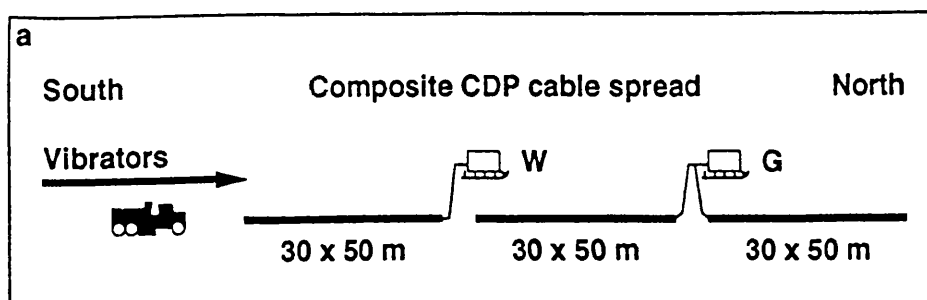


Fig. 7-3. Layout of composite CDP spread of 90 3-component stations linked to sledge-mounted dighouses W (Wyoming University) and G (Glasgow University). The vibrators moved up from south to north. (After Smythe *et al.* 1994)

Figure 7-2. The station spacing of 50 m was used to achieve a maximum 35-fold subsurface coverage near the main line and an average of about 3-4 fold per 50-m square bin in the area around the SG-3 well. The result is a unique 3-dimensional, 3-component crustal reflection data set, complete with well control, to a depth of 12 km. The aperture and density of the data are far too small for orthodox 3-dimensional processing, but the data could permit a test of hypothesis that there are horizontal reflectors at the well.

Positioning was based on a high-quality 1:50,000-scale topographic map enlarged to 1:10,000 scale. Three-dimensional global positioning satellite (GPS) fixes were made at key locations. Absolute positioning is better than 20 m and relative positioning is 5 m or better, which is satisfactory for processing purposes (Smythe *et al.* 1994).

7.3 Wave patterns

The complete wave field was observed in a 3-component mode, and all raw data were preserved in an unsummed, uncorrelated form. After demultiplexing, the surface seismic data amounts to some 40 Gb (Smythe *et al.* 1994). Although the data suffered from the noise problems from pumps at the SG-3 well, the quality is generally good. Fortunately the quality of the vertical component is much better than the horizontal component. The author's contribution to the processing described below starts from the demultiplexed SEG-Y shot records with geometry information applied to the trace headers.

The identification of wave patterns from various images of the complex interferential wave field is possible only near the beginning of the traces where they can be clearly characterised.

7.3.1 *Ground roll*

A repetitive source such as a vibrator generates unwanted noise. One of them is ground roll, which is a type of dispersive waveform propagating along the surface. It is low-frequency and large-amplitude in character. Ground roll usually arises because of the coupling of the compressional wave (P) and the vertical component of shear waves (SV). From the field records in Figure 7-4 and 7-5, we see how ground roll can dominate the shallow area in these shot gathers.

Ground roll is one of the prominent sources of coherent noise in the Kola data. It has a frequency lower than 15 Hz and its amplitude is very high, especially on short-offset records, arriving shortly behind the direct S-wave. The intensity of the contamination from ground roll varies only slightly for the repetitive eight sweeps at same shot station (with a 5 m move-up between sweeps), but sometimes varies rapidly for the records collected at different stations, due to the variation of the earth's surface conditions; see, for example, the shot gather shown in Figure 7-5. Ground roll contamination can be attenuated by bandpass filtering, F-K filtering and CDP stacking.

7.3.2 *First arrivals*

The first arrivals are visible on almost all records in the Kola data. They correspond to the direct P-wave energy in a complicated way. Its dominant frequency and waveform depends on the injected source sweep energy conditions and varies from 25 to 35 Hz at different shot points.

As the first arrivals usually have the strongest energy with the biggest amplitude, the sidelobe noise is likely to be introduced into the correlated dataset by sweep signal correlation. This sort of the sidelobe noise could degrade the data quality and overwhelm later reflections. It should be removed, or at least minimised as much as possible. So far

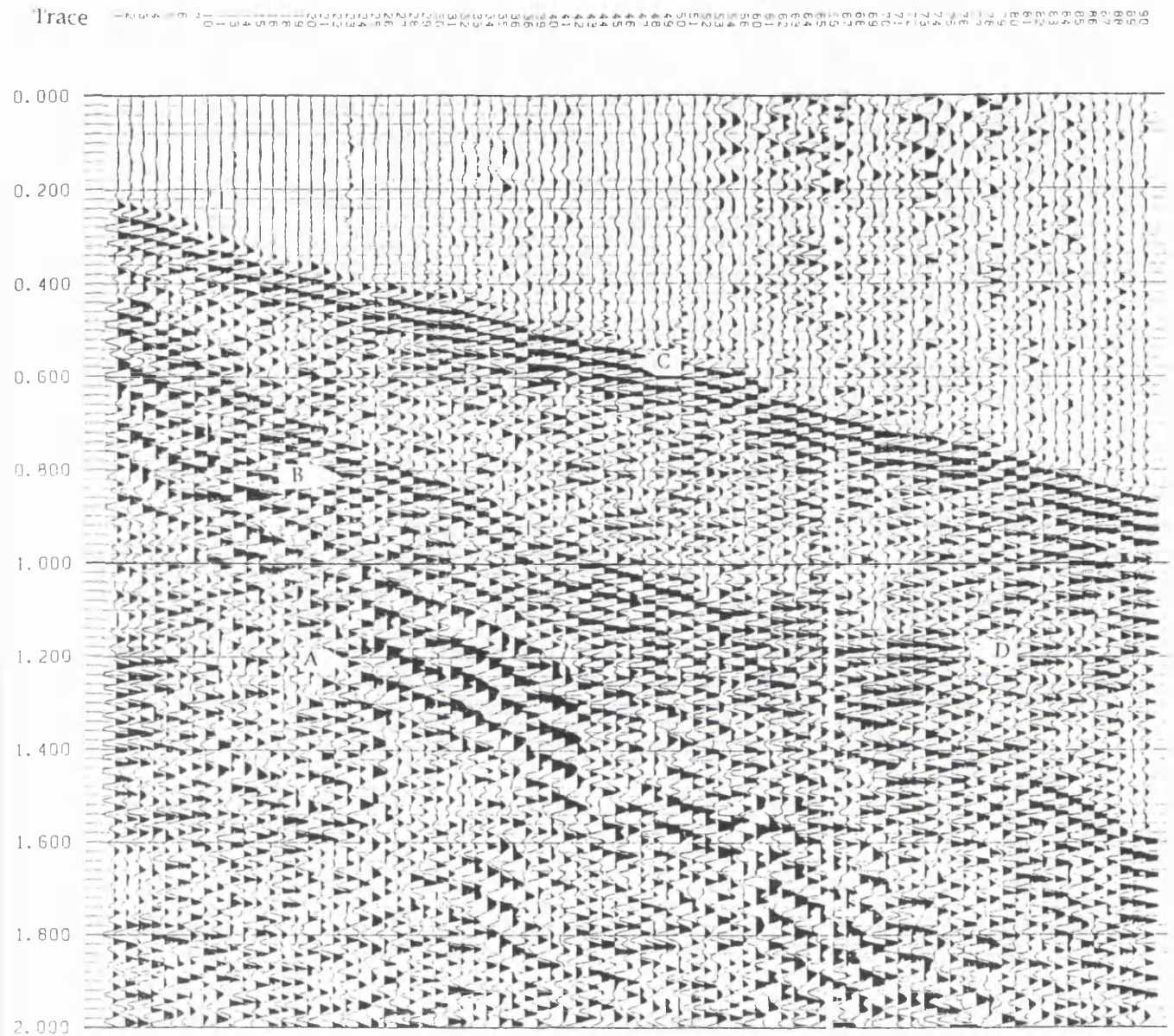


Fig. 7-4. The four types of prominent wave patterns in most Kola data (vertical component). This is an example of one of the common source (shot) gathers, showing ground roll marked as (A), shear wave as (B), direct P-wave as (C), and a reflection as (D). Note that the amplitude of the ground roll does not change much compared with the example shot gather from a different shot point shown in Fig. 7-5. Trace spacing 50 m, vertical scale in seconds.

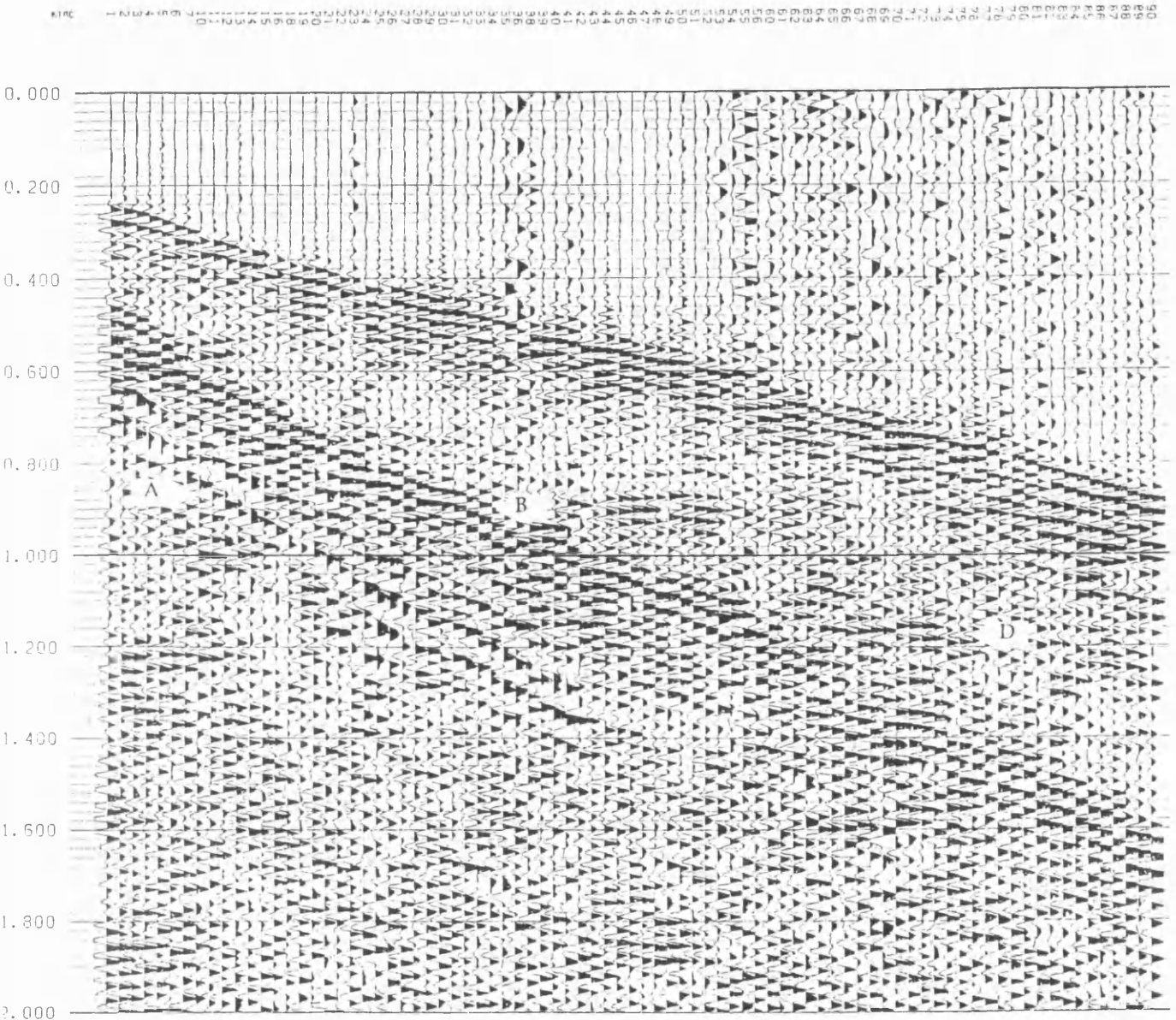


Fig. 7-5. Variation in the amplitude of ground roll marked as (A) is seen in this shot gather. The shear wave marked as (B), direct P-wave as (C), and a reflection as (D).

Trace spacing 50 m, vertical scale in seconds.

the SFU and DOLS filters are the only treatments available to suppress the correlation noise due to the direct wave energy in the pre-correlation domain. Examples of the application of SFU and DOLS to the Kola shot gathers are illustrated in Figures 4-10 and 5-7 above.

7.3.3 *Shear waves*

The large amplitude of the direct S-wave is visible on almost all vertical component shot gathers of Kola data, as indicated in Figure 7-4 and 7-5. It propagates following the direct P-wave with a low apparent velocity, around 2700-2800 m/s. The reflected S-wave energy should be visible on the Kola data, but is hard to distinguish it from reflected P-waves on the vertical component records. As 3-component data have been recorded in the Kola project, it should be possible to separate or remove the undesired S-wave energy from the P-wave reflection by using polarisation filters, for example, the signal enhancement polarisation filter (SEPF) designed by Ma (1990). For the P-wave reflection processing and imaging, S-waves may be considered as unwanted noise and need therefore to be removed.

7.3.4 *P-wave reflections*

A genuine reflection is usually recognised on common-shot gathers by its hyperbolic nature. Since the primary lithological layering of the Proterozoic supracrustal rocks dips at 40°- 50° in the survey area, the P-wave reflection hyperbola is skewed in the updip direction on all shot gathers. The strong reflection energy is only recognised in the relatively shallow section in some pre-processed raw data, and most shot gathers seem to have no clear events with the expected skewed hyperbolic moveout, which are perhaps buried in the strong ambient and coherent noise. As we have seen from the two typical examples of Figures 7-4 and 7-5, the dominant characteristic of reflections in the Kola data is the poor continuity of P-wave reflectors. As we shall show below, the stacked sections suggest that the reflectors are short and discontinuous. Weak velocity contrasts and discordance of interfaces, as we would expect from volcanic layering within a greenstone belt, do not stimulate the generation of strong reflections in this northern

section of the Kola survey area. This contrasts with the southern segment of the main survey line, where a brute stack of vertical component data, shot on gneisses, presents much stronger reflection energy corresponding to the primary dipping interfaces at depth (Smythe *et al.* 1994). Multiples are secondary reflections with interbed or intrabed ray paths. The subsurface medium near the SG-3 well is not favourable for the generation of multiples.

7.3.5 Noise

As the energy propagating within the earth is subject to decay in amplitude because of wavefront divergence and frequency-dependent absorption from the intrinsic attenuation of rock. The desired P-wave signal strength therefore decreases in time, while random noise persists and eventually dominates. Any gain corrections to restore signal strength at later times also boost the random and coherent noise, so that the strong direct P-waves, S-waves and dispersive waves (ground roll) makes up the early part of most Kola shot gathers, while the remaining part contains primarily random and various coherent noise.

The random noise has various sources. A poorly planted geophone on the snow surface, wind motion, transient movements in the vicinity of the recording cable and electrical noise from the recording instruments - all could contribute to the ambient noise. The net result of scattered noise from many scatterers in the subsurface could also cause the random noise. However, the more serious problem is coherent noise. This includes an approximate 18 Hz hum from a pump and other frequencies from various machinery sources at the SG-3 well site. These coherent noise sources usually align in shot gathers, concentrating at the channels located near the well head. The moveout of the constant frequency sinusoidal noise on the B (Blue system) set of traces in Figure 7-6 is to the left (south); that is, it increases with the offset between the the well site (located offset, approximately between the Blue and the White spreads) and receiving stations. It has a velocity similar to that of the ground roll.

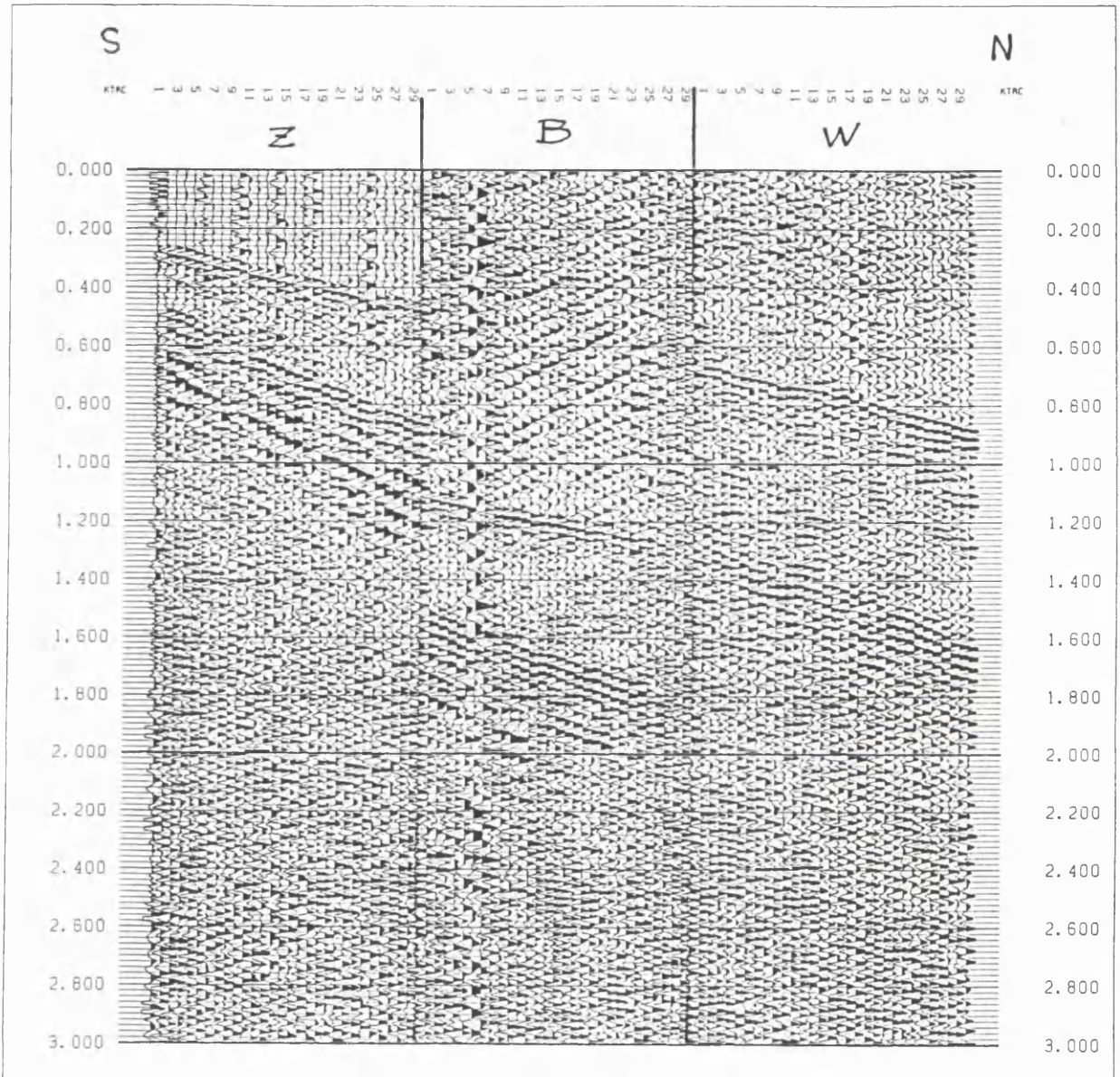


Fig. 7-6. A common source gather consisting of the data of FFID=12681, FFID=22681 and FFID=32681 (from left to right) from three recording systems Z, B and W respectively, without the timing compatibility correction. Note the relative delay of the B system. Note also the strong left-dipping constant-frequency sinusoidal noise seen clearly on the B-system before the direct wave. Trace spacing 50 m, vertical scale in seconds.

7.4 New processing modules

7.4.1 Module /QSHIFT in SierraSEIS 1.4

The new module /QSHIFT has been developed to carry out the correction to ensure that all data from the three different recording systems, each with different trigger circuits, have same time break. It searches for the onset time of the recorded pilot sweep in a common source gather, then shifts all traces up or down to reset the beginning of each trace based on an analysis using autocorrelation and crosscorrelation. The usage and parameters of the processor /QSHIFT, which has been added into SierraSEIS 1.4 as a routine module, is described in Appendix I 1.

7.4.2 Module /QZERO in SierraSEIS 1.4

The new module /QZERO is developed to identify bad traces automatically. It has been added to the SierraSEIS 1.4 package as a routine module. The new processor searches for noise-contaminated traces based on a statistical analysis of amplitude within a certain time window of each trace, and by a comparison of the statistical parameters among the traces in one shot gather. All the bad traces passed through this processor are set to zero. It is very useful when handling a large amount of data with poor quality. It is described in Appendix I 2.

7.4.3 Module /QNOTCH in SierraSEIS 1.4

Stationary sinusoidal noise, such as 50 Hz power-line interference, often contaminates seismic data. When the noise is large compared to wanted signals, it adversely affects pre-stack seismic processing and subsequent interpretation. Analogue notch filter and digital notch filters can be applied to remove this sort of interference. They are easy to use and run extremely fast. Unfortunately they also attenuate signals at the notch frequency, as well as frequencies around the notch point. To solve the problem, the new module /QNOTCH has been developed to cancel any stationary sinusoidal noise in the seismic data. It is based on the digital least-squares filtering algorithm of Linville and Meek (1992). /QNOTCH differs from the usual notch-filtering techniques because the sinusoidal

noise is cancelled without notching the signal spectrum. The usage and parameters of the processor /QSHIFT is described in Appendix I 3.

7.5 Processing parameter table

Processing cannot yield signals from field data without any signal. At best, it suppresses whatever noise is in the field data and brings up the reflection energy that is buried in the noise. In this chapter, the main goal in processing the vertical component data of the Kola reflection seismic survey is to enhance P-wave reflection signals by suppressing the common unwanted energy in the form of coherent and random ambient noise.

As a preliminary processing phase, and due to limited hard disk space, a profile along the main survey line (line 1) was processed to 20 s using only the source points on the same line. The geometry base map with the CDP line, the CMP locations and the statics/elevation profile are presented in Figures 7-7, 7-8 and 7-9 respectively. An interactive and iterative processing sequence with some newly developed processors was used in the preliminary processing phase as shown in Table 7-1.

7.6 Preprocessing

Kola data were recorded in a multiplexed mode using SEG-B format in field. The data were then demultiplexed and converted to the SEG-Y format that is used throughout the subsequent processing discussed in this chapter. Mathematically, demultiplexing is seen as transposing a large matrix so that the columns of the resulting matrix can be read as seismic traces recorded at different offsets with a common shot point. The multi-component Kola data traces is finally sorted out in the order of $x_1, y_1, z_1, x_2, y_2, z_2, \dots, x_n, y_n, z_n$, where n is the receiver station number in a common shot gather, and z represents the vertical component, and x and y the two horizontal components respectively.

Table 7-1. Processing Parameter List

SORT VERTICAL COMPONENT FROM SEG-Y EXABYTE TAPES

Only SierraSEIS processor "IN" Valid.

Separate Exabyte tapes contain SEG-Y shot gathers for Z, B, and W recording systems.

DATA EDITING

Timing compatibility correction	Automatic
Trace kills	Automatic
Summing of 8 shot gather	Interactive
Muting	First-break muting

PRE-CORRELATION FILTERING

Spectral analysis From 0 to 80 Hz

Z system:

Notch Filtering Frequencies and Gaps in Table 3

Blue system:

Notch Filtering Frequencies and Gaps in Table 3

White system

Notch Filtering Frequencies and Gaps in Table 3

CORRELATION

Synthetic or pilot sweep From 10 to 60 Hz in 20 s with 0.5 s linear tapers

SPHERICAL DIVERGENCE COMPENSATION

End time 12 s

Scalar

CROOKED LINE GEOMETRY

Bin length 25 m

Bin width 80 m

VELOCITY ANALYSIS

Semblance analysis Some done using ISX interactively

NMO**F-K FILTERING**

Filter design Initially by ISX interactively

Pie-slice filter

Coordinates of the area to filter: 0.5, 10 Hz -- 0.5, 80 Hz in $f-k$ domain

STACK**RESIDUAL STATICS CORRECTION**

Cross-correlation window 1800 - 2400 ms at CDP 30; 1000 - 1700 ms at CDP 230

POST-STACK

Bandpass filtering 10-35 Hz

Auto-gain-control Window: 1 s

Plot

Coherency filtering Searching 8 traces

Auto-gain-control Window: 1 s

Plot

DECONVOLUTION

Length of autocorrelation window 2400 ms

Maximum lag for operator 2400 ms

Length of prediction lag 4 ms

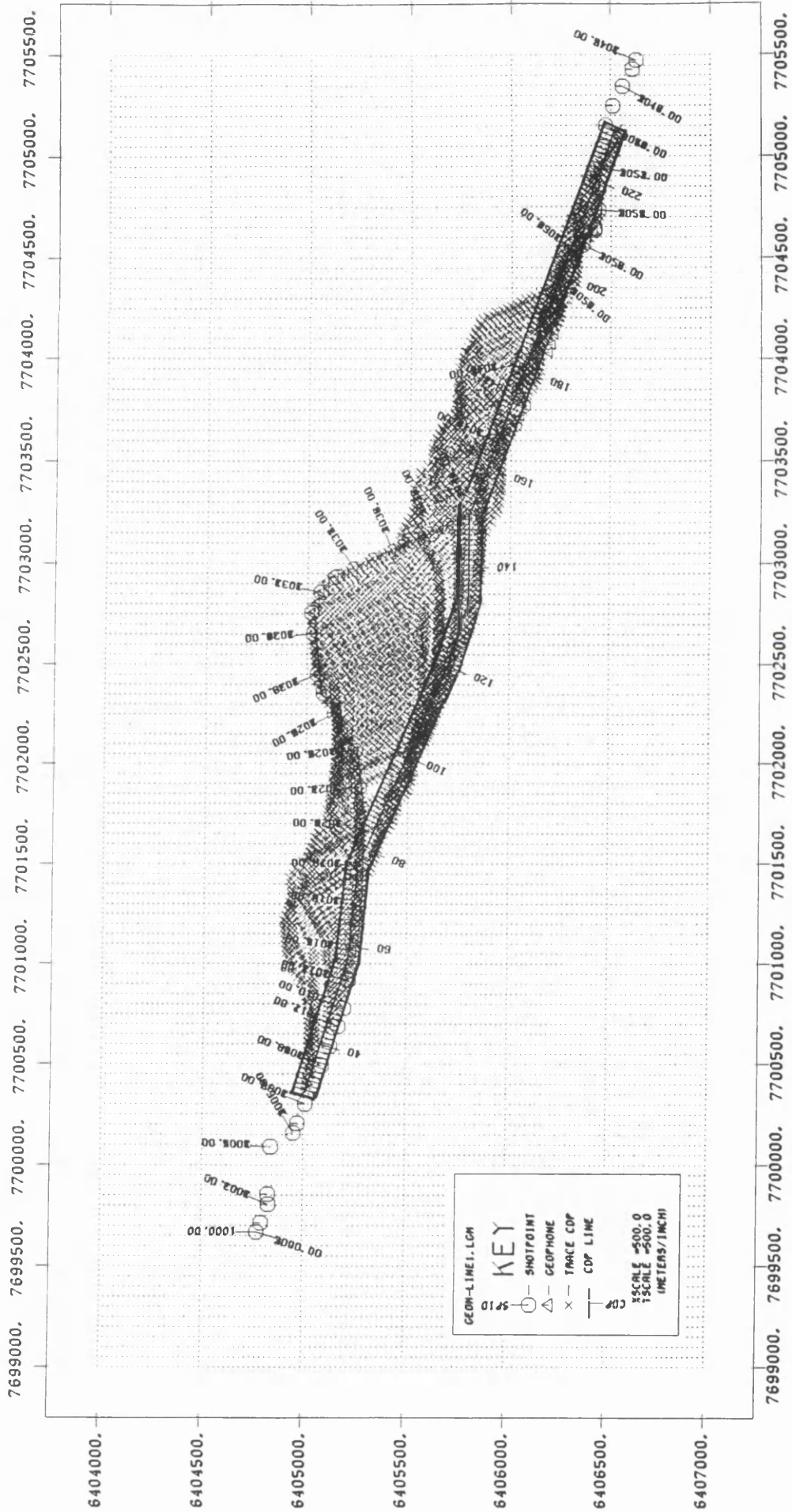


Fig. 7-8. The base map showing the location of CMPs and the bins. It is designed for the vibrator array on Line 1 in Fig. 7-7 with same scale.

7.6.1 Compatibility correction for the recording systems

As mentioned in the section 7.2.3, three recording systems had to be merged into one 90-channel 3-component system. Unfortunately one of them (the Blue system) had a different electrical trigger circuit from the other two. That resulted in a different recording start time. When correlated with a synthetic sweep, the traces from the three recording system are not compatible in time, as shown in Figure 7-6. The new module /QSHIFT in SierraSEIS 1.43 has been applied to all Kola shot gathers to reset the beginning time of the data traces from the different recording systems. After this correction, the traces in one shot gather will have the correct recording time relative to the shot instant. For instance, the corrected version of the gather of Figure 7-6 is demonstrated in Figure 7-10. This timing system compatibility correction is sometimes necessary for the data recorded on different recording systems, and the processor /QSHIFT provides an excellent solution. Refer to section 7.4.1 for details about /QSHIFT.

7.6.2 Data editing

Because the Kola data were acquired on a deep snow surface in the Arctic, varying from 0-2 m depth, poor coupling between geophone and the Earth's surface often led to very bad signal-to-noise ratio at some stations. Another prominent source of interfering noise came from the SG-3 wellhead operations, as the northern portion of the survey line passes through the drilling site. There are usually some 3 to 8 bad or dead traces in any one 30 trace vertical component shot gather on any one of the three systems. As eight shot gathers were collected for each shot position, there are in total some 1464 shot gathers for those shots on the main survey line (Line 1). This is too laborious to edit one-by-one, either manually or interactively. Therefore we have used the newly developed processor /QZERO in SierraSEIS 1.4 to identify these bad traces automatically. /QZERO searches for noise-contaminated traces based on a statistical analysis of amplitude within a certain time window of each trace, and by comparison with the traces in each shot gather. For the data from Z- and W-recording systems, default thresholds are used due to their good average quality, which is specified by the amplitude analysis in each shot gather. For the data from the B-recording system, we first use /QZERO with parameter SWITCH to check the relative noisy level by printing the statistical indicators of average amplitude of

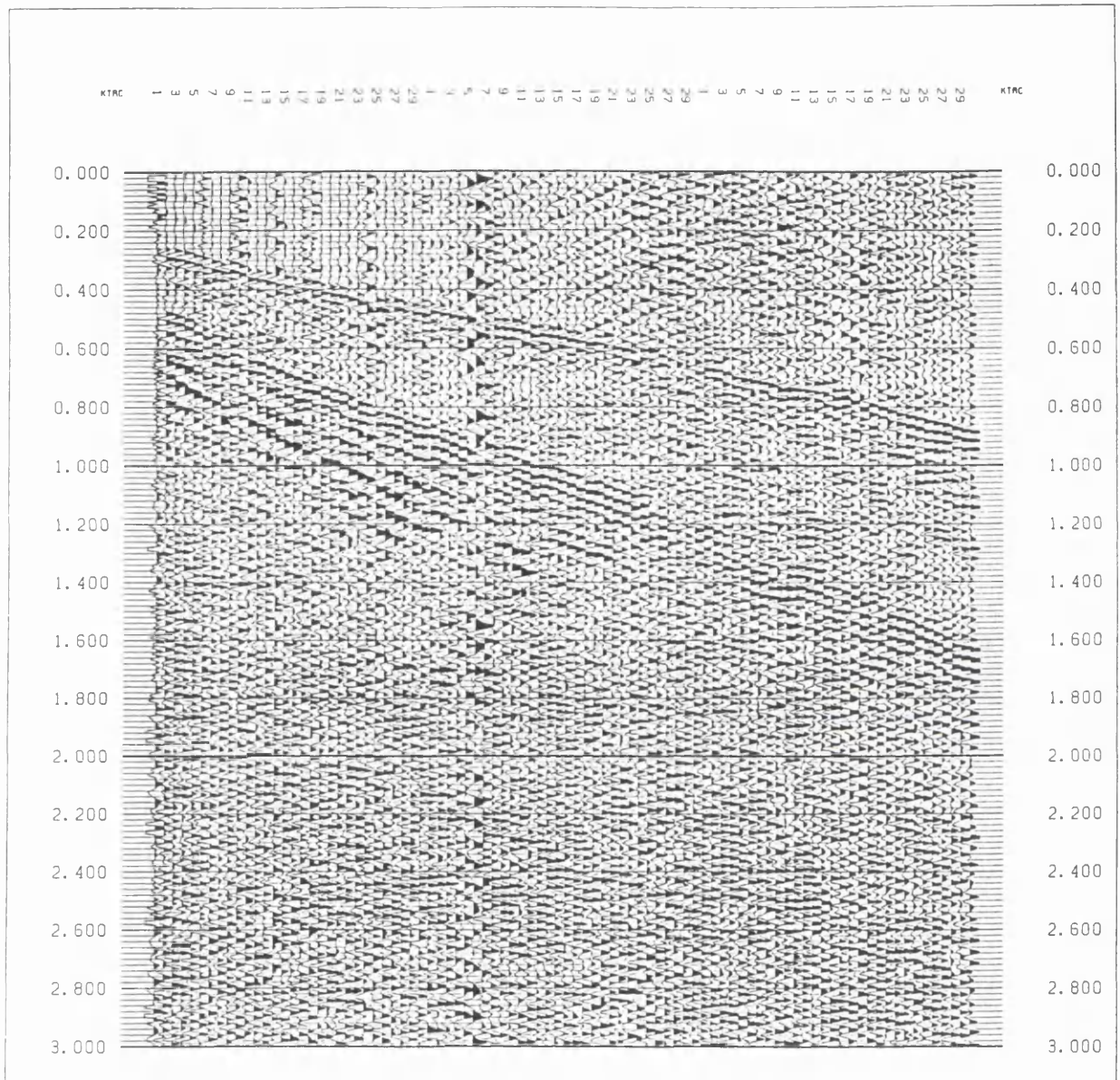


Fig. 7-10. The same common source gather in Figure 7-6-1, but after compatibility correction by /QSHIFT. It shows that the records of the B system are shifted to a reasonable onset time. Trace spacing 50 m, vertical scale in seconds.

each trace in one shot gather. The auto-trace-zeroing process was then applied with a range of threshold values to find out the desired parameters. All the overly noisy or dead traces passed through this processor are set to zero. Some of the processed Kola shot gathers are shown as an example in Figure 7-11, which are in shot gather order. /QZERO works well in processing the Kola data. It is very useful when handling a large amount of data with poor quality.

In addition to the auto-killing of the traces with low signal-to-noise ratio using the new processor /QZERO, some bad shot gathers due to occasionally faulty amplifiers in the recording systems are removed manually before the summing. In total, 25 shot gathers were eliminated from the Z recording system, 76 bad shot gathers from the B recording system, and 35 shot gathers from the W recording system.

7.6.3 Geometry

Finally, the field geometry is incorporated into the Kola data in line 1. Based on the information from a high-quality 1:50,000-scale topographic map enlarged to 1:10,000 scale the coordinates and elevation of shot and receiver locations for all 3-component traces are used at this stage to carry out static correction, and move the traveltimes to a common datum level as shown in Figure 7-9. The detailed SierraSEIS processing job file is listed in Appendix J. Some types of processing problems could arise from incorrectly setting up the Kola field geometry. We will discuss them in the following section.

7.6.4 Application of gain

Gain is a time-variant scaling in which the scaling function is based on a desired criterion. In the Kola data processing, the gain for spherical spreading correction is applied to compensate for the geometric spreading decay of the wave amplitude with depth. The primary velocity of 5000 m/s at surface, linearly increasing to 6000 m/s at 20 s, is used to calculate the gain function, as no significant velocity variation is observed in the Kola survey area. Time-windowed AGC gain is used in most of the data displays of this chapter with a time gate from 200 ms to 1000 ms. As we see in all the plots, while the desired

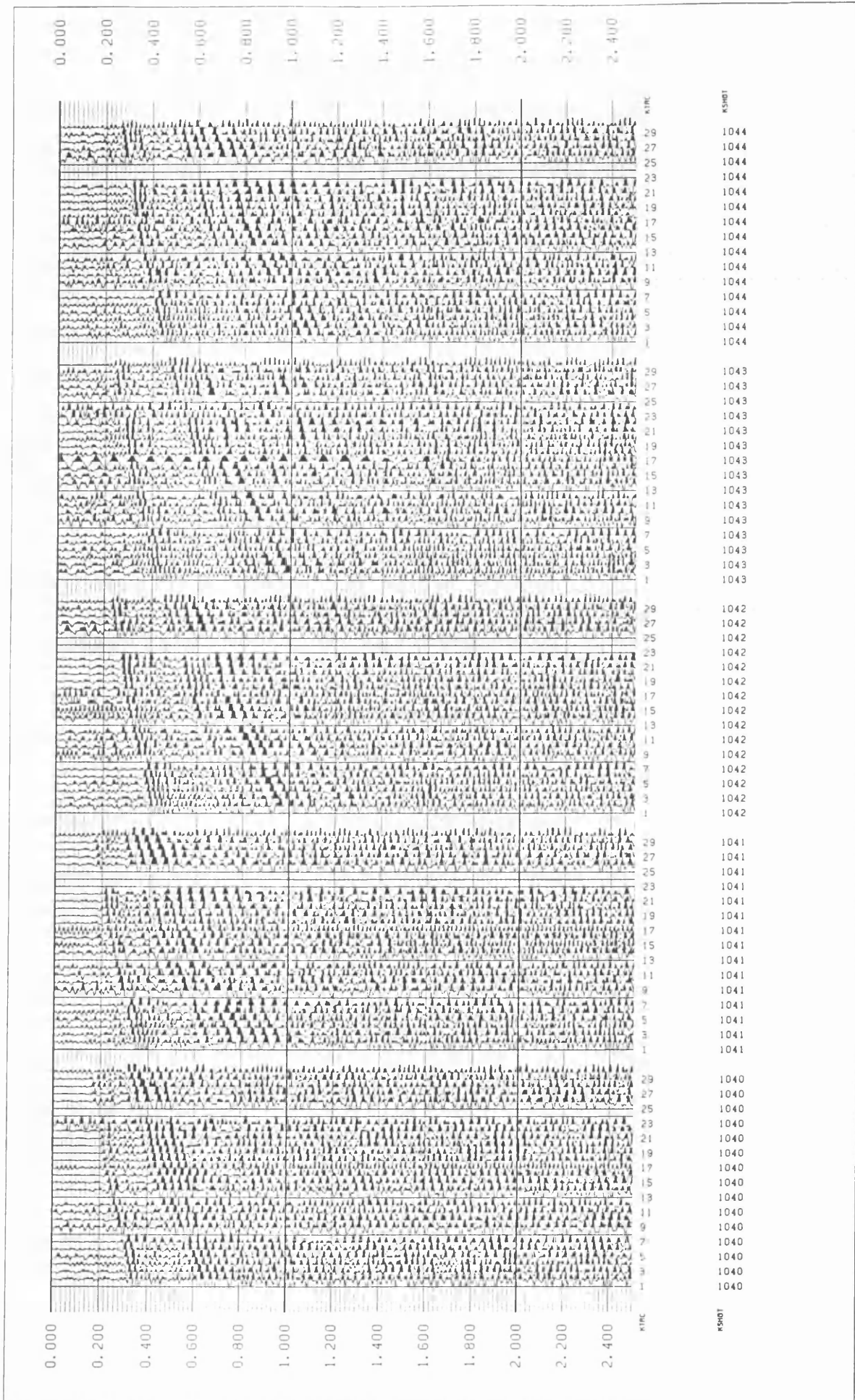


Fig. 7-11. The five shotgathers (from Z-system) out of the new developed processor /QZERO, which sets bad and dead traces to zero automatically. Trace spacing 50 m, vertical scale in seconds.

signals have been brought up in strength, noise components in the data have also been boosted. This is one undesirable aspect of both types of gain application.

7.7 Spectral Characteristics and filtering

The frequency content of the most prominent reflectors is in the 10-45 Hz range. The optimum results were produced when processing took place on data spectrally balanced between 20-45 Hz.

7.7.1 Application of notch filter

The data were examined carefully to find out the amount of stationary sinusoidal contamination caused by the rotating machinery, generators of the SG-3 well site, water pumps, vibrator and doghouses, as shown in the examples in Figure 7-12. The frequencies of some sinusoidal noise components vary slightly with time, so that different notches had to be used to ensure a minimum loss of desired signal. Table 7-2 shows details of these prominent frequencies and the notch gaps applied to cancel the stationary sinusoidal noise. Figure 7-13 presents a comparison of the filtered shot with original version.

In the field, an analogue notch filter was used to attenuate power-line interference which corrupted the recording data with 50 Hz noise. However it is not flawless. The first flaw is that the frequency gap of the analogue filter is so big that a wide signal spectrum is notched off around 50 Hz, resulting in the degradation of data quality as shown in Figure 7-12d. The second flaw is that analogue filters sometimes performed poorly due to the instability of the electrical circuits in the recording systems, as shown in Figure 7-14. Since most of the other sinusoidal noise components shift somewhat in time, the newly developed filter /QNOTCH, described in section 5.4.3 above, could not be successfully applied to the data described in this chapter, so the conventional digital notch filter was used instead.

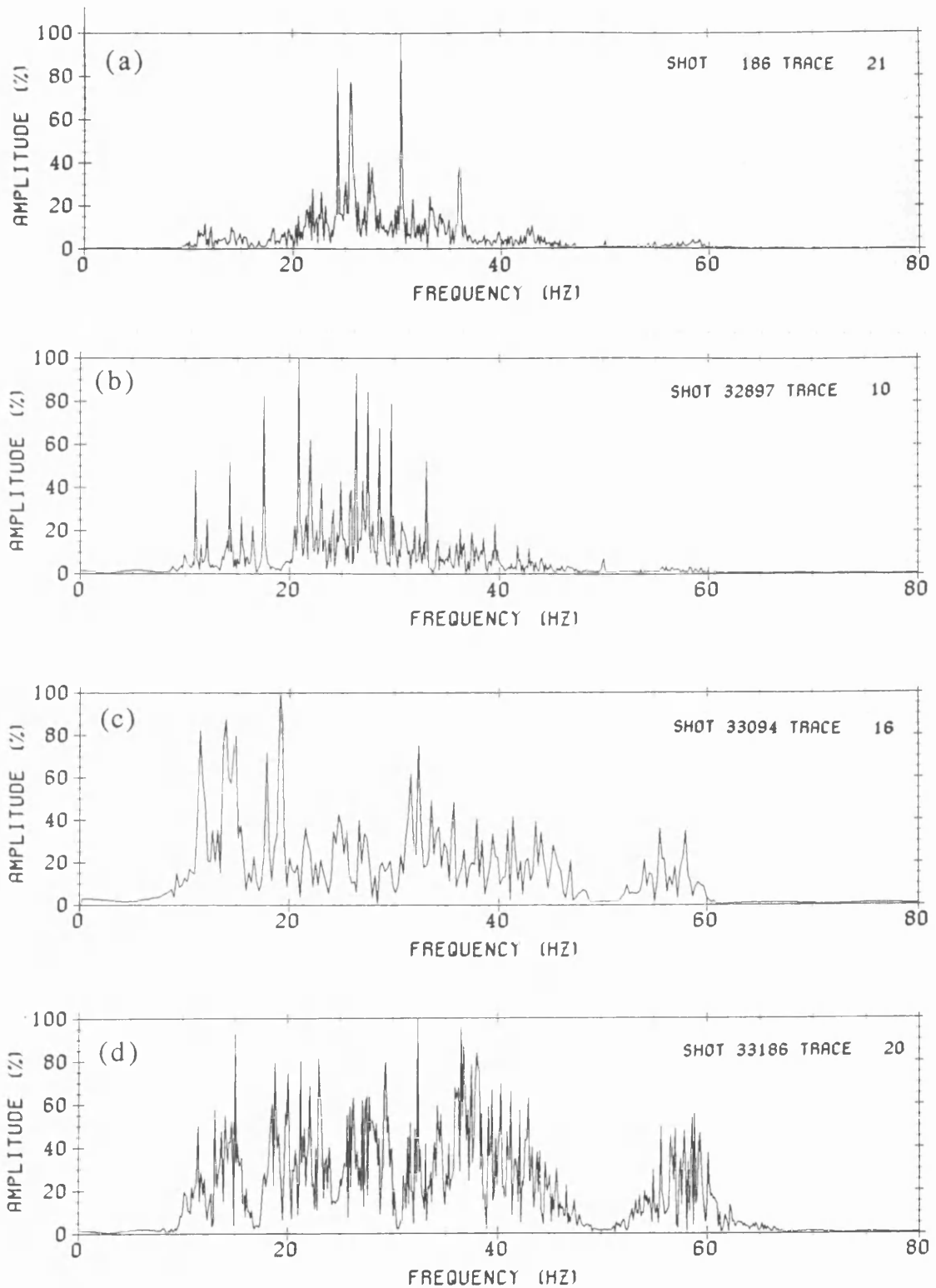


Fig. 7-12. Frequency amplitude spectra for (a) shot 13186 trace 21, (b) shot 32897 trace 10 and (c) shot 33094 trace 16 show how the Kola data are corrupted by various stationary sinusoidal noise components. (d) is an example how the 50 Hz analogue notch filtering in field leads to the degradation of Kola data because a big gap was used.

Table 7-2. Frequencies of stationary sinusoidal contamination

System	Centre Frequency (Hz)	Notch Gap	Field file nos. (FFID)
Z	50	1	All data
	16.5	2	All data
	25.5	2	12870 - 112898
B	50.0	1.0	All data
	12.3	0.3	All data
	16.7	1.0	All data
	25.5	1.0	22681 - 22711
			22713 - 22719
			22751 - 22753
			22777 - 22798
	18.5	0.8	22810 - 22823
			22825 - 22858
			22886 - 22919
			22921 - 23008
			23065 - 23224
W	50.0	1.0	All data
	12.3	0.3	All data
	16.8	2.0	All data
	24.7	0.5	All data
	33.4	0.5	All data
			22810 - 22823
			22825 - 22858
			22886 - 22919
			22921 - 23008
			23065 - 23224
			22810 - 22823
			22825 - 22858
		22886 - 22919	
		22921 - 23008	
		23065 - 23224	

Note: SG-3 well is located between B- and W-recording systems.

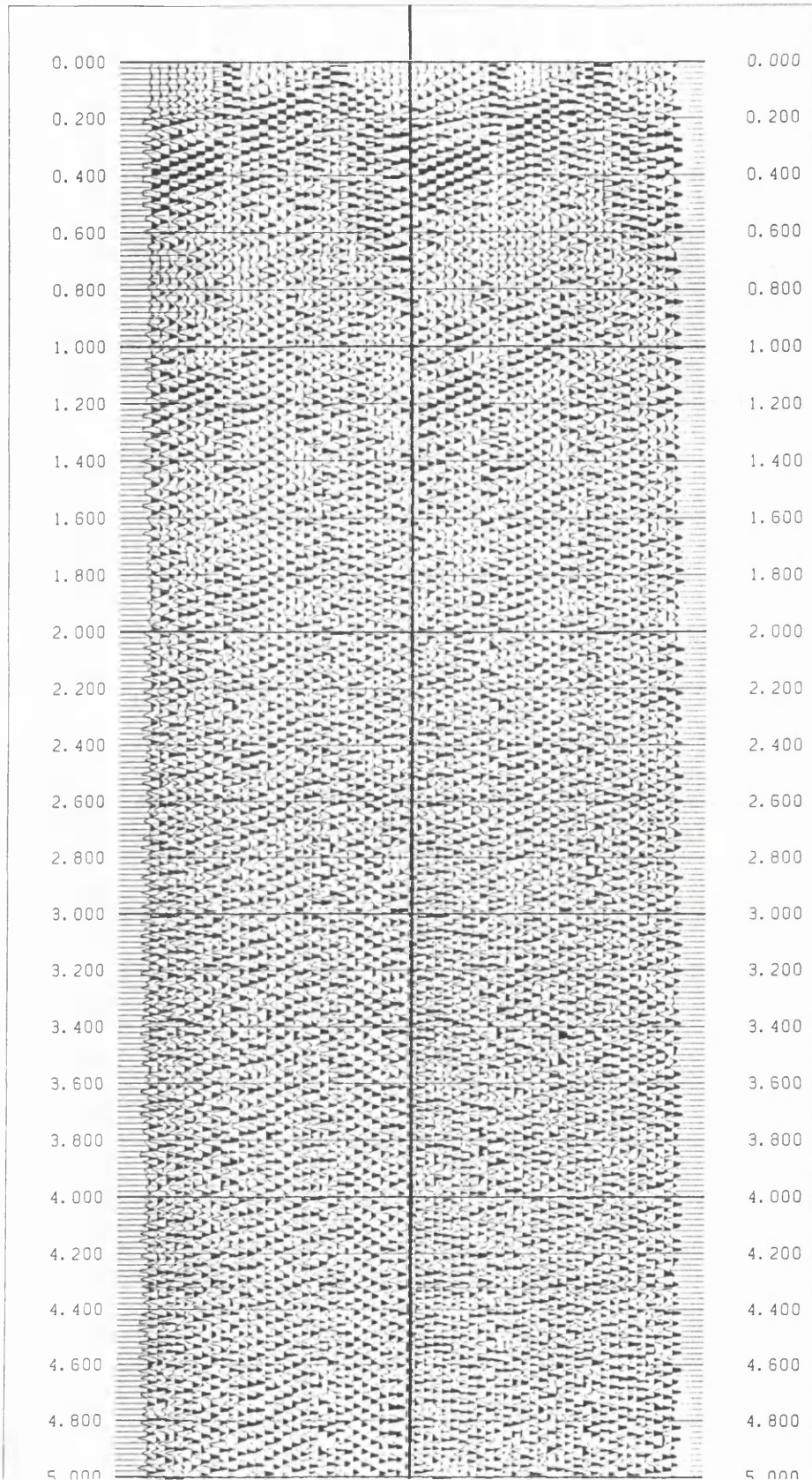


Fig. 7-13. Comparison of a filtered common shot gather (right) from the W-system FFID=33207 with its original version (left). The stationary sinusoidal noise components are mostly suppressed as shown on the right panel. Fig. 7-13. Trace spacing 50 m, vertical scale in seconds.

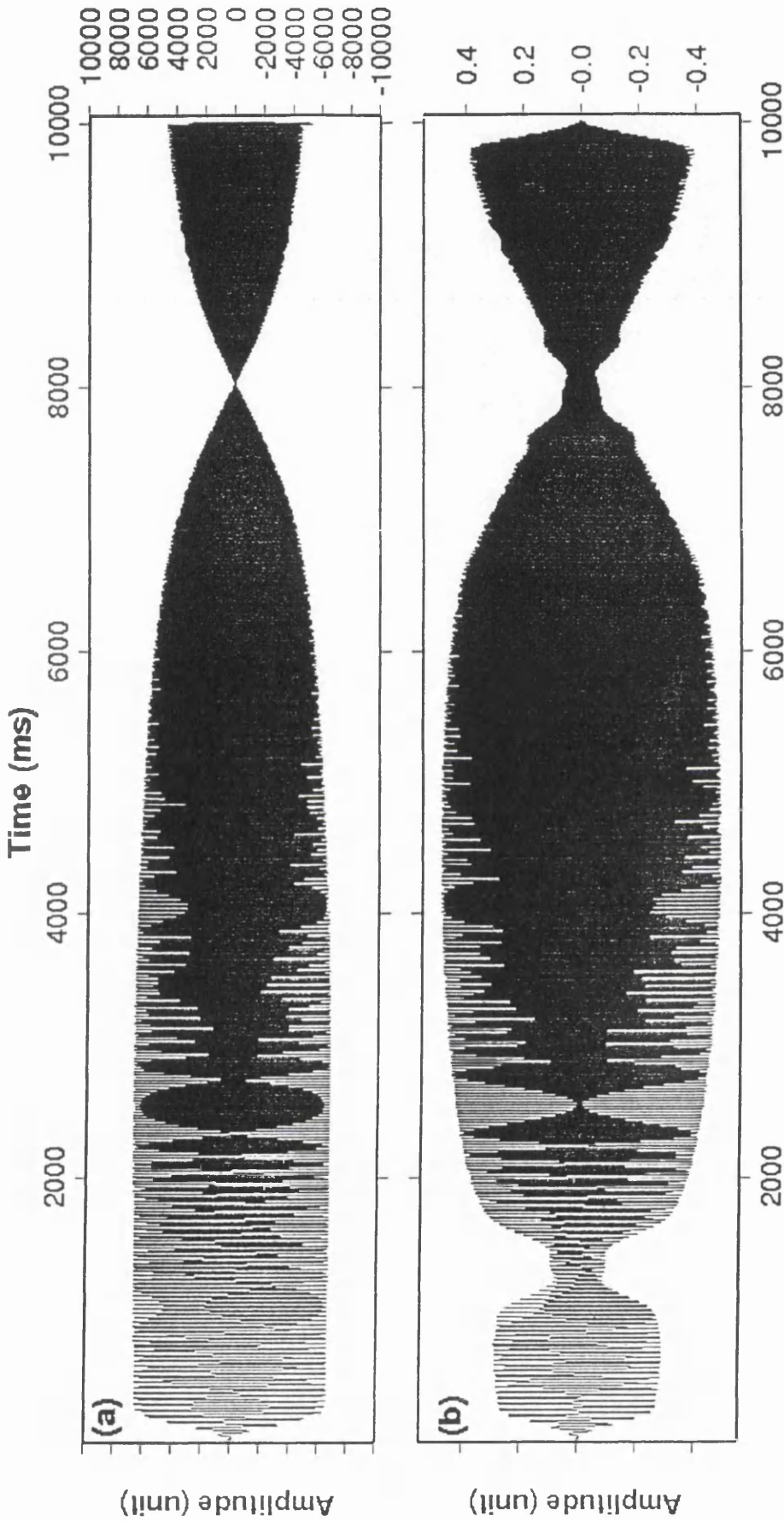


Fig. 7-14. Flawless analogue notch filtering on a recorded sweep from the W-system is shown in (a). Sometimes the instability of the electrical circuits in the recording systems results in bad analogue notch filtering as shown in (b), which is from the Z-system. Note that their amplitudes are different from each other as different amplifiers were used in the different recording systems.

7.7.2 Application of f - k filter

In addition to the application of a notch filter to suppress the stationary sinusoidal noise, an f - k filter is used as well to eliminate unwanted energy, e.g. coherent linear noise (in the form of ground roll), guided waves and side-scattered energy, which commonly obscures the genuine reflections.

2-D Fourier transformation is a way to decompose a wave field into its plane-wave components. Each plane wave carries a monochromatic signal that propagates at a certain angle from the vertical. Events with the same dip in the (t,x) plane, regardless of location, are mapped onto a single line in the radial direction on the $(f-k)$ plane. This is the basis for the f - k dip filter, where we define and apply a reject fan in the transform domain. In the Kola data processing, the reject fan in the f - k domain is depicted in the processing parameter table (Table 7-1) 0.5, 10 Hz to 0.5, 80 Hz. The k units here are spatial Nyquist units. Figure 7-15 is a comparison of an f - k filtered Kola shot gather with the original unfiltered version.

7.7.3 Application of new SFU filter

To test the new pre-correlation SFU filter some shot gathers from the Z-recording system were used to show how well the vibroseis direct wave is removed without attenuating desired signals. The method is described in Chapter 4, and a sample shot gather from the Kola dataset is shown in Figure 4-10.

As the correlation noise problem caused by the direct wave is not very serious in the case of the shallow Kola data (the uppermost 4 s or so), and because the filter would have taken too long to apply to the full 40 s uncorrelated trace length, SFU filtering was only applied to some shot gathers as a test. However, we would recommend using SFU filtering in a processing project, if the aim is to improve the reflection data from the lower crust.

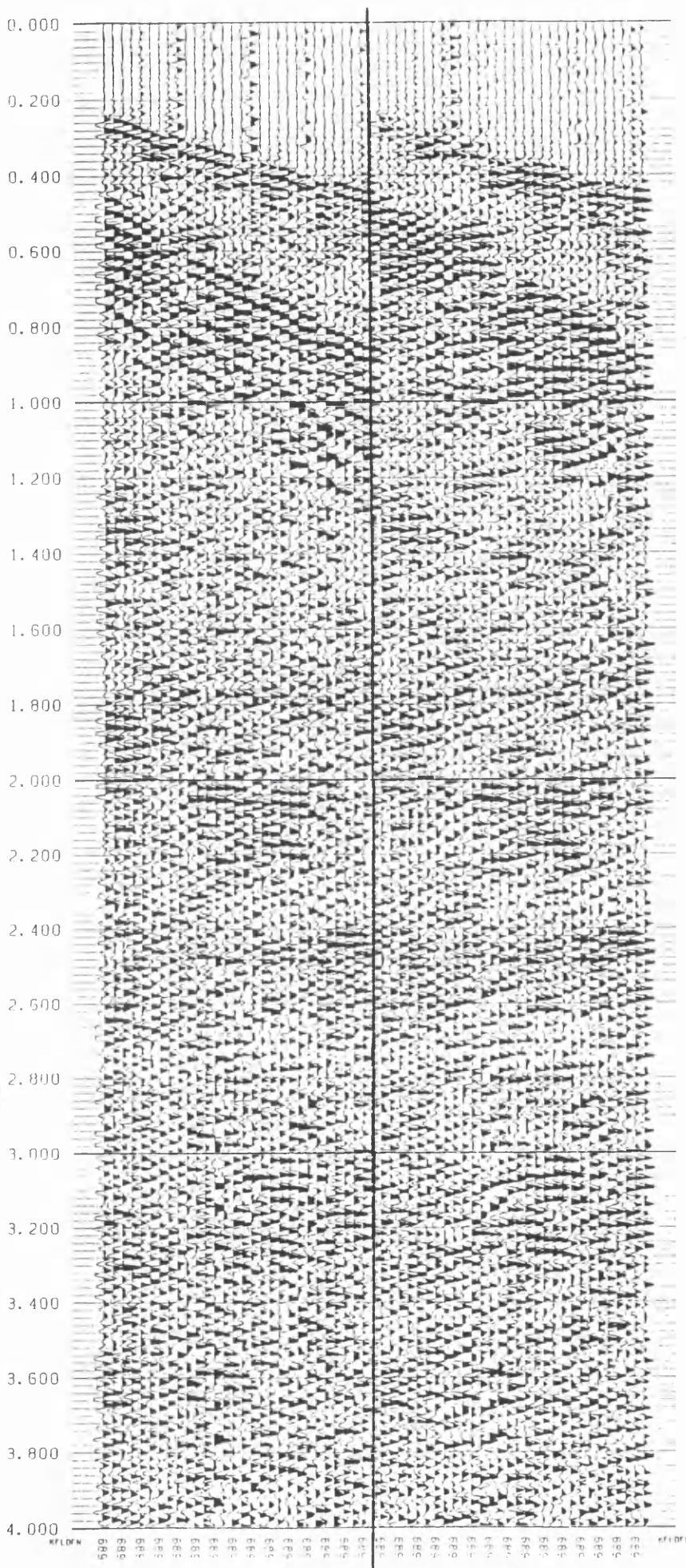


Fig. 7-15. Comparison of a filtered version (right) after 2-D F-K filtering with its original version (left), common shot gather FFID=12689 from Z recording system. Trace spacing 50 m, vertical scale in seconds.

7.8 CMP sorting

Seismic data acquisition with multifold coverage, like Kola data, is usually done in shot-receiver coordinates, and seismic data processing is conventionally done in midpoint-offset coordinates. Therefore, after the initial signal processing described above, the Kola data are sorted from the shot-receiver to the common midpoint-offset (CMP) domain. The CDP gather is equivalent to a CMP gather only when reflectors are horizontal and velocity does not vary horizontally.

7.8.1 Summing shot gathers

The latest version 2.1 of the SierraSEIS package cannot handle the 1500 shot gathers individually in the application of geometry information. We have to sum the 8 sweeps at each shotpoint to reduce the data volume, regardless of the 5 m moveup of each sweep. This could lead to the degradation of the Kola data to a certain extent, since the summed source has been horizontally smeared over 35 m.

7.8.2 Crooked line binning

The problem of coping with a crooked survey line is especially serious for the Kola high-resolution reflection experiment. Figure 7-7 shows that the main survey line contains a big dog-leg between CDP stations 80-150 that results in scattering of the shot to receiver midpoint positions (CMPs). Some of them are offset away from the survey line by as much as 800 m, as shown in Figure 7-8. We examined two binning strategies in which the position and width of CMP bins, together with the restrictions of SierraSEIS package on definition of the first and last bins on the CMP line, were varied. Early tests seemed to indicate that moving the CMP line away from the crooked station line toward the dense trace midpoints produced a significantly improved section near the dog leg. However, information about the uppermost 700 ms below the Earth's surface is then lost, due to the lack of short source-receiver offsets in the stacked section. After more careful specification, the best CMP section was found to be a nearly straight one, positioned near to the recording station line at either end, ensuring that the densest CMPs were included in the bins, as shown in Figure 7-8. Two bin sizes were tested. The default one has a size of

25 m of CMP interval and width of 50 m. The enlarged one has same CMP interval, but with a width of 80 m. The CMP section with small bins is more reasonable for the stacking of shallow signals in the CMP gather. The bigger bins results in higher fold near bends along the main survey road, and this is the one which is used for the following processing. The result is presented in Figure 7-16 (following page) and at full 10 cm/s scale in the pocket inside the rear cover (Fig. 7-16a).

7.8.3 *Velocity analysis and NMO correction*

As the survey is targeting on the deep reflectors below 3000 m, a constant velocity of 5000 m/s and thickness of 10 m is used for weathering surficial cover. Velocity data from the well were not available. The velocity analysis was conducted using both the interactive interpretation environment ISX and the normal batch processing system SierraSEIS. Velocity depth functions could not be picked from semblance plots, because of the weakness of the reflection signals from depth, which differ qualitatively and quantitatively from those obtained when investigating thick sedimentary sections. A constant-velocity moveout correction method was used for the velocity analysis in this chapter. Finally the normal moveout correction (NMO) based on a linearly varying function from 5000 m/s to 6000 m/s was then applied to the Kola data. The CMP stack is obtained by summing over the offset. It is an approximation to a zero-offset section.

7.8.4 *Muting*

As a result of the NMO correction, a frequency distortion occurs, particularly for shallow events and at large offsets. This is called NMO stretch. Because of the stretched waveform, stacking the NMO-corrected CMP gather will severely damage the shallow events. This problem can be solved by muting the stretched zones in the gather. In our case, the muting is done with 80% stretch limit for all NMO-correct gathers. In addition, a top mute is designed for each shot gather interactively in ISX to remove the direct wave energy since the SFU and DOLS filters were not applied in this preliminary processing phase. The muting zone was positioned close to the first breaks so as to retain as much shallow information as possible.

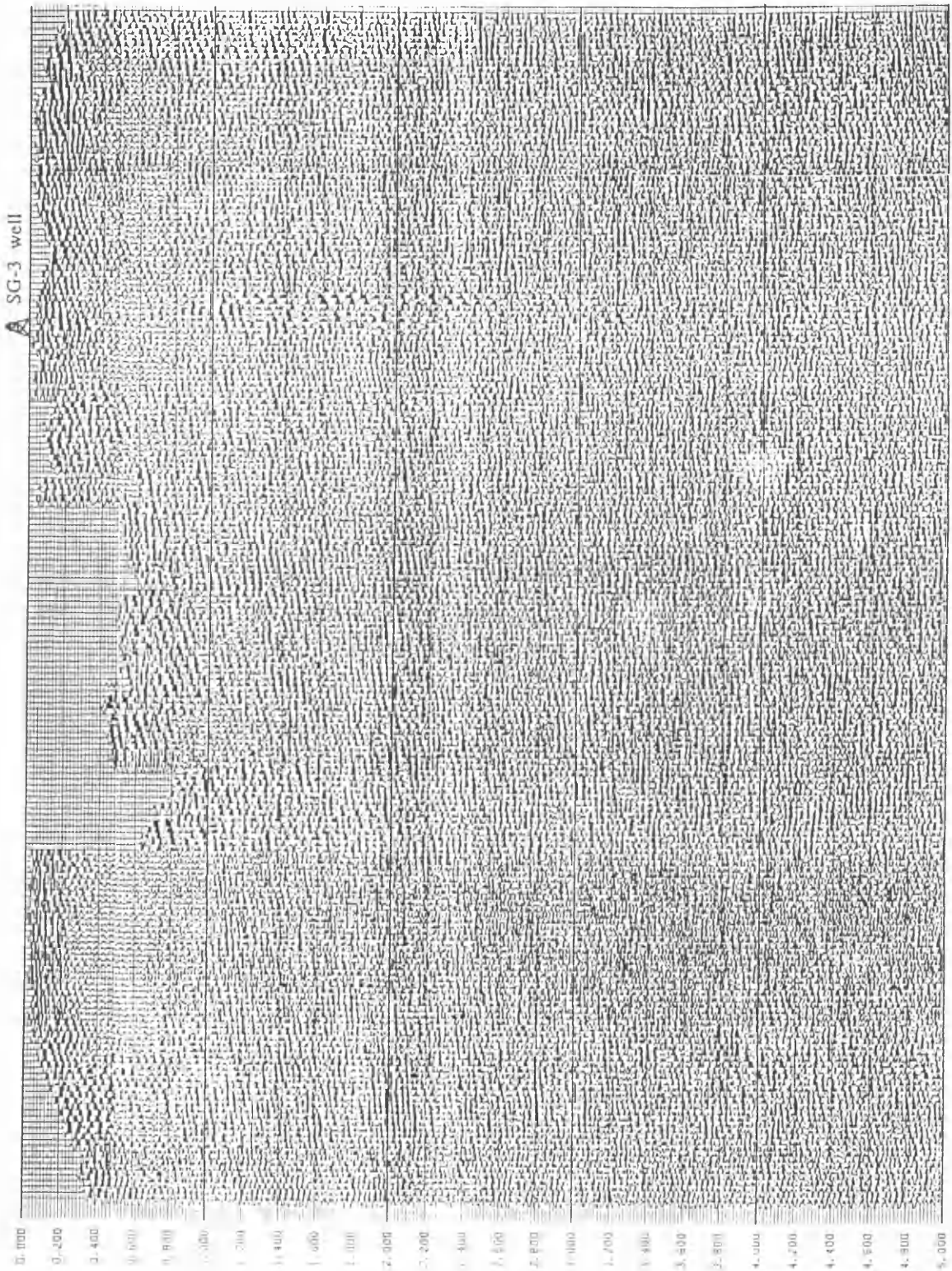


Fig. 7-16. Final stacked section without migration. The SG-3 well is marked at top. Trace spacing 25 m, vertical scale in seconds of two-way travel time. NB a large-scale version of this section is enclosed as Figure 7-16a inside the pocket of the rear cover.

7.8.5 Residual statics correction

The moveout in CMP gathers is not always exactly correct, because of near-surface velocity irregularities that cause a static shift. Lateral velocity variations due to complex overburden can cause moveout that can even be negative locally. To improve stacking quality, residual statics corrections are performed on the moveout-corrected Kola CMP gathers. This is done in a surface-consistent manner; that is, time shifts are dependent only on shots and receiver locations, not on the raypaths from shots to receivers. The cross-correlation window is defined from 1800-2400 ms at CDP 30 to 1000-1700 ms at CDP 230 in the reference stacked section. The estimated residual corrections are applied to the original CMP gathers with no NMO correction. In addition, we found that the SierraSEIS version 2.1 could cause the extra linear moveout with the application of module /RSESTIM.

7.9 Poststack processing

The primary goal of poststack processing is to improve the quality of stacked data. The processing methods include predictive deconvolution, time-variant bandpass filtering, migration, and some gain scaling. In our case, three kinds of processing methods are used in the final stage. These are described below

7.9.1 Deconvolution

Deconvolution is a general term for data processing methods designed to improve the temporal resolution of seismic data by compressing the basic seismic wavelet, to remove effects which tend to mask the primary reflected events. The predictive deconvolution filter is applied in the post-stack Kola data to suppress reverberations, further whitening the spectrum and obtaining higher resolution. But we found that no significant improvement is achieved as shown in Figure 7-17. It is suspected that the discordance of the interfaces degraded the performance of deconvolution. There are about six assumptions that underlie predictive deconvolution. Our case violates at least two of them; firstly, the noise component is not zero in the Kola data, and secondly, the subsurface is not made up of horizontal layers of constant velocity.

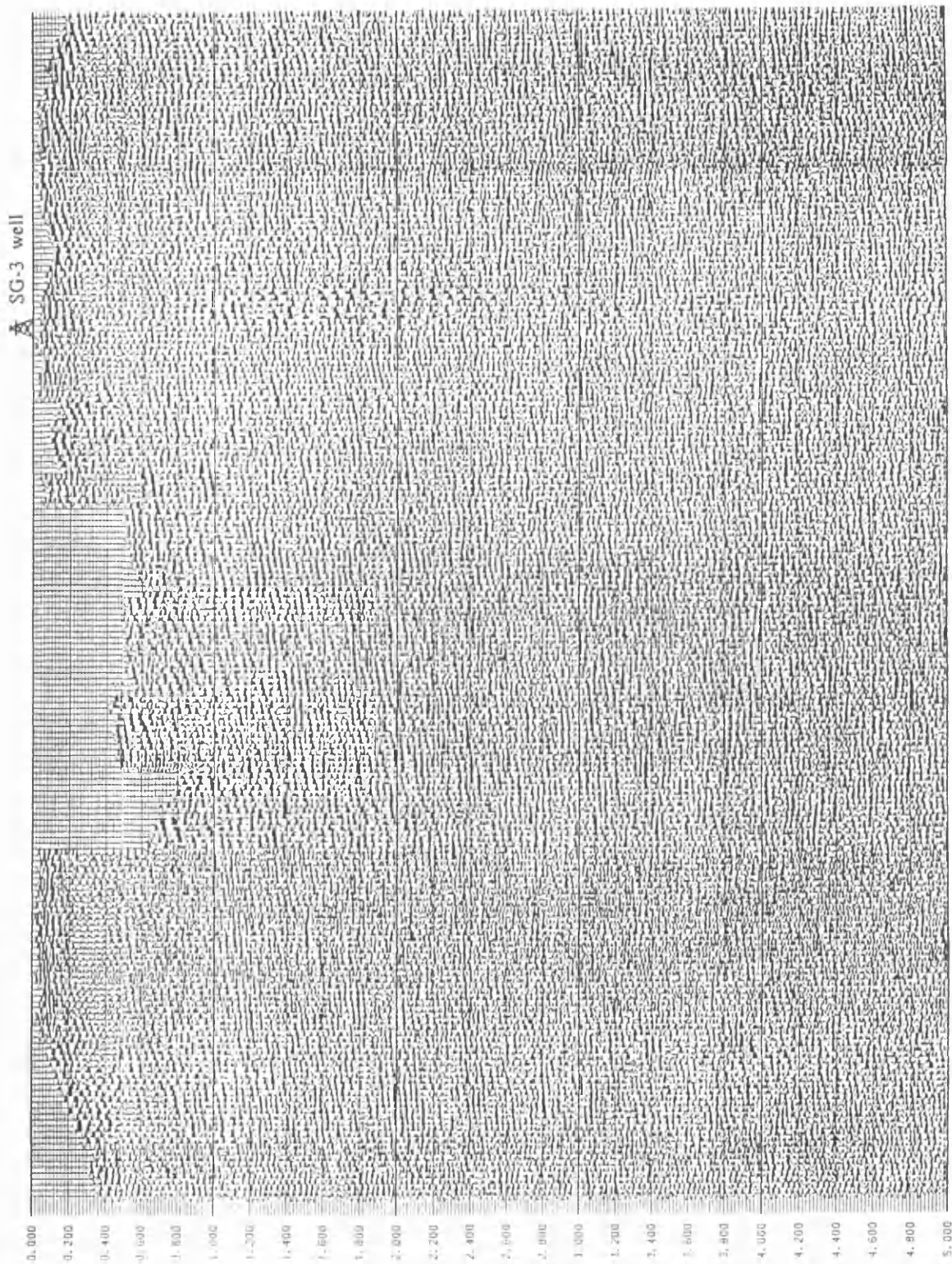


Fig. 7-17. Result of poststack predictive deconvolution processing, plotted in variable area form with wiggly trace. Trace spacing 25 m, vertical scale in seconds of two-way travel time.

7.9.2 Coherency filtering

As the dominant characteristics of reflection in the Kola data are the poor continuity of P-wave reflectors and their frequent unconformity, it is necessary to enhance the stacked section using some image enhancement techniques. A useful method is coherency filtering, which can enhance the events with lateral continuity within a specified dip range. In our case, 8 traces and a 40° dip angle were used in the post-stack coherency filter. The final output of this process is shown in Figure 7-18.

7.9.3 Band-pass filtering

Band-pass filtering is used most because a seismic trace typically contains some low-frequency noise, such as ground roll, and some high-frequency ambient noise. It is standard practice to apply a time-variant bandpass filter to stacked data. The usable seismic reflection energy usually is confined to a band-width of approximately 10 to 70 Hz, with a dominant frequency around 30 Hz. As the relatively strong high-frequency ambient noise dominates the Kola stack section, a narrow band-pass filter is applied, from 10 to 35 Hz.

7.10 Problems and discussion

The final stack of the main line is presented in conventional wiggle-variable area form in Figure 7-16. The coherency-enhanced version of the stack is shown in Figure 7-18. Overall, the data quality is disappointing, but it is hoped that further improvement could be achieved by increasing the CMP coverage, by including the shots from the shots on line 2 and line 3, and resolving the following problems during a future processing phase.

7.10.1 Extra moveout problem for Blue recording system

We found that a few common shot gathers from the B-system seem to have their polarity reversed, compared to the data recorded by the Z- and W-systems, as shown for example in Figure 7-19. So far we have been unable to simply apply a routine processor to reverse the polarity, because only some of the gathers from the B-system have the problem, and

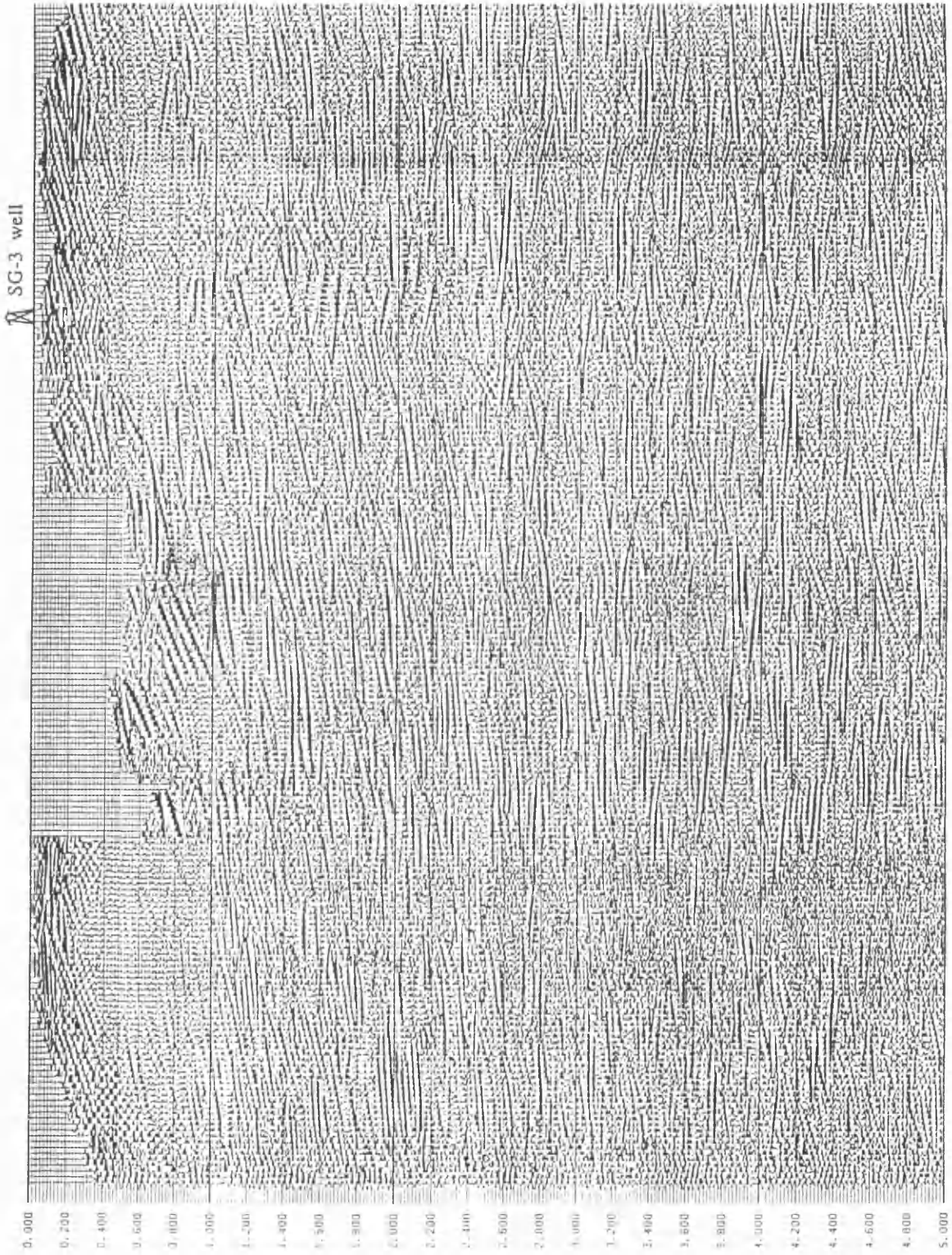


Fig. 7-18. Result of poststack coherency filtering to enhance the events with lateral continuity. The specified filtering dip range is 8 traces and 40°. Trace spacing 25 m, vertical scale in seconds of two-way travel time.

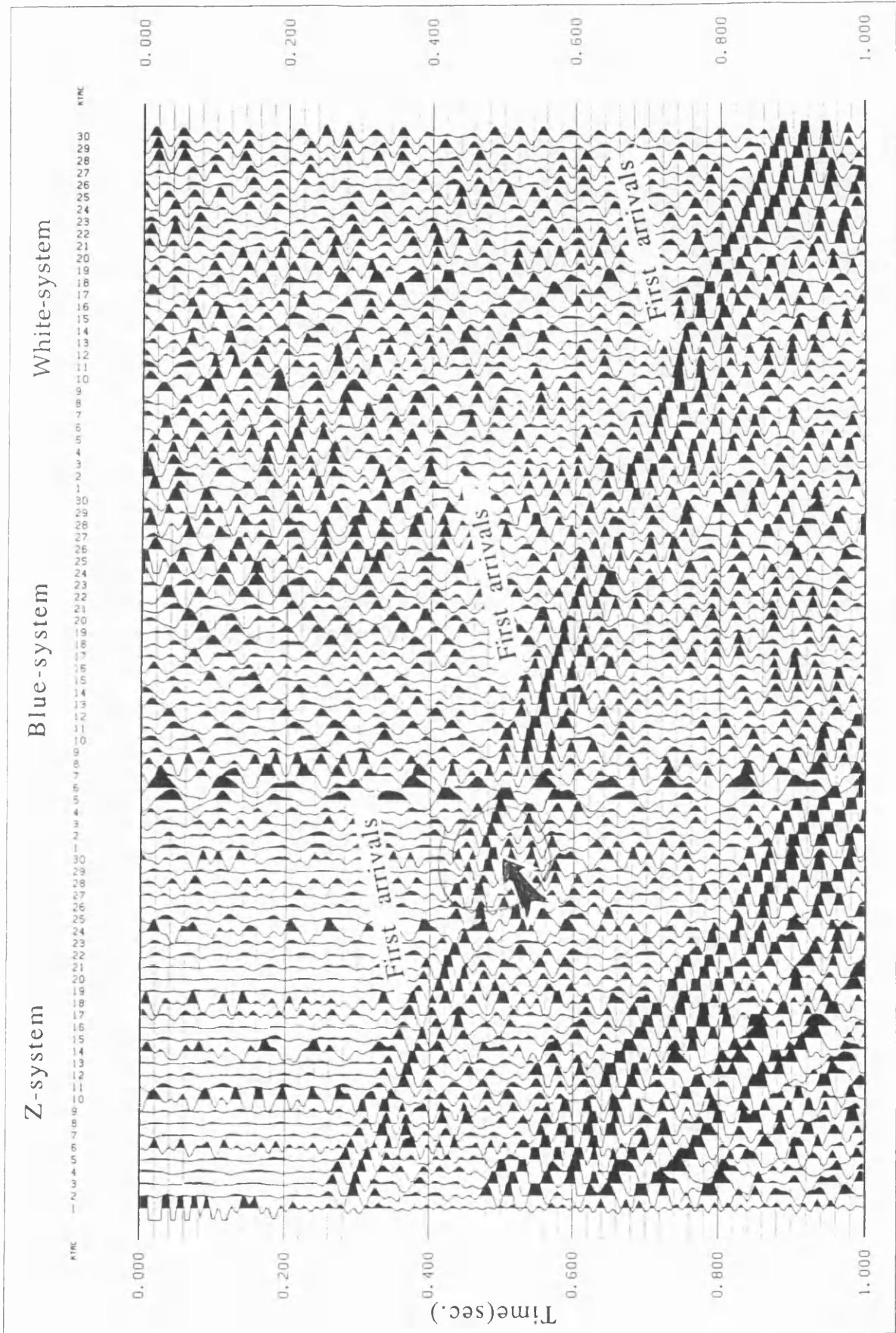


Fig. 7-19. The misaligned moveout of the traces in a common source gather FFID=22681 from Blue recording system (middle) is marked by an arrow. Trace spacing 50 m, vertical scale in seconds.

the first breaks are not always clear within those shot gathers. The reasons for the problem could be related to (1) a hardware flaw in the recording system, or (2) near-surface velocity variation. The following is a discussion of the second potential reason.

Residual static corrections are needed because field statics and datum corrections almost never totally compensate for the effects of near-surface velocity variations. This is because the near-surface velocity variations are not known and therefore exact corrections cannot be made. The method of surface-consistent statics estimation based on reflections works well in accommodating short-wavelength variations, but performs poorly in handling the long-wavelength variations. The main reason for this is that the input to reflection-based statics algorithms is arrival time differences between traces, not absolute times. Refraction-based static methods are based on absolute first-break arrival times and, in theory, are able to estimate the long-period statics components.

7.10.2 Separation of P- and S-waves

As shown in Figures 7-4 and 7-5, a strong S-wave can be observed on almost all shot gathers. Its amplitude is usually bigger than that of the direct P-wave. The correlation sidelobe problem due to the direct S-wave could be worse than that due to the direct P-wave energy. In addition, the strong direct S-wave itself complicates other wave patterns, leading to reduction of the signal-to-noise ratio, particularly in the shallow section. For this preliminary phase of conventional P-wave data processing, the undesired S-wave has not been removed prior to correlation. Fortunately 3-component data were acquired in the Kola deep reflection experiment. It is hopeful that the newly developed polarisation enhance algorithm (Ma 1992) could be applied to separate the P- and S-waves, so that only the P-waves in the Kola data will be used in a future processing phase.

7.10.3 Statics estimation

At each shot station the vibrator array moved up 5 m before every sweep injection. At the last sweep it is therefore 35 m away from the original station position. However we have had to simply sum these 8 shot gathers together, neglecting this moveup, to calculate the statics, due to the limited capacity of the SierraSEIS package. It would be reasonable in

future, if processing facilities permit, to calculate statics based on the unsummed corrected sweeps.

7.10.4 Velocity analysis

Velocity analysis is an essential step for stacking. The linearly varying velocity function from 5000 m/s to 6000 m/s was applied in the normal moveout correction (NMO) of the Kola data because the velocity spectra were noisy and difficult to interpret. The complex crustal structure also leads to the weakness of the reflection signals from depth. However it is hoped that some improvement in the stacked section can result if more accurate velocity-depth functions can be interactively picked from semblance plots in the first 3-4 s, where the signal strength of reflection is likely to be strong enough.

Chapter 8

Conclusions

8.1 New near-zero-offset methods based on the RAZOR array

To simulate and study the new near-zero-offset method based on the RAZOR array, we used the Sierra products, one of the standard industry geophysical processing and geological interpretation systems, to carry out numerical experiments. In our discussion two array design modes are proposed for modelling RAZOR array surveys. The first is the crooked line mode which is suitable to the experiment with a single RAZOR array. The second is the five-line mode which is more suitable to simulate roll-along experiments of the RAZOR array using QUIKSHOT, one of the Sierra subsystems. A new Fortran-77 program RAZORSORT.F is developed for the required post-raytracing sorting. In addition, a new quick display tool QPLOT.F was developed, supported by the UNIRAS packages. To image the subsurface structure from the P-wave of recorded RAZOR data, slant-stack processing is applied to extract the maximum reflection energy and improve the signal to noise ratio. The aim of the slant-stack operation in the RAZOR array is to image geological structure and improve the signal/noise ratio in three dimensions rather than to suppress multiples or pursue other purposes, for which the slant-stack processing is usually performed in CDP gather in two dimensions. The synthetic data test examines the performance of the 3-D RAZOR slant-stack. As a undesired aliasing occurs in the τ -p domain from the RAZOR slant-stack processing, and leading to the degradation of the imaging, two techniques, an image enhancement operator (IEO) and diversity stack, are proposed to suppress this kind of noise without distortion of the signal components in the stacked trace. Both methods work effectively during the synthetic data experiments. Finally we examine the RAZOR point-source data from the point of view of seismic illumination, or so called controlled directional source (CDS) method. By superposing the common-receiver traces corresponding to the continuous point source, the response of RAZOR array to a plane source is simulated. Based on the analysis of the 4-D data set from the RAZOR array rolling along a survey line, the RAZOR profile is obtained.

After the experimenting with the synthetic RAZOR data processing, we realised that some problems still remained and that further development work would be required. These problems are listed as follows:

(1) The IEO attenuates alias artifacts effectively in the synthetic data test, but improper specification of the IEO operator parameters could lead to poor resolution of the output IEO image. The relationship between the image resolution and its defining parameters has not yet been figured out. How best to specify those parameters still remains a problem. In addition, we have not yet tested whether the IEO would work as well on real noisy RAZOR data.

(2) In the author's point of view, the RAZOR diversity slant-stack is a better alternative for carrying out slant-stacking in the RAZOR domain. However the performance of this diversity slant-stack is affected by the choice of the dispersion aperture length, as mentioned in section 3.4 of chapter 3. According to the test results, the extent of aliasing noise attenuation increases with the enlargement of the dispersion aperture, but it is very hard to give some criteria to define the optimum parameters. This deserves further study. The Fortran-77 program QDSTACK for performing diversity slant-stack processing should also be added into SierraSEIS to go along with the RAZORSORT module.

(3) The RAZOR profiling is based on the analysis of the 4-D data set from CDS sections. Each RAZOR CDS section represents the reflections generated by an invariant subsurface illuminated by a planar source wave with a particular inclination and azimuth. According to the discussion by some authors the point-sources should be spaced less than $1/4$ of the shortest wave length apart in order properly to generate plane waves or a controlled wavefront. For the geometrical definition of the original RAZOR array, the simulated plane wave is suitable for a maximum reflection frequency of 20 Hz, since the maximum station spacing is 75 m when the velocity of the rocks is 5000 m/s. It is obvious that this maximum frequency of 20 Hz is too low for many exploration purposes, and implies that the geometrical definition of the RAZOR array should adjusted in some situations to simulate a plane source wave at higher frequencies. In addition, if there were a 3-dimensional interactive display tool available with a flexible access I/O port, the

interpretation and analysis of RAZOR CDS sections would become much faster and easier to understand.

(4) Imaging the subsurface structure using the P-wave information of recorded RAZOR data is based on the assumption that the offsets between the shot and receivers in RAZOR array are small relative to the depth of the subsurface target. If this assumption is violated, the wavefront of P-wave reflections cannot be approximated by a flat plane. Can we still apply the slant-stack processing to extract the maximum reflection energy and improve the signal to noise ratio in the 3-dimensional spatial domain? This question remains unanswered.

Finally we have to point out that only the vertical component of the RAZOR data has been discussed in this first research phase of the new near-zero-offset reflection method. Further discussion and experiments should continue to study the application of other two horizontal components of the RAZOR data in the future.

8.2 Removing the direct wave

The SFU algorithm for removing the direct wave in uncorrelated vibroseis data demonstrates, using both synthetic data and field recorded data, that the filter can provide excellent correlation noise cancellation when the onset time of the direct wave sweep is known. The SFU algorithm does not require any additional conditions on field acquisition (other than that the uncorrelated data are preserved) and is suitable for all common vibroseis data acquired using linear or non-linear sweeps. The algorithm has the following costs and benefits:

- Requires uncorrelated data
- Requires a knowledge of the source sweep
- It is a single trace processor (no geometry information required)
- Does not degrade the trace in any way
- It has no special acquisition requirements
- It works with a variety of source sweeps
- It is cpu intensive, but automatic, so not labour-intensive.

The version of SFU with the application of an OLS filter appears to be much more effective at cancelling the noise without attenuating signal frequency components near the terminal frequency than the version using a notch filter. However if the tapers on either end of the sweep are unknown, severe harmonic distortion is introduced. In that case SFU with the notch filter should replace SFU with the OLS filter. The field data examples demonstrate that SFU requires the onset time of direct wave sweep to be known precisely. In cases where the onset time is known only approximately, a correlation analysis can be used to find the exact onset time needed for the squeezing and unsqueezing transforms to work automatically. If the auto-pick still fails or performs poorly, SFU with the notch filter should replace SFU with the OLS filter. Even when the sweep formula is unknown or cannot be described as an explicit function of time, SFU is still valid for vibroseis data recorded with both linear or non-linear sweeps. In this case we search for and pick the zero nodes on the recorded sweep directly, without deriving an explicit transformation algorithm. Although we have investigated the SFU algorithm as a means of removing correlation noise from first breaks, there is no reason why SFU should not be applied to the removal of any undesired signal, as long as the exact onset time of the unwanted signal in the pre-correlation domain is known or determinable.

The DOLS filter is the second method developed to remove the direct wave in the pre-correlation domain. It is the simplified version of the 'squeeze-filter-unsqueeze' (SFU) algorithm, and can also provide excellent correlation noise cancellation when the onset time of the direct wave sweep is known. The DOLS filter differs from SFU filtering, since the latter is dependent upon the squeezing and unsqueezing transformation pair. The DOLS filter does not require any additional restrictions on field acquisition, and is suitable for all common vibroseis data acquired using linear or non-linear sweeps as well. However, the synthetic examples demonstrate that the DOLS filter requires the onset time of direct wave sweep to be known precisely as does SFU. Although both the SFU and the DOLS filters can provide excellent results in cancelling the direct wave in the pre-correlation domain, some problems still remain, as follows:

- (1) The SFU and DOLS filters are based on two assumptions: (a) that the undesired vibroseis direct wave is a copy of the source sweep, and (b) that the onset time of the

direct wave sweep is known well. As discussed in Chapter 4, if the sidelobes caused by a strong direct wave constitute the dominant source of coherent noise, the first assumption can be easily satisfied. However the second assumption would be often violated in the real world. Further study should be carried out in the future.

(2) Improper specification of the operator length will result in poor performance of the DOLS filter. To select an optimum operator length, we proposed a method in Chapter 5, which was dependent upon an empirical method. In practice, this is not a ideal way to find out the optimum operator length. We should therefore continue the study of the relationship of the optimum operator length to the specification and characteristics of the injected sweep. In addition, the DOLS filter could lead to possible attenuation or distortion of the signal at and near the direct wave. In Chapter 5 we concluded that this disadvantage of DOLS is related to the approximation error of the onset time for direct wave; however, it is necessary to find out more solid evidence for this explanation.

(3) The resolution of the SFU operation is restricted by the sampling rate. Decreasing the sample interval to 1 ms will mean that the computation time is four times more than that of common sampling rate of 4 ms, as used by the current program. So the further development of this new module /QSFU within the SierraSEIS package is necessary.

8.3 Improving Reflection Images with 3-component filtering

A new 3CFH filter is proposed for enhancing P-wave reflections, by using 3-component recording. The process is able to generate a unique 3-D velocity semblance for each CMP gather. By iteratively repeating the processing on each 3-component CMP shot gather, a final improved subsurface image can be extracted by using the optimum projection velocity. A new module /QTCFH for 3CFH filter processing was programmed and added into the SierraSEIS 1.43. In addition the /QGATHER module is added into SierraSEIS as a routine processor to gather the unique 3-C CMP data into an appropriate format for 3CFH.

The 3CFH filter is based on three main assumptions:

- (1) The earth is made up of horizontal isotropic layers of constant velocity;
- (2) P-wave energy dominates in the 3-component data compared with other modes, and
- (3) The velocities of the multi-layer model do not vary very much.

Assumption 1 and 3 are the basis for the 3CFH filtering of the recorded 3-component seismogram. In practice, 3CFH filtering often yields good results in areas where these three assumption are not strictly valid. Assumption 2 can be relaxed by applying some effective filter to separate P-wave and S-wave before filtering. Further experiments on the processing procedure should be conducted. If assumption 3 is violated - for example, if there is a low velocity layer, and/or if the earth is not made up of horizontal layers, then we would have a problem in extracting the maximum P-wave energy from the desired interfaces. Although the experiments with synthetic data show a considerable improvement of the signal to noise ratio, we still have to experiment further before we can expect good results to be obtained from real data.

We realise that further tests of 3CFH filtering on real data are very important. As we stated in Chapter 6, SierraSEIS cannot handle 3-component data, and the newly added /QGATHER module can only process limited shot gathers in one batch processing job. Although the 3-component CMP data from the Kola CDP crustal reflection experiment is available, we cannot at present test the 3CFH filtering on it. So it is necessary to further develop both the new /QTCFH and /QGATHER processors in the future. Despite the fact that the 3CFH filtering works well with synthetic data, its usefulness or its practicality still is uncertain, and should be examined further.

8.4 Application of new methods to the Kola data

The Kola data processing described in Chapter 7 follows a conventional sequence of seismic data processing. Three new processing techniques have been developed for some preprocessing phases. Firstly, a new module carries out a timing compatibility correction for the three field recording systems which had different trigger circuits. Secondly, a new module is developed to pick up and automatically set to zero the bad traces, based on a statistical analysis of amplitudes within a certain time window of each trace, and by

comparison among the traces in shot gather. Lastly, a new notch filter is developed to cancel any stationary sinusoidal noise in the seismic data, based on a recently published digital least-squares filtering algorithm (Linville and Meek, 1992). An F-K filter has been applied to remove coherent noise such as ground roll. The notch filter suppresses a large amount of stationary sinusoidal contamination caused by the mechanical noise near the well-head. Band-pass filtering is used to attenuate very low- and high-frequency random noise. Residual statics correction is done to improve stacking quality. Post-stack deconvolution achieves compression of the wavelet to increase the temporal resolution. Coherency filtering enhances the events with lateral continuity within a specified dip range. Migration has not been applied in this preliminary processing phase. The quality of the processed Kola data is disappointing at present, although the stacked sections (e.g. Fig. 7-16) suggest the presence of reflectors in the uppermost 1-2 s dipping to the left (south) at a rate of about 1 s TWT over 2.5 km. Assuming 5 km/s for the Proterozoic volcanics, this would correspond to a dip of around 45°. This matches the primary lithological layering of the Proterozoic supracrustal rocks, which are observed at the surface and in the well dipping at 40-50°. However, we are unsure of the validity of the results, as the processing techniques applied have been extensive, and it is difficult to assess seismic reflection quality within such a hard-rock environment.

Although some preliminary results have been achieved by the current processing sequence, we still have to point out some potential factors which could affect the final processed version of the Kola data, and some further work we could do to improve the processing quality. They are listed as follows:

(1) Merging the East Road and Nikel Road lines with the Main line. As over 8000 CMPs are too many for the SierraSEIS 2.1 to sort, we have had to exclude the CMPs from the shots on the East Road and Nikel Road lines. Including the common mid points associated with the East and Nikel Road lines into the bins will certainly increase the CDP fold, and subsequently improve S/N ratio for the deep section. It would be best if CDP gathering could be carried out by another processing package in the future. The geometry job file would have to be re-written, though this is only a technical problem.

(2) *Amplitude correction for Kola 3-component surface seismic data.* As the Kola multicomponent seismic data were recorded on the poor snow surface conditions during the winter season, and the survey was over a hard-rock outcrop area, the data quality was probably degraded by the complicated interaction between the field recording system and the near surface. The factors which affect the target amplitudes in the multicomponent data may be divided into two groups. One is related to the surface or near surface, including geometrical spreading, and source and receiver distortions due to interactions with the near-surface. The other is related to the subsurface, including attenuation, scattering and anisotropy. These complications may perhaps be corrected by an overburden-correction scheme developed by Winterstein and Meadows (1991); MacBeth *et al.* (1992, 1993); Li (1994a, b). These corrections could be essential for preserving and recovering the amplitude information of the target area in the Kola 3-component surface seismic data.

(3) *Slant stack processing to separate refraction and reflection, then mute out refraction.* Concerns over apparent lack of continuous reflections and the relatively low S/N ratio in the deep section below 2 s have been raised by this current processing phase of the Kola data. It is suggested that the noise could be related to the reverberating refractions and multiple reflections associated with the primary reflections near 2 s. The τ - p domain is an effective place to separate refraction and reflections according to their different ray parameters. The filtering could be carried out by passing the events of low p (high velocity) and rejecting events of high p (low velocity) in the τ - p domain. Then the data are transformed back into the x - t domain.

(4) *Velocity analysis at selected CDP control points with good primary reflections.* A constant stacking velocity was used for NMO correction during the current processing phase of the Kola data, although the velocity of the subsurface rocks doubtless varies vertically and horizontally. The reason for this is that the low CDP fold resulted in low S/N ratio on most CDP gathers, so that conventional velocity analysis is difficult. Nevertheless, variation of velocity should be considered in this area. It is expected that some of the CDP gathers could have relatively high S/N ratio, enough to carry out

semblance analysis as the velocity analysis control points, after a variety of filters have been applied to enhance primary reflections, for instance muting in the τ - p domain.

(5) Programming a new processor to sort out 3 component CDPs for the newly developed 3CFH filter. As neither SierraSEIS versions 1.4 nor 2.1 are able to sort out the 3-component CDPs into the required format, the newly developed filter 3CFH cannot yet be applied to any real field data, although the synthetic example demonstrated that filtering version is very satisfactory, with much improved reflections. The difficulty in dealing with programming a new 'sort' processor is that the internal data bus management in SierraSEIS is too complicated to understand in a limited time and to be manipulated at the full level. More time is needed to analyse the SierraSEIS internal data bus, given that there is no support, nor a detailed manual. A new 'sort' processor is the essential gateway to further analysis and development of multicomponent reflection processing methods.

References

- Al-Sadi, H. N. 1980, *Seismic exploration technique and processing*, Birkhauser Verlag Basel Press.
- Bernhardt, T. and Peacock, J. H. 1978, Encoding techniques for the vibroseis system: *Geophys. Prosp.* **26**, 184-193.
- Bortfeld, R., Hurtgen, H. and Koppel, H. 1960, Direction shooting. *Geophysical Prospecting* **8**, 534-562.
- Claerbout, J. F. 1971, Toward a unified theory of reflector mapping, *Geophysics* **36**, 467-481.
- Claerbout, J. F. 1978, A short review of retarded Snell midpoint coordinates. Stanford Exploration Project No. 14, 73-80.
- Crampin, S. and Lovell, J. H. 1991, A decade of shear-wave splitting in earth's crust: what does it mean? what use can we make of it? and what should we do next, *Geophys. J. Int.* **107**, 387-408.
- Cunningham, A. B. 1979, Some alternate vibrator signals: *Geophysics*, **44**, 1901-1921.
- Edelmann, H. 1966. New filtering methods with Vibroseis. *Geophysical Prospecting* **14**, 455-469.
- Edelmann, H. A. K. and Werner, H. 1982, Combined sweep signals for correlation noise suppression. *Geophysical Prospecting* **30**, 786-813.
- Embree, P. 1968, Diversity seismic record stacking method and system, *U.S. Patent* 3,398,396.
- Ensing, L. 1983. The autobalancer - an automatic system for the reduction of powerline interference with seismic signals. *Geophysical Prospecting* **31**, 591-607.
- Garotta, R. 1980, Bi-radial imaging and complicated tectonics. Presented at 42nd EAEG Meeting, Istanbul.
- Key, S. C. and Smithson, S. B. 1990, New approach to seismic reflection event detection and velocity determination, *Geophysics* **55**, 1057-1058.
- Kirk, P. 1981, *Vibroseis processing*, Developments in geophysical exploration methods-2, Society of Exploration Geophysicists, Tulsa, OK, 37-52.
- Klauder, J. K. Price, A. C. Darlington, S. and Albersheim, W. J. 1960, The theory and design of chirp-radars: *The Bell System Technical Journal* **39**, 745-808.

- Li, X. P. 1994a, Decomposition of vibroseis data by multiple filter technique, *64th ann. internat. Society of Exploration Geophysicists conf. Expanded Abstracts*, 711-714.
- Li, X. P. 1994b, Elimination of harmonic distortion in vibroseis data, *64th ann. internat. Society of Exploration Geophysicists conf. Expanded Abstracts*, 886-889.
- Linville, A. F. and Meek, R. A. 1992, Cancelling stationary sinusoidal noise. *Geophysics* **57**, 1493-1501.
- Lynn, W., Doyle, M. Lerner, K. and Marschall, R. 1987, Experimental investigation of interference from seismic crews, *Geophysics* **50**, 539-550.
- Ma, X. Q. 1990, *New methods in gravitational and seismic reflection exploration*, Unpublished Ph.D thesis, Univ. Glasgow.
- Mitchell, G. D. 1951, Seismic prospecting method, including generation of a cylindrical wave front, *U.S. Patent 2,555,806*, Patented June 5, 1951.
- Monk, D. J. and Cowan, P. B. 1991, An approach to optimum slant stack, its application as a seismic noise attenuator, *Halliburton Geophysical Services, Inc.*
- Pierau, H. and Muller, W. 1960, Improvement in the quality of deep reflections by uniformly linear shotpoint arrays, *Geophysical Prospecting* **8**, 154-163.
- Pierau, H. and Rosenbach, O. 1960, Comparative considerations on the energy content of seismic waves in central and linear pattern shooting, *Geophysical Prospecting* **8**, 164-177.
- Potts, M. J. and Wason, C. B. 1986, Amplitude balancing and approaches to optimum stack: Presented at Society of Exploration Geophysicists workshop on Near Surface Effects, Hyannis.
- Press, W. H. et al. 1989, *Numerical Recipes*: Cambridge Univ. Press.
- Schultz, P. S. 1976. *Velocity estimation by wavefront synthesis*. PhD Thesis, Stanford Exploration Project Report no. 9.
- Schultz, P. S. 1982, A method for direct estimation of interval velocities, *Geophysics* **47**, 1657-1671.
- Schultz, P. S. and Claerbout, J. F. 1978, Velocity estimation and downward continuation by wavefront synthesis, *Geophysics* **43**, 691-714.
- Smythe, D. K. Smithson, S.B. Gillen, C. Humphreys, C. Kristoffersen, Y. Karaev, N.A. Garipov V.Z. Pavlenkova, N.I. and the Kola-92 Working Group, 1994, Project images crust, collects seismic data in world's largest borehole. *EOS Trans. Am. Geophys. Union*, **75**, 473-476.

- Taner, M. T. 1976, *Simplan - simulated plane wave exploration*, Presented at 46th Society of Exploration Geophysicists Meeting, Houston, Texas.
- Taner, M. T. 1978, *Simulated plane-wave seismic sections, an update*, Presented at 48th Society of Exploration Geophysicists Meeting, San Francisco.
- Taner, M. T., Baysal, E. and Koehler, F. 1988, CDS - the controlled directional source method. In Gardner, G.H.F. and Lu, L. (Editors), *Slant Stack Processing*, 390-418, Society of Exploration Geophysicists.
- Taner, M. T. and Koehler, F. 1969, Velocity spectra-digital computer derivation and applications of velocity functions, *Geophysics* **39**, 859-881.
- Werner, H. and Krey, T. H. 1979, Combisweep - a contribution to sweep techniques, *Geophysical Prospecting* **27**, 78-106.
- Wiener, N, 1949, *Extrapolation, interpolation, and smoothing of stationary time series with engineering applications*, M.I.T Press and John Wiley & sons, Inc.
- Yilmaz, O. 1987, *Seismic data processing*, Society of Exploration Geophysicists.

Appendices

Appendix A:

BIRPS S-wave experiment 1988 Field layout of the Glasgow piggyback experiment

This note describes the array of 12 3-component seismometers designed to be beam-steered at approximately zero offset. Figure 1 shows the proposed pattern, with the shot point at the centre. The dimension of the pattern is the same as the shot spacing, viz. 75 m. Thus the seismometers can be thought of as lying on one of two concentric circles of radii 75 and 130 m.

The reasons for this array are as follows:

1. For a maximum phase shift of half a wavelength, the diameter of the array should be of the order of 200-300 m, for the events of interest (see Appendix for derivation).
2. The station spacing is big enough so that different near-surface ground conditions will be sampled. Rogue stations can be identified by comparison with other stations, and rejected from the beam-steered stack.
3. The 75 m radius of the inner circle is large enough so that the stations will not interfere with the firing of the shots; there is no station at the shot point.
4. Summation of 12 stations (if all can be used) produces a respectable signal-to-noise increase of 3.5, after polarisation filtering of each 3-component station separately.
5. During shooting, only 6 of the 12 stations have to be shifted between each shot point. Furthermore, 8 station sites are used 3 times, 2 are used twice, and only 2 are used once, thus minimising the preparation of sites for planting the geophones.
6. The multiplicity of station use allows the possibility of separating shot and receiver statics.
7. If reciprocity of shot and receiver applies, two further stations can be added to the 12 for each shot point.
8. Larger in-line arrays for beam-steering can be simulated, if necessary, by summing data for several consecutive shots.

Figure 2 gives an indication of the effective array pattern for two azimuths, which are periodic every 60° . Azimuths of between $0-30^\circ$ and $30-60^\circ$ will have patterns that are intermediate in form, but still symmetrical about the centre of the projection onto the azimuthal plane.

- 2 -

Appendix

Consider a normal-incidence ray leaving a reflector, which dips at an angle θ , in the lower crust, which has P-wave velocity V . The horizontal slowness is clearly

$$p = \sin \theta / V$$

The ray emerges at an angle of incidence α , corresponding to a planar wavefront dipping at the same angle α . We require a suitable dimension of x , the width of the array, over which the phase difference of a planar arrival will not differ by more than half a wavelength. This half-cycle definition is analogous to the definition of a Fresnel zone for a spherical wavefront.

The path difference across the array is

$$\Delta l = V_0 \Delta t$$

where V_0 is the velocity at the surface, and Δt is the time delay. Assuming a horizontally stratified velocity layering in the crust, the same horizontal slowness p applies at the surface. So

$$p = \sin \alpha / V_0 = \Delta l / (x \cdot V_0)$$

Substituting and re-arranging, we get

$$x = V \Delta t / \sin \theta$$

For a half-cycle of a 25 Hz wavelet, $\Delta t = 40 / 2 = 20$ ms. Taking a lower crustal velocity of $V = 6.5$ km/s, and a typical dip of an event that we might realistically expect to enhance or reject of, say, 30° , we get

$$x = 20 * 6.5 / \sin 30^\circ = 260 \text{ m.}$$

DKS 3.5.88

Fig. 1. Aerial pattern of 12 3-component receivers round each shot.

Lower figure shows the fold of coverage obtained if shot spacing is equal to the array spacing (75m)

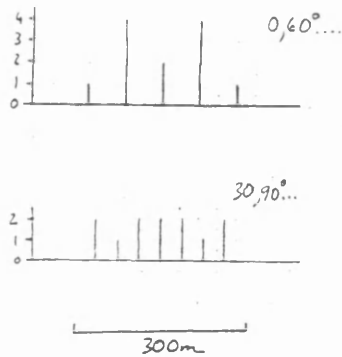
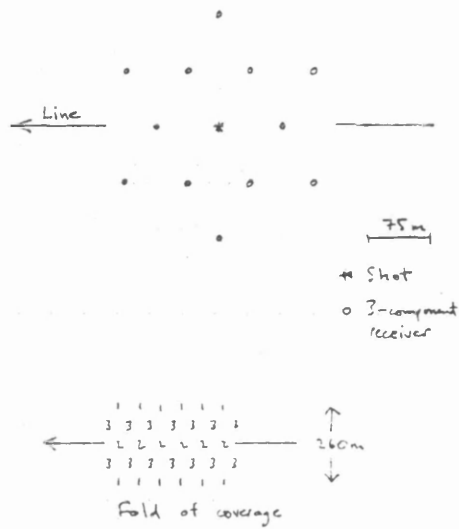
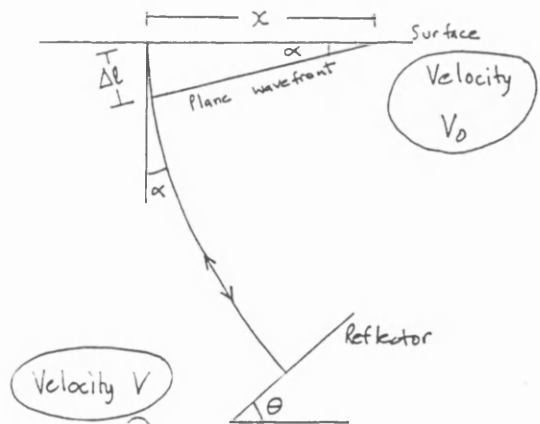


Fig. 2. Array weighting patterns for different azimuths

Fig. 3. Geometry of normal-incidence ray from lower crustal reflector dipping at θ . Plane wavefront is incident across an array of receivers of width x .



Appendix B: Fortran-77 source code

Source code for these programs can be found in the attached floppy disk.

Appendix C: The new processor /QDSTACK

To run the program, we have to define several calculation parameters at beginning. For example:

```
$ INPUT FILE NAME FOR RAZOR DIVERSITY SLANT-STACK  
DATA1.QR  
$ INPUT PROJECTION AZIMUTH (DEFAULT:90)  
90 (degrees)  
$ INPUT THE DIVERSION APERTURE (DEFAULT:100 MS)  
100 (ms)  
$ INPUT RAY PARAMETER LIMITS FOR SLANT-STACK  
                                (DEFAULT: 0.02)  
0.02  
$ INPUT THE NUMBER OF TRACES IN TAU-P DOMAIN  
                                (DEFAULT: 60)  
60  
$ INPUT FILE NAME FOR OUTPUT  
OUT.QR
```

Appendix D: A note on vibroseis direct wave suppression

Dave Smythe, 29 July 1992

Reflection data recorded at short source-receiver offsets can be swamped by direct waves from the source. This apparently limits the use of geometries such as RAZOR to deeper data. With vibrators, receivers nearby are unplugged since the source direct waves continue to swamp the receiver for an extended period, as well as producing cross-talk onto other channels. This note proposes a pre-correlation filtering procedure for vibroseis data, aimed at removing the direct waves.

A sketch of the combined time-frequency (t-f) spectrum (Cohen 1989) of an uncorrelated trace at zero offset is shown in Figure 1. The direct wave starts at time zero and sweeps up linearly in (t-f) space. The procedure to remove this is:

- (1) Linearly squeeze the portion of the trace from time zero to the end of the sweep, such that the direct wave sweep becomes a constant frequency signal (Figure 2). This constant frequency is equal to the end frequency of the sweep.
- (2) Apply a zero-phase high-cut filter to the trace, to remove all frequencies above the sweep end frequency.
- (3) Unsqueeze the squeezed portion of the trace, i.e. undo the compression applied in (1) (Figure 3).
- (4) Correlate the trace.

The above procedure could be applied to other unwanted signals, e.g. multiples, as long as we know the start time of the unwanted phase. This can be determined by inspection of a correlated trace. Direct waves at finite offsets could also be removed by this method, also cross-talk from near-offset traces contaminating other traces.

The problem remaining might be that after removing the unwanted signal, there is no dynamic range left in the filtered portion of the trace to record reflections.

Implementation of this idea

1. Write the squeezing and unsqueezing algorithms for SierraSEIS. Use can probably be made of trace-resampling processors already in SierraSEIS.
2. Write a t-f procedure to display a trace, so that we can see the effect.
3. Use standard SierraSEIS processors for the filtering and correlation.
4. Test it with Kola data.

References and further reading

Barnes, A. E. 1992. Another look at NMO stretch. *Geophysics* 57, 749-751.

Cohen, L. 1989. Time-frequency distributions - a review. Proc. IEEE 77, 941-981.

Follow up other references in Cohen (1989). Use the Science Citation Index to check up on other geophysical applications apart from Barnes (1992).

Fig. 1.

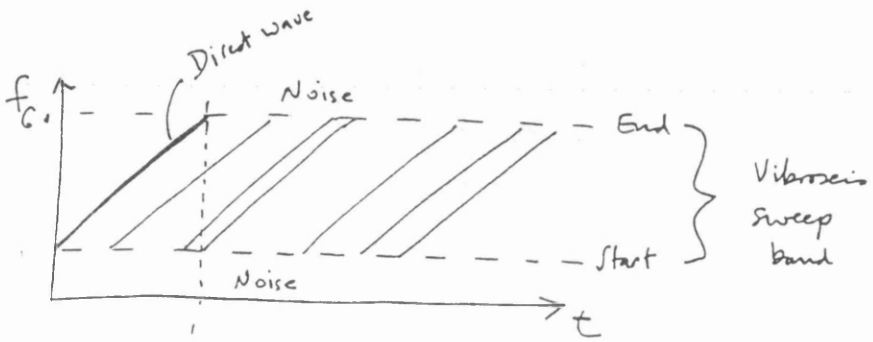


Fig. 2.

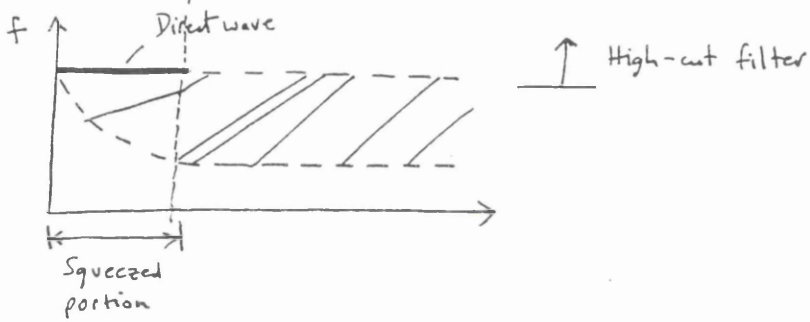
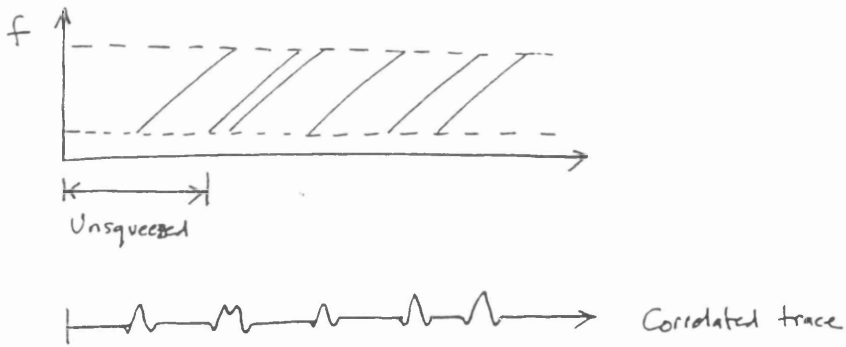


Fig. 3.



Appendix E: The new processor /QSFU

(1) Notes on usage

The new processor /QSFU should be called prior to correlation of common shot gathers. To run /QSFU, two disk files are need as buffers in your current subdirectory. They are named refer1.dat and refer2.dat respectively. You can create these filters initially using any text editor or copy them from /bin subdirectory before running. To verify the operation of SFU filtering, the application "hodogram" can be used as a screen view utility to display the recorded pilot sweep in refer1.dat and its squeezed version in refer2.dat. In the specification of the parameters for /QSFU, at least two control points must be defined in each calling for the window scanning, one on the first trace, and another on the last trace. Otherwise the processor will use default values.

(2) Parameter Description and Definition in /QSFU

SWEEP begin-frequency, end-frequency, sweep-duration

SWEEP defines the synthetical reference sweep to identify and correct the recorded pilot sweep based on the correlation analysis.

Required ? : Yes
 Parameter dependencies: None
 Value type : Real
 Units : Seconds and Hz
 Default : None

SCAN N1, begin-window1, scanning-window1
 N2, begin-window2, scanning-window2
 ...
 ...
 Nm, begin-windowm, scanning-windowm

Nm defines the trace number of control point for linear interpolation of window.

begin-window-Nm is the beginning time of scanning window on trace

No.Nm

scanning-window-Nm specifies the window length from begin-windowm

Required ? : Yes

Parameter dependencies: None

Value type : Real

Maximum no. of points : 50

Units : Seconds

Default : None

LINEAR

define the linear interpolation in squeezing and unsqueezing
transformation

Required ? : No

Parameter dependencies: None

Value type : None

Default : 4-point cubic spline interpolation

NOTCH The linear recursive notch algorithm will be applied

Required ? : No

Parameter dependencies: None

Value type : None

Default : The OLS algorithm

(3) Example of job file

...

/RESAMP

SR 2

/QSFU

SWEEP 10. 60. 20.

SCAN 1 0.63 0.06

11	0.72	0.08
17	0.78	0.1
30	0.86	0.076

/VCORR

SWEEP 10 60 20000

TAPER 1 500 500

TAPESWP

DATASWP 1

/RESAMP

SR 4

...

Appendix F: The new processor /QDOLS

(1) Notes on usage

The new processor /QDOLS should be called prior to correlation of common shot gathers. For /QDOLS, only one disk file is needed as the temporary buffer under the current subdirectory, named refer1.dat. You can create the refer1.dat file initially using any text editor or copy it from the /bin subdirectory before running the batch job. To verify the operation of DOLS filtering, the application "hodogram" can be used as a screen view utility to display the recorded pilot sweep in refer1.dat. In the specification of the parameters for /QDOLS, at least two control point must be defined in each calling for the window scanning, one control point at the first trace, and another at the last trace. Otherwise the processor will use the default value. The default operator length is 20 sampling units.

As the DOLS filter can use the original pilot sweep to design the filter parameters directly, we do not have to re-sample the data trace, as the /QSFU, in order to minimise the signal distortion associated with the squeezing and unsqueezing transformation.

(2) Parameter Description and Definition

SWEEP begin-frequency, end-frequency, sweep-duration

SWEEP defines the synthetic reference sweep to identify and correct the recorded pilot sweep based on the correlation analysis.

Required ? : Yes
 Parameter dependencies: None
 Value type : Real
 Unit : Seconds and Hz
 Default : None

SCAN N1, begin-window1, scanning-window1
 N2, begin-window2, scanning-window2
 ...
 ...
 Nm, begin-window, scanning-window

Nm defines the trace number of control point for linear interpolation of window.

begin-window-Nm is the beginning time of scanning window on trace

No. Nm

scanning-window-Nm specifies the window length from begin-window

Required ? : Yes
 Parameter dependencies: None
 Value type : Real
 Maximum of Points : 50
 Unit : Seconds
 Default : None

NTROPLZ nn

nn define the operator length of the DOLS filter.

Required ? : No
 Parameter dependencies: None
 Value type : Integer
 Default : 20

HODOGRAM

The switch is to generate the output of any desired trace in HODO format,
which can be viewed by application "hodogram"

Required ? : No

Parameter dependencies: None

value type : None

Default : off

CLENG cl

cl defines the lags of the reference sweep truncated from pilot trace
for correlation analysis to find out the onset time of direct sweep.

Required ? : NO

Parameter dependencies: None

Value type : Integer

Default : One third length of sweep duration

(3) Example of job file

...

/NOTCH

FREQUENCY 50

/QDOLS

SWEEP 10. 60. 20.

SCAN	1	0.63	0.06
------	---	------	------

	11	0.72	0.08
--	----	------	------

	17	0.78	0.1
--	----	------	-----

	30	0.86	0.076
--	----	------	-------

NTROPLZ 25

/VCORR

SWEEP 10 60 20000

TAPER 1 500 500

TAPESWP

DATASWP 1

/DISPLAY

...

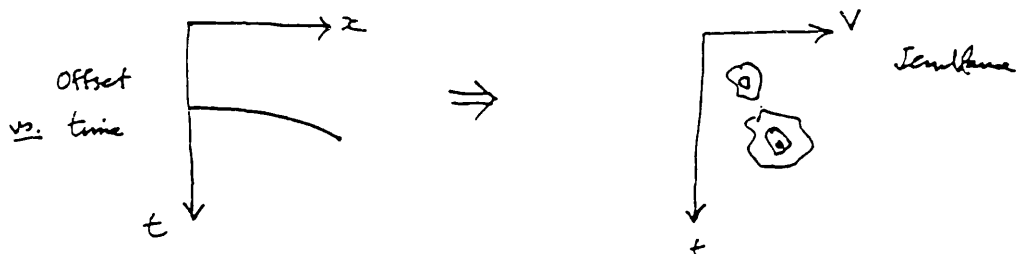
Appendix G: Note on 3-component semblance

by Dave Smythe, 10.6.93

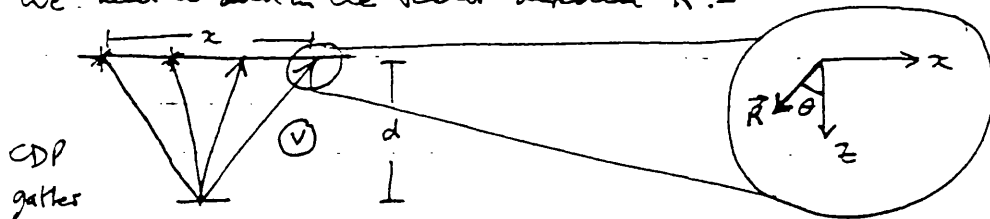
General problem We have an areal coverage of 3-component data through the Kola well. We wish to image horizontal reflectors (if they exist), not the steeply dipping lithological boundary reflectors.

Method: 3-component semblance

As a first step towards imaging we want to derive the velocities for stacking CDP gathers, using the full 3-component trace.



We need to add in the vector direction \vec{R} :-



$$V^2 t^2 = x^2 + 4d^2 \quad \dots \dots \dots (1)$$

$$\tan \theta = \frac{x}{2d} \quad \dots \dots \dots (2)$$

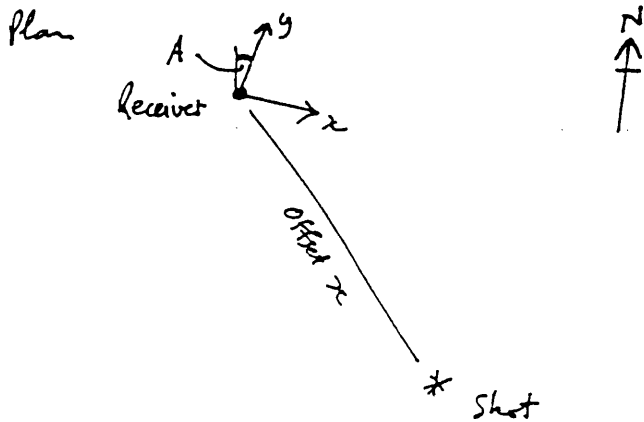
From (1)

$$2d = \sqrt{V^2 t^2 + x^2}$$

$$\therefore \theta = \tan^{-1} \left(\frac{x}{\sqrt{V^2 t^2 + x^2}} \right)$$

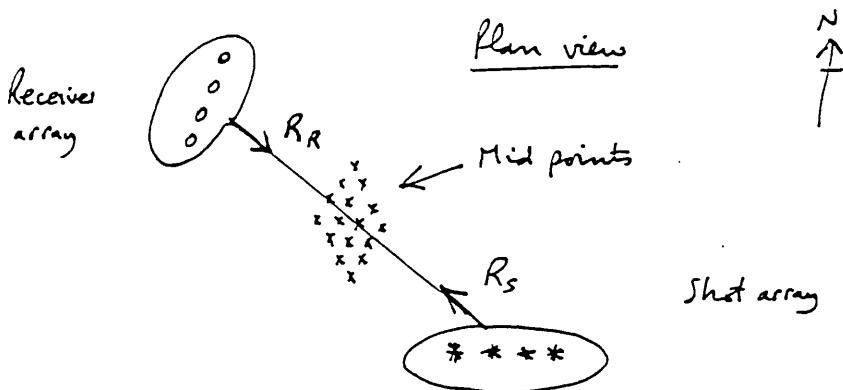
Use this $\theta(x, t, V)$ in a generalised semblance calculation for each CDP gather. The amplitude ϕ that goes into the semblance statistic is the component of the 3-cpt trace in the direction of \vec{R} .

In practice using direction cosines is probably the best way. The directions of the 3 components may not be related to the shot-receiver offset in a simple way:-



\vec{R} is in the vertical plane through shot & receiver. We will need to know the azimuth A of the 3-cpt. phone as well as the shot-receiver geometry. This will have to be obtained by study of 1st breaks.

Further work This will lead on to stacking the gathers using the vector \vec{R} derived from the 3-cpt. trace. We can also try beam-steering small shot and receiver arrays to improve the data:-



This will involve calculating the time delays for a short line of shots / receivers ^{laid} along an arbitrary line, to get the vectors R_R and R_S . In effect the array of mid-points is all put into one bin or CDP gather.

Appendix H: The new processors /QTCFH and /QGATHER

(1) Module /QTCFH in SierraSEIS 1.43

The 3CFH filter has been added into SierraSEIS package as a routine processor, named /QTCFH. It is used in processing 3-component data to obtain the enhanced P-wave reflection based on the three assumptions. /QTCFH must be applied to the 3-component CMP gather data stream prior to NMO correction and stacking. The 3-component trace stream should be in the order of $X_1, Y_1, Z_1, X_2, Y_2, Z_2, \dots, X_i, Y_i, Z_i, \dots$. The /QTCFH processor can extract the offset and velocity information attached to each trace attribute to calculate the angle between the raypath and vertical axis. However, you can also alternatively manipulate those input information by specifying the parameters in the batch job file. These parameters are described as follows:

AVELOCI vel

The "vel" defines a constant projection velocity for all stations in the 3CFH filtering.

Required ? : No
 Parameter dependencies: None
 Value type : Real
 Units : m/s
 Default : Velocity attached to each trace attribute

BELTAR beltar

The "beltar" defines a constant azimuth angle rotating from North axis in a field coordinate system $O_1(N, E, V)$ to the X radial axis in the required coordinate system $O_2(X, Y, Z)$ for 3CFH filtering.

Required ? : No
 Parameter dependencies: None
 Value type : Real
 Units : Degrees
 Default : by calculating the azimuth information
 attached to trace attributes

HODOGRAM n, m

This switch is to output the filtered version of any desired trace to HODO format, which can be viewed by the programme "hodogram".

The "n" define the gather number and "m" the trace number.

Required ? : No

Parameter dependencies: None

Value type : None

Default : Off

(2) Module /QGATHER in SierraSEIS 1.43

/QGATHER can sort out 3-component CMP gathers from any shot gather input. The maximum of the input is restricted not more than 8 shot gathers, each of which can have up to 24 data traces. No restrictions are placed on the trace length and sample rate. As the operation of the /QGATHER needs a large temporary disk buffer, we must always ensure that there is enough free disk space before running it. Alternatively the /QGATHER can also sort out the 3-component CMP in to different orders for other applications. The latest version is developed to output the CMP gather in three kinds of order:

- (1) $X_1, Y_1, Z_1, X_2, Y_2, Z_2, \dots, X_i, Y_i, Z_i, \dots$
- (2) $Y_1, Z_1, X_1, Y_2, Z_2, X_2, \dots, Y_i, Z_i, X_i, \dots$
- (3) $Z_1, X_1, Y_1, Z_2, X_2, Y_2, \dots, Z_i, X_i, Y_i, \dots$

To verify the operation of the 3CFH filtering, the application "hodogram" can be used as a screen view utility to display any desired trace data after 3CHF filtering. The /QGATHER filter has been added into SierraSEIS1.43 version as a routine processor, but it is not yet advanced enough to apply to processing real data. Further development of this new module is necessary in the future.

JCDP j

The "j" is the switch number, which defines the order of 3-component data in the output.

- | | |
|-----|---|
| j=1 | $X_1, Y_1, Z_1, X_2, Y_2, Z_2, \dots, X_i, Y_i, Z_i, \dots$ |
| j=2 | $Y_1, Z_1, X_1, Y_2, Z_2, X_2, \dots, Y_i, Z_i, X_i, \dots$ |

$j=3$ $Z_1, X_1, Y_1, Z_2, X_2, Y_2, \dots, Z_i, X_i, Y_i, \dots$

Required ? : No

Parameter dependencies: None

Value type : Integer

Units : None

Default : $j=1$

HODOGRAM n, m

The switch is to output the filtered version of any desired trace in HODO format, which can be viewed by the programme "hodogram".

The "n" define the gather number and "m" the trace number.

Required ? : No

Parameter dependencies: None

Value type : None

Default : Off

Appendix I: The new processors /QSHIFT, /QZERO and /QNOTCH

(1) Module /QSHIFT in SierraSEIS 1.43

The new module /QSHIFT has been developed to carry out the correction to ensure that all data from the three different recording systems, each with different trigger circuits, have same beginning of recording time. The parameters of /QSHIFT are described as below:

Notes:

1. Use /QSHIFT prior to correlation in shot-gather order.
- 2*. /QSHIFT can indicate if the recorded pilot sweep is bad.
- 3*. Use CHECK to explicitly switch off the checking procedure,
Otherwise the processor will analyse the pilot sweep first

SWEEP f1 f2 length

SWEEP specifies a synthetic sweep to identify the recorded sweep base on the correlation analysis. f1 and f2 are beginning and ending frequencies of sweep respectively. Length is the duration of sweep.

Required ?	: Yes
Parameter dependencies	: None
value type	: Float
Unit	: Hz and Second
Default	: None

NTRACE n

n defines the trace number of the pilot sweep for correlation analysis.

Required ?	: No
Parameter dependencies	: None
value type	: integer
Unit	: None
Default	: 1

HODOGRAM

HODOGRAM is a switch to output an ASCII file in hodogram format, which contains the original pilot sweep defined by **NTRACE**, and its shifted version. **HODOGRAM** is useful for check the operation of the new processor.

Required ?	: No
Parameter dependencies	: None
value type	: None
Unit	: None
Default	: Off

Example:

```
/JOB ACCT 'RD EX BY TE'
```

```
/IN
```

```
FORMAT SEG Y
```

```
DATA 1 40000 4 95 0
```

```
NOMATCH
```

```
REEL 1
```

```

...
/QSHIFT
SWEEP 10 60 20.
NTRACE 1
/VCORR
SWEEP 10 60 20000
TAPER 1 500 500
...
$EOJ

```

(2) Module /QZERO in SierraSEIS 1.43

/QZERO should be used prior to any other operation in the shot gather. The default value are strongly recommended, excluding some special cases. The parameter SWITCH is for printing the average amplitude of each trace in one shot gather, and list them in the order of their values. The parameter SHRE is to specify explicitly a threshold value for all of the shot gathers passed through the processor manually. Otherwise the thresholds will be specified by the amplitude analysis in the shot gather. The maximum number of traces per shot gather is allowed to be 100 and the maximum number of samples per trace 6000. The detailed description for these parameters is listed as follows:

SWITCH

SWITCH is a switch to carry out the zeroing of bad traces. Otherwise
The processor only list the results out of amplitude analysis.

Required ?	: Yes
Parameter dependencies	: None
Value type	: None
Unit	: None
Default	: only print the results of amplitude analysis on screen.

WINDOWB timeb

WINDOWB defines the beginning of time window for amplitude
analysis.

Required ?	: No
Parameter dependencies	: None

Value type	: Real
Unit	: ms
Default	: Set at the half of the trace length

WINDOWE timee

WINDOWE defines the end of time window for amplitude analysis.

Required ?	: No
Parameter dependencies	: None
Value type	: Real
Unit	: ms
Default	: Set at the end of the trace length

SHRE Threshold

SHRE specifies the threshold value for zeroing manually. All the trace with average amplitude value in time window greater or equal to this value are set to zero.

Required ?	: No
Parameter dependencies	: None
value type	: Real
Unit	: None
Default	: specify by the amplitude analysis in shot gather automatically. Thresholds would vary gather by gather.

BCUT n

n specifies the parameter value for a special filtering in amplitude analysis. It is usually set to default.

Required ?	: No
Parameter dependencies	: KNTR
value type	: Integer
Unit	: None
Default	: =KNTR/3

SCALE m

m specifies the times to amplify the trace values. It is usually set to default

Required ?	: No
Parameter dependencies	: None
value type	: real
Unit	: None
Default	: 1.0

CUTSCALE maxcut

CUTSCALE specifies the times to set maximum value of threshold. It is usually set to default

Required ?	: No
Parameter dependencies	: None
value type	: real
Unit	: None
Default	: 8.0

MINSCALE mincut

mincut specifies the times to set minimum value of threshold. It is usually set to default

Required ?	: No
Parameter dependencies	: None
value type	: real
Unit	: None
Default	: 5.0

(3) Module /QNOTCH in SierraSEIS 1.43

/QNOTCH requires that the undesired line frequency be accurately known, and takes somewhat more computer time than conventional notch filtering. As the 50 Hz analogue notch filter has been applied in all Kola data in the field, /QNOTCH is not used in the data

processing of Chapter 7. The detailed description of the operator's parameters is given as follows:

FREQUENCY freq

"freq" specifies the undesired line frequency

Required ?	: Yes
Parameter dependencies	: None
Value type	: Real
Unit	: Hz
Default	: None

OPERL operlen

"operlen" specifies the operator length of the least-squares filtering algorithm

Required ?	: No
Parameter dependencies	: None
Value type	: Integer
Unit	: Sampling rate (Points)
Default	: 20 points

Appendix J: SierraSEIS geometry processing job file (Chapter 7).

This is listed in the attached floppy disk.

Appendix K: Acronyms, abbreviations and definitions of symbols

Chapter 1

RAZOR	Roll-along zero-offset receiver array
IEO	Image enhancement operator
SFU	Squeeze-filter-unsqueeze algorithm
DOLS	Direct optimum least-squares algorithm
3CFH	3-component P-wave image enhancement operator

Chapter 2

BIRPS	British Institutions' Reflection Profiling Syndicate
θ	Dip of an interface in the lower crust
V	P-wave velocity of the crust

p	Horizontal slowness
α	Incidence angle of ray
$\Delta\lambda$	Phase difference of planar arrival on RAZOR array
V_0	Velocity at the surface
Δt	Time delay at the surface
x	Station spacing

Chapter 3

p	Slowness or the ray parameter
x	Offset
t	Two-way traveltime
τ	Linearly moved out time
α	Projection azimuth or azimuth of linear move out
α_0	Instance of projection azimuth α
$P(x, t)$	Observed seismic data
$S(p, \tau)$	Plane wave with ray parameter $p = \sin \theta / V$
x_i	Projected offsets of the 12 RAZOR receivers, $i = 1, 2, \dots, 12$
g	Observed seismic traces
$h_{\alpha_0}(p, \tau)$	Input image from the slant-stack processing with azimuth α_0 for one RAZOR shot gather
$f_{\alpha_0}(p, \tau)$	Processed IEO version of $h_{\alpha_0}(p, \tau)$
T	IEO operator.
A and B	IEO parameters leading with the resolution
K_i	Slope of the i th linear noise aliasing event, where $i = 1, 2, \dots, 5$.
g_{α_0}	Projected version of the RAZOR shot gather at the azimuth α_0
\bar{g}_{α_0}	Time averaged version of g_{α_0} , or dispersion aperture
i	Station number of a RAZOR array, or trace number of a RAZOR gather.
$h'_{\alpha_0}(p, \tau)$	Output of the RAZOR power diversity slant-stack
v_0	Medium velocity near the surface
θ	Angle between desired source wavefront direction and vertical z axes
β	Azimuth of wavefront inclination
T_i	Delay firing interval time, $i = 1, 2, 3, 4, \dots, 12$

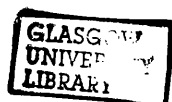
Chapters 4 and 5

f_1	Start frequency of sweep
f_2	End frequency of sweep
T	Duration of sweep
$\Phi(\tau)$	Autocorrelation
τ	Processed record time
A	Sweep signal amplitude
$\Delta f = f_2 - f_1$	Frequency bandwidth of sweep
$f_0 = \frac{(f_2 + f_1)}{2}$	Centre frequency of sweep
t	Time before squeezing transform
$x(t)$	Recorded data trace

$s(t)$	Vibroseis direct wave from linear sweep
$y(t)$	Primary reflection signal
	Squeezing transform
t_1	Time in squeezed domain
$s^1(t_1)$	Squeezed direct wave linear sweep with constant frequency f_0
$y^1(t_1)$	()
$x^1(t_1)$	
x_n^1	
y_n^1	Output trace sequence of a linear recursive notch filter
c_k and b_k	Filter coefficients of a linear recursive notch filter
θ	Desired width of notch filter
s_t^1	Squeezed direct wave signal
x_t^1	Recorded data trace
h_t	Squeezed synthetic reference sweep
v_t	Wiener-Levinson filter coefficients
L	Least-squares error of Wiener-Levinson filter

Chapter 6

$t(x)$	Travel time in homogeneous isotropic medium
v	Velocity
x	Offset
d	Depth between surface and reflection interface
θ	Angle between vertical component and raypath of a plane wave
$Z(t,x)$	Recorded vertical component data
$H(t,x)$	Recorded horizontal component data in the 'sagittal' or 'arrowhead' plane
$U(t,x)$	New scalar measurement as output of 3-component 3CFH filter
c_i	Complicated functions that depend on layer thickness and interval velocities
V_{rms}	RMS velocity
V_{nmo}	NMO velocity
V_{st}	Stacking velocity
V_i	Interval velocity
N	North axis
X	Horizontal component of a vector stands for the radial axis
Y	Horizontal component of a vector stands for the transverse axis
Z	Vertical component of a vector
β	Angle of rotation from the N axis clockwise to the X axis
\bar{V}_n	Average velocity down to nth reflector
o_i	Traveltime from surface to the i th reflector
$V_{rms,i}$	RMS velocity from surface to the i th reflector



FOLD — Fig. 7-16a. Final stacked section from Kola (CDP map shown in Fig. 7-8). The approximate location of the Kola SG-3 superdeep well is marked by the arrow. CDP interval 25 m; horizontal scale 1:10,000; vertical scale 10 cm/s; units are seconds of two-way time.

